I 1503/3

BULETINUL INSTITUTULUI POLITEHNIC DIN IAŞI

Tomul XLI (XLV)
Fasc. 1-2

Secția III **ELECTROTEHNICĂ**
ENERGETICĂ
ELECTRONICĂ

1995

ORSZÁGOS KÖZPONT ÉS KÖNYVTÁR 1981 INFORMÁCIÓS MŰSZAKI

BULETINUL INSTITUTULUI POLITEHNIC DIN IAŞI

Tomul XLI (XLV)
Fasc. 1–2

Secţia III

ELECTROTEHNICĂ. ENERGETICĂ. ELECTRONICĂ

1995

EDITORIAL STAFF

Prof. dr. eng. **VITALIE BELOUSOV** (President)
Prof. dr. eng. **PAULICĂ RĂILEANU** (Secretary)
Prof. dr. eng. **EFTIMIE NIŢESCU**
Prof. dr. doc. **ALFRED BRAIER** (Editor)
Prof. dr. eng. **HUGO ROSMAN** (Editor)
Prof. dr. eng. **MIHAIL VOICU** (Head of the Exchange Service)
Prof. dr. **AUREL BEJANCU**
Prof. dr. eng. **VICTOR BULACOVSCHI**
Prof. dr. eng. **DIMITRIE ALEXA**
Prof. dr. eng. **SPIRIDON CREŢU**
Prof. dr. eng. **ADRIAN RADU**
Prof. dr. eng. **ION GIURMA**
Prof. dr. eng. **MIRCEA MATEESCU**

The Bulletin of the Polytechnic Institute of Jassy is edited by
the **Technical University "Gh.Asachi"** (the former Polytechnic Institute), Jassy.

TEXredaction:
B. Grigoriu, A. Rotaru
Technical University of Jassy

BULETINUL INSTITUTULUI POLITEHNIC DIN IAŞI
BULLETIN OF THE POLYTECHNIC INSTITUTE OF JASSY
Tomul XLI (XLV), Fasc. 1-2 1995

Secţia III

ELECTROTEHNICĂ. ENERGETICĂ. ELECTRONICĂ

SUMAR

Pag.

FLORIN CONSTANTINESCU, MIRUNA NIŢESCU şi ANIŞOARA GEORGESCU, O metodă iterativă rapidă pentru analiza circuitelor neliniare în regim permanent. I. Teorie (engl., rez. rom.) 7

HUGO ROSMAN, Câteva observaţii referitoare la condiţiile de simetrie ale unui biport generalizat liniar, neautonom, în regim permanent armonic (franc., rez. rom.) 15

TUDOR MOROŞAN, Observaţii asupra erorilor metodelor numerice utilizate în studiul câmpului electromagnetic (engl., rez. rom.) 21

RADU URSULEAN, Senzitivitatea în domeniul timp a circuitelor electrice liniare în regim tranzitoriu (engl., rez. rom.) 27

PAUL COTAE, Calculul densităţii spectrale de putere pe baza anvelopei complexe pentru semnalele din banda de bază (engl., rez. rom.) 33

N.D. ALEXANDRU, Codare Miller combinată cu codare corelativă (engl., rez. rom.) ... 41

N.D. ALEXANDRU, Un circuit de codare *M*3 modificat (engl., rez. rom.) 47

VALERIU MUNTEANU, M. LUCANU şi DANIELA TĂRNICERIU, Creşterea siguranţei în funcţionarea dispozitivelor electronice prin folosirea unui cod bloc liniar corector de o eroare (II) (engl., rez. rom.) 51

ROMEO CIOBANU, TRAIAN BALAN şi MARINEL TEMNEANU, O aproximare teoretică a estimării fiabilităţii condensatoarelor de forţă funcţionând în regim periodic nesinusoidal (engl., rez. rom.) 57

ADRIAN BARABOI, MARICEL ADAM şi P. LEONTE, Utilizarea reactorului comandat ortogonal în tratarea neutrului instalaţiilor de medie tensiune (franc., rez. rom.) ... 65

EUGEN HNATIUC şi ADRIAN BARABOI, Asupra proiectării optimale a electromagneţilor monofazaţi de curent alternativ (franc., rez. rom.) 71

R.J. GREEN, Restricţii în calitatea imaginilor TV de înaltă fidelitate (engl., rez. rom.) . 77

LAURENŢIU DIMITRIU, Sistem de telecomandă multicanal cu radiaţie infraroşie. Decodorul (franc., rez. rom.) 85

Pag.

M. LUCANU, DORIN NEACŞU şi VICTOR DONESCU, Strategii de control optimal al puterii pentru invertoare cu MID vectorială (engl., rez. rom.) 97

LIVIA COCIU şi RADU COCIU, Traductor optic pentru controlul lăţimii foliei de polietilenă în instalaţii de extrudere (franc., rez. rom.) 103

C. ASAFTEI, MIRCEA GUŞĂ, MARCEL ISTRATE şi N. GAVRILAŞ, Semnalizarea la distanţă a scurtcircuitelor în reţelele de medie tensiune (franc., rez. rom.) 111

GH. GEORGESCU, M. GAVRILAŞ, GH. CÂRŢINĂ şi VIRGIL ALEXANDRESCU, Planificarea optimală a reţelelor electrice de distribuţie de medie tensiune (engl., rez. rom.) 117

RECENZII 125

BULETINUL INSTITUTULUI POLITEHNIC DIN IAŞI
BULLETIN OF THE POLYTECHNIC INSTITUTE OF JASSY
Tome XLI (XLV), Fasc. 1–2 1995

Section III

ELECTROTECHNICS. ENERGETICS. ELECTRONICS

CONTENTS

Pp.

FLORIN CONSTANTINESCU, MIRUNA NIŢESCU and ANIŞOARA GEORGESCU, A Shooting Method for the Computation of the Steady State in Nonlinear Circuits. I. Theory (English, Romanian summary) 7

HUGO ROSMAN, Quelques observations concernant les conditions de symétrie d'un biporte généralisé linéaire, nonautonome, en régime permanent harmonique (French, Romanian summary) 15

TUDOR MOROŞAN, Remarks on the Numerical Methods Errors in Electromagnetic Field Analysis (English, Romanian summary) 21

RADU URSULEAN, Time Domain Sensitivity of Linear Circuits. The Transient Case Study (English, Romanian summary) 27

PAUL COTAE, Computation of Power Spectral Density Based on Complex Envelope for Baseband Signals (English, Romanian summary) 33

N.D. ALEXANDRU, Combined Delay-Modulation and Correlative Level Coding (English, Romanian summary) 41

N.D. ALEXANDRU, A Modified *M*3 Coder (English, Romanian summary) 47

VALERIU MUNTEANU, M. LUCANU and DANIELA TĂRNICERIU, Increasing of the Safety in the Working of the Electronic Devices Using a Single-Error Correcting Linear Block Code (II) (English, Romanian summary) 51

ROMEO CIOBANU, TRAIAN BALAN and MARINEL TEMNEANU, A Theoretical Approach in Reliability Estimation of Power Capacitors Working in Periodical Nonsinusoidal Steady State (English, Romanian summary) 57

ADRIAN BARABOI, MARICEL ADAM et P. LEONTE, Emploi du réacteur commandé orthogonalement pour le traitement du neutre dans les installations moyenne tension (French, Romanian summary) 65

EUGEN HNATIUC et ADRIAN BARABOI, Sur le calcul optimal des électro-aimants à courant alternatif (French, Romanian summary) 71

R.J. GREEN, Picture Quality Restrictions in HDTV Systems (English, Romanian summary) 77

LAURENŢIU DIMITRIU, Système multicanal de télécommande par rayonnement infrarouge. Le décodeur (French, Romanian summary) 85

Pp.

M. LUCANU, DORIN NEACŞU and VICTOR DONESCU, Optimal Power Control Strategies for Space Vector PWM Inverters (English, Romanian summary) 97

LIVIA COCIU et RADU COCIU, Traducteur optique pour le contrôle de la largeur du film de polyéthylène dans les installations d'extrusion (French, Romanian summary) 103

C. ASAFTEI, MIRCEA GUŞĂ, MARCEL ISTRATE et N. GAVRILAŞ, Sur la signalisation à distance des court-circuits dans les réseaux de moyenne tension (French, Romanian summary) 111

GH. GEORGESCU, M. GAVRILAŞ, GH. CÂRŢINĂ and VIRGIL ALEXANDRESCU, The Optimal Planning of Medium Voltage Power Distribution Networks (English, Romanian summary) 117

BOOK REVIEWS 125

BULETINUL INSTITUTULUI POLITEHNIC DIN IAŞI
Tomul XLI (XLV), Fasc. 1–2, 1995
Secţia III
ELECTROTEHNICĂ. ENERGETICĂ. ELECTRONICĂ

D.C. 621.316

A SHOOTING METHOD FOR THE COMPUTATION OF THE STEADY STATE IN NONLINEAR CIRCUITS
I. THEORY

BY
FLORIN CONSTANTINESCU, MIRUNA NIŢESCU
and ANIŞOARA GEORGESCU

1. Introduction

The computation of the steady state of a nonlinear circuit by the "brute-force" method (the integration of circuit equations until all transients decay) is often too expensive [1],[2]. There are three classes of efficient methods to overcome this difficulty: shooting methods, finite difference methods and harmonic balance methods. The most efficient ones are the shooting methods.

The most known shooting method is the shooting with N e w t o n–R a p h s o n. In this method the circuit equations are integrated over a period, and before starting the next period, the final state is corrected with the N e w t o n–R a p h s o n formula. This correction speeds up the reaching of the steady state.

In this paper we propose a shooting method of the N e w t o n–R a p h s o n type which uses new models for the nonlinear circuit elements. These models have some properties that speed up the computation required for circuit equation integration. The computations are performed using the discrete circuit model; this model is a nonlinear resistive circuit which is solved by the method described in [3].

The elements of the discrete circuit model are presented in the section **2** and the solving of this circuit is described in the section **3**. Section **4** presents the shooting procedure including a computation method for the Jacobian in the N e w t o n–R a p h s o n formula.

This first part of the paper will be followed by the second one dealing with the implementation of the method.

2. The Elements of the Discrete Circuit Model

We consider a dynamic circuit containing nonlinear elements (voltage-controlled two-terminal resistors, voltage-controlled current sources, voltage-controlled capacitors) and independent current sources. The building of the discrete circuit model as well as the method of steady-state computation can be easily extended to a larger class of circuits.

As it is well known [1], the transient analysis of a nonlinear dynamic circuit

can be done by solving a nonlinear resistive circuit (the discrete circuit model) for each time step. In the following we shall develop resistive circuit models suitable to an iterative method proposed in [3].

Choosing as unknows the voltages u_k of the capacitors, resistors and current sources the circuit equations are:

$$\sum_{k\in N} \hat{q}_k(u_k) + \sum_{k\in N} \hat{i}_k(u_k) = \sum_{k\in N} j_k(t), \quad \text{for a node } N, \tag{1}$$

$$\sum_{k\in L} u_k = 0, \quad \text{for a loop } L, \tag{2}$$

where $q_k = \hat{q}_k(u_k)$ are the characteristics of the capacitors, $i_k = \hat{i}_k(u_k)$ are the characteristics of the resistors and of the controlled sources and $j_k(t)$ – the currents of the independent sources. Considering that the time step h is constant we denote by u_k the voltages at $t = mh$ and by $\overline{u}_k$ the voltages at $t = (m-1)h$. Using the backward E u l e r method, the equations (1) for $t = mh$ become:

$$\sum_{k\in N} \frac{1}{h}[\hat{q}(u_k) - \hat{q}(\overline{u}_k)] + \sum_{k\in N} \hat{i}_k(u_k) = \sum_{k\in N} j_k(t_m). \tag{3}$$

The equations (3) and (2) describe the nonlinear resistive discrete circuit model of the dynamic circuit.

The basic idea in [3] is to replace a nonlinear resistor by a linear one and a nonlinear controlled source. For example, a voltage-controlled resistor having the characteristic $i_k = \hat{i}_k(u_k)$ is replaced by a linear resistor with resistance R and a voltage-controlled current source (Fig.1).

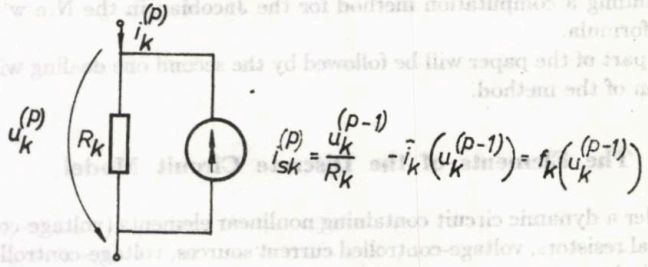

Fig. 1

The iterative procedure used in [3] for solving the nonlinear resistive circuit is to consider at the first iteration the sources $i_{sk}^{(1)}$ null, to solve the linear circuit

(having resistors with resistances R_k) computing $u_k^{(1)}$, to compute $i_{sk}^{(2)} = f_k(u_k^{(1)})$, to solve the linear circuit with sources $i_{sk}^{(2)}$ computing $u_k^{(2)}$ and so on, i.e.:

$$(4) \qquad i_{sk}^{(1)} = 0 \to u_k^{(1)} \to i_{sk}^{(2)} \to \cdots \to u_k^{(p)} \to i_{sk}^{(p)} \to \cdots$$

The nonlinear voltage-controlled current source in Fig.2 *a* is replaced by a linear voltage-controlled current source and a current source depending on the voltage in the previous iteration (Fig.2 *b*).

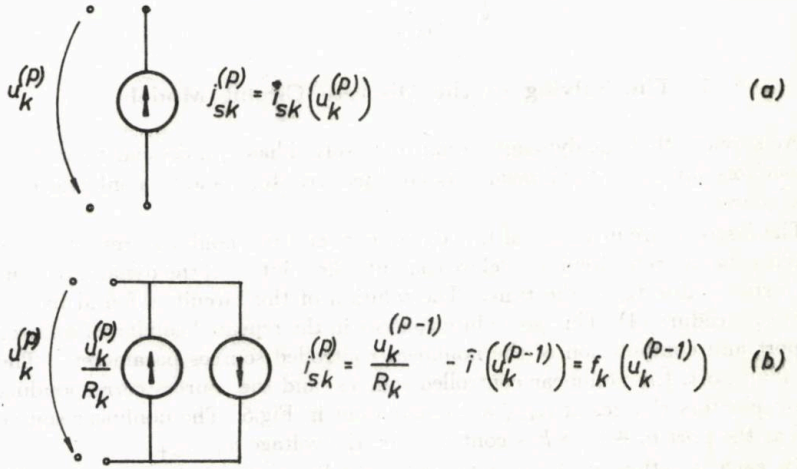

Fig. 2

A linear capacitor with the equation $i_k = C_k(u_k - \overline{u}_k)/h$ is replaced by the circuit in Fig.3 containing a linear resistor with resistance h/C_k and a current source controlled by the capacitor voltage in the previous time step $\overline{u}_k$.

The constitutive relation of a nonlinear voltage-controlled capacitor $q_k = \hat{q}_k(u_k)$ is written as $u_k = q_k/C_k + s_k(u_k)$, where C_k is a constant and $s_k = u_k - \hat{q}_k(u_k)/C_k$. Taking into account the equation $i_k = [\hat{q}_k(u_k) - \hat{q}_k(\overline{u}_k)]/h$, it follows:

$$(5) \quad i_k^{(p)} = \frac{1}{h}\left[C_k u_k^{(p)} - C_k u_k^{(p-1)} + \hat{q}_k(u_k^{(p-1)})\right] - \frac{\hat{q}_k(\overline{u}_k)}{h}.$$

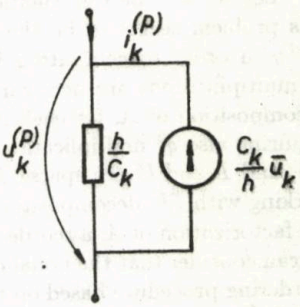

Fig. 3

The equation (5) leads to the circuit in Fig.4 – the discrete circuit model of a nonlinear voltage-controlled capacitor.

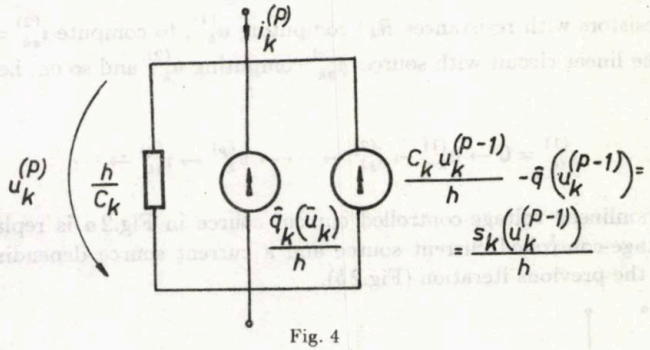

Fig. 4

3. The Solving of the Discrete Circuit Model

We suppose that the dynamic circuit to be solved has n_i independent sources, n_c capacitors (linear and nonlinear), n_r nonlinear resistors, and n_s nonlinear controlled sources.

The discrete circuit model of this dynamic circuit is a nonlinear resistive one; by solving the discrete circuit model we compute the solution of the dynamic circuit for a certain value t_m of the time. The solution of this circuit is found by the iterative procedure (4). This procedure consists in the repeated solving of a linear multiport and computation of the nonlinear controlled sources parameters. The linear multiport, the nonlinear controlled sources, and the sources corresponding to the capacitors charges at t_{m-1} are pointed out in Fig.5. The nonlinear source placed at the port $n_c + n_r + k$ is controlled by the voltage $u_{n_c+n_r+k}$.

For each iteration in (4) we must solve the linear circuit in Fig.5 and this solving is repeated many times for each value of the time t_m. If the time step h is constant the linear circuit is the same for all iterations in (4) and for any t_m.

Let $Ax = y$ be the equation of the linear circuit. The simplest way to solve this problem seems to be the computation of A^{-1} followed by a multiplication $A^{-1}y$ in order to compute x in each iteration in (4). If A is a $q \times q$ matrix, q^2 multiplications are necessary for each iteration. If we perfom firstly the LU decomposition of A, for each iteration we need to do only the back substitution requiring also q^2 multiplications [1]. Taking into account that A is sparse, A^{-1} is full, and L and U are sparse, it is clear that a shorter running time is obtained working with LU decomposition. In order to obtain a minimum number of fills in the factorization of A, a reordering procedure [1] is used. Taking into account that we can consider that the nodal circuit matrix A is structurally symmetric, a simple reordering procedure based on the properties of the circuit graph [1] may be used.

In [3] the convergence of the iterative procedure (4) is proved for a resistive circuit having nonlinear resistors and nonlinear controlled sources with Lipschitzian characteristics. If the characteristics of the nonlinear resistors, nonlinear controlled sources and nonlinear capacitors of the dynamic circuit are Lipschitzian, it follows

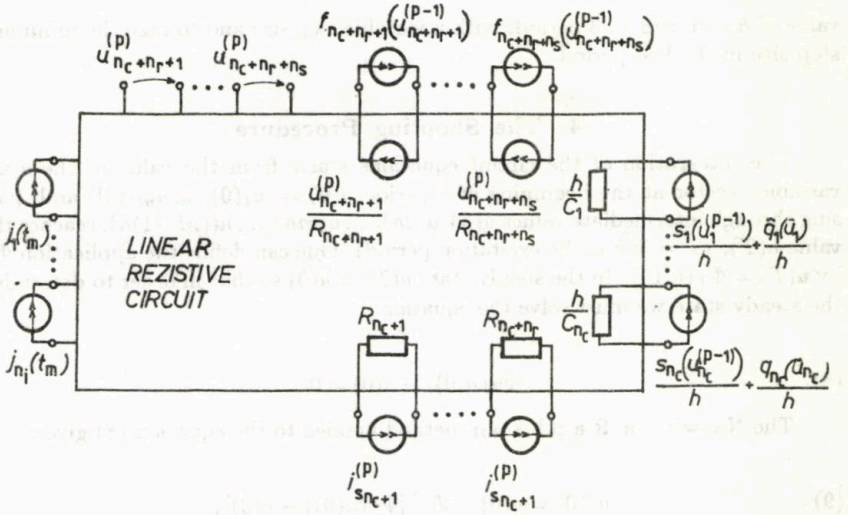

Fig. 5

that the characteristics of the nonlinear resistive circuit model elements satisfy the conditions of convergence of (4).

As it is pointed out in [3] we can choose the value of R_k and C_k to obtain the fastest convergence of (4). If the slopes of the nonlinear characteristics are bounded by

$$G_{k-} = \min \frac{\partial \hat{i}_k(u_k)}{\partial u_k}, \quad G_{k+} = \max \frac{\partial \hat{i}_k(u_k)}{\partial u_k}, \quad C_{k-} = \min \frac{\partial \hat{q}_k(u_k)}{\partial u_k}, \quad C_{k+} = \max \frac{\partial \hat{q}_k(u_k)}{\partial u_k},$$

the optimal values for R_k and C_k are:

$$R_k = \frac{2}{G_{k-} + G_{k+}}, \qquad C_k = \frac{C_{k-} + C_{k+}}{2}. \tag{6}$$

According to [3] the iteration are stopped in the p-th step if the following relation:

$$\sum_{k=1}^{n_c} \frac{C_k}{h^3} \left[s_k(u_k^{(p)}) - s_k(u_k^{(p-1)}) \right]^2 + \sum_{k=n_c+1}^{n_c+n_r+n_s} \frac{1}{R_k} \left(i_{sk}^{(p)} - i_{sk}^{(p-1)} \right)^2 < \varepsilon \tag{7}$$

is fulfilled, where ε is an imposed global absolute error.

The magnitude of the maximum constant time step h which ensures the convergence of the circuit equations integration depends on the circuit element nonlinearities and the excitation waveforms. A simple procedure for establishing the

value of h is to run 2...3 periods with a variable step size and to take the minimum step size in the last period.

4. The Shooting Procedure

The integration of the circuit equations starts from the value of the state variables vector at the beginning of a period $u(0) = [u_1(0), ..., u_{nc}(0)]^t$ and, passing through intermediate values $u(h), u(2h), ..., u(mh), ..., u((M-1)h)$, reaches the value $u(T)$, ($T = Mh$ is the excitation period). One can define the application Φ_T by $u(T) = \Phi_T(u(0))$. In the steady state $u(T) = u(0)$ so that in order to determine the steady state we must solve the equation:

$$\Phi_T(u(0)) - u(0) = 0. \tag{8}$$

The N e w t o n–R a p h s o n method applied to the equation (8) gives:

$$u^*(0) = u(0) - J^{-1}\left[\Phi_T(u(0)) - u(0)\right], \tag{9}$$

where $u^*(0)$ is the corrected value of $u(0)$, J is the $n_c \times n_c$ matrix:

$$J = \begin{bmatrix} \frac{\partial u_1(T)}{\partial u_1(0)} & \cdots & \frac{\partial u_1(T)}{\partial u_{n_c}(0)} \\ \vdots & & \vdots \\ \frac{\partial u_{n_c}(T)}{\partial u_1(0)} & \cdots & \frac{\partial u_{n_c}(T)}{\partial u_{n_c}(0)} \end{bmatrix} - 1_{n_c} = \frac{\mathrm{d}u(t_0+T)}{\mathrm{d}u(t_0)} - 1_{n_c};$$

u_k is the k-th component of the state variable vector and 1_{n_c} is the unity matrix. The matrix $\mathrm{d}u(T)/\mathrm{d}u(0)$ may be computed as follows [2]:

$$\frac{\mathrm{d}u(T)}{\mathrm{d}u(0)} = \frac{\mathrm{d}u(h)}{\mathrm{d}u(0)} \cdot \frac{\mathrm{d}u(2h)}{\mathrm{d}u(h)} \cdots \frac{\mathrm{d}u(Mh)}{\mathrm{d}u((M-1)h)}. \tag{10}$$

The computation of $\mathrm{d}u(Mh)/\mathrm{d}u((M-1)h)$ may be effectuated using the small signal equivalent circuit of the discrete circuit model around the operating point corresponding to t_m (Fig.6).

The parameters in the Fig.6 have the following values:

$$\begin{aligned} &C_1 = \frac{1}{h} \cdot \frac{\partial \hat{q}_1}{\partial u_1}\bigg|_{t_m}, ..., C_{n_c} = \frac{1}{h} \cdot \frac{\partial \hat{q}_{n_c}}{\partial u_{n_c}}\bigg|_{t_m}; \\ &G_{n_c+1} = \frac{1}{h} \cdot \frac{\partial \hat{i}_{n_c+1}}{\partial u_{n_c+1}}\bigg|_{t_m}, ..., G_{n_c+n_r} = \frac{1}{h} \cdot \frac{\partial \hat{i}_{n_c+n_r}}{\partial u_{n_c+n_r}}; \\ &G_{n_c+n_r+1} = \frac{\partial \hat{i}_{n_c+1}}{\partial u_{n_c+n_r+1}}\bigg|_{t_m}, ..., G_{n_c+n_r+n_s} = \frac{\partial \hat{i}_{n_c+n_r+n_s}}{\partial u_{n_c+n_r+n_s}}. \end{aligned} \tag{11}$$

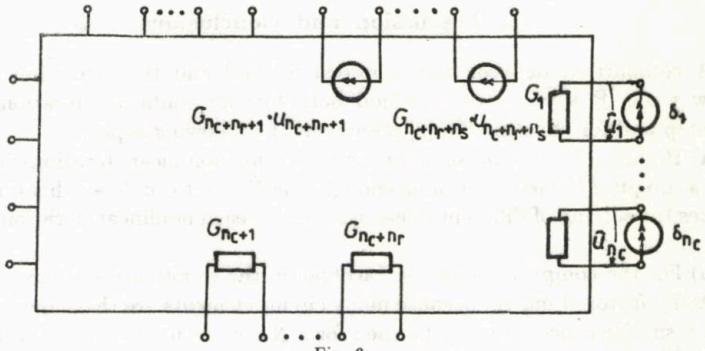

Fig. 6

This circuit may be obtained from the one in Fig.5 by removing the independent sources and by replacing the linear resistors attached to the other current ports by the small signal equivalent resistors and controlled sources having the parameters given in (11).

Solving this circuit for $\delta_1 = 1$ and $\delta_k = 0$, $k \neq 1$, we obtain the voltages $\hat{u}_1,\ \hat{u}_2, ..., \hat{u}_{n_c}$ where $\hat{u}_k = \mathrm{d}u_k(t_m)/\mathrm{d}\delta_1$, $(k = 1, ..., n_c)$. It follows:

$$\frac{\mathrm{d}u_k(t_m)}{\mathrm{d}u_1(t_{m-1})} = \frac{\mathrm{d}u_k(t_m)}{\mathrm{d}\delta_1} \cdot \frac{\mathrm{d}\delta_1}{\mathrm{d}u_1(t_{m-1})} = \hat{u}_1 \frac{1}{h} \cdot \frac{\mathrm{d}\hat{q}_1(u_1(t_{m-1}))}{\mathrm{d}u_1(t_{m-1})}. \tag{12}$$

The computation of $\mathrm{d}u_k(t_m)/\mathrm{d}u_j(t_{m-1})$ is performed similarly by solving the circuit with $\delta_j = 1$. By this way, after finishing the integration procedure for a period T, the matrix J is computed and the corrected value of the state variables $u^*(0)$ is given by (9). The integration procedure for the following period starts from $u^*(0)$. If the values $u(0)$ and $u(T)$ satisfy the relation

$$\left| \sum_{k=1}^{n_c} u_k^2(0) - \sum_{k=1}^{n_c} u_k^2(T) \right| < \varepsilon_T^2,$$

where ε_T is an imposed error, we consider that the steady state is reached and the integration procedure is finished.

The computation of $\mathrm{d}u(t_m)/\mathrm{d}u(t_{m-1})$ is performed using LU factorization of the small signal equivalent circuit matrix. Taking into account that the conductances given by (11) are changing often each time step, the reordering procedure is modified so that the nodes adjacent to the corresponding resistors are among the last. By this way a partial LU factorization may be performed only once.

5. Discussion and Conclusions

A comparison between the proposed method and the algorithm using the N e w t o n–R a p h s o n method both for the nonlinear iterations in each time step and for shooting [1], [2] points out the following aspects:

a) Because we use the same linear circuit for nonlinear iterations in all time steps a unique *LU* factorization is enough; the N e w t o n–R a p h s o n method requires the solving of different linear systems for each nonlinear iteration in a time step.

b) For the computation of the Jacobian in the shooting procedure (9) we use a partially factored matrix because many circuit elements are the same for all time steps; a similar procedure may be used for a N e w t o n–R a p h s o n method.

c) The convergence of the iterative method [3] used by us is linear and the convergence of the N e w t o n–R a p h s o n method is quadratic.

Taking into account all these features we appreciate that the two methods are competitive. A method of the harmonic balances type using a similar manner to deal with nonlinear circuit elements was published in [4]; in this paper the nonlinear iterative procedure (4) and the conditions for its convergence are not very clear.

Received, January 6, 1994 *University "Polytechnica", Bucharest*

REFERENCES

1. C h u a L.O., L i n P.M., *Computer-aided Analysis of Electronic Circuits.* Prentice Hall, 1975.
2. K u n d e r t K.S., S a n g i o v a n n i–V i n c e n t e l l i, S u g a w a r a T., *Techniques for Finding the Periodic Steady-state Response of Circuits.* In *Analog Methods for Computer Aided Circuit Analysis and Diagnosis*, edited by T. O z a w a, Marcel Dekker Inc., New York, Basel, 1988, 169-203.
3. H ă n ţ i l ă F., *A Method for Solving Nonlinear Resistive Networks.* Rev. Roum. Sc. Techn., s. Electrotechn. et Energ., **24**, *2*, 217-226 (1979).
4. F r e y D.R., N o r m a n O., *An Integral Equation Approach to the Periodic Steady-state Problem in Nonlinear Circuits.* IEEE Trans. on Circuits and Systems, **CAS-39**, *9*, 744-755 (1992).

O METODĂ ITERATIVĂ RAPIDĂ PENTRU ANALIZA CIRCUITELOR NELINIARE ÎN REGIM PERMANENT

(Rezumat)

Se utilizează noi modele ale elementelor circuitelor neliniare cu scopul de a accelera procedeul de analiză. Este utilizat în acest scop un circuit liniar, drept model al celui neliniar analizat, pentru toate iteraţiile neliniare şi în toate treptele de timp.

BULETINUL INSTITUTULUI POLITEHNIC DIN IAŞI
Tomul XLI (XLV), Fasc. 1–2, 1995
Secţia III
ELECTROTEHNICĂ. ENERGETICĂ. ELECTRONICĂ

C.D. 621.392.5

QUELQUES OBSERVATIONS CONCERNANT LES CONDITIONS DE SYMÉTRIE D'UN BIPORTE GÉNÉRALISÉ LINÉAIRE, NONAUTONOME, EN RÉGIME PERMANENT HARMONIQUE

PAR
HUGO ROSMAN

1. Le problème de la détermination des conditions de symétrie d'un biporte généralisé linéaire nonautonome (BGLN), en régime permanent harmonique, a donné naissance à de nombreuses discussions dans la littérature de spécialité. Ainsi, S i g o r s k y, dans une monographie fondamentale dédiée à l'étude de tels biportes [1], a introduit la notion de symétrie d'un BGLN par rapport à certains axes, qu'on a denommée dans Note precédente [2] *symétrie axiale*. Dans la même Note, citée ci-dessus, on a défini encore la *symétrie ordinaire* et dans une autre Note [3], la *symétrie totale* d'un BGLN.

Dans ce qui suit on poursuit à déterminer les conditions qui assurent la réalisation d'un autre type de symétrie d'un BGLN qu'on va la denommer *partielle*. Tels biportes sont rencontrés assez souvent en divers cas pratiques. Un esquisse de ce problème a été donné dans la Note précédente [2] sans y déterminer, d'une façon explicite, les conditions qui assurent la réalisation d'un tel type de symétrie.

2. On considère le BGLN représenté dans la Fig.1 *a* dont les équations sont de la forme:

$$(1) \qquad \begin{bmatrix} \underline{U}_1 \\ \underline{I}_1 \\ \underline{U}_3 \end{bmatrix} = \begin{bmatrix} \underline{A}_{11} & \underline{A}_{12} & \underline{A}_{13} \\ \underline{A}_{21} & \underline{A}_{22} & \underline{A}_{23} \\ \underline{A}_{31} & \underline{A}_{32} & \underline{A}_{33} \end{bmatrix} \begin{bmatrix} \underline{U}_2 \\ \underline{I}_2 \\ \underline{I}_3 \end{bmatrix},$$

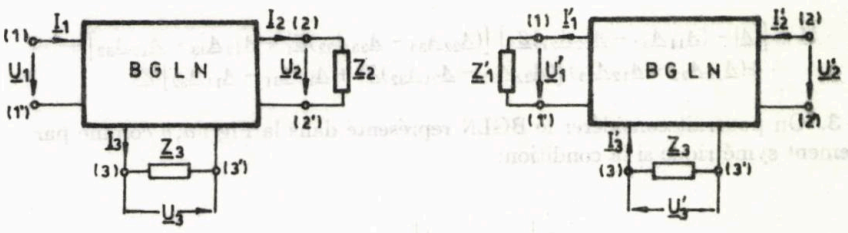

Fig. 1

et soient

(2)
$$\begin{bmatrix} \underline{U}'_2 \\ \underline{I}'_2 \\ \underline{I}'_3 \end{bmatrix} = \frac{1}{|\underline{A}|} \begin{bmatrix} \underline{A}_{22}\underline{A}_{33} - \underline{A}_{23}\underline{A}_{32} & \underline{A}_{12}\underline{A}_{33} - \underline{A}_{13}\underline{A}_{32} & \underline{A}_{13}\underline{A}_{22} - \underline{A}_{12}\underline{A}_{23} \\ \underline{A}_{21}\underline{A}_{33} - \underline{A}_{23}\underline{A}_{31} & \underline{A}_{11}\underline{A}_{33} - \underline{A}_{13}\underline{A}_{31} & \underline{A}_{13}\underline{A}_{21} - \underline{A}_{11}\underline{A}_{23} \\ \underline{A}_{22}\underline{A}_{31} - \underline{A}_{21}\underline{A}_{32} & \underline{A}_{12}\underline{A}_{31} - \underline{A}_{11}\underline{A}_{32} & \underline{A}_{11}\underline{A}_{22} - \underline{A}_{12}\underline{A}_{21} \end{bmatrix} \begin{bmatrix} \underline{U}'_1 \\ \underline{I}'_1 \\ \underline{U}'_3 \end{bmatrix}$$

les équations du même biporte renversé (Fig.1 *b*) avec:

(3) $$|\underline{A}| = \det |\underline{A}_{ij}|, \quad (i,j = 1,2,3).$$

Si on introduit les notations:

(4) $$\frac{\underline{U}_2}{\underline{I}_2} = \underline{Z}_2, \qquad \frac{\underline{U}'_1}{\underline{I}'_1} = \underline{Z}'_1, \qquad \frac{\underline{U}_3}{\underline{I}_3} = \frac{\underline{U}'_3}{\underline{I}'_3} = \underline{Z}_3,$$

les équation (1) permetteront à déterminer le courant $\underline{I}_3$ en fonction de la tension $\underline{U}_1$, des impédances $\underline{Z}_2$, $\underline{Z}_3$ et des paramètres $\underline{A}_{i,j}$, $(i,j = 1,2,3)$, du biporte à savoir:

(5) $$\underline{I}_3 = \frac{(\underline{A}_{31}\underline{Z}_2 + \underline{A}_{32})\underline{U}_1}{(\underline{A}_{11}\underline{Z}_2 + \underline{A}_{12})\underline{Z}_3 - (\underline{A}_{11}\underline{A}_{33} - \underline{A}_{13}\underline{A}_{31})\underline{Z}_2 - \underline{A}_{12}\underline{A}_{33} + \underline{A}_{13}\underline{A}_{32}}.$$

Toutefois, à l'aide des équations (2) il est possible à obtenir le courant $\underline{I}_3$ en fonction de la tension $\underline{U}'_2$, les impédances $\underline{Z}'_1$, $\underline{Z}'_3$ et les paramètres $\underline{A}_{ij}$, $(i,j = 1,2,3)$:

(6) $$\underline{I}'_3 = \frac{|\underline{A}|\left[(\underline{A}_{22}\underline{A}_{31} - \underline{A}_{21}\underline{A}_{32})\underline{Z}'_1 + \underline{A}_{12}\underline{A}_{31} - \underline{A}_{11}\underline{A}_{32}\right]\underline{U}'_2}{\underline{M}},$$

où on a utilisé la notation:

(7) $$\begin{aligned} \underline{M} = &\left[|\underline{A}| - (\underline{A}_{11}\underline{A}_{22} - \underline{A}_{12}\underline{A}_{21})\underline{Z}_3\right]\left[(\underline{A}_{22}\underline{A}_{33} - \underline{A}_{23}\underline{A}_{32})\underline{Z}'_1 + \underline{A}_{12}\underline{A}_{33} - \underline{A}_{13}\underline{A}_{32}\right] + \\ &+(\underline{A}_{13}\underline{A}_{22} - \underline{A}_{12}\underline{A}_{23})\left[(\underline{A}_{22}\underline{A}_{31} - \underline{A}_{21}\underline{A}_{32})\underline{Z}'_1 + \underline{A}_{12}\underline{A}_{31} - \underline{A}_{11}\underline{A}_{32}\right]\underline{Z}_3. \end{aligned}$$

3. On pourrait considérer le BGLN représenté dans la Fig.1 *a*, *b* comme partiellement symétrique si la condition:

(8) $$\underline{I}_3\Big|_{\underline{U}_1 = \underline{E}} = \underline{I}'_3\Big|_{\underline{U}'_2 = \underline{E}}$$

sera satisfaite lorsque

$$\underline{Z}_2 = \underline{Z}_1'. \tag{9}$$

Compte tenu de (5) et (6) la condition (8) conduit à l'identité:

$$\underline{\alpha}\,\underline{Z}_2^2\underline{Z}_3 + \underline{\beta}\underline{Z}_2\underline{Z}_3 + \underline{\gamma}\underline{Z}_2^2 + \underline{\delta}\,\underline{Z}_2 + \underline{\varepsilon}\,\underline{Z}_3 + \underline{\varphi} \equiv 0, \tag{10}$$

qui doit être satisfaite pour n'importe quelles valeurs des impédances $\underline{Z}_2$, $\underline{Z}_3$, où:

$$\begin{aligned}
\underline{\alpha} &= -|\underline{A}|\left[\underline{A}_{22}\underline{A}_{31} + \underline{A}_{11}(\underline{A}_{22}\underline{A}_{31} - \underline{A}_{21}\underline{A}_{32})\right],\\
\underline{\beta} &= -|\underline{A}|\left[\underline{A}_{12}(\underline{A}_{22}\underline{A}_{31} - \underline{A}_{21}\underline{A}_{32}) - \underline{A}_{11}(\underline{A}_{11}\underline{A}_{32} - \underline{A}_{12}\underline{A}_{31}) + \underline{A}_{12}\underline{A}_{31} + \underline{A}_{22}\underline{A}_{32}\right],\\
\underline{\gamma} &= |\underline{A}|\left[\underline{A}_{31}(\underline{A}_{22}\underline{A}_{33} - \underline{A}_{23}\underline{A}_{32}) + (\underline{A}_{22}\underline{A}_{31} - \underline{A}_{21}\underline{A}_{32})(\underline{A}_{11}\underline{A}_{33} - \underline{A}_{23}\underline{A}_{31})\right],\\
\underline{\delta} &= |\underline{A}|\left[\underline{A}_{31}(\underline{A}_{12}\underline{A}_{33} - \underline{A}_{13}\underline{A}_{32}) + \underline{A}_{32}(\underline{A}_{22}\underline{A}_{33} - \underline{A}_{23}\underline{A}_{32}) + (\underline{A}_{22}\underline{A}_{31} - \underline{A}_{21}\underline{A}_{32}) \times\right.\\
&\qquad \left.\times(\underline{A}_{12}\underline{A}_{33} - \underline{A}_{13}\underline{A}_{32}) + (\underline{A}_{12}\underline{A}_{31} - \underline{A}_{11}\underline{A}_{32})(\underline{A}_{11}\underline{A}_{33} - \underline{A}_{13}\underline{A}_{31})\right],\\
\underline{\varepsilon} &= -|\underline{A}|\underline{A}_{12}(\underline{A}_{32} + \underline{A}_{12}\underline{A}_{31} - \underline{A}_{11}\underline{A}_{32}),\\
\underline{\varphi} &= |\underline{A}|(\underline{A}_{12}\underline{A}_{33} - \underline{A}_{13}\underline{A}_{32})(\underline{A}_{32} + \underline{A}_{12}\underline{A}_{31} - \underline{A}_{11}\underline{A}_{32}).
\end{aligned} \tag{11}$$

Afin que l'identité (10) soit satisfaite il est nécessaire et suffisant que:

$$\underline{\alpha} = 0,\quad \underline{\beta} = 0,\quad \underline{\gamma} = 0,\quad \underline{\delta} = 0,\quad \underline{\varepsilon} = 0,\quad \underline{\varphi} = 0. \tag{12}$$

Compte tenu que, par des raisons évidentes, $\underline{A}_{11} \neq 0$, $|\underline{A}| \neq 0$, la condition $\underline{\alpha} = 0$ conduit à:

$$\underline{A}_{12}\underline{A}_{32} - \underline{A}_{22}\underline{A}_{31} = \frac{\underline{A}_{22}\underline{A}_{31}}{\underline{A}_{11}}. \tag{13}$$

Si l'on examine les expressions de $\underline{\varepsilon}$ et $\underline{\varphi}$ on constatera aisément que celles-ci s'annulent lorsque

$$\underline{A}_{11}\underline{A}_{32} - \underline{A}_{12}\underline{A}_{31} = \underline{A}_{32}. \tag{14}$$

Dans les conditions où on tient compte de (13) et (14) les expressions de $\underline{\beta}$, $\underline{\gamma}$ et $\underline{\delta}$ deviennent:

$$\begin{aligned}
\underline{\beta} &= -\frac{|\underline{A}|}{\underline{A}_{11}}(\underline{A}_{11} - \underline{A}_{22})(\underline{A}_{12}\underline{A}_{31} - \underline{A}_{32}),\\
\underline{\gamma} &= |\underline{A}|\frac{\underline{A}_{31}}{\underline{A}_{11}}(\underline{A}_{13}\underline{A}_{22}\underline{A}_{31} - \underline{A}_{11}\underline{A}_{23}\underline{A}_{32}),\\
\underline{\delta} &= \frac{|\underline{A}|}{\underline{A}_{11}}\left[\underline{A}_{33}(\underline{A}_{11} - \underline{A}_{22})(\underline{A}_{12}\underline{A}_{31} - \underline{A}_{11}\underline{A}_{33}) - \underline{A}_{32}(\underline{A}_{11}\underline{A}_{23}\underline{A}_{32} - \underline{A}_{13}\underline{A}_{22}\underline{A}_{31})\right].
\end{aligned} \tag{15}$$

Vu que $\underline{A}_{12}\underline{A}_{31} \neq \underline{A}_{22}$ (v. la relation (14)) on peut aboutir à la conclusion que $\underline{\beta} = 0$ si

$$\underline{A}_{11} = \underline{A}_{22}. \tag{16}$$

Dans ce cas il résulte que $\underline{\gamma}$ et $\underline{\delta}$ s'annulent simultanément si, en outre

$$\underline{A}_{13}\underline{A}_{31} = \underline{A}_{23}\underline{A}_{32}. \tag{17}$$

Par conséquent *les conditions nécessaires et suffisantes afin qu'un biporte généralisé linéaire nonautonome soit partiellement symétrique sont que les paramètres fondamentaux de celui-ci satisfassent les relations (13), (14), (16), (17).*

Observations.

1. Si on tient compte de (16) la condition (13) devient

$$\underline{A}_{21}\underline{A}_{32} - \underline{A}_{22}\underline{A}_{31} = \underline{A}_{31}. \tag{13'}$$

2. Compte tenu que les conditions de symétrie partielle d'un BGLN impliquent la nécessité que les paramètres fondamentaux satisfassent quatre relations il résulte que seulement cinq de ceux-ci sont indépendants.

4. Dans une Note antérieure [2] on a prouvé que afin qu'un BGLN soit *réciproque* il est nécessaire et suffisant que ses paramètres fondamentaux satisfassent les relations:

$$\underline{A}_{11}\underline{A}_{22} - \underline{A}_{12}\underline{A}_{21} = 1, \quad |\underline{A}| = \underline{A}_{33}. \tag{18}$$

Il est facile à observer que si les paramètres fondamentaux d'un BGLN satisfont aux relations (13), (14), (16), (17), alors les relations (18) seront une *conséquence* de celles-ci. Il s'ensuit que *tout BGLN partiellement symétrique est, necessairement, réciproque.*

5. Dans la même Note [2] on a prouvé que afin qu'un BGLN ait une symétrie ordinaire, ses paramètres fondamentaux doivent satisfaire les relations (16) et (17). Dans ces conditions le biporte considéré étant en même temps et partiellement symétrique il s'ensuit que, en réalité, on réalise la symétrie *totale.* Par conséquent *tout BGLN ayant une symétrie ordinaire, qui en même temps est partiellement symétrique est, au fond, totalement symétrique.* Autrement dit si les relations (8), (9) sont satisfaites alors, nécessairement seront satisfaites et les relations:

$$\underline{U}_2' = \underline{U}_1, \quad \underline{I}_2' = \underline{I}_1, \quad \underline{U}_2' = \underline{U}_2, \quad \underline{I}_1' = \underline{I}_2. \tag{19}$$

6. En conclusion si la symétrie axiale ou celle usuelle peut être réalisée par un BGLN, soit il réciproque où nonreciproque, la symétrie partielle (donc et celle générale) ne peut être réalisée que par un BGLN réciproque.

Reçue le 1 décembre 1993

Université Technique „Gh. Asachi", Jassy,
Chaire d'Électrotechnique

BIBLIOGRAPHIE

1. S i g o r s k y V.P., *Obshčaya teoria četyrekhpoliusnikov.* Izd. Akad. Nauk Ukr. SSR, Kiev, 1955.
2. R o s m a n H., *Sur les conditions de réciprocité et de symétrie d'un biporte nonautonome généralisé en régime permanent harmonique.* Bul. Inst. polit., Iaşi, **XL (XLIV)**, *1-4*, s.III, 23-30 (1994).
3. R o s m a n H., *Über die Symmetriebedingungen eines allgemeinen nichtautonomen Vierpole in harmonischen Dauerbetrieb.* Beiträge zur theoretischen Elektrotechnik, *1*, 78-89 (1988).

CÂTEVA OBSERVAŢII REFERITOARE LA CONDIŢIILE DE SIMETRIE ALE UNUI BIPORT GENERALIZAT LINIAR, NEAUTONOM, ÎN REGIM PERMANENT ARMONIC

(Rezumat)

Se stabilesc condiţiile necesare şi suficiente pentru ca un biport generalizat liniar, neautonom, în regim permanent armonic, să fie parţial simetric. Simetria parţială a unui astfel de biport este caracterizată prin condiţiile (8), (9), implicând necesitatea ca parametrii fundamentali $\underline{A}_{ij}$, $(i, j = 1, 2, 3)$, să satisfacă relaţiile (13), (14), (16), (17).

BULETINUL INSTITUTULUI POLITEHNIC DIN IAŞI
Tomul XLI (XLV), Fasc. 1–2, 1995
Secţia III
ELECTROTEHNICĂ. ENERGETICĂ. ELECTRONICĂ

D.C. 621.319.7; 517.9

REMARKS ON THE NUMERICAL METHODS ERRORS IN ELECTROMAGNETIC FIELD ANALYSIS

BY
TUDOR MOROŞAN

1. Introduction

Electromagnetic field analysis is often possible only by use of numerical methods. With this purpose the variational and integral methods have been theoretically developed during past years namely: the finite element method and the boundary element method [1], [2]. The evaluation of result error is necessary in all these cases. Various formulae which rely on the relative and absolute errors have been used, namely: relative energy error [1] and relative error [2], [3].

In this paper we show that relative error, in its classical formulation, causes some difficulties in the electromagnetic field analysis, and it can be replaced with other expressions that can be more easily used.

2. Disadvantages of the Relative Error Using

Let us consider a real "exact" number A and let a be an approximation of A. The difference $\Delta a = A - a$ is named *error*, and $|\Delta a| = |A - a|$ is the *absolute error* [4]. For an efficient estimation, if $A \neq 0$, one can define the *relative error* [4], [5]:

$$\delta a = \frac{|\Delta a|}{|A|}. \tag{1}$$

Some features of the relative error (1) are pointed out here:

i) If a is an approximation of A, than $\delta a = 0$ if and only if $a = A$. The *proof* is self-evident.

ii) If a and b are two approximations of a, and if $|a - A| > |b - A|$, then

$$\delta a > \delta b.$$

The *proof* is also self-evident.

iii) For any positive real number M and any $\varepsilon > 0$, there exist $\beta > 0$ so that for any real number A with $|A| < \varepsilon \bigwedge |a| > \beta$ the inequality

$$\delta a > M$$

is valid.

P r o o f. If $a > A$ and $A > 0$, we have from (1) $\delta a = a/A - 1$. Let $M > 0$ and $\varepsilon > 0$; then from $\delta a > M$ we obtain $a/A - 1 > M$, hence $a > A(1+M) > \varepsilon(1+M)$.

If β is chosen so that $\beta > \varepsilon(1+M)$ then $\alpha > \beta$ and iii) is satisfied.

For $\alpha < A$ and $A < 0$ the *proof* is similar.

The i) and ii) are convenient features because they make an usable relationship between (a, A) pair and the $\mathbf{R}$ set.

The iii) feature exhibits a great disadvantage, namely, if A is a near zero value, the relative error δ is very large, and at limit, since A is a zero value, any approximation a is considered to be completely wrong because δ has infinite magnitude.

This constraint is very inconvenient in electromagnetic field analysis, where the pieces boundary connected to the zero reference potential always exist.

As an example we consider the electrostatic problem:

$$\Delta u = 0, \qquad u : [0,1] \times [0,1] \to \mathbf{R}.$$

The potential u is known on the boundary of the definition domain:

$$u(x,y) = \begin{cases} 0, & y = 0, \\ \frac{1}{3}y^3 - y, & x = 1, \\ \frac{1}{3} - x^2, & y = 1, \\ \frac{1}{3}y^3, & x = 0, \end{cases}$$

and the exact solution also is known:

$$u(x,y) = \frac{1}{3}y^3 - x^2 y.$$

The problem was numerically solved by the boundary element method [2], [7] with 16 constant elements and the boundary values of u were approximatively recalculated in order to establish the accuracy of the method.

Let a counter-clockwise parametrisation of the boundary be. The exact and approximate values of u are graphically represented in the Fig.1.

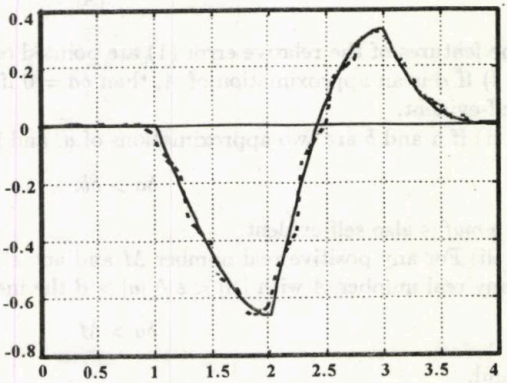

Fig. 1.– Exact (—) and approximated (...) boundary values of function u.

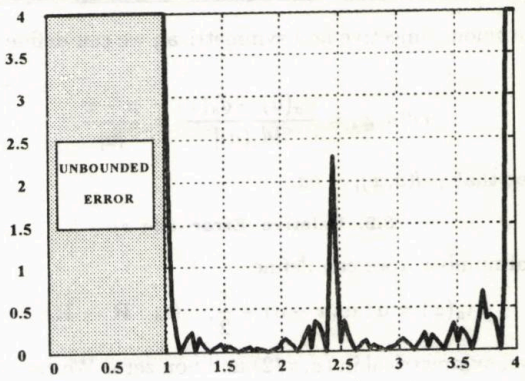

Fig. 2.– Classical relative error.

The δ relative error offers an inefficient picture of the precision, and it can't be used to make a realistic comparison between the different boundary points error, especially when the exact values are 0, because the δ error is unbounded (Fig.2).

3. A New Method to Define Relative Error

From i), ii) and iii) we propose a more general

D e f i n i t i o n. The function $e : D \subseteq R^2 \to \mathbf{R}$ is named *relativ error* of a if:

1°. $e(a,x) = 0$ if and only if $a = x$, for any $(a,x) \in D$ pair.

2°. If $x, y \in \mathbf{R}$ so that $|x-a| > |y-a|$, the inequality $|e(a,x)| > |e(a,y)|$ is valid.

The function e is named L-bounded relative error if 1°, 2° and 3° are proved, where

3°. There exist $L \in (0,\infty)$ so that for any $(a,x) \in D$ pair, the inequality $|e(a,x)| \leq L$ is valid.

The error Δa, the absolute error Δ and the relative error δ satisfy 1° and 2°.

We'll show some examples for L-bounded relative error.

If a is a real number, let $f_a : \mathbf{R} \to \mathbf{R}$ be an injective, continuous, symmetrical in $(a, f_a(a))$ function. Then,

$$e(a,x) = \frac{f_a(a) - f_a(x)}{|f_a(a)|}, \quad (e : \mathbf{R}^2 \to \mathbf{R}),$$

is a relative error in the *definition* sense, 1°and 2°being proved immediately.

If f_a is a bounded function, one can obtain an L-bounded relative error.

We'll particularise f_a to obtain some relative error functions.

3.1. Relative Error $ed(a,x)$

If a is a non-negative real number, the function

$$d_a(x) = x - 2a, \quad (d_a : \mathbf{R} \to \mathbf{R}),$$

is evidently continuous, injective and symmetrical; we can define the relative error function:

$$ed(a,x) = \frac{d_a(a) - d_a(x)}{|d_a(a)|} = \frac{a-x}{|a|}.$$

It is easily to see that $|ed(a,x)| = \delta a$.

3.2. Relative Error $et(a,x)$

For any real number a we can define

$$t_a(x) = a\tan(x-a) + \frac{\pi}{2}, \quad (t_a : \mathbf{R} \to \mathbf{R}),$$

which is injective, symmetrical in $(a, \pi/2)$ and non zero. We can define the relative error function

$$et(a,x) = \frac{t_a(a) - t_a(x)}{|t_a(a)|} = \frac{2}{\pi} a\tan(a-x),$$

that is a L-bounded relative error, with $L = 1$.

The use of the et relative error in the place of δ is advantageous because it is defined for $a = 0$ and the values of $et(a,x)$ are situated in [-1,1] interval, obtaining reasonable values for the errors.

3.3. The Normal en Relative Error

Another formulation for relative error could be obtained using the normal probabilistic distribution. This is a new and very interesting relationship between the probabilistic distributions and the relative error evaluation.

The normal probabilistic distribution, with a and σ parameters, is [6]:

$$N_a(x) = \int_{-\infty}^{x} \frac{1}{\sigma\sqrt{2\pi}} \exp\left[-\frac{(t-a)^2}{2\sigma^2}\right] \mathrm{d}t.$$

It is easy to observe that the bounded function

$$n_a(x) = N_a(x), \quad (n_a : \mathbf{R} \to (0,1)),$$

satisfies the 1°, 2°, 3° conditions.

We can so introduce the normal relative error

$$en_\sigma(a,x) = \frac{n_a(a) - n_a(x)}{|n_a(a)|} = \frac{1}{\sigma\sqrt{2\pi}} \int_x^a \exp\left[-\frac{(t-a)^2}{2\sigma^2}\right] \mathrm{d}t.$$

For different values of σ we can obtain a lot of definitions of the normal en relative error.

4. Examples

In order to show the validity of the proposed definition we'll consider again the elliptic problem, presented in §2, and we'll calculate the et and en relative error.

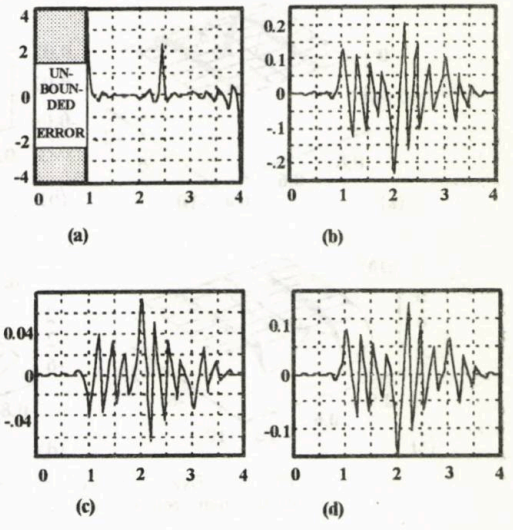

Fig. 3.– The *ed* (*a*), *et* (*b*), *en* with σ=1 (*c*) and σ=0.5 (*d*), for presented potential errors.

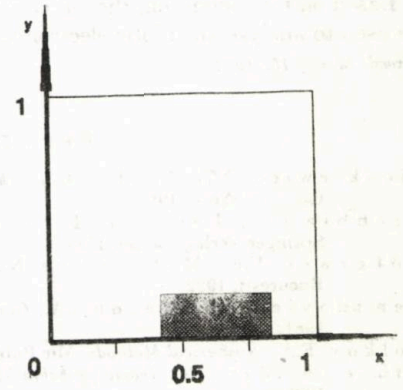

Fig. 4.– Analysed domain.

One can see that unlike the δ and *ed* relative errors, the *et* and *en* relative errors do away with the difficulties of zero exact values (Fig.3).

One can point out similar advantages in the *et* or *en* using on the domains with near zero exact values.

To exemplify this, we analysed the same electrostatic problem in the proximity of one boundary element (Fig.4) and we show in Fig.5 the exact and the approximate solutions with the δ and *et* calculated relative errors.

5. Conclusions

The relative errors which appear in the proximity of zero value boundary conditions of the electromagnetic field problems were analysed. The disadvantages of the δ classical relative error was pointed out, and a new definition for the relative error was presented.

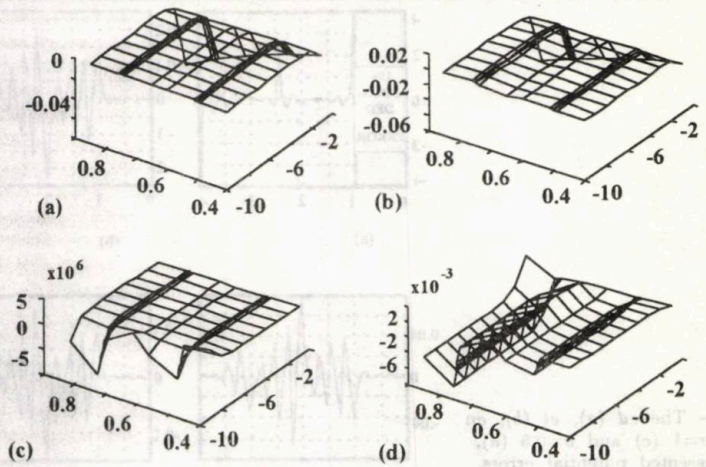

Fig. 5.– Exact (*a*) and approximated (*b*) potential, their relative *ed* (*c*) and *et* (*d*) errors.

Based on this definition, the *ed*, *et* and *en* relative error was built, and these were used to analyse an elliptic electromagnetic problem.

Received, March 15, 1994

University "Ştefan cel Mare", Suceava,
Department of Electrical Engineering

REFERENCES

1. Zienkiewicz O.C., Taylor R.L., *The Finite Element Method.* Mc Graw-Hill Book Co., New-York, 1989.
2. Brebbia C.A., Telles J.C.F., Wrobel L.C., *Boundary Element Techniques.* Springer Verlag, Berlin, 1984.
3. Poteraşu V.F., Mihalache N., *Elemente de contur. Aplicaţii.* Ed. Militară, Bucureşti, 1992.
4. Demidovich B.P., Maron I.A., *Computational Mathematics.* Mir Publ., Moscow, 1981.
5. Volkov E.A., *Numerical Methods.* Mir Publ., Moscow, 1986.
6. Mihoc Gh., Micu N., *Teoria probabilităţilor şi statistică matematică.* EDP, Bucureşti, 1980.
7. Moroşan T., *Computer-Aided Analysis of Electromagnetic Field Using Boundary Element Method.* An. Univ. "Ştefan cel Mare", Suceava, s.Elect., **I**, *1*, 46-50 (1994).

OBSERVAŢII ASUPRA ERORILOR METODELOR NUMERICE UTILIZATE ÎN STUDIUL CÂMPULUI ELECTROMAGNETIC

(Rezumat)

Se prezintă o nouă posibilitate de studiu al erorilor care apar cu ocazia rezolvării numerice a problemelor de câmp electromagnetic. Se scot în evidenţă câteva proprietăţi ale erorii relative, aşa cum este ea definită în modul clasic şi se arată că utilizarea ei este uneori neconvenabilă, chiar imposibilă: existenţa unor zone de câmp cu potenţial nul (conectate deci la referinţă) conduce la valori infinite ale erorii. Se propune o definiţie axiomatizată, construindu-se pe baza acesteia, prin particularizare, pe lângă eroarea relativă clasică şi alte erori relative în sensul definiţiei propuse.

În final se prezintă câteva exemple referitoare la rezolvarea unei probleme de câmp laplacean prin metoda elementului de frontieră, analizându-se eroarea relativă în puncte aflate în imediata apropiere a potenţialului zero.

BULETINUL INSTITUTULUI POLITEHNIC DIN IAŞI
Tomul XLI (XLV), Fasc. 1–2, 1995
Secţia III
ELECTROTEHNICĂ. ENERGETICĂ. ELECTRONICĂ

D.C. 538.551.23

TIME DOMAIN SENSITIVITY OF LINEAR CIRCUITS
THE TRANSIENT CASE STUDY

BY
RADU URSULEAN

1. Introduction

Time domain sensitivity of linear circuits is less studied mostly because of the complicated calculus and also because the significance of the sensitivities in the time domain is somehow lost since the function that gives the sensitivity has several variables (one of them being time, of course), [1].

If in the frequency domain sensitivities can be computed easily, this is not the case in the time domain. Most of the authors focused their efforts on developing techniques that use already known methods from circuit analysis in the frequency domain, adapting them to the desired purpose [1], [2]. That is why we have now well developed techniques for frequency domain calculus of the sensitivities, which, due to their simplicity, look appropriate for calculating time domain sensitivities if we are able to find a method which, by means of an operator, is qualified to transform the equations containing derivatives and integrals in algebraical ones, whenever possible. Anyway, using different transforms (Fourier, Laplace, z) to calculate time domain sensitivities is still an open problem. It is essential to find the conditions in which these methods can be used, to adjust them in order to obtain the results in an efficient manner from the already known circuit analysis and to reveal their correct significance.

From the beginning we must say that most of the authors focused to one purpose when dealing with time domain sensitivities: finding the gradients for the objective functions in optimization problems.

Of course, this is due to the development of the mathematical background of the problem. Only few authors concentrate on calculating time domain sensitivities, [1], [3]. When they do, they intend to find a better way to get the steady state of the circuit when dealing with nonlinear circuit elements, [1], and as an application to an already existing software, which analyses the circuit in the time domain when there are no initial conditions, [3]. In the first case, in spite of their compactness

and accessible form, the algorithms are memory and time consuming when used in developing software for this purpose. Also, when dealing with nonlinear circuits, we cannot talk about a global approach, one which takes advantage of the already known functions to model nonlinearities looks more efficient from the programmer's point of view not only because the time and memory costs, but, which is more important, for an improved precision.

The main advantage of this approach is the simultaneous computing of the time domain solution, the sensitivities and eventually its use in the case of nonlinear circuits. The main drawback is the rise of computing costs as the number of parameters to which the sensitivities are computed grows.

In the second case, [3], the method is highly restrictive as soon as there are not allowed initial conditions and the software package is almost unknown.

2. A Method to Compute Sensitivities of Linear Circuits in the Transient Case

The following method concerns linear circuits and the type of sensitivity used is the so called "small change sensitivity".

Taking into account the linearity of the circuit we are able to find for the functions involved the Laplace transform:

$$F(s) = \int_0^\infty f(t) \exp(-st) \mathrm{d}t. \tag{1}$$

The conditions that must be obeyed by $f(t)$ are well known, [4], [5].

The function $f(t)$ is dependent not only by time; it is also a function of the parameters of the circuit itself: resistance, inductance, capacities and all the other parameters of controlled sources which model the active devices.

To calculate the sensitivity of function f when a parameter h has a small change it is necessary to evaluate the derivative of function $f(t)$ to this parameter:

$$S_h^f = \frac{\mathrm{d}f}{\mathrm{d}h}. \tag{2}$$

The main idea of the proposed method is based on the fact that the function has a derivative no matter which parameter is of interest and so in (1) we can change the order of the operations. To put it another way, one can compute the derivative of function $f(t)$ in the complex domain and then to transfer the result in the time domain. The benefit of this fact is that we can find an exact solution and therefore we won't use numerical methods involving sometimes a considerable amount of inaccuracies.

At first sight one can consider the amount of calculus the same, no matter the domain, time or complex, taking into account the fact that the characteristic variables of the domains, t and s, appear as parameters during the calculus. However,

taking into account the fact that obtaining sensitivities in the frequency domain is an already solved problem and formally the circuits associated with the real one by applying the Laplace transform are practically the same, we can use the same methods for the sensitivities, methods based on the transposed circuit.

Let us consider a linear circuit which has independent and/or controlled current and/or voltage sources. We want to compute the sensitivity of a voltage V between two arbitrary chosen nodes when the operational admittance $Y_0(s)$ changes. We consider another circuit, having the same topology, which has its elements determined [2] by the following rules, imposed by the ease of computing the desired sensitivity: a) the admittances of the circuit remain unchanged; b) in parallel with the operational admittance $Y_0(s)$ we put a 1 A independent current source; c) the independent voltage source are replaced by short-circuits; d) the independent current sources are replaced by open circuits; e) for the controlled sources the control and the controlled ports are interchanged.

In this manner we obtain the so called "transposed circuit".

To obtain the desired sensitivity there are necessary two analyses of the initial circuit and of the transposed one. If we denote by V and V' the two values of the voltage, then the sensitivity when the operational admittance $Y_0(s)$ changes is given [2] by:

$$S_Y^V = -VV'. \tag{3}$$

To compute sensitivities in the transient case, one can follow the next algorithm: a) starting from the initial circuit and taking into account the initial conditions for inductors and capacitors, establish the operational diagram of the circuit introducing the current and/or voltage sources which model the initial conditions [4], [5]; b) analyse the circuit obtained at a) to get the voltage V; c) analyse the transposed circuit to get V'; the current and/or voltage sources that model the initial conditions will be considered independent ones; d) compute the sensitivity by means of (3); e) obtain the time function using a reverse transformation formula.

The above mentioned algorithm can also be used for computing multiparametric sensitivities.

3. Application

For the circuit represented in Fig.1 the switch is closed at $t = 0$ and the initial voltage on capacitor C_1 is U. We need to calculate the sensitivity of the voltage on capacitor C_2, for the transient case, when G_2 varies.

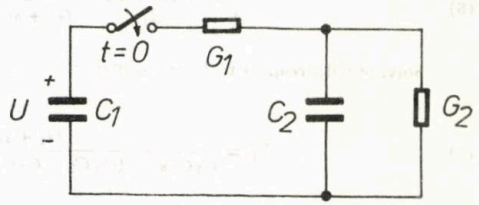

Fig. 1

The circuit obtained using operational admittances is represented in Fig.2.

To get V_1 we use the nodal analysis:

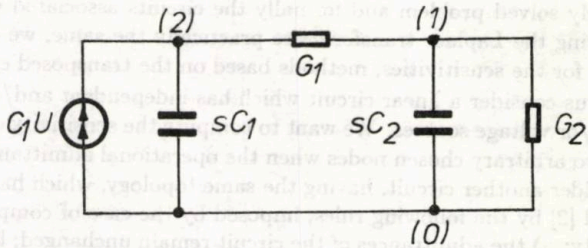

Fig. 2

(4) $$\begin{bmatrix} G_1+G_2+sC_2 & -G_1 \\ -G_1 & G_1+sC_1 \end{bmatrix} \begin{bmatrix} V_1 \\ V_2 \end{bmatrix} = \begin{bmatrix} 0 \\ C_1U \end{bmatrix}.$$

Solving with respect to V_1 we obtain:

(5) $$V_1 = \frac{G_1C_1U}{C_1C_2s^2 + (G_1C_2 + G_1C_1 + G_2C_1)s + G_1G_2}.$$

The transposed circuit is represented in Fig.3.

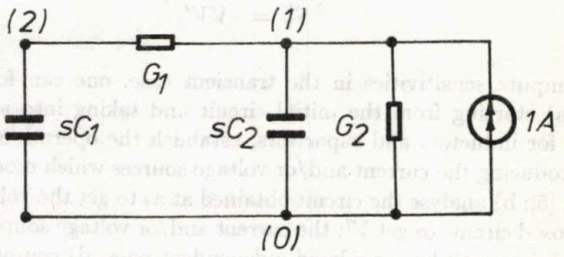

Fig. 3

The nodal equations for this circuit are:

(6) $$\begin{bmatrix} G_1+G_2+sC_2 & -G_1 \\ -G_1 & G_1+sC_1 \end{bmatrix} \begin{bmatrix} V_1' \\ V_2' \end{bmatrix} = \begin{bmatrix} 0 \\ 1 \end{bmatrix}.$$

Solving with respect to V_1' it results:

(7) $$V_1' = \frac{G_1+sC_1}{C_1C_2s^2 + (G_1C_2 + G_1C_1 + G_2C_1)s + G_1G_2}.$$

The sensitivity is:

(8) $$S_{G_2}^{V_1} = -V_1V_1' = \frac{-G_1C_1U(G_1+sC_1)}{[C_1C_2s^2 + (G_1C_2 + G_1C_1 + G_2C_1)s + G_1G_2]^2}.$$

It can be easily verified taking the derivative that this result is the same with the one obtained by direct derivation.

The time domain function for (8) can be obtained using tables or Heaviside's theorems. Noting s_1 and s_2 the double roots of the denominator of the fraction (8), we can write:

$$S_{G_2}^{V_1} = \frac{K_1}{s-s_1} + \frac{K_2}{(s-s_1)^2} + \frac{K_3}{s-s_2} + \frac{K_4}{(s-s_2)^2}, \tag{9}$$

where K_1, K_2, K_3 and K_4 are given by:

$$K_1 = \frac{G_1 U}{C_1 C_2^2} \cdot \frac{2G_1 + C_1(s_1+s_2)}{(s_1-s_2)^3}, \tag{10}$$

$$K_2 = \frac{-G_1 U}{C_1 C_2^2} \cdot \frac{G_1 + s_1 C_1}{(s_1-s_2)^2}, \tag{11}$$

$$K_3 = -K_1, \tag{12}$$

$$K_4 = \frac{-G_1 U}{C_1 C_2^2} \cdot \frac{G_1 + s_2 C_1}{(s_1-s_2)^2} \tag{13}$$

The time function that gives the sensitivity of V_1 when G_2 varies is:

$$S_{G_2}^{V_1} = K_1 e^{s_1 t} + K_2 t e^{s_1 t} + K_3 e^{s_2 t} + K_4 t e^{s_2 t}. \tag{14}$$

To compare the obtained results we used the MathCAD software to get the direct derivative. We denoted by $F(t)$ the sensitivity obtained with the proposed method and with $H(t)$ the one got by direct derivation. It can be seen that there are no differences between the two graphs and therefore there is a perfect concordance between the two methods (Fig.4). The parameters of the circuit are as follows: R_1=12 kohms, R_2=510 ohms, C_1=0.47 μF, C_2=330 μF, U=100 V. For these values the constants in (14) are: s_1=−177.566, s_2=−5.933, K_1= 2.59, K_2=0.679, K_3=2.59, K_4=−445.172.

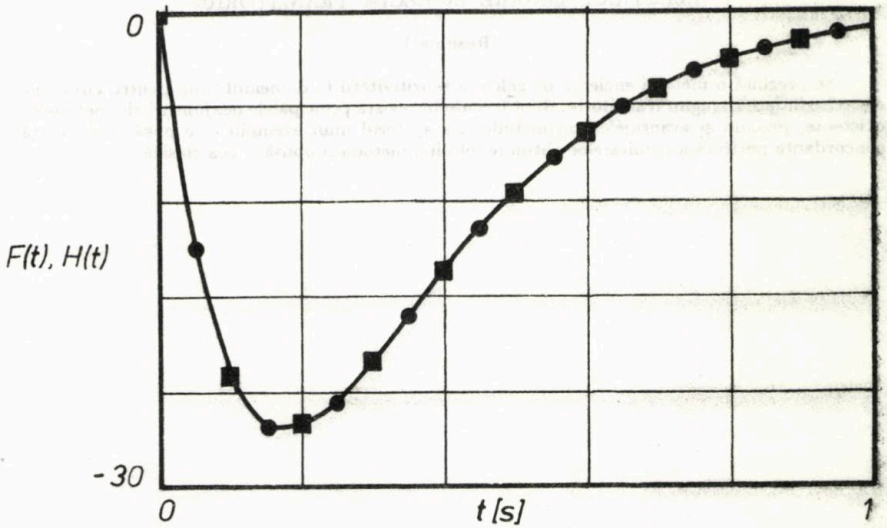

Fig. 4

4. Conclusion

The proposed method is based on an efficient algorithm that can be easily adapted for existing software; it permits the computing of the sensitivities in the transient case. Its main advantage is that using the already known results it can give the exact solution when the involved circuits are linear, while the existing methods deal with approximate solutions. The open problems that still exist in the field are concerning the multiparametric sensitivity and the large change sensitivity.

Received, March 2, 1994

Technical University "Gh.Asachi", Jassy,
Department of Electrotechnics
and Electrical Machines

REFERENCES

1. Vlach J., Singhal K., *Computer Methods for Circuit Analysis and Design.* Van Nostrand Reinhold Co., N.Y., 1983.
2. Brayton R., Spence R., *Sensitivity and Optimisation.* Elsevier Scientific Publishing Company, N.Y., 1980.
3. Chojcan J., Izydorczyk J., *Computer-Aided Time Domain Sensitivity Analysis of Linear Networks Using IZTIS Program.* Proc. of Internat. Brighton Conf. Signals & Systems, AMSE Press, Vol. **4**, 239-248, 1989.
4. Rosman H., Savin Gh., *Circuite electrice liniare.* Partea a II-a. *Analiza circuitelor liniare în regim tranzitoriu.* Inst. polit., Iaşi, 1977.
5. Timotin Al. et al., *Lecţii de bazele electrotehnicii.* Vol. **II**, E.D.P., Bucureşti, 1964.

SENZITIVITATEA ÎN DOMENIUL TIMP A CIRCUITELOR ELECTRICE LINIARE ÎN REGIM TRANZITORIU

(Rezumat)

Se prezintă o metodă eficientă de calcul a senzitivităţii în domeniul timp pentru circuitele electrice liniare în regim tranzitoriu. Sunt trecute în revistă principalele neajunsuri ale metodelor existente, precum şi avantajele noii metode. Cu ajutorul unui exemplu este pusă în evidenţă concordanţa perfectă a rezultatelor obţinute folosind metoda propusă şi cea clasică.

BULETINUL INSTITUTULUI POLITEHNIC DIN IAŞI
Tomul XLI (XLV), Fasc. 1–2, 1995
Secţia III
ELECTROTEHNICĂ. ENERGETICĂ. ELECTRONICĂ

D.C. 621.391

COMPUTATION OF POWER SPECTRAL DENSITY BASED ON COMPLEX ENVELOPE FOR BASEBAND SIGNALS

BY
PAUL COTAE

1. Introduction

In Fig.1 we present the process through which the data signal in BB $d(t, \alpha_i)$ is obtained, as well the complex envelope of modulated signal.

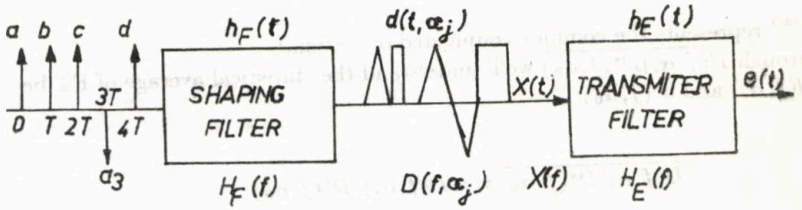

Fig. 1

The source emits random at the iT moment of time the symbol a_i with a certain probability.

The data sequence α_i is a discrete random variable one, corresponding to a particular succession of signals at input, under the form:

$$\alpha_i = ...a_{i-1}a_{i-2}...a_{-1}a_0... \tag{1}$$

In the time domain, when at the output of the shaping filter, whose answer to the Dirac impulse is $h(t)$, the data signal is obtained in BB, given by the relation:

$$d(t, \alpha_i) = \sum_i h(t - iT, a_i) = \sum_i h_i(t, a_i), \tag{2}$$

which depends on the transfer function of the shaping filter as well as on the a_i symbol transmitted on the time interval $iT \leq t < (i+1)T$.

In Fig.1 we have associated to symbols a_0, a_1, a_2, a_3 and a_4 the shaping functions 1TR, 1NRZ, 1HS, 1TR and respectively 1RZ [1], [2] having their polarity and amplitude.

The complex envelope $x(t)$ is given by the relation:

$$x(t) = A \sum_i d(t - iT, \alpha_i) \tag{3}$$

and represents a random process.

Let's have $D(f, \alpha_i)$, Fourier Transform (FT) of data signals $d(t, \alpha_i)$, corresponding to the relation:

$$D(f, \alpha_i) = F\{d(t, \alpha_i)\}. \tag{4}$$

In the same way we have the complex FT:

$$D^*(f, \alpha_0) = F\{d(t, \alpha_0)\}, \tag{5}$$

where "*" represents the complex conjugated operation.

Through $\overline{D(f, \alpha_i)D^*(f, \alpha_0)}$ we'll understand the statistical average of FT between $d(f, \alpha_i)$ and $d^*(f, \alpha_0)$:

$$\overline{D(f, \alpha_i)D^*(f, \alpha_0)} = < D(f, \alpha_i), D^*(f, \alpha_0) > . \tag{6}$$

We define $R_x(t + \tau, t)$ the autocorrelation function of complex envelope, according to the relation:

$$R_x(t + \tau, t) = \overline{x(t + \tau)x^*(t)}. \tag{7}$$

In [1], [2] we have obtained for $R_x(t + \tau, t)$ the expression:

$$R_x(t + \tau, t) = A^2 \sum_i \sum_k \overline{d(t + \tau - iT, \alpha_i)d^*(t - kT, \alpha_k)}. \tag{8}$$

2. Power Spectral Density of Complex Envelope

The autocorelation function $R_x(t + \tau, t)$ is periodical with T period. Indeed starting with the relation (8) we obtain:

$$(9)\quad R_x(t+\tau+T,t+T)=A^2\sum_i\sum_k\overline{d[t+\tau-(i-1)T,\alpha_i]d^*[t-(k-1)T,\alpha_k]}.$$

Operating the variables change $i-1=i'$, $k-1=k'$ and taking into consideration the stationarity symbol we can replace the sequence pair (α_i,α_k) with (α_i',α_k') and obtain the relation (7).

That's why the autocorrelation function will depend only on τ and will be given by the relation:

$$(10)\qquad R_x(\tau)=\frac{1}{T}\int_0^T R_x(t+\tau,t)\mathrm{d}t.$$

Replacing (8) in (10), we get for $R_x(\tau)$ the expression:

$$(11)\qquad R_x(\tau)=\frac{A^2}{T}\sum_i\int_{-\infty}^{+\infty}\overline{d(t+\tau-iT,\alpha_i)d^*(t,\alpha_0)}\mathrm{d}t.$$

Using the W i e n e r–K h i n č i n theorem, we obtain:

$$(12)\qquad X(f)=\frac{A^2}{T}\int_{-\infty}^{+\infty}\sum_i\int_{-\infty}^{+\infty}\overline{d(t+\tau-iT,\alpha_i)d^*(t,\alpha_0)}\mathrm{d}t\,\mathrm{e}^{-\mathrm{j}2\pi f\tau}\mathrm{d}\tau.$$

The operation of statistical average, defined by the relation (6), implying an integration operation (relation (12)), after a suitable grouping, can also written:

$$(13)\qquad X(f)=\frac{A^2}{T}\int_{-\infty}^{+\infty}\sum_i\left\{\int_{-\infty}^{+\infty}d^*(t,\alpha_0)\left[\int_{-\infty}^{+\infty}d(t+\tau-iT,\alpha_i)\mathrm{e}^{-\mathrm{j}2\pi f(t+\tau-iT)}\right]\mathrm{d}\tau\times\right.$$
$$\left.\times\mathrm{e}^{j2\pi ft}\mathrm{d}t\right\}\mathrm{e}^{-2\pi fiT}.$$

Utilizing the variable change $\tau'=t+\tau-iT$ and recognizing $D(f,\alpha_i)$, we obtain the relation:

$$(14)\qquad X(f)=\frac{A^2}{T}\sum_i\overline{D(f,\alpha_i)D^*(f,\alpha_0)}\mathrm{e}^{-j2\pi fiT}.$$

Using notation:

$$X_{d,i}(f) \triangleq \overline{D(f,\alpha_i)D^*(f,\alpha_0)}, \tag{15}$$

we obtain for PSD of complex envelope an extremely simple relation:

$$X(f) = \frac{A^2}{T}\sum_i X_{d,i}(f)e^{-j2\pi fiT}. \tag{16}$$

We denote:

$$R_{d,i}(t,t') = \overline{d(t,\alpha_i)d^*(t',\alpha_0)}, \tag{17}$$

which is the autocorrelation of $d(t,\alpha_i)$ and changing order of statistical and integration average of operation in (15) we get:

$$\begin{aligned} X_{d,i}(f) &= \int_{-\infty}^{+\infty}\int_{-\infty}^{+\infty} \overline{d(t,\alpha_i)d^*(t',\alpha_0)}e^{-j2\pi(t-t')}dtdt' = \\ &= \int_0^T\int_0^T R_{d,i}(t,t')e^{-j2\pi(t-t')}dtdt', \end{aligned} \tag{18}$$

where we have supposed that $d(t',\alpha_0)$ is limited in time in the $[0,T]$ interval.

In (18) we make the variables change $x = t'$ and $z = t - t'$. This the area of integration change from $0 \le t \le T$, $0 \le t' \le T$ to $-x \le z \le T - x$, $0 \le x \le T$ as represented in Fig.2.

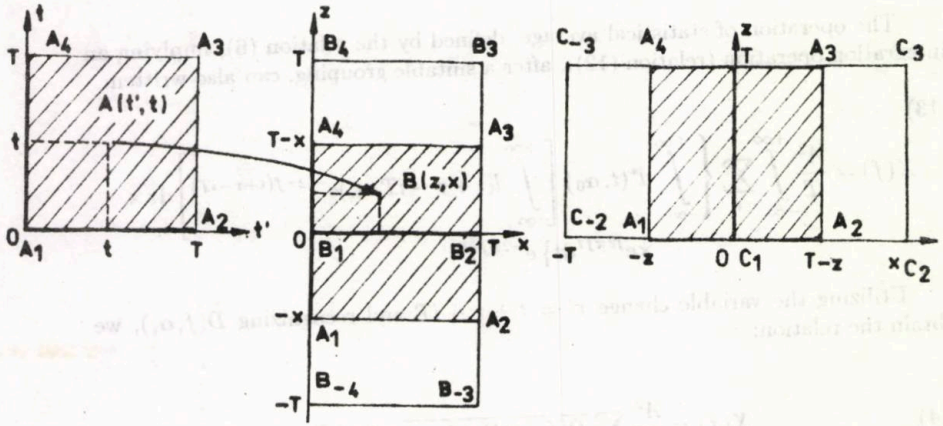

Fig. 2

According to the variables change we get:

$$X_{d,i}(f) = \int_0^T \left[\int_{-x}^{T-z} R_{d,i}(z+x,x) \mathrm{e}^{-\mathrm{j}2\pi f z} \mathrm{d}z \right] \mathrm{d}x. \tag{19}$$

Changing the integration order in the above relation we obtain, according to Fig.2:

$$\begin{aligned} X_{d,i}(f) = &\int_0^T \left[\int_0^{T-z} R_{d,i}(z+x,x)\mathrm{d}x \right] \mathrm{e}^{-\mathrm{j}2\pi f z}\mathrm{d}z + \\ &+ \int_{-T}^0 \left[\int_{-z}^{T} R_{d,i}(z+x,x)\mathrm{d}x \right] \mathrm{e}^{-\mathrm{j}2\pi f z}\mathrm{d}z. \end{aligned} \tag{20}$$

If, continuing, the variables change $z' = -z$, $x' = x - z$ is performed, after which we come back to the initial variables (x, z), the relation (20) becomes:

$$X_{d,i}(f) = \int_0^T \int_0^{T-z} R_{d,i}(z+x,x)\mathrm{d}x\mathrm{e}^{-\mathrm{j}2\pi f z}\mathrm{d}z + \int_0^T \int_0^{T-z} R_{d,i}(x,z+x)\mathrm{d}x\mathrm{e}^{\mathrm{j}2\pi f z}\mathrm{d}z. \tag{21}$$

3. Particular Cases

a) If condition

$$R_{d,i}(z+x,x) = R^*_{d,i}(x,z+x) \tag{22}$$

is fullfilled, then relation (21) becomes:

$$X_{d,i}(f) = 2\int_0^T \Re e \left[\int_0^{T-z} R_{d,i}(z+x,x)\mathrm{d}x \right] \mathrm{e}^{-\mathrm{j}2\pi f z}\mathrm{d}z \tag{23}$$

and if, in addition, $R_{d,i}(x, z+x)$ is real, then we obtain:

$$X_{d,i}(f) = 2\int_0^T \left[\int_0^{T-z} R_{d,i}(x,z+x)\mathrm{d}x \right] \cos 2\pi f z \mathrm{d}z. \tag{24}$$

b) Sequences α_i and α_0 are independent and stationary for $i \geq k$. In this case, (15) becomes:

$$X_{d,i}(f) = \overline{D(f,\alpha_i)D^*(f,\alpha_0)} = |\overline{D(f,\alpha_0)}|^2 \triangleq X_{d,k}(f). \tag{25}$$

Relation (16) may be written under the suitable form:

$$X(f) = \frac{A^2}{T}\sum_{|i|<k} X_{d,i}(f)\mathrm{e}^{-\mathrm{j}2\pi fiT} + \frac{A^2}{T}\sum_{|i|\geq k} X_{d,i}(f)\mathrm{e}^{-\mathrm{j}2\pi fiT}. \tag{26}$$

Substracting and adding in (26) the term

$$X_{d,k}(f)\sum_{|i|<k}\mathrm{e}^{-\mathrm{j}2\pi fiT},$$

we get:

$$X(f) = \frac{A^2}{T}\sum_{|i|<k}(X_{d,i} - X_{d,k})\mathrm{e}^{-\mathrm{j}2\pi fiT} + \frac{A^2}{T}\sum_{i} X_{d,i}(f)\mathrm{e}^{-\mathrm{j}2\pi fiT}. \tag{27}$$

According to the equality:

$$T\sum_{i}\mathrm{e}^{-\mathrm{j}2\pi fiT} = \sum_{k}\delta\left(f - \frac{k}{T}\right) \tag{28}$$

and to the relation (23), we obtain finally the well-known result:

$$X(f) = \frac{A^2}{T}\sum_{|i|<k}[X_{d,i}(f) - X_{d,k}(f)]\mathrm{e}^{-\mathrm{j}2\pi fiT} + \frac{A^2}{T^2}X_{d,k}\sum_{k}\delta\left(f - \frac{k}{T}\right). \tag{29}$$

The relation (29) can also be put under the form:

$$X(f) = X_c(f) + X_d(f), \tag{30}$$

where:

$$X_c(f) = \frac{A^2}{T}\sum_{|i|<k}[X_{d,i}(f) - X_{d,k}(f)]\mathrm{e}^{-\mathrm{j}2\pi fiT}, \tag{31}$$

$$X_d(f) = \frac{A^2}{T^2}X_{d,k}(f)\sum_{k}\delta\left(f - \frac{k}{T}\right) \tag{32}$$

represent the continuous and, respectively, the discrete part of the spectrum. In (31) we can replace the terms with negative indices, having in view that:

$$X_{d,-i}(f) = \overline{D(f,\alpha_{-i})D^*(f,\alpha_0)} = \overline{D(f,\alpha_0)D^*(f,\alpha_i)} = \tag{33}$$
$$= \overline{D^*(f,\alpha_i)D(f,\alpha_0)} = \left[\overline{D(f,\alpha_i)D^*(f,\alpha_0)}\right]^* = X^*_{d,i}(f).$$

For $i = 0$, from (15) we obtain:

$$X_{d,0} = \overline{|D(f,\alpha_0)|^2}. \tag{34}$$

According to (33) and (34), expression (31) may be written under the form:

(35)
$$X_c(f) = \frac{A^2}{T}\left(X_{d,0}(f) - X_{d,k}(f) + 2\Re e\left\{\sum_{i=1}^{k-1}[X_{d,i}(f) - X_{d,k}(f)]e^{-j2\pi fiT}\right\}\right).$$

c) The sequence α_i is formed of a single symbol and the a_i symbols are independent. So:

$$d(t,\alpha_i) = d(t,a_i), \quad D(f,\alpha_i) = d(f,a_i). \tag{36}$$

Relation (17) becomes:

$$R_{d,i}(t,t') = \overline{d(t,a_i)d^*(t',a_0)} = \begin{cases} \overline{d(t,a_0)d^*(t',a_0)}, & i = 0, \\ d(t,a_0)d(t',a_0), & i \neq 0. \end{cases} \tag{37}$$

Making the relation (25) particular, we'll have:

$$X_{d,i}(f) = \begin{cases} \overline{|D(f,a_0)|^2} = X_{d,0}, & i = 0; \\ \overline{|D(f,a_0)|^2} = X_{d,1}, & i \neq 0. \end{cases} \tag{38}$$

For $k = 1$, the relation (35) becomes:

$$X_c(f) = \frac{A^2}{T}[X_{d,0}(f) - X_{d,1}(f)] + \frac{A^2}{T^2}X_{d,1}(f)\sum_k \delta\left(f - \frac{k}{T}\right). \tag{39}$$

d) The shaping filter $h(t)$ has the same form for all symbols and it is supposed to be linear. In consequence, the relation (2) becomes:

$$d(t,a_i) = \sum_i a_i h(t) \tag{40}$$

and for PSD of BB signals an extremely simple expression results, which depends only on $h(t)$:

$$X(f) = \frac{A^2}{T}|H(f)|^2 \sum_i a_i a_0 e^{-j2\pi fiT} =$$

$$= \frac{A^2}{T}|H(f)|^2 \left[\overline{a_0^2} - \overline{a_0}^2 + \frac{a_0^2}{T}\sum_k \delta\left(f - \frac{k}{T}\right)\right]. \tag{41}$$

4. Conclusions

A procedure for obtaining the digital signal in BB, by means of associating to each symbol transmitted by the information source a transfer function of the shaping filter is proposed. We demonstrate that the autocorrelation function of complex envelope is periodical. Applying the W i e n e r–K h i n č i n theorem we come across PSD of complex envelope, also for certain particular cases known in the literature. The calculation method is much more general and the obtained formula extremely simple making better evidence of the influence of shaping filter on the modulated signal.

Received, April 30, 1992

Technical University "Gh. Asachi", Jassy,
Department of Communications

REFERENCES

1. C o t a e P., *Contribuţii la îmbunătăţirea tehnicilor de modulaţie din sistemele de transmisiuni de date cu mare viteză.* Ph. D. Diss., Polyt. Inst., Bucharest, 1991.
2. C o t a e P., *Comunicaţii digitale.* Part I, *Modulaţia digitală.* Inst. polit., Iaşi, 1992.
3. G a r d n e r W.A., *Introduction to Random Processes with Applications to Signals and Systems.* McGraw-Hill Book Company, NY, 1989.
4. B l a h u t R.E., *Digital Transmission of Information.* Addison-Wesley Publishing Company, NY, 1990.
5. P i e r o b o n G.L., P u p o l i n S.G., T r o n c a G.P., *Power Spectrum of Angle Modulated Correlated Digital Signals.* IEEE Trans. on Commun., **COM-30**, *2*, 389-396 (1982).

CALCULUL DENSITĂŢII SPECTRALE DE PUTERE PE BAZA ANVELOPEI COMPLEXE PENTRU SEMNALELE DIN BANDA DE BAZĂ

(Rezumat)

Pornind de la proprietăţile statistice ale secvenţei de date emise de sursă, se deduce funcţia de autocorelaţie a datelor în BB. Se propune o metodă mai generală decât cea cunoscută în literatura de specialitate pentru deducerea DSP a semnalelor în BB.

Se particularizează rezultatele obţinute pentru o serie de semnale modulatoare necesare tehnicilor de modulaţie.

BULETINUL INSTITUTULUI POLITEHNIC DIN IAŞI
Tomul XLI (XLV), Fasc. 1–2, 1995
Secţia III
ELECTROTEHNICĂ. ENERGETICĂ. ELECTRONICĂ

D.C. 621.394.9

COMBINED DELAY-MODULATION AND CORRELATIVE LEVEL CODING

BY
N.D. ALEXANDRU

1. Introduction

The delay modulation (DM) or M i l l e r coding is widely used in digital magnetic recording and data transmission due to its very attractive spectral properties [1]. Its power spectral density [2] is given by

$$\frac{S(f)}{E_s} = \frac{1}{2\theta^2(17+8\cos 8\theta)}(23 - 2\cos\theta - 22\cos 2\theta - 12\cos 3\theta + \\ + 5\cos 4\theta + 12\cos 5\theta + 2\cos 6\theta - 8\cos 7\theta + 2\cos 8\theta), \tag{1}$$

where $\theta = \pi f T$; $E_s = A^2 T$.

Taking into account the poor d.c. response of the magnetic recording systems due to the inherent differentiation in the read-back process, variations of the M i l l e r code have been deviced in order to decrease its d.c. component [3], [4]. The recording channel can also be regarded as a partial-response channel [3], with a discrete transfer function

$$F(D) = 1 - D, \tag{2}$$

where D is the delay operator.

2. Combining DM and Correlative Level Coding

A correlative level coding can be applied to a delay-modulation coded signal to make it more suitable for digital magnetic recording, as shown in Fig. 1.

Taking into account that the elementary interval is $T/2$ seconds wide, a correlative level coding implying a delay of $nT/2$, (n = 1, 2 and 3), is applied to the M i l l e r coded data signal. The polynomials $F(D) = 1 - mD$ and

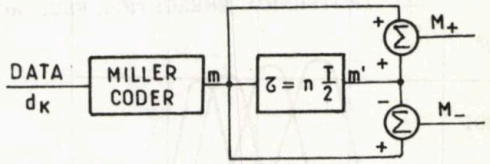

Fig. 1

$F(D) = 1 + mD$, ($m = 0.5$, 1 and 1.5), are used. The first polynomial creates a null at d.c., while the second one produces a null at $f - 1/mT$. We obtain the ternary codes described by the state transition diagrams depicted in Fig. 2

The waveforms illustrated in Figs. 3 and 4 are obtained for $n = 1$ and $n = 2$ ($m = 0.5$ and $m = 1$).

3. Power Spectral Density of the New Codes

We shall consider only the ternary codes based on the polynomial $F(D) = 1 - mD$. The power spectral density (p.s.d.) is given by

$$W(f) = |Y(f)|^2 S(f), \tag{3}$$

where $S(f)$ is p.s.d. of the DM coded signal, $Y(f)$ – transfer function of the correlative level coding circuit.

Obviously,

$$|Y(f)|^2 = \left|1 - e^{-j2\pi f n \frac{T}{2}}\right|^2 = 2\left(\sin\frac{n\pi fT}{2}\right)^2, \tag{4}$$

or

$$|Y(f)|^2 = 2\left(\sin\frac{n\theta}{2}\right)^2. \tag{5}$$

Using the approach outlined in [5] and [6], we get for $p = 0.5$ (p is the probability of a mark in the data string) and $n = 2$:

$$W(f) = \frac{1}{8(17 + 8\cos 8\theta)}(4\cos 9\theta - 8\cos 8\theta - 24\cos 7\theta + 16\cos 6\theta + \\ + 62\cos 5\theta + 20\cos 4\theta - 82\cos 3\theta - 116\cos 2\theta + 40\cos\theta + 88), \tag{6}$$

which after some trigonometric manipulations becomes

$$W(f) = 2(\sin\theta)^2 S(f). \tag{7}$$

The p.s.d. plots illustrated in Fig. 5 are obtained.

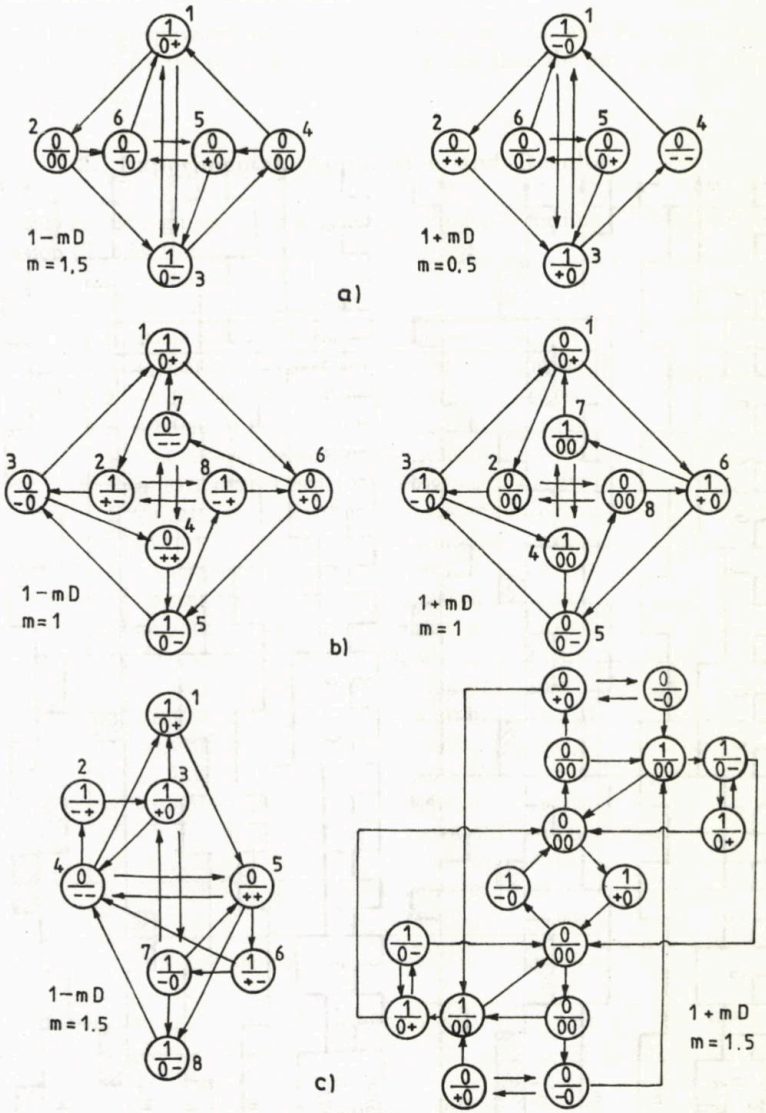

Fig. 2

4. Conclusions

1. A few ternary codes, based on delay-modulation and correlative level coding were introduced. They exhibit attractive spectral properties. Those based on the

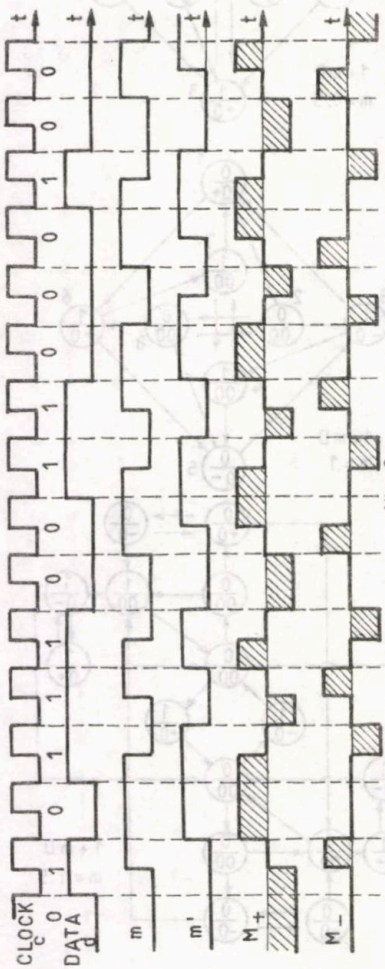

Fig. 3

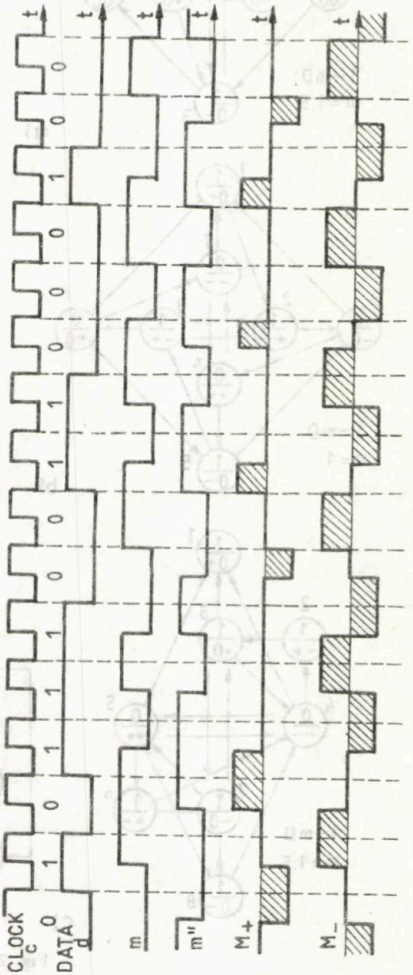

Fig. 4

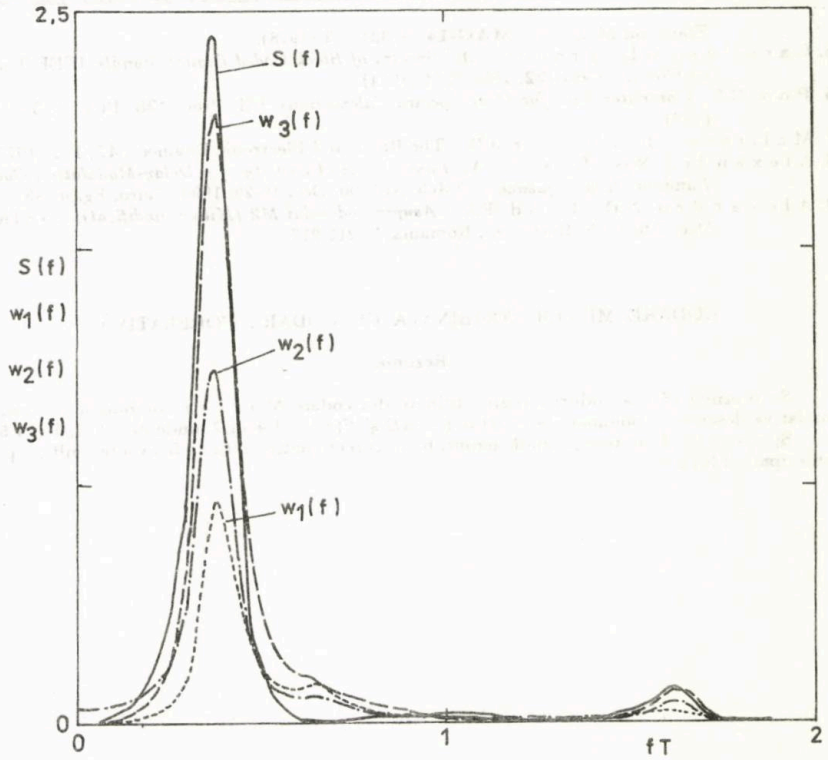

Fig. 5

polynomial $F(D) = 1 - mD$, ($m = 0.5$, 1 and 1.5), exhibit a null at d.c. in the power spectrum.

2. A set of original transition diagrams were introduced for the proposed codes.

3. We checked their power spectrum using the method based on the autocorrelation function and applying the W i e n e r–K h i n č i n theorem and found the same result.

Received, April 20, 1992

Technical University "Gh. Asachi", Jassy, Department of Communications

REFERENCES

1. H e c h t M., G u i d a A., *Delay Modulation.* Proc IEEE, **57**, 1314-1316 (1969).
2. L i n d s e y W.C., *Telecommunication Systems Engineering.* Prentice Hall, Englewood Cliffs, New Jersey, 1973, ch.1.
3. K o b a y a s h i H., T a n g D.T., *Application of Partial-Response Channel Coding to Magnetic Recording Systems.* IBM J. Res. Develop., **14**, 368-375 (1970).
4. L i n d h o l m D.A., *Power Spectra of Channel Codes for Digital Magnetic Recording.* IEEE

Trans. on Magnetics, **MAG-14**, *5*, 321-323 (1978).
5. C a r i o l a r o G.L., T r o n c a G.P., *Spectra of Block Coded Digital Signals*. IEEE Trans. on Comm., **Com-22**, 1555-1564 (1974).
6. P o o G.S., *Computer Aids for Code Spectra Calculations*. IEE Proc, **128**, Pt.F, *5*, 323-330 (1981).
7. M a l l i n s o n J.C., M i l l e r J.W., The Radio and Electronic Engineer, **47**, 172 (1977).
8. A l e x a n d r u N.D., B o a r i u A., *Power Spectral Density of a Delay-Modulation Coded Random Data Sequence*. COMCONEL 90, Dec. 16-20, 1990, Cairo, Egipt, 83.
9. A l e x a n d r u N.D., I m a d F.M., *Asupra coderului M2 (Miller modificat)*. CNETAC, Dec. 7-9, 1988, Bucharest, Romania, **2**, 215-217.

CODARE MILLER COMBINATĂ CU CODARE CORELATIVĂ

(Rezumat)

Se prezintă câteva coduri ternare obţinute din codare M i l l e r combinată cu codare corelativă descrise de polinoamele $F(D) = 1 - mD$ şi $F(D) = 1 + mD$, unde $m = 0,5$; 1 şi 1,5.

Spectrele lor de putere prezintă zerouri fie în curent continuu, fie la frecvenţe multipli pari sau impari ai lui $1/mT$.

BULETINUL INSTITUTULUI POLITEHNIC DIN IAŞI
Tomul XLI (XLV), Fasc. 1–2, 1995
Secţia III
ELECTROTEHNICĂ. ENERGETICĂ. ELECTRONICĂ

D.C. 621.394.9

A MODIFIED $M3$ CODER

BY
N.D. ALEXANDRU

1. Introduction

In a previous work [5], a method of synthesizing the modified $M2$ coding circuit was presented. The modified $M2$ code is derived from the M i l l e r code or delay-modulation (DM). A restriction was introduced for the last mark in a string of at least two successive marks, which is coded as a single space, by the lack of transition. This is not the M i l l e r-squared code (M^2), where this restriction applies for the last mark only if the number of marks in the string is even.

The modified $M2$ code, besides the intervals with the length T, $1.5T$ and $2T$, specific to DM code, exhibits other intervals with a length of $2.5T$ and $3T$. They can be used for eliminating the phase ambiguity.

The synthesis method for the modified $M2$ coder [6] is based on the fact that, starting from the DM code, the $M2$ one can be obtained as a SIK digital modulation [7], where the carrier is the DM code and the data are an auxiliary signal a, which is obtained from the NRZ-L coded data, replacing every mark by a space, excepting the last mark in a string of at least two successive marks. We can write then

$$M2 = M \oplus a, \tag{1}$$

where M represents the DM coded signal and a is the auxiliary signal and the operation involved is an exclusive-or operation.

2. The $M3$ Code

A new code is introduced, denoted by $M3$. It is similar to the DM and $M2$ codes with the exception that the last two marks in a string of consecutive marks with a length of at least 3, and the last space in a string of at least two successive spaces are coded by the lack of transition. The associated transition diagram is represented in Fig.1.

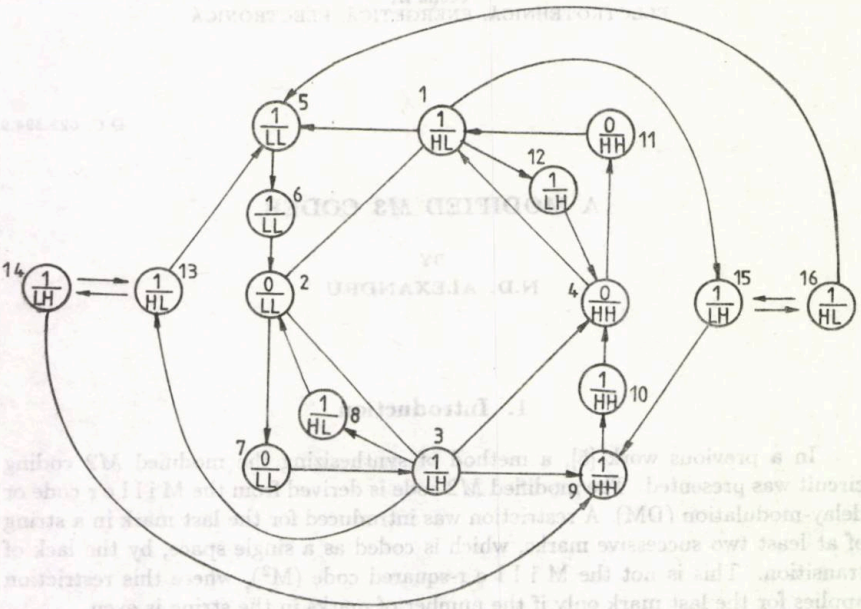

Fig. 1

A diagram of the coding circuit is presented in Fig.2. This implementation is based on the relation

$$M3 = M \oplus x_1 \oplus x_2, \tag{2}$$

where: M denotes the DM encoded data sequence; x_1 represents a signal evidencing the strings of successive spaces composed of at least two spaces, which is further frequency-divided by two; x_2 – a signal evidencing the strings of successive marks with a length of at least three.

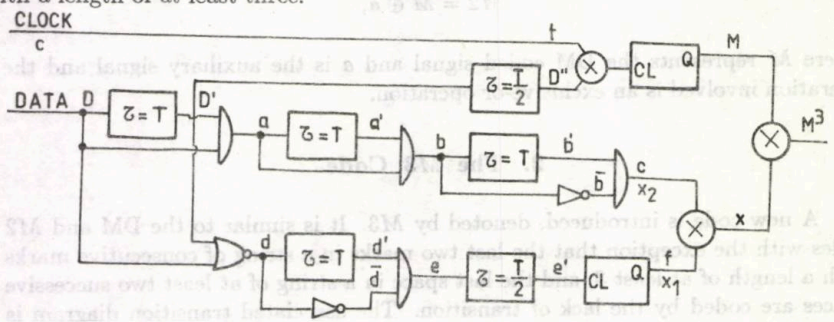

Fig. 2

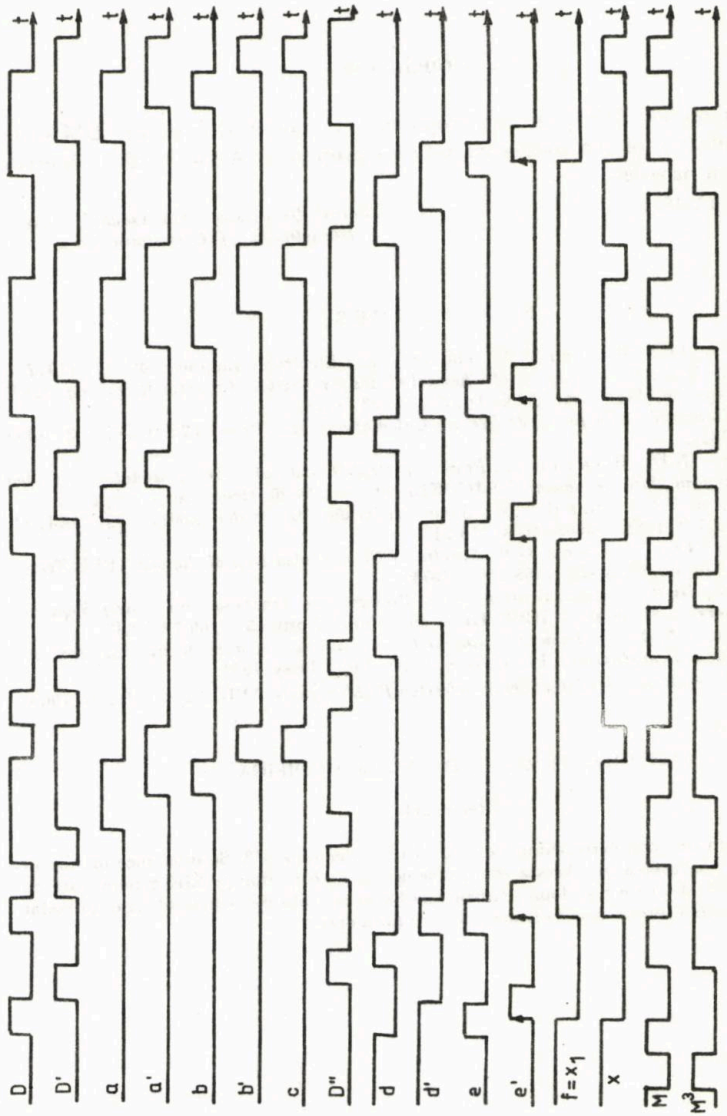

Fig. 3

The waveforms illustrating the operation of the coding circuit are represented in Fig.3.

3. Conclusion

A new modified $M3$ code was proposed. It is derived from the DM code. An implementation of the coding circuit was proposed. A study of its spectral properties is in progress.

Received, April 30, 1992

Technical University "Gh.Asachi", Jassy,
Department of Communications

REFERENCES

1. Mallinson J.C., Miller J.W., The Radio and Electronic Engineer, **47**, 172 (1977).
2. Lindholm D.A., *Power Spectra of Channel Codes for Digital Magnetic Recording.* IEEE Trans. on Magnetics, **MAG-14**, *5*, 321-323 (1978).
3. Poo G.S., *Computer Aids for Code Spectra Calculations.* IEE Proc., **128**, Pt.F, *5*, 323-330 (1981).
4. Alexandru N.D., Boariu A., *Power Spectral Density of a Delay-Modulation Coded Random Data Sequence.* COMCONEL 90, Dec. 16-20, 1990, Cairo, Egipt, 83.
5. Alexandru N.D., Imad F.M., *Asupra coderului M2 (Miller modificat).* CNETAC, Dec. 7-9, 1988, Bucureşti, **2**, 215-217.
6. Cariolaro G.L., Tronca G.P., *Spectra of Block Coded Digital Signals.* IEEE Trans. on Comm., **Com-22**, 1555-1564 (1974).
7. Ward R.B., *Digital Communications on a Pseudonoise Tracking Link Using Sequence Inversion Modulation.* IEEE Trans. on Comm., **Com-15**, *1*, 69-78 (1967).
8. Alexandru N.D., *Contribuţii la studiul transmisiunilor de date de tip FSK (privind codarea şi modularea).* Ph. D. Diss, Polyt. Inst., Jassy, 1981.
9. Nave P.M.W., *Spektrum des biternaerer codierten PCM-Signals.* AEÜ, **23**, *4*, 216-218 (1969).

UN CIRCUIT DE CODARE $M3$ MODIFICAT

(Rezumat)

Se prezintă un nou cod derivat din codul Miller, denumit $M3$. Se introduce un circuit de codare pentru producerea lui. Acesta este implementat ca o modulaţie SIK generalizată cu o purtătoare codată Miller şi două semnale auxiliare, derivate din semnalul de date codat NRZ-*L*. Codul prezintă interes pentru transmisiile pe fibră optică.

BULETINUL INSTITUTULUI POLITEHNIC DIN IAŞI
Tomul XLI (XLV), Fasc. 1-2, 1995
Secţia III
ELECTROTEHNICĂ. ENERGETICĂ. ELECTRONICĂ

D.C. 621.3.088.6

INCREASING OF THE SAFETY IN THE WORKING OF THE ELECTRONIC DEVICES USING A SINGLE-ERROR CORRECTING LINEAR BLOCK CODE (II)

BY
VALERIU MUNTEANU, M. LUCANU and DANIELA TĂRNICERIU

1. Introduction

On the basis of a property of single-error correcting linear block codes, demonstrated in [8], we deduce in this paper a synthesis method for a protection circuit of the electronic devices in the presence of disturbances.

In the proposed method each time one or more errors occur, a command will be firstly provided to block all of the electronic devices, then one of the p information words for the correct working of the electrical circuit will be provided. Thus, disregarding the number of errors occurred in the transmitting process, a correct command of the electronic devices shall be ensured, removing the risk of damage.

2. Protection Circuit Design of the Electrical Devices

Let us consider an electrical diagram containing k electronic devices, which must be driven according to a given program at discrete time moments t_1, $t_2, ..., t_p$. To design a protection circuit for electronic devices we must go through the following steps:

1°. For each of the p imposed commands in a working cycle, we determine the informational symbols in each code-word.

2°. We determine the number of parity-check symbols by relation (1) [8].

3°. We calculate the parity-check symbols in each code-word by relation (5) [8], then the code-words are constructed.

4°. We calculate the syndrome's components by relation (9) [8], considering that the received word form is:

$$[v_e] = [c_1' \; c_2' \; I_3' \; c_4' \; I_5' \; I_6' \; I_7' \; c_8' \; I_9' ... I_n']. \tag{1}$$

5°. The syndrome components will be applied, on one hand, to the binary-decimal decoder, and on the other hand they will provide a command to block all the electronic devices.

6°. If only $p < 2^k$ information words out of the 2^k possible ones are used, then

each time one of the $2^k - p$ information words not included in the working program occurs, a blocking command will be provided for every electronic device.

7°. If the associated syndrome of the received word is not equal to a column in the parity check matrix, a blocking command will be provided for every electronic device.

3. Three Phase Inverter Protection Scheme

In Fig.1 we present the electrical circuit of a 3-phase bridge inverter with separated reversed commutation circuits for each thyristor.

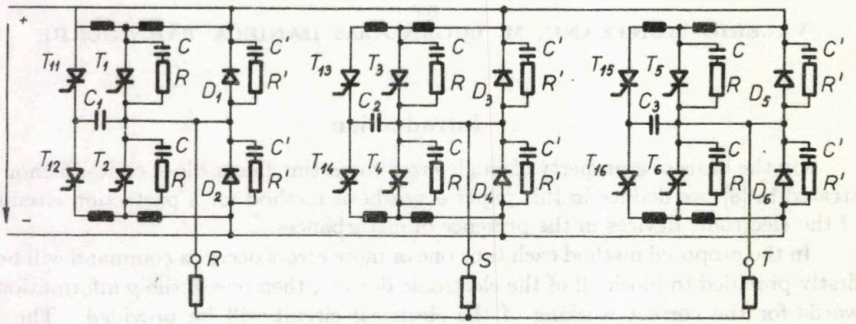

Fig. 1

The inverter contains the main thyristors $T_1, ..., T_6$ and the auxiliary commutation thyristors $T_{11}, ..., T_{16}$.

In Table 1 we present the diagram of the thyristor drive pulses. From Table 1 one can notice that if the correspondences $T_1 - T_{12}$; $T_2 - T_{11}$; $T_3 - T_{14}$; $T_4 - -T_{13}$; $T_5 - T_{16}$; $T_6 - T_{15}$ are made, then the information words will be identical for the driving of the corresponding thyristors. That means one may use a single decoder for both, the main and the auxiliary thyristors' driving, provided that the commands are applied firstly on the auxiliary, then on the main.

Also from Table 1 one can notice that at any moment three thyristors will be driven: either 2 in the upper branch plus 1 in the lower branch, or conversely.

Moreover, when thyristors T_i, $(i = 1, 3, 5)$, are driven for turning-on, thyristors T_j, $(j = 2, 4, 6)$, must be turned-off. It means that if, for instance, we construct the information words to drive thyristors T_1, T_4, T_5, then the information words driving thyristors T_2, T_3, T_6 are obtained by inverting the first ones.

From these observations it comes out that only the code-words for driving the thyristors T_1, T_4, T_5 must be generated by the computer, that is $k = 3$ information symbols.

From relation (1) [8], it results that each code-word will contain $m = 3$ parity-check symbols. Denoting I_{T_1}, I_{T_4}, I_{T_5} the information symbols in each code-word, it follows:

Table 1

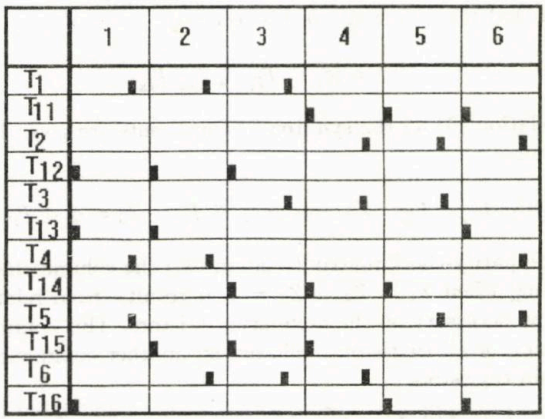

(2) $$[v] = [c_1\ c_2\ I_{T_1}\ c_4\ I_{T_4}\ I_{T_5}].$$

The parity-check matrix will then have 3 rows and 6 columns, that is:

(3) $$[H] = \begin{bmatrix} 0 & 0 & 0 & 1 & 1 & 1 \\ 0 & 1 & 1 & 0 & 0 & 1 \\ 1 & 0 & 1 & 0 & 1 & 0 \end{bmatrix}.$$

Substituting relations (2), (3) in relation (5) [8], it results:

(4) $$c_1 = I_{T_1} \oplus I_{T_4},\quad c_2 = I_{T_1} \oplus I_{T_5},\quad c_4 = I_{T_4} \oplus I_{T_5}.$$

Substituting in relation (4) only the information symbols necessary to drive the T_1, T_4, T_5 thyristors, according to Table 1, the following code-words result:

(5) $$[v_7] = [0\ 0\ 1\ 0\ 1\ 1],\quad [v_6] = [0\ 1\ 1\ 1\ 1\ 0],\quad [v_4] = [1\ 1\ 1\ 0\ 0\ 0],$$
$$[v_0] = [0\ 0\ 0\ 0\ 0\ 0],\quad [v_1] = [0\ 1\ 0\ 1\ 0\ 1],\quad [v_3] = [1\ 1\ 0\ 0\ 1\ 1].$$

These code-words must be generated by the computer in a sequence according to system (5).

The code-words $[v_2]$, $[v_5]$ are missing in the total of $2^3 = 8$ possible code-words. These code-words would correspond to the informational words to drive the thyristors T_1, T_4, T_5 by sequences 010 and 101, respectively. Because these information words are not included in Table 1, they must be avoided any time they occur in the driving process. When one of these two information words occurs, a command will be provided on the auxiliary thyristors, which will lead to the

blocking of all thyristors, followed by a command to cancel the next command on the main thyristors.

Supposing that the following word is received:

$$[v'] = [c'_1\ c'_2\ I'_{T_1}\ c'_4\ I'_{T_4}\ I'_{T_5}], \tag{6}$$

according to relation (9) [8] the syndrome components are given by the following equations system:

$$Z_1 = c'_4 \oplus I'_{T_4} \oplus I'_{T_5},\quad Z_2 = c'_2 \oplus I'_{T_1} \oplus I'_{T_5},\quad Z_3 = c'_1 \oplus I'_{T_1} \oplus I'_{T_4}. \tag{7}$$

Since in the parity-check matrix (relation (3)) the column that contains only unities is missing, when $Z_1 = Z_2 = Z_3 = 1$, it results, from relation (7), that a command will be necessary on the auxiliary thyristors. This command will determine the blocking of all thyristors, followed by another command to inhibit the drive of the main thyristors.

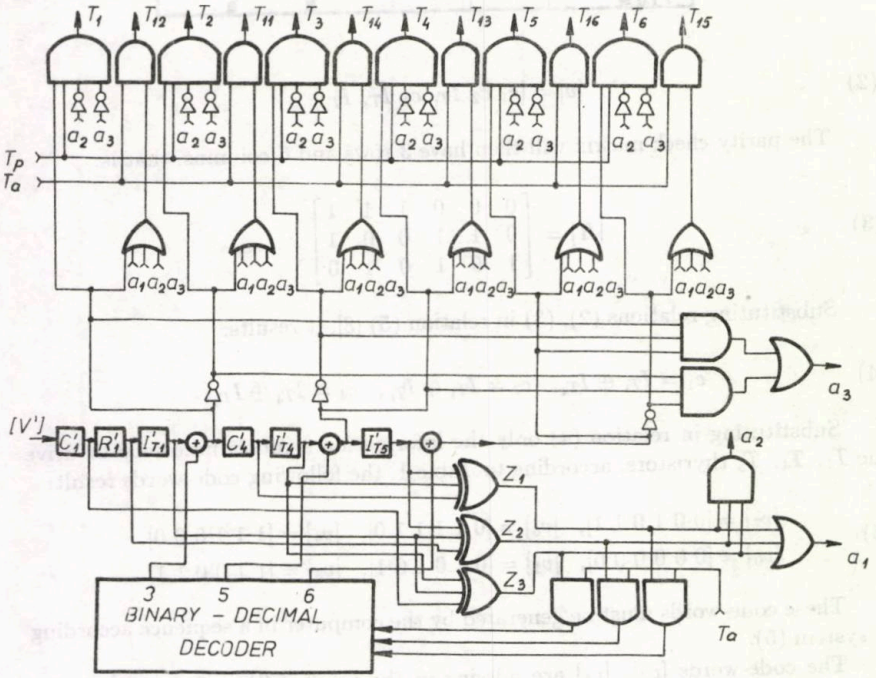

Fig. 2

The thyristors drive and protection circuit is shown in Fig.2.

In the protection scheme, shown in Fig.2, only outputs 3, 5 and 6 of the binary-decimal decoder have been used, because only these ones correspond to the

modification of the received information symbols, which will finally command the thyristors. That will obviously lead to component saving, without affecting the correct working of the protection circuit.

After the word $[v']$ is stored into the shift register one calculates the syndrome's components Z_1, Z_2 and Z_3. If at least one component Z_i, $(i = 1, 2, 3)$, equals 1, it results $a_1 = 1$, which will determine one turning-off impulse for auxiliary thyristors $T_{11}, ..., T_{16}$, leading thus of all the main thyristors to turn-off.

One denotes by T the clock pulse period of the transmission of the binary symbols in each computer code-word. The clock driving the auxiliary thyristors will be then $T_a = 6T$. The clock driving the main thyristors will be also $T_p = 6T$, but delayed from the clock T_a by a time necessary to a thyristor reversed commutation.

If $Z_1 = Z_2 = Z_3 = 1$ it results $a_2 = 1$, which will determine at clock T_a the command to turn on the auxiliary thyristors $T_{11}, ..., T_{16}$, followed at clock T_p by the inhibition of the command on the main thyristors $T_1, ..., T_6$.

At the occurrence of information words 010 and 101 respectively it results $a_3 = 1$, which will determine the same commands as $Z_1 = Z_2 = Z_3 = 1$. The detection of states 010 and 101 respectively is achieved simply by synthesizing a three-input and one-output circuit, which must provide a logical "1" on the output only when the inputs are in 010 and 101, respectively.

4. Conclusions

At the occurrence of one error in the command sequence at any moment t_i, $(i = 1, 2, ..., p)$, the protection scheme synthesized according to the proposed method sends firstly a turning-on command for the auxiliary thyristors, then the t_i moment correct command is applied.

At the occurrence of two or more errors the protection scheme will provide firstly a conduction command for the auxiliary thyristors, then it will send one of those p correct commands in the working program of the electrical circuit.

When three or more errors have occurred, it is possible that a transmitted code-word turns into an other code-word. In this case, a false command may occur.

The probability of a false command equals the product of the probability of three – or more – errors occurrence in the transmitted code-word and the probability that a code-word should be turn into an other code-word.

If one uses a symmetric binary channel, then the probability of a three – or more – errors occurrence may be calculated by the relation:

$$P_1 = \sum_{i=3}^{n} \binom{n}{i} Q^1 (1 - Q)^{n-1},$$

where Q is the error-probability of a binary symbol, and n is the code-word length.

The probability for a code-word to turn into an other code-word in presence of disturbances is:

$$P_2 = \frac{p}{2^n},$$

where p is the number of code-words used in the driving program of the electrical circuit. Then the probability of a false command is:

$$P_3 = P_1 P_2 = \frac{p}{2^n} \sum_{i=3}^{n} \binom{n}{i} Q^1 (1-Q)^{n-1}.$$

In case of the analyzed electrical circuit, $p = n = 6$ and for an ordinary transmission $Q = 0.01$. Taking into account these values, it really results that the false command probability is very small. In absence of a such protection, the false command probability equals Q.

If however, for some practical purposes, the P_3 probability proves to be unsatisfactory, a many-error-correcting block code may be used.

The theorem and the corollary, proved in [8], stay also true in case of the decoder for many-error correcting linear block codes.

For instance, if a double-error-correcting code would be used, then a false command might occur when on the transmitting channel at least five errors occur.

Generally, using an e-error-correcting code, a false command might occur, only if in the received word at least $2e + 1$ errors have occurred.

Obviously the decreasing of the probability of a false command is balanced by increasing the protection circuit complexity.

In ordinary purpose, it is enough to use a decoder for a single-error-correcting code, thus resulting the simplest protection circuit and a small enough false command probability.

Received, December 12, 1994

Technical University "Gh.Asachi", Jassy, Department of Applied Electronics

REFERENCES

1. Hamming R.W., *Error-Detecting and Error-Correcting Codes.* Bell Syst. Tech. J., **29**, 147-160 (1950).
2. Berlekamp E.R., *Algebraic Coding Theory.* McGraw-Hill, Book Company, New York, 1968.
3. Gallager R.G., *Information Theory and Reliable Communication.* John Wiley & Sons, New York, 1968.
4. Peterson W.W., Weldom E.J.Jr., *Error Correcting Codes.* Massachusetts, the MIT Press, 1972.
5. Lucanu T.M., *Industrial Electronic* (in Romanian). Polyt. Inst., Jassy, 1980.
6. Munteanu B.V., *Theory of Information Transmission* (in Romanian). Polyt. Inst., Jassy, 1979.
7. Bimal K.B., *Microcomputer Control of Power Electronics and Drives.* IEEE Press, New York, 1987.
8. Munteanu B.V., Lucanu T.M., Tărniceriu D., *Increasing of the Safety in the Working of the Electronic Devices Using a Single-Error Correcting Linear Block Code.* (I). Bul. Inst. polit., Iaşi, **XL (XLIV)**, *1-4*, s.III (1994).

CREŞTEREA SIGURANŢEI ÎN FUNCŢIONAREA DISPOZITIVELOR ELECTRONICE PRIN FOLOSIREA UNUI COD BLOC LINIAR CORECTOR DE O EROARE (II)

(Rezumat)

Pe baza a două noi proprietăţi ale codurilor bloc liniare corectoare de o eroare, se expune o metodă economică de comandă a dispozitivelor electronice din orice circuit electric, supus perturbaţiilor care pot cauza un număr nedefinit de erori în secvenţa de comandă. Se exemplifică metoda în cazul unui invertor trifazat în punte cu circuite de comutaţie inversă, separate pentru fiecare tiristor.

BULETINUL INSTITUTULUI POLITEHNIC DIN IAŞI
Tomul XLI (XLV), Fasc. 1–2, 1995
Secţia III
ELECTROTEHNICĂ. ENERGETICĂ. ELECTRONICĂ

D.C. 621.319.4; 538.551

A THEORETICAL APPROACH IN RELIABILITY ESTIMATION OF POWER CAPACITORS WORKING IN PERIODICAL NONSINUSOIDAL STEADY STATE

BY

ROMEO CIOBANU, TRAIAN BALAN and MARINEL TEMNEANU

1. Introduction

The integral form of thermal accumulated dose [1], [2] can be used with the aim of equating any unisothermal service regime with an isothermal one, an equivalent temperature value for this new regime being estimated. This temperature value can be generally determined, based on specific dielectric (temperature – frequency) characteristic and includes all the secondary effects (both exterior conditions and material thermal behaviour), so that the classical complicated, expensive and vague method of restriction coefficients estimation (for a certain regime, purpose or material), used in addition with endurance profile estimation [3], is avoided.

Thus the classical thermal endurance tests regarding a selected quality characteristic of the material (that reflects properly the material behaviour under the service circumstances) are used in connection with the new equivalent temperature value, still being the basis in determination of activation energy value of the intimate destruction process.

The problem of power capacitors reliability estimation consists in a specific dependence on temperature and voltage frequency of $\tan\delta$-factor [4], e.g. Fig.1, and peculiar frequency spectrum of each real nonsinusoidal electric regime.

The previous researches [4], [5], including the definition of an equivalent service $\tan\delta$-factor, or of the isotanδ-characteristics couldn't solve the general practical part of the problem.

2. Theoretical Considerations

There was observed that power capacitors are suffering only thermal breakdowns, that appear even the requests of the P.E.-143/80 standard of M.E.E.-ICEMENERG, Bucharest, are accomplished, regarding the critical value of voltage

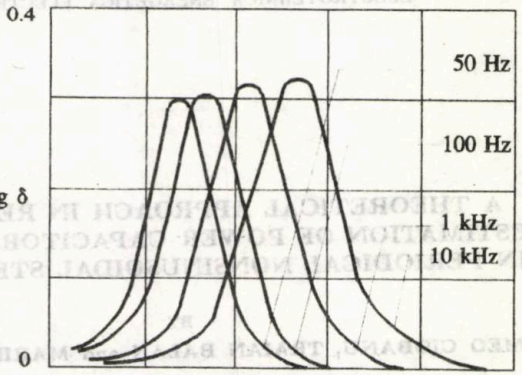

Fig. 1

distortion coefficient.

The multiple degree of nominal frequency is more important than its weight and exterior temperature influences the measurement results.

For a certain periodical nonsinusoidal service steady state the spectral Fourier form is used and according to [4],...,[6], a heating formula for power capacitors is proposed:

$$\frac{T - T_a}{T_n - \min(T_a, T_k)} = \sum_n n^2 p_n^2 = K_s > 1, \tag{1}$$

where: T is the final regime temperature, T_a – the exterior temperature, T_n – the nominal (standard admitted) temperature, T_k – the temperature value corresponding to minimum tanδ-value according to the dielectric characteristic (a new proposed parameter), n – multiple degree, p_n – the frequency component weight (reported to the nominal one), K_s – the equivalent overheating coefficient, according to the real nonsinusoidal steady state.

For the theoretical case of a single temporal electric regime T-value becomes T_e-equivalent temperature of the regime.

Usually there exist more than a temporal nonsinusoidal electric steady state and according to [2], a cumulative equation form is needed to estimate the real T_e-value. Here is proposed:

$$te^{-\frac{b}{T_e+273}} = \sum_i t_i e^{-\frac{b}{T_i+273}} \tag{2}$$

where: b is the activation energy coefficient, $t = \sum_i t_i$ – total observation period (hour, day, week, year, etc.), T_i – calculated using (1) for every electric i-regime.

The real heating equivalent value must be correlated to T_e and so, the lifetime, determined using [3] for the real regime T_e-value, is less than the anticipated value, corresponding to T_n.

3. Experimental, Application and Results

Two real electric regimes, more significant, founded according [7], were chosen for application (Tables 1 and 2).

Table 1

n	Amplitude	in sin	in cos	p_n, [%]
1	+1.389E+01	+1.388E+01	-4.664E-01	+100.000
2	+2.065E-06	+2.055E-06	+2.027E-07	+0.000
3	+2.946E-01	-1.217E-01	-2.683E-01	+1.121
4	+1.025E-06	+9.942E-07	+2.503E-07	+0.000
5	+1.697E+00	-1.293E+00	-1.099E+00	+12.217
6	+1.224E-06	-1.094E-06	-5.484E-07	+0.000
7	+1.201E+00	+8.204E-01	-8.770E-01	+8.646
8	+1.466E-06	+4.125E-07	-1.407E-06	+0.000
9	+2.560E-01	-1.151E-01	+2.286E-01	+0.843
10	+4.243E-07	-3.020E-07	-2.980E-07	+0.000
11	+2.519E-01	+1.950E-01	-1.595E-01	+1.813
12	+6.465E-07	+1.372E-07	-6.318E-07	+0.000
13	+6.045E-02	-3.953E-02	-4.573E-02	+0.435
14	+6.495E-07	-1.940E-07	-6.199E-07	+0.000
15	+1.973E-02	+6.533E-03	+1.861E-02	+0.142
16	+6.925E-07	-2.554E-07	-6.437E-07	+0.000
17	+2.376E-01	-3.422E-02	+2.351E-01	+1.710
18	+4.957E-07	-3.303E-07	+3.696E-07	+0.000
19	+1.201E-01	-9.988E-02	-6.676E-02	+0.865
20	+9.124E-07	-9.124E-07	+1.062E-11	+0.000

$K_{s_1} = 1.9657$, corresponding to a 13.5% distortion factor.

The first, very usual before 1989, is now not so wide in teritory. The second is the up-to-date usual one, reflecting the industrial level; it represents minimum average level of real distortions.

During a day, for a certain power capacitor station, there were found an average of 18 hours of first regime (tramway travel) and 6 hours of the second. The estimation adopted, $T_n = 50°C$ (standard), $T_a = 20°C$ (usual reference temperature in study) and $T_k = 8°C$ (for the Pyralene 1476 (pentachlordiphenyl) dielectric, from firm promotion characteristic, [5]).

The b-parameter values are $b_1 = 10,550$ K for breakdown strength and $b_2 = 8,820$ K for $\tan\delta$ thermal ageing estimation of the devices, using this dielectric.

Table 2

n	Amplitude	in sin	in cos	p_n, [%]
1	+1.042E+01	+1.025E+01	−1.864E+00	+100.000
2	+1.795E−06	+1.570E−06	−8.702E−07	+0.000
3	+1.875E−01	+8.920E−02	+1.649E−01	+0.799
4	+3.372E−07	+3.338E−07	−4.768E−08	+0.000
5	+5.280E−01	+1.719E−01	−4.992E−01	+5.366
6	+7.283E−07	+2.620E−07	−6.795E−07	+0.000
7	+1.010E−01	+9.542E−02	−3.304E−02	+0.969
8	+4.909E−07	+4.608E−08	−4.888E−07	+0.000
9	+1.084E−01	+1.083E−01	+3.515E−03	+0.140
10	+4.539E−07	+1.478E−07	−4.292E−07	+0.000
11	+7.114E−02	−3.716E−02	+6.066E−02	+0.683
12	+2.329E−07	−2.001E−07	−1.192E−07	+0.000
13	+7.049E−02	−3.192E−02	−6.284E−02	+0.676
14	+3.729E−07	−3.272E−07	−1.788E−07	+0.000
15	+6.196E−02	+1.192E−02	−6.080E−02	+0.095
16	+3.455E−07	−3.321E−07	−9.536E−08	+0.000
17	+9.549E−02	−1.294E−02	−9.461E−02	+0.916
18	+5.401E−07	−4.847E−07	−2.384E−07	+0.000
19	+3.277E−02	+2.913E−02	−1.501E−02	+0.314
20	+3.586E−07	−3.584E−07	−1.191E−08	+0.000

$K_{s_2} = 1.1289$, corresponding to a 5.45% distortion factor.

Table 3

b	T_e, [°C]
b_1	98.99
b_2	98.46

Table 4

T, [°C]	Lifetime, [hours]
70	40,000 (standard)
99	3637 (normal)
74	27,100 (elec.res.)

The obtained results are summarised in Tables 3 and 4.

There was observed that the difference between the estimations regarding the b-value is insignificant (less than 1%) and the real found service time is according to the long time experiment (about half a year, in winter period, in stead of 4.5 years proposed for the adopted power capacitors). For decreasing T_a-values, the lifetime is even less (Fig.2) that justify this proposed method, that is in correlation with the noticed tanδ-values increasing at low temperatures [3] and the theory of dielectric local overheating and thermal breakdown.

Overall there was noticed that a certain dielectric behaviour can be fully characterised only using the b and T_k specific values, e.g. the equivalent T_e-temperature values presented in Fig.2, where x – Pyralene dielectric, y – BNC-dielectric with $b_2 = 6,685$, $T_n = 50°C$ and $T_k = 35°C$ and z – PXE-dielectric with $b_2 = 9,540$, $T_n = 40°C$ and $T_k = 35°C$.

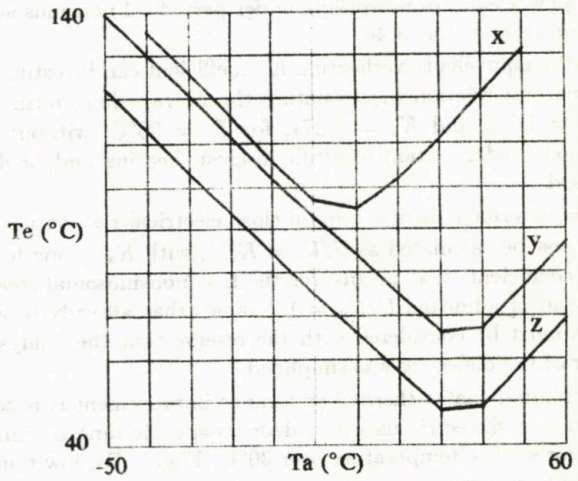

Fig. 2

If, as usual, a reliability improvement by electrical reservation (20% breakdown strength increasing) is adopted, the theoretical lifetime is according to Table 4 and T_e-values according to Fig.3, x, y, z having the same significance.

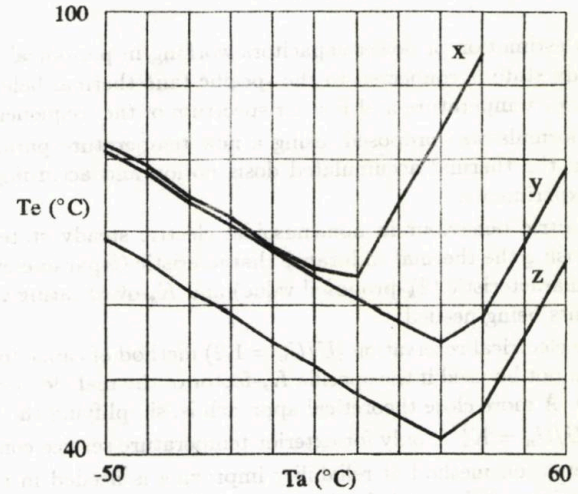

Fig. 3

We may anticipate that the lifetime increasing for this real electric regime is less than expected (only 1.2 years) and this method of reliability improvement is

not so usefull for power capacitors working under periodical nonsinusoidal steady state with K_s-value greater than 1.40.

A real long term equivalent overheating K_s-coefficient can be estimated using T_e-equivalent value and relation (1), equating the average long term distortion regime, e.g. $K_s = 1.833$ and $K_s = 1.271$, for $T_e = 99°C$, without and with electrical reservation; under certain scientific interest, heating and/or distortions analysis can be used.

Regarding the described theory, a more close electrical reservation for reliability improving must be calculated as $U/U_n = K_s^{1/2}$, with K_s – long term equivalent overheating coefficient; that means, for the first nonsinusoidal steady state, $U/U_n = 1.41$ instead of admitted $U/U_n = 1.2$ value (that allready provided too low). Such values must be considered with the reserve that the analysis of real thermal behaviour of the dielectric was simplified.

There was estimated that a thermal endurance improvement is needed, even by a careful selection of dielectric nature and/or its specific $\tan\delta$ thermal service regime, especially for service temperature over 30°C (Fig.3). For low temperature values a dielectric with a corresponding T_k-value must be used (e.g. for continental-underpolar climate, Pyralene 1499-trichlordiphenyl (Fig.1), having $T_k = -20°C$).

However a general condition in dielectric chosing is a T_k value close to average value of exterior service temperature.

4. Conclusions

The reliability estimation of power capacitors working in periodical nonsinusoidal electric steady state is connected to the specific $\tan\delta$ thermal behaviour of the dielectric, exterior temperature and Fourier spectrum of the frequencies.

A theoretical formula was proposed, using a new temperature parameter of dielectric, based on the thermal accumulated dosis notion and according to the long time service experiments.

A certain dielectric behaviour in nonsinusoidal electric steady state can be fully characterised using the thermal endurance characteristic (b-parameter value), $\tan\delta$ temperature characteristic (T_k-proposed value) and K_s-overheating value, no restriction coefficients being needed.

The up-to-date electrical reservation ($U/U_n = 1.2$) method of capacitors reliability improving can not be used if the specific K_s-factor of the real electric regime is greater than 1.40. A more close theoretical approach is, simplifying the thermal regime conditions, $U/U_n = K_s^{1/2}$, only for exterior temperature service conditions.

A thermal reservation method of reliability improving is needed in practice, concerning the capacitors dielectric behaviour, especially if ambient temperature is over 30°C.

Received, May 6, 1994

Technical University "Gh.Asachi", Jassy,
Department of Electrical Measurements

REFERENCES

1. C i o b a n u R., *Contribuţii privind analiza şi îmbunătăţirea tehnologică a fiabilităţii materialelor compozite.* Ph. D. Diss., Polyt. Inst., Bucharest, 1992.
2. C i o b a n u R., *The Thermal Accumulated Dose Notion and Reliability Estimation of Composite Materials.* Int. Conf. I.C.A.T.E.'93, Craiova, Ses. A, 27.
3. * * * N.F.-C.-26-205-1981.
4. K i e r s z t y n S. et al., *Thermal Analyse of Locomotive Cables under Variable Charge.* IEEE Trans. Ind. Applic., **IA-21**, *4*, 882 (1982).
5. B a l a n T. et al., *Some Contributions Concerning the Behaviour of Polar Dielectrics in Periodic Nonsinusoidal Electric Field.* Bul. Inst. polit., Iaşi, **XXXII (XXXVI)**, *1-4*, s.III, 65 (1986).
6. B a l a n T. et al., *The Thermal Behaviour of Polar Liquid Dielectrics; Iso-tanδ-characteristics.* Bul. Inst. polit., Iaşi, **XXXIV (XXXVIII)**, *1-4*, s.III, 33 (1988).
7. * * * *Analiza regimului deformant al condensatoarelor de forţă.* Techn. Univ. "Gh. Asachi", Jassy, Res. Contract, *182* (1993).

O APROXIMARE TEORETICĂ A ESTIMĂRII FIABILITĂŢII CONDENSATOARELOR DE FORŢĂ FUNCŢIONÂND ÎN REGIM PERIODIC NESINUSOIDAL

(Rezumat)

Se stabileşte un model matematic de echivalare a comportării condensatoarelor de forţă în regim periodic nesinusoidal, bazat pe noţiunea de doză termică acumulată.

Determinând o temperatură echivalentă se poate utiliza direct metoda clasică de estimare a profilului de anduranţă termică, nefiind necesari alţi parametri restrictivi determinaţi empiric.

BULETINUL INSTITUTULUI POLITEHNIC DIN IAŞI
Tomul XLI (XLV), Fasc. 1-2, 1995
Secţia III
ELECTROTEHNICĂ. ENERGETICĂ. ELECTRONICĂ

C.D. 621.3.052.3; 621.318.423

EMPLOI DU RÉACTEUR COMMANDÉ ORTHOGONALEMENT POUR LE TRAITEMENT DU NEUTRE DANS LES INSTALLATIONS MOYENNE TENSION

PAR

ADRIAN BARABOI, MARICEL ADAM et P. LEONTE

1. Introduction

Le traitement du neutre des installations moyenne tension s'avère l'une des actions nécessaires d'être effectuées dans le but de maintenir ces installations-ci en bon état de service.

L'une ou l'autre des solutions techniques concernant le traitement de neutre peut être appliquée, prenant en considération les critères suivants [1]: a) le niveau des surtensions transitoires et temporaires; b) la continuité dans l'alimentation à l'énergie électrique; c) le rapport entre les amplitudes des courants de court-circuit à la terre, respectivement triphasé; d) les possibilités de détecter et d'éliminer les défauts; e) l'intensité de la perturbation des télécommunications; f) le niveau des tensions de contact et de pas.

Les méthodes de traitement dans les réseaux moyenne tension sont différentes, à partir du neutre mis à la terre (USA, Canada) jusqu'au neutre isolé (Italie).

Pour les réseaux moyenne tension contenant seulement des consommateurs linéaires, en Roumanie on recommande [1] le traitement du neutre par la bobine d'extinction, munie d'un contrôle automatique de l'accord.

En ce qui concerne l'accord de la bobine d'extinction, on peut le réaliser par un réglage discontinu, à l'aide des prises ou, par contre, continu, si l'on utilise une bobine commandée. À ce point de vue, l'emploi d'un réacteur commandé orthogonalement comme bobine d'extinction pour le traitement du neutre dans les réseaux moyenne tension peut s'avérer avantageux, compte tenu des caractéristiques de celle-ci, qui assurent de meilleures possibilités de réglage.

2. Les caractéristiques constructives et fonctionnelles du réacteur commandé orthogonalement

S'il est utilisé comme équipement électrique dans l'énergétique, le réacteur commandé orthogonalement (RCO) s'avère avantageux par rapport au réacteur commandé longitudinalement (RCL), le dernier étant étudié en detail dans la littérature.

Le RCO est un dispositif électromagnétique, constitué en principe (Fig.1 *a*) par un noyau ferromagnétique *1*, muni par des enroulements de commande *2* et

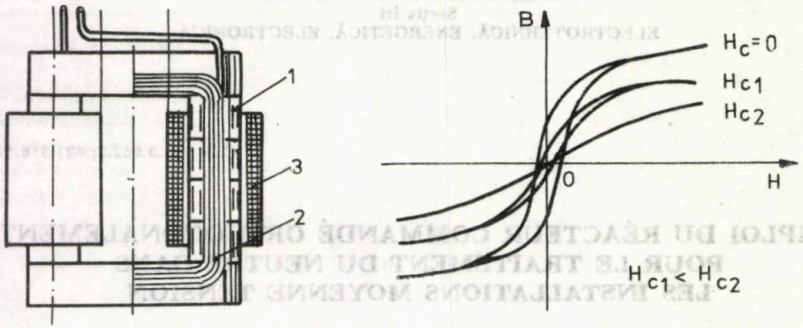

Fig. 1

d'excitation 3, dont les axes sont perpendiculaires [3].

Le fonctionnement du RCO est basé sur la modification de la courbe d'aimantation $B(H)$, considérée dans la direction d'excitation, fonction des valeurs du signal de commande, finalement exprimé par un champ magnétique H_c, perpendiculaire sur la direction d'excitation.

L'illustration de cette propriété est indiquée dans la Fig.1 *b*, où on met en évidence que l'augmentation des valeurs du champ magnétique continu H_c produit des diminutions des valeurs de l'induction rémanente, du champ coercitif et de la surface du cycle d'hystérésis, toutes les trois caractérisant l'aimantation dans la direction d'excitation.

Il est très important à remarquer que, par l'accroissement du signal de commande, on obtient des diminutions des pertes par hystérésis et du caractère nonlinéaire de la caractéristique d'aimantation $B(H)$.

Dans la construction des RCO fonctionnant à haute tension et ayant de grandes puissances, il est nécessaire que l'on assure une efficience augmentée du refroidissement des enroulements et, en même temps, le niveau d'isolement imposé par les tensions des réseaux.

Quoique les caractéristiques du RCO s'avèrent favorables à son emploi dans l'énergétique, les exemples de ce type sont relativement rares, parce que des essais dans ce but ont été marqués par des difficultés technologiques notables, surtout en ce qui concerne la construction du noyau ferromagnétique. Pourtant, quelques utilisations des RCO dans l'énergétique sont connues; ainsi on peut mentionner leurs emploi pour obtenir des sources statiques et réglables de puissance réactive, dans la construction des filtres qui éliminent les harmoniques ou comme bobine d'extinction [3],[4].

L'analyse du fonctionnement des schémas électriques, attachés aux différentes utilisations des RCO, peut être effectuée seulement à l'aide des expressions des caractéristiques de ces dispositifs-ci.

Les caractéristiques des RCO sont déterminées en acceptant des hypothèses simplificatrices, concernant spécialement l'isotropie du matériel du noyau ferromagnétique et la possibilité de négliger la hystérésis magnétique du noyau et les

résistances électriques des enroulements [2], [4].

Généralement, les caractéristiques d'un RCO sont décrites par des fonctions polynômiales, dont une approximation satisfaisante peut être limitée aux polynômes de troisième degré, ayant la forme:

$$(1) \qquad \begin{cases} \theta(\Psi, \Psi_c) = b_{10}\Psi + b_{30}\Psi^3 + b_{12}\Psi\Psi_c^2, \\ \theta_c(\Psi, \Psi_c) = b_{10}^c\Psi_c + b_{30}^c\Psi_c^3 + b_{12}^c\Psi_c\Psi^2, \end{cases}$$

où on a noté avec θ, θ_c et Ψ, Ψ_c les t. m. m. et les flux magnétiques d'excitation, respectivement de commande, b_{10}, b_{30}, b_{12}, b_{10}^c, b_{30}^c, b_{12}^c étant des coefficients variables par rapport aux matériaux et aux dimensions du RCO.

3. Le fonctionnement du RCO comme bobine d'extinction

Par le traitement du neutre dans un réseau moyenne tension on poursuit, dans le cas d'une mise accidentelle à la terre, la compensation du courant capacitif, parcourant le tracé en court-circuit; cet effet est dû au courant inductif qui traverse la bobine d'extinction, branchée entre le neutre du réseau et la terre.

En admettant l'hypothèse que la mise à la terre s'avère métallique, le schéma électrique équivalent, attaché au fonctionnement du réseau avec une mise monophasée à la terre, est donné dans la Fig.2, où C_e représente la capacité équivalente du réseau, R_e – la résistance de pertes, U_0 – la tension entre le point neutre et la terre [5].

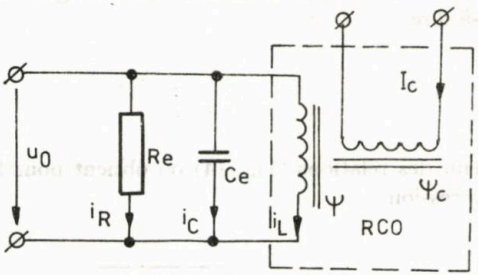

Fig. 2

Vu que les caractéristiques de la bobine d'extinction doivent être linéaires, il est nécessaire que le noyau ferromagnétique du RCO soit muni, tout au moins le long du circuit d'excitation, par des entrefers; étant données ces conditions, dans les expressions (1) on peut considérer:

$$(2) \qquad b_{30} = b_{30}^c = 0,$$

de sorte que, pour l'intensité du courant traversant l'enroulement d'excitation du RCO, il résulte l'expression:

$$I_L = \frac{U_0(b_{10} + b_{12}\Psi_c^2)}{\omega N}, \tag{3}$$

N étant le nombre de spires de l'enroulement d'excitation. Pour une série de valeurs de la tension U_0 du neutre, les caractéristiques (3) sont représentées dans la Fig.3.

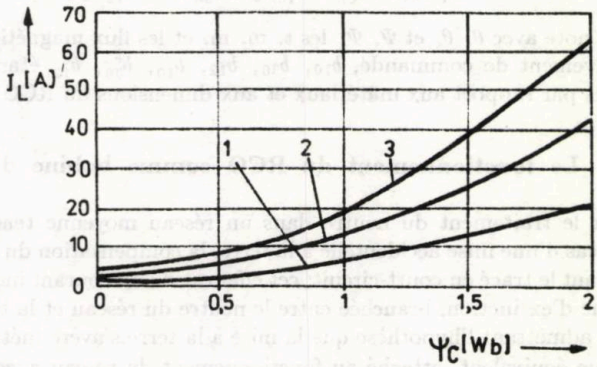

Fig. 3

L'effet de la compensation du courant capacitif i_c (Fig.2) est obtenu par la commande automatique du RCO, de sorte que le régime du circuit soit (ferro)-résonant, c'est-à-dire:

$$i_L = i_C. \tag{4}$$

Compte tenu des relations (1),...,(4) on obtient pour le flux magnétique de commande l'expression:

$$\Psi_c = \sqrt{\frac{\omega^2 NC - b_{10}}{b_{12}}}. \tag{5}$$

À l'aide de l'expression (5) on peut établir le procédé de commande du RCO, fonction de la place du défaut dans le réseau; la courbe $\Psi_c(C)$ est représentée dans la Fig.4.

Selon la commande du RCO, l'enroulement d'excitation est traversé par le courant d'intensité I_L qui, compte tenu de (4), est donné par:

$$I_L = \omega C U_0. \tag{6}$$

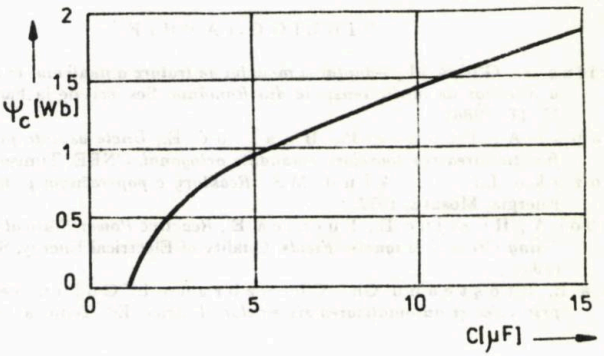

Fig. 4

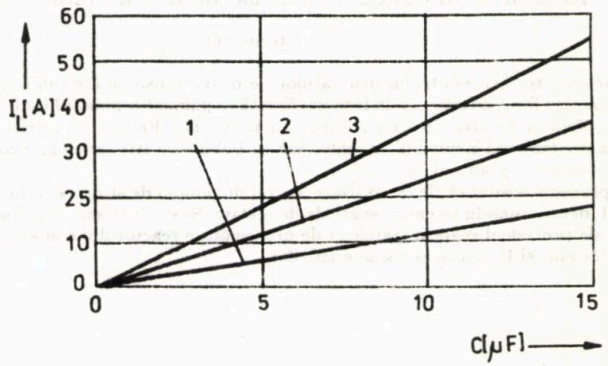

Fig. 5

Dans la Fig.5 on a représenté, pour quelques valeurs de la tension U_0, les courbes $I_L(C)$; habituellement, dans les réseaux moyenne tension, les valeurs de l'intensité du courant inductif traversant la bobine d'extinction peuvent atteindre quelques dizaines d'ampères.

4. Conclusions

On étudie la possibilité d'employer un RCO en tant que bobine d'extinction pour le traitement du neutre dans les réseaux moyenne tension.

Compte tenu des caractéristiques du RCO, ce mode d'emploi peut s'avérer avantageux, surtout concernant la rapidité de la réponse et la linéarité de la courbe d'aimantation.

Reçue le 14 juin 1993

Université Technique „Gh. Asachi", Jassy,
Chaire d'Énergétique

BIBLIOGRAPHIE

1. Gavrilaş N., Guşă M., *Adaptarea modului de tratare a neutrului la stadiul de dezvoltare a reţelelor de medie tensiune din România.* Ses. sci. de la Fac. d'Eléctrot., Jassy, **II**, 11 (1986).
2. Baraboi A., Leonte P., Hnatiuc E., *Unele aspecte privind construcţia şi funcţionarea reactoarelor comandate ortogonal.* CNEE, Timişoara, **9**, 9 (1982).
3. Dorozhko L.I., Libkind M.S., *Reaktory c poperečnym podmagničivaniem.* Izd. Energia, Moskva, 1977.
4. Baraboi A., Hnatiuc E., Furnică E., *Reactive Power Statical Source with Reactor Using Crossed Magnetic Fields.* Quality of Electrical Energy, Spala, Poland, **II**, 81 (1991).
5. Badea I., Broşteanu Gh., Chenzbraun I., Columbeanu P., *Protecţia prin relee şi automatizarea sistemelor electrice.* Ed. Tehnică, Bucureşti, 1973.

UTILIZAREA REACTORULUI COMANDAT ORTOGONAL ÎN TRATAREA NEUTRULUI INSTALAŢIILOR DE MEDIE TENSIUNE

(Rezumat)

Problema tratării neutrului instalaţiilor de medie tensiune are multiple rezolvări, soluţiile tehnice aplicate fiind diferite, de la legarea directă la pământ a punctului neutru (în ţări ca SUA, Canada), până la funcţionarea cu neutrul izolat (Italia). Parţial, în reţelele de medie tensiune din România, tratarea neutrului se realizează cu bobine de stingere, prevăzute cu dispozitive de reglare automată a gradului de acord.

Se prezintă posibilităţile de utilizare, cu rol de bobină de stingere, a unui reactor comandat ortogonal, determinându-se caracteristicile de reglare. Se evidenţiază avantajele soluţiei, legate în principal de procedeul reglării statice şi de proprietăţile reactorului comandat ortogonal: rapiditatea în răspuns şi liniarizarea caracteristicilor.

BULETINUL INSTITUTULUI POLITEHNIC DIN IAŞI
Tomul XLI (XLV), Fasc. 1-2, 1995
Secţia III
ELECTROTEHNICĂ. ENERGETICĂ. ELECTRONICĂ

C.D. 538.244.2

SUR LE CALCUL OPTIMAL DES ÉLECTRO-AIMANTS À COURANT ALTERNATIF

PAR
EUGEN HNATIUC et ADRIAN BARABOI

1. Introduction

Le calcul des électro-aimants monophasés à courant alternatif doit tenir compte des bagues de déphasage placées sur les pièces polaires [1]. Ce calcul devient optimal en réalisant „l'accord" des valeurs du rapport entre les aires embrassée et pas embrassée par la spire en court-circuit sur les pièces polaires, $m = S_1/S_2$ et les paramètres de cette bague, c'est-à-dire des valeurs de son angle de déphasage, φ_{sc}, en résultant des valeurs minimales de la section transversale du noyau ferromagnétique. Ainsi on indique pour les électro-aimants de type U-I les valeurs $m = 4$ et $\sin^2 \varphi_{sc} = 0,0625$, [1], [2].

Afin de respecter ces restrictions il est nécessaire d'adopter les valeurs du rapport m et de déterminer les valeurs nécessaires de la résistance électrique de la bague de déphasage, R_{sc}.

Dans ce qui suit on se propose d'évaluer la valeur de la résistance électrique de cette bague de déphasage, pour réaliser le calcul optimal de ces électro-aimants à courant alternatif.

2. Le schéma magnétique équivalent pour les pièces polaires munies avec de bagues de déphasage

La spire en court-circuit, placée sur l'une des pièces polaires des électro-aimants monophasés à courant alternatif, assure l'action locale des deux flux magnétiques ϕ_{e1} et ϕ_{e2} déphasés l'un par rapport à l'autres avec l'angle θ, [1], qui traversent les circuits magnétiques ayant la section transversale S_1 ou S_2. Les réluctances magnétiques $\Re_{e1}$ et $\Re_{e2}$ seront (v. Fig.1):

$$\Re_{e1} = \frac{\rho_{m1} l}{S_1}, \qquad \Re_{e2} = \frac{\rho_{m2} l}{S_2}. \tag{1}$$

Le schéma magnétique équivalent (v. Fig.2) met en évidence tant les réluctances des entrefers δ_{e1} et δ_{e2} que les composants $\Re_{sc}$, $\mathcal{X}_{sc}$ de l'impédance magnétique de la bague de déphasage, [3]:

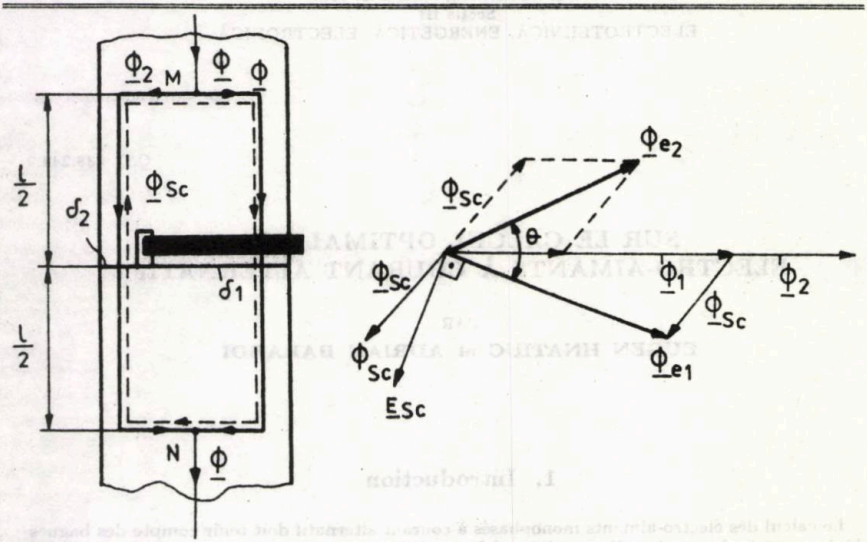

a b

Fig. 1

$$(2) \qquad \mathcal{R}_{sc} = \frac{\omega X_{sc}}{Z_{sc}^2}, \quad \mathcal{X}_{sc} = \frac{\omega R_{sc}}{Z_{sc}^2}, \quad \operatorname{tg}\varphi_{sc} = \frac{X_{sc}}{R_{sc}} = \frac{\mathcal{R}_{sc}}{\mathcal{X}_{sc}},$$

où R_{sc}, X_{sc}, Z_{sc} représentent la résistance électrique, la réactance inductive et l'impédance électrique de la spire en court-circuit et ω – la pulsation de la source.

Le fonctionnement à courant alternatif impose aussi à considérer les réactances magnétiques $\mathcal{X}_{e1}$ et $\mathcal{X}_{e2}$ (v. Fig.2) [3]:

$$(3) \qquad \mathcal{X}_{e1} = \frac{\rho_{x1} l}{S_1}, \qquad \mathcal{X}_{e2} = \frac{\rho_{x2} l}{S_2},$$

où les constantes ρ_{x1} et ρ_{x2} peuvent être obtenues à l'aide des courves $\rho_x(B)$ de la Fig.3.

La tension magnétique $\underline{U}_{M-N}$ peut être évaluée à l'aide des relations:

$$(4) \qquad \begin{cases} \underline{U}_{M-N} = [(\mathcal{R}_{e1} + \mathcal{R}_{\delta_1} + \mathcal{R}_{sc}) + j(\mathcal{X}_{e1} + \mathcal{X}_{sc})]\,\underline{\phi}_{e1} = \underline{U}_{me1}, \\ \underline{U}_{M-N} = [(\mathcal{R}_{e2} + \mathcal{R}_{\delta_2}) + j\mathcal{X}_{e2}]\,\underline{\phi}_{e2} = \underline{U}_{me2}. \end{cases}$$

À partir des relations (4) on peut représenter le diagramme vectoriel (Fig.4) où on met en évidence l'angle ε.

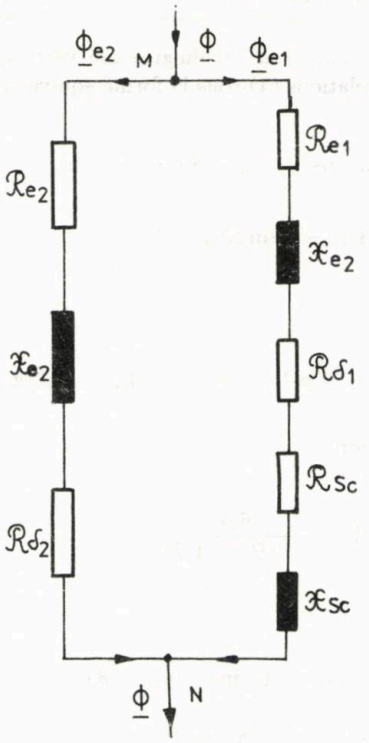

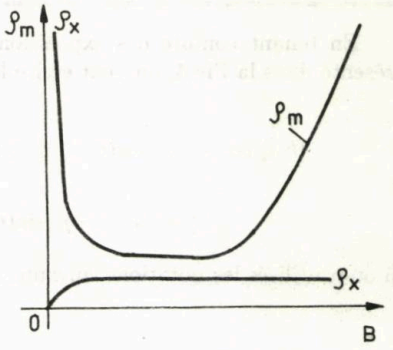

Fig. 3

Fig. 2

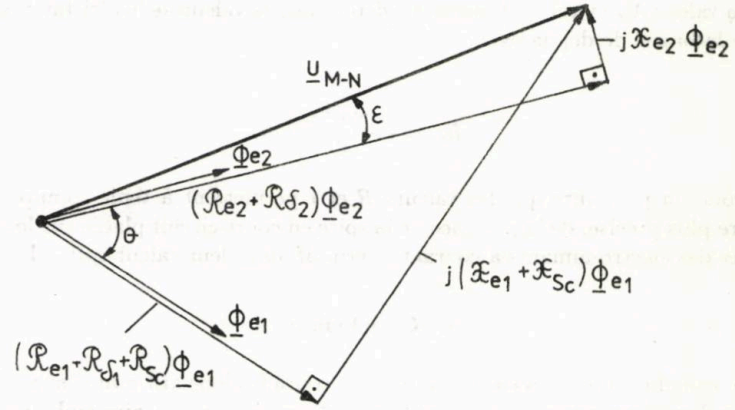

Fig. 4

En tenant compte des expressions (1),...,(3) et du diagramme vectoriel représenté dans la Fig.4, on peut écrire les relations (4) sous la forme équivalente:

$$\begin{aligned}&[k_1 Q\cos\varepsilon - k_2\cos(\theta+\varepsilon)]\,l + Q\mathcal{X}_{sc}\cos\varepsilon\,\mathrm{tg}\,\varphi_{sc} = \Re_{\delta_2}\cos(\theta+\varepsilon),\\ &[p_1 Q\sin\varepsilon - p_2\sin(\theta+\varepsilon)]\,l + Q\sin\varepsilon\mathcal{X}_{sc} = 0,\end{aligned} \tag{5}$$

où on a utilisés les notations suivantes:

$$\Re_{e1} = k_1 l,\quad \Re_{e2} = k_2 l,\quad \mathcal{X}_{e1} = p_1 l,\quad \mathcal{X}_{e2} = p_2 l,\quad Q = \frac{\phi_{e1}}{\phi_{e2}},\quad \Re_{sc} = \mathcal{X}_{sc}\,\mathrm{tg}\,\varphi_{sc}. \tag{6}$$

Le système d'équations (5) a les solutions:

$$l = \frac{B_2 C_1}{A_1 B_2 - A_2 B_1},\qquad \mathcal{X}_{sc} = \frac{A_2 C_1}{A_2 B_1 - A_1 B_2}, \tag{7}$$

où:

$$\begin{cases} A_1 = k_1 Q\cos\varepsilon - k_2\cos(\theta+\varepsilon),\quad A_2 = p_1 Q\sin\varepsilon - p_2\sin(\theta+\varepsilon),\\ B_1 = Q\cos\varepsilon\,\mathrm{tg}\,\varphi_{sc},\quad B_2 = Q\sin\varepsilon,\quad C_1 = \Re_{\delta_2}\cos(\theta+\varepsilon). \end{cases} \tag{8}$$

La valeur $\mathcal{X}_{sc}$ (v.rel.(7_2)) permet à déterminer la valeur de la résistance électrique de la bague de déphasage:

$$R_{sc} = \frac{\omega^2\cos^2\varphi_{sc}}{\mathcal{X}_{sc}}. \tag{9}$$

Donc on peut dire que les valeurs R et l permettent à tenir compte, d'une manière plus précise, de la présence de la spire en court-circuit placée sur les pièces polaires des électro-aimants à courant alternatif, dans leur calcul optimal.

3. Conclusions

Le calcul optimal des électro-aimants à courant alternatif munis avec des bagues de déphasage suppose „l'accord" des valeurs du rapport aire embrassée/aire pas embrassée des pièces polaires, m, avec les paramètres de ces spires en court-circuit, par l'intermédiaire des valeurs établies de l'angle φ_{sc}, [2], [4].

On propose d'adopter les valeurs du rapport m et puis, en tenant compte des conditions d'optimum indiquées ci-dessus, on détermine les valeurs nécessaires de

la résistance électrique de la bague en court-circuit, selon ce qui résulte des valeurs minimales de la section transversale du noyau ferromagnétique. Il faut ajouter aussi que le calcul de la bobine de l'électro-aimant devient plus précis à l'aide des valeurs de la tension magnétique U_{M-N} qu'on peut la déterminer avec les relations (4).

Reçue le 14 juin 1993

Université Technique „Gh. Asachi", Jassy, Chaire d'Énergétique

BIBLIOGRAPHIE

1. H n a t i u c E., *Sur le fonctionnement des électro-aimants monophasés à courant alternatif de type U-I munis avec des bagues de déphasage.* Bul. Inst. polit., Iaşi, **XXXIV (XXXVIII)**, *1-4*, s.III (1988).
2. H n a t i u c E., *Cu privire la proiectarea optimală a electromagneţilor monofazaţi de curent alternativ de tip U-I prevăzuţi cu spire ecran.* II-ème Symp. d'Appar. électr., 19-20 oct. 1989, Bucharest.
3. T a e v I.S., *Osnovy teorii električeskih apparatov.* Vysšaia Škola, Moskva, 1987.
4. H n a t i u c E., *Sur le fonctionnement des électro-aimants à courant alternatif de type E-I munis d'une bague de déphasage sur la colonne mediane du noyau magnétique.* Bul. Inst. polit., Iaşi, **XXXV (XXXIX)**, *3-4*, s.III (1989).

ASUPRA PROIECTĂRII OPTIMALE A ELECTROMAGNEŢILOR MONOFAZAŢI DE CURENT ALTERNATIV

(Rezumat)

Se propune luarea în considerare a particularităţilor de funcţionare ale spirelor ecran în zona pieselor polare şi a condiţiilor de optim din punct de vedere al „acordului" între raportul arie ecranată/arie neecranată faţă de parametrii electrici ai spirei, în scopul definirii unui algoritm capabil să permită proiectarea optimală a acestor electromagneţi.

BULETINUL INSTITUTULUI POLITEHNIC DIN IAŞI
Tomul XLI (XLV), Fasc. 1–2, 1995
Secţia III
ELECTROTEHNICĂ. ENERGETICĂ. ELECTRONICĂ

D.C. 621.397.5

PICTURE QUALITY RESTRICTIONS IN HDTV SYSTEMS

BY

R.J. GREEN

1. Introduction

The quality of television pictures in general, and high definition television pictures in particular, is a complex function of many factors. Those that may be exemplified include: a) correct luminance fidelity; b) correct colour rendition; c) aspect ratio correct, and no pin cushion and other geometric type distortions; d) good signal to noise ratio; e) low level of coding artefacts when compression is used.

In the assessment of picture quality, it is very useful to consider fundamental quality trade-offs, e.g. it is possible to increase the bandwidth of a television signal so that the sharpness of the image is optimized, but this is at the expense of bandwidth itself and signal to noise ratio. The quality of a picture is difficult to define because there are many variables which include experience of the observer, ambient lighting conditions, viewing distance, etc. The term HDTV implies a picture of high quality, but this is not so in all aspects of the picture at the same time. In any form of communication system, the electronic noise is the basic limitation to the achievement of desired performance. In TV systems of the current 4:3 aspect ratio type, the characterisation of noise is based on work of B a i r s t o w and C h r i s t o p h e r [1] of the 1960s. The implication is that the noise weighting characteristics in use now are mainly defined by monochrome criteria. Incomplete allowance has been made for the colorimetric noise in modern TV images, except for the use of low-base filter weighting of chrominance and luminance noise. Noise measurements tend to be made in the middle of the TV chain generally and not at the display end of the system, i.e. the consumer end.

2. Noise Analysis

For all video systems the ultimate limitation to performance lies is the noise which is always present in the head amplifiers. The noise in the sensors (CCDs

or vacuum tubes) tends to be masked by this head amplifier noise, which exists in the form of shot- and channel noise in the front end amplifier devices. The consequence of the process of acquisition for the signals from the sensor is that the noise spectrum at the output of the head amplifier tends to be triangular in nature, above a low frequency break point given by

$$F_0 = \frac{1}{\omega C_D R_L},$$

where C_D is the accumulated capacitance at the output of the sensor and the input device capacitance at the front end of the amplifiers, R_L the effective load resistance which is accounted for by the bias resistor and the input shunt resistance of the head amplifier front end device. Analysis of the noise spectrum at the output of the head amplifier leads to the conclusion that:

$$P_n = kB^3,$$

where B is the signal bandwidth.

This powerful function of noise with bandwidth may be demonstrated by a simple example. If a HDTV system of 20 MHz luminance bandwidth is considered, the signal to noise ratio at the output of the head amplifiers under identifiable conditions of light level and sensor response is 18 dB lower than for a standard video system of bandwidth 5 MHz. This implies either use of the HDTV cameras in higher lighting conditions or a degradation of picture quality. One of the problems with the many HDTV systems being proposed is the apparent lack of compatibility between them. No two are directly comparable because of the different coding/compression methods utilised. The question is how might they be compared? One way is to analyse the underlying system aspects which are in common. A meaningful comparison may then be made, albeit tentatively.

3. Display Signal to Noise Ratio (DSNR)

The basis of the comparison between such systems is an examination of the fundamental luminance and chrominance signal coding and decoding. Other signal processing will add to the complexity of the system model. A figure of merit, known as the Display Signal to Noise Ratio, is utilised, based on real system measurements and simulation [2]. This figure of merit takes into account the essential coding and decoding process in any TV system which has been designed around compatibility with monochrome. This model in order to achieve this method of assessment, may be modified easily to accommodate variations in the ratio of, for example, luminance to chrominance bandwidths, and also different luminance bandwidths themselves. A very important feature of this figure of merit is the ability to distinguish between luminosity noise and chromaticity noise, as distinct from luminance noise achieved in current assessment methods. Fig.1 shows the block diagram of a whole TV chain, taking into account the essential signal processing referred to. As far as limiting noise is concerned, the important features include noise added in

the head amplifiers ($n_r(t)$, etc.), gamma correction, coding–decoding and display gamma, etc. Within the coding–decoding matrix, further signal processing takes place, as shown in Fig.2, which gives the example of a standard TV system for which the luminance bandwidth was chosen to be 5 MHz. The individual signal processing blocks may, of course, be modified for any system such as HDTV, in which the basic luminance bandwidth may extend to over 12 MHz.

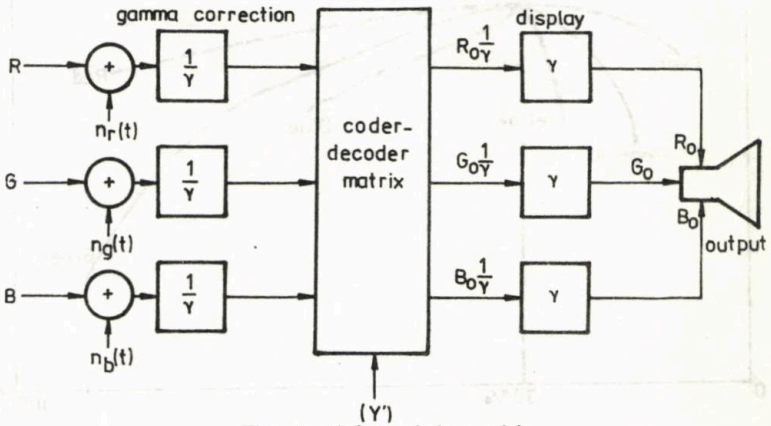

Fig. 1.– Colour chain model.

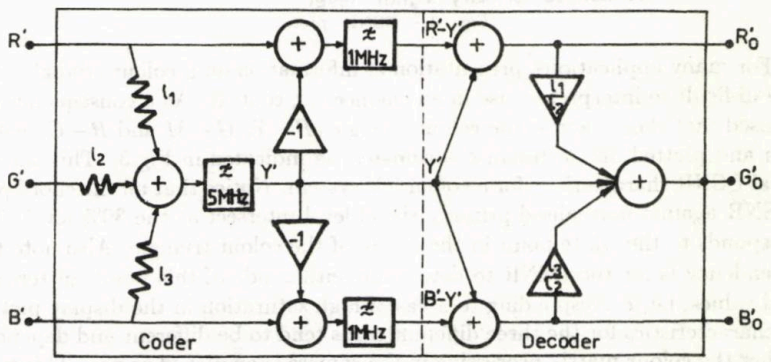

Fig. 2.– Internal form of coder-decoder block.

In view of certain statistical properties of a standard TV signal, the following conditions are proposed for the definition of the display signal to noise ratio:

1. All evaluations are undertaken for 30% luminance, which corresponds to the peak value of luminance which is transmitted for 90% of air time.

2. For objective tests, a cathode ray tube simulator is employed. This has the same non-linear characteristics as the real display tube, but allows electronic measurements of the noise as distinct from visual tests undertaken by eye.

3. In the case of subjective tests, the environment surrounding the monitor being viewed is set at 10% peak luminance, which statistically is the average luminance.

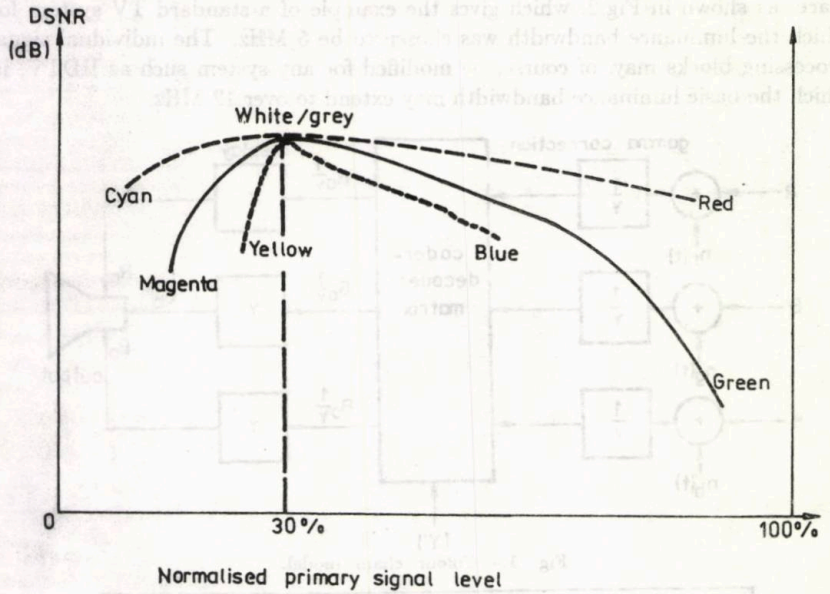

Fig. 3.– DSNR plot.

For many applications, presentation of information on a colour triangle tends to be difficult to interpret or use in an engineering context. As a consequence it is proposed that chords across the colour triangle ($B-Y$, $G-M$ and $R-C$) will be taken and plotted on Cartesian co-ordinates, as indicated in Fig.3. This shows a typical DSNR characteristic for a colour TV system. Notice that all the chord plots of DSNR against normalised primary signal level intersect at the 30% level. This corresponds to the white point in the centre of the colour triangle. Also note that the tendency is for the DSNR to deteriorate either side of this point, in terms of signal values, i.e. corresponding to areas of high saturation in the display picture. The characteristics for the three different cords tend to be different and depend on whether the colour matrix processing in the camera is employed or not. This tends to emphasise noise in certain parts of the colour space and reduce its visibility in other parts.

4. Application of the DSNR Evaluation in Three Example HDTV Systems

The three HDTV systems examined were: a) MAC (Multiplexed Analogue Component video); b) MUSE (Japanese sub-Nyquist proposals); c) NYIT (New York Institute of Technology).

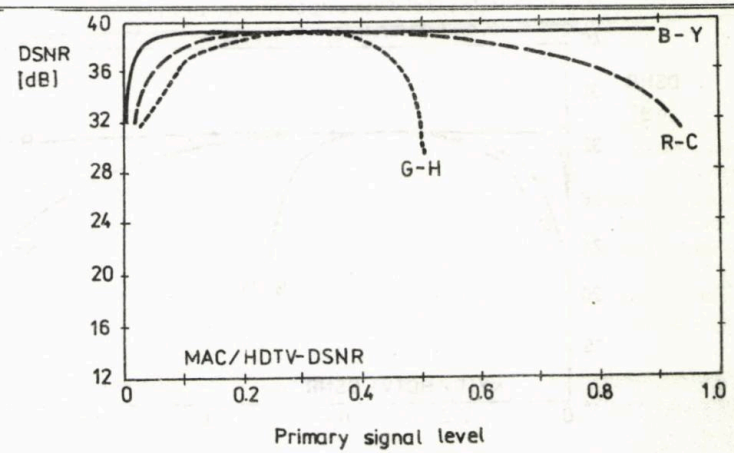

Fig. 4.– MAC.

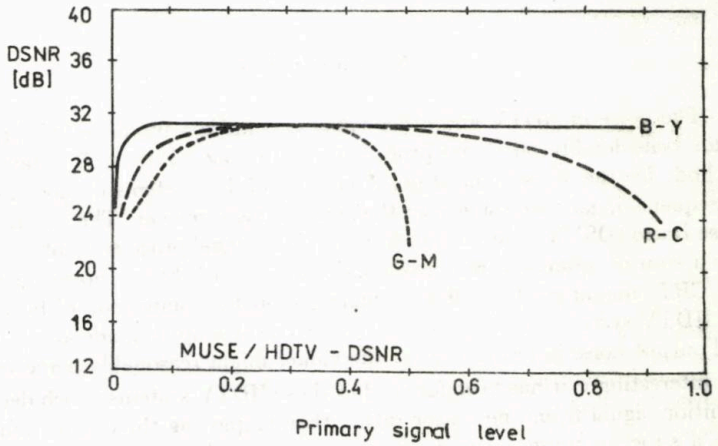

Fig. 5.– MUSE.

No allowance was made for digital artifacts for the comparison. Figs.4,...,6 indicate the DSNR plots for the three systems, respectively, under the same starting conditions, under the same CCIR-defined signal to noise ratios at the head amplifiers. The MAC system was found to be the best under the test conditions, with a DSNR of 39 dB for greys at 30% luminance. The NYIT system was found to be second best with a DSNR of 23 dB and the MUSE at a DSNR of 35 dB, again at the white point. The reason for this difference is concerned with how the individual systems see the primary signal bandwidths. For example, the NYIT system uses a monochrome luminance signal rather than employing three broad band primary signals.

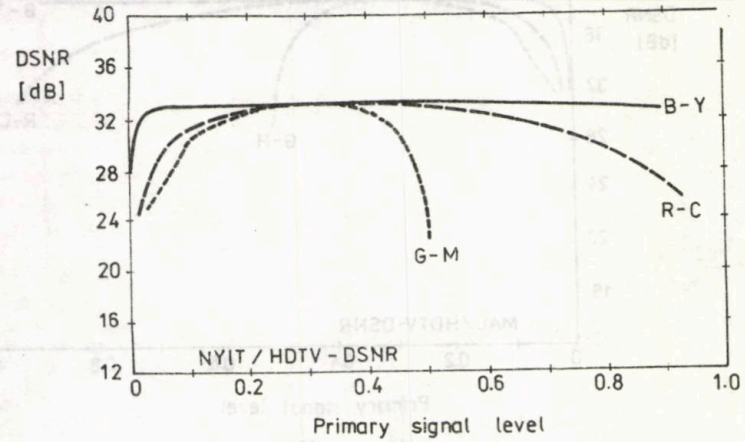

Fig. 6.- NYIT.

5. Conclusions

The noise in HDTV and other video systems is a fundamental limit and depends considerably on signal processing at all stages in the TV chain. Current methods for the assessment of noise qualities of TV systems do not allow for the subsequent signal processing after the point of measurement. The Display Signal to Noise Ratio (DSNR) takes in much more of the signal processing into account and uses a sum of squares of red, green and blue channel display noise, with the help of a CRT simulator. This allows a more reasonable comparison of both standard and HDTV systems. bearing in mind that some attempt is made at evaluating the final output noise in terms of what the viewer might reasonably perceive.

Interestingly, it has been found that those HDTV systems which derive a high definition signal from one sensor rather than employing three wide band signals, have a superior noise performance and consequently picture quality. This also means that these systems are, in effect, more sensitive and can operate in lower light conditions. This in turn means that their application areas, for various dramatic effects, are more diverse ad more easily accommodated.

Received, February 2, 1994

Electronic Imaging Unit,
Bradford University England, UK

REFERENCES

1. Barstow J.M., Christopher H.N., *Measurements of Random Video Interferance to Monochrome Colour TV Pictures.* Commun. a. Electronics, 312-320 (1962).

2. Green R.J., Selvan B., *Objective Noise Performance Evaluation of Component Video Signals Using an Electronic Colour Video Simulator.* IEEE Trans. on Broadcasting, **38**, *3*, 327-330 (1993).

RESTRICŢII ÎN CALITATEA IMAGINILOR TV DE ÎNALTĂ FIDELITATE

(Rezumat)

Se prezintă o metodă de evaluare cantitativă a calităţii sistemelor TV de înaltă definiţie, bazată pe determinarea raportului semnal de imagine / zgomot.

Criteriul de apreciere a performanţelor unui sistem TV bazat pe măsurarea raportului semnal de imagine / zgomot are în vedere procesul de codare – decodare TV color, putându-se face, astfel, o distincţie între zgomotul de luminanţă şi cel de crominanţă.

Condiţiile în care se defineşte raportul semnal de imagine / zgomot pentru un semnal TV standard normat sunt: a) luminanţă 30%; b) la ieşirea lanţului video, în locul tubului cinescop, se plasează un simulator de tub catodic permiţând măsurarea obiectivă pe cale electronică a zgomotului de imagine în locul aprecierii vizuale; c) pentru aprecieri subiective ale raportului semnal de imagine / zgomot mediul ambiant de vizualizare a imaginii va avea o luminanţă echivalentă cu 10% din luminanţa maximă a imaginii TV.

BULETINUL INSTITUTULUI POLITEHNIC DIN IAŞI
Tomul XLI (XLV), Fasc. 1-2, 1995
Secţia III
ELECTROTEHNICĂ. ENERGETICĂ. ELECTRONICĂ

C.D. 535.61-15; 621.39

SYSTÈME MULTICANAL DE TÉLÉCOMMANDE PAR RAYONNEMENT INFRAROUGE
LE DÉCODEUR

PAR
LAURENŢIU DIMITRIU

1. Introduction

Les systèmes de télécommande par rayonnement infrarouge sont les plus utilisés pour les applications courantes (la télécommande d'un téléviseur, par exemple), grâce à leur prix réduit et à leur portée suffisante.

À l'aide d'une méthode originale [1], on a réalisé un système multicanal pour 11 canaux.

Dans ce qui suit on présente la réalisation du décodeur, conformément au principe mentionné ci-dessus.

2. Le schéma synoptique du décodeur

Le signal reçu par le décodeur est sous la forme des trains d'impulsions de basse fréquence. Le récepteur fournit ce signal sous la forme TTL. La forme du signal est présentée dans la Fig.1.

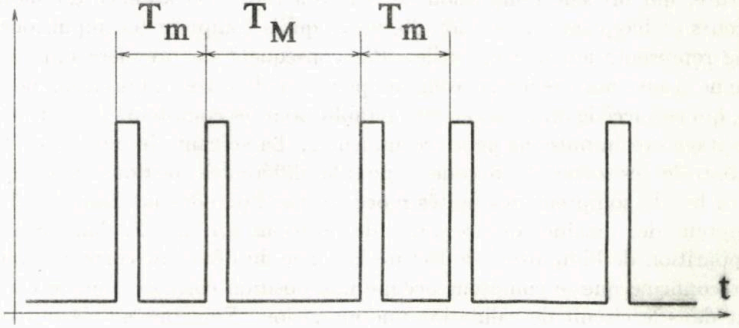

Fig. 1

Si on note par $0,1,...,8,9,C$ les 11 canaux, un canal $0,1,...,8,9$ sera défini conformément à [1] par une des valeurs de temps pour T_m ou T_M:

(1) $(10k+2)t$, $(10k+3)t$, $(10k+4)t$, $(10k+5)t$, $(10k+6)t$, $(10k+7)t$, $(10k+8)t$,

où $k = 4,5,6,7,8$ et $t = t_m$ ou $t = t_M$; t_m et t_M doivent satisfaire la condition:

$$\frac{t_m}{t_M} < \frac{3}{7}, \tag{2}$$

pour une séparation correcte des canaux [1].

L'identification de la commande C nécessite la réalisation simultanée d'une paire de la forme [1]:

$$T_m = (96 \text{ ou } 97 \text{ ou } 98)t_m \quad \text{et} \quad T_M = (96 \text{ ou } 97 \text{ ou } 98)t_M. \tag{3}$$

Le schéma synoptique du décodeur qui permet l'identification des canaux définis par les relations (1),...,(3) est présenté dans la Fig.2.

Le circuit de déclenchement des signaux fournit au début de chaque période du signal capté par le récepteur des impulsions de lecture, READ, et de remise à zéro des compteurs, RESET. Les canaux *0,1,2,3,4* sont décodés par la section: base de temps étalon *1*, compteur *1*, décodeur *1*, validation *1* et les canaux *5,6,7,8,9* par la section: base de temps étalon *2*, compteur *2*, décodeur *2*, validation *2*. L'impulsion de remise à zéro, d'une durée très réduite, met à l'état zéro les compteurs. Depuis, les compteurs comptent les impulsions des bases temps étalon. Le moment où le compteur occupe les positions $10x + 2$, $(x = 4,5,6,7,8)$, le décodeur pour le canal respectif change son état. Il revient à l'état initial après une impulsion de remise à zéro ou le compteur a dépassé la position $10x+8$, $(x = 4,5,6,7,8)$. Un compteur est constitué en fait de deux compteurs décimaux montés en cascade: l'un comptant les unités et l'autre les dizaines. La sélection d'un canal est réalisée par l'impulsion de lecture, qui précède l'impulsion de remise à zéro. En absence du signal, les compteurs se bloquent en position 99, après qu'ils comptent 99 impulsions. Cet état ne représente aucun code utile. Par conséquent, la première impulsion de lecture ne trouve aucune information qui peut être décodée. L'impulsion de remise à zéro, qui se succède immédiatement, rétablit pour les compteurs la position 00 et le comptage des impulsions peut recommencer. La suivante impulsion de lecture peut contrôler les sorties des décodeurs pour les différentes positions des compteurs. Dans ce but le compteur des unités n'occupe pas l'une des positions 9,0,1 et/ou le compteur des dizaines occupe l'une de positions 0,1,2,3. Si dans le moment de l'apparition de l'impulsion de lecture la sortie du décodeur correspondante au code x confirme que le compteur occupe une position correcte pour le canal, on obtient dans le circuit de validation une impulsion. Évidemment, la durée entre deux impulsions de lecture est fixée par le canal sélectionné.

Pour éviter les fausses commandes, dues aux régimes transitoires ou aux impulsions parasites captées, on utilise une intégration des impulsions délivrées par le circuit de validation. À ce fin les impulsions sont unifiées à l'aide de l'étage mixer

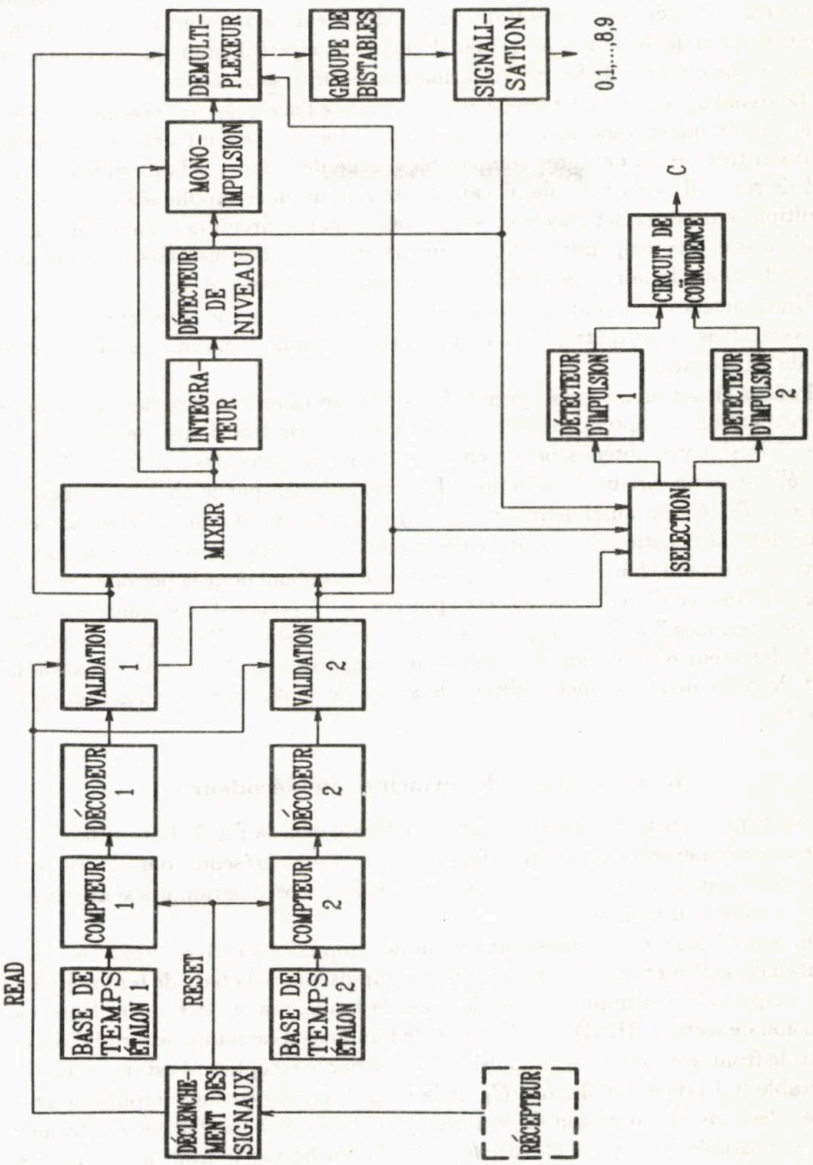
READ
BASE DE TEMPS ÉTALON 1
COMPTEUR 1
DÉCODEUR 1
VALIDATION 1
RESET
BASE DE TEMPS ÉTALON 2
COMPTEUR 2
DÉCODEUR 2
VALIDATION 2
DÉCLENCHEMENT DES SIGNAUX
RÉCEPTEUR
MIXER
INTEGRATEUR
DÉTECTEUR DE NIVEAU
MONO-IMPULSION
DEMULTI-PLEXEUR
GROUPE DE BISTABLES
SIGNALISATION
0,1,...,8,9
DÉTECTEUR D'IMPULSION 1
DÉTECTEUR D'IMPULSION 2
SELECTION
CIRCUIT DE COÏNCIDENCE
C

Fig. 2

et appliquées à un circuit intégrateur. Seulement l'application répétitive du signal utile permet de dépasser le seuil du circuit détecteur de niveau. Par conséquent, seulement pour la situation où le signal capté est répétitif pour quelques fois, en signifiant une commande ferme, l'information décodée serra utilisée.

Le signal de sortie du détecteur de niveau valide l'accès des impulsions délivrées par le circuit mixer vers un circuit monoimpulsion. Ce circuit délivre une seule impulsion très brève, de durée comparable à celle de lecture, à la modification de l'état de sortie du détecteur de niveau. Cette impulsion est appliquée à un circuit démultiplexeur et permet l'accès du signal délivré par le circuit de validation vers la bascule bistable correspondante du groupe de bistables. Les bistables fonctionnent comme diviseurs binaires; pour chaque commande ils changent leur état.

Une nouvelle commande est possible seulement après que le détecteur de niveau est revenu dans l'état d'attente. L'état de chaque canal est indiqué en utilisant le LED de signalisation.

Pour la situation du canal spécial C, les deux sections *1* et *2* du décodeur (base de temps étalon, compteur, décodeur, validation) travaillent d'une manière simultanée. Les signaux obtenus par le chronométrage des périodes $T_m(C)$ et $T_M(C)$ sont délivrés à un circuit de sélection. Le signal obtenu par le chronométrage de la période $T_M(C)$ est aussi délivré vers l'étage mixer et il est traité également tout comme dans la situation du décodage des canaux *0,1,...,8,9*. Après l'intégration, le détecteur de niveau change son état. Cet état est maintenu pour la période pendant la quelle la touche C de l'émetteur est appuyée. La présence d'une manière simultanée des périodes $T_m(C)$ et $T_M(C)$ assure le changement de l'état aux sorties des circuits détecteur d'impulsion *1* et détecteur d'impulsion *2*. Dans cette situation le circuit de coïncidence permet d'obtenir le signal de confirmation de l'action de la touche C.

3. Le schéma de principe du décodeur

Le schéma de principe du décodeur est présenté dans la Fig.3. Les oscillogrammes de fonctionnement pour le décodage du canal *0* sont présentés dans la Fig.4 et pour le décodage de la commande C dans la Fig.5. Les oscillogrammes sont relevés en divers points du montage.

On a noté par: t – la durée maximum des impulsions délivrées par les deux monostables de l'émetteur; t_1 – la période des impulsions de la base de temps étalon *1*; t_2 – la période des impulsions de la base de temps étalon *2*; t_3 – la durée de l'impulsion de lecture READ; t_4 – la durée de l'impulsion de remise à zéro RESET.

Sur le front ascendant de l'impulsion fournie par le récepteur il est déclenché le monostable IC1 (type 74123), R_1, C_1. À la sortie *5* on obtient une impulsion avec la durée de 3 ms. L'impulsion de lecture, ayant la durée $t_3 = 250$ μs, est formée par le monostable IC1 (type 74123), R_2, C_2, déclenché par le front ascendant de l'impulsion du premier monostable. Sur le front descendant de l'impulsion de lecture on déclenche le monostable IC2 (type 74121), R_3, C_3. On obtient l'impulsion de remise à zéro, RESET, qui a une durée $t_4 = 150$ μs. La base de temps étalon

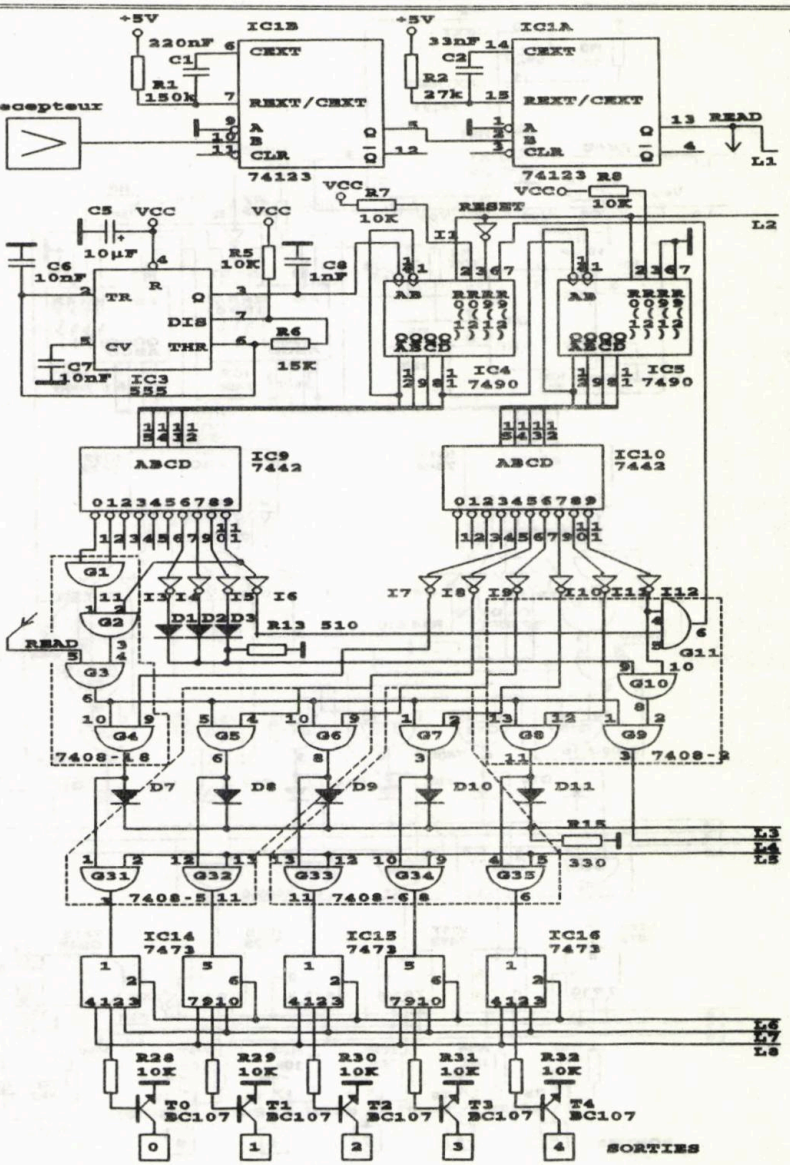

Fig. 3*a*

1 est réalisée par le circuit intégré IC3 (type 555). On peut régler la fréquence en actionnant le curseur de l'ajustable S_6, de façon que la période du signal ait une valeur de 200...400 μs. Le réglage est nécessaire pour mettre au point le décodeur.

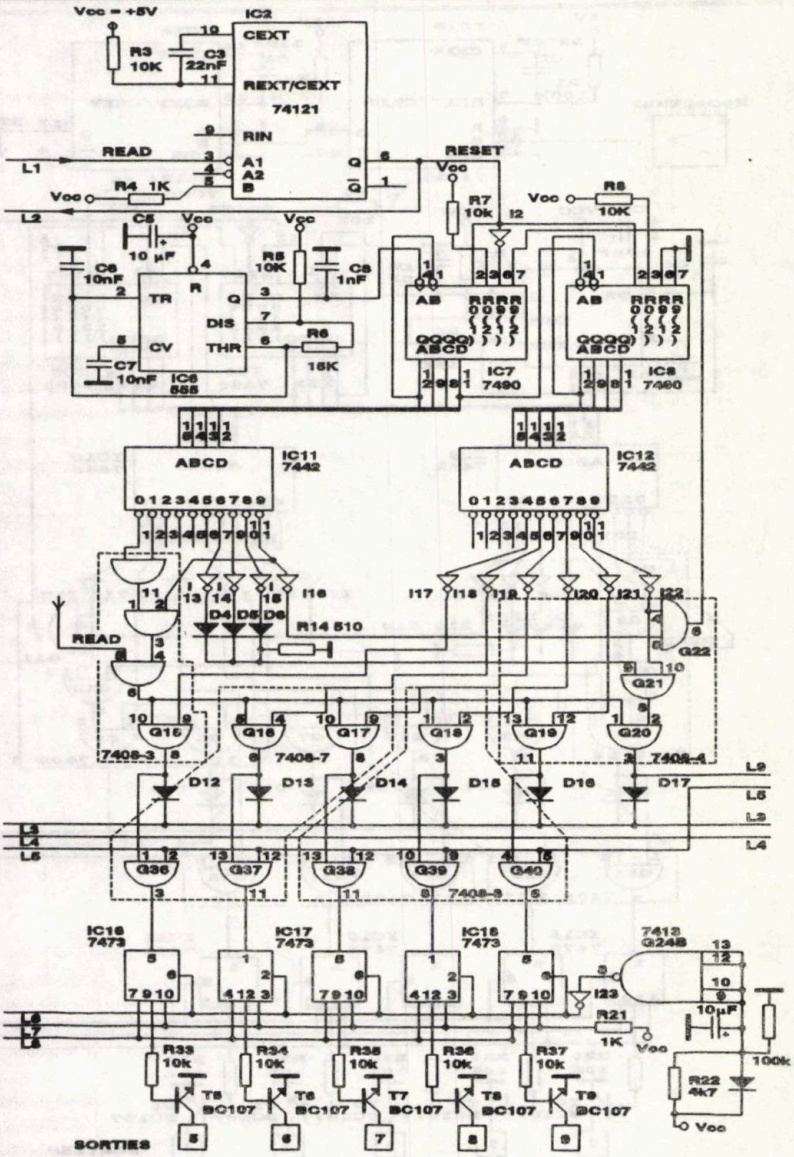

Fig. 3*b*

La base de temps étalon 2 est réalisée par un circuit intégré de type 555, IC6. Le réglage est assuré par l'ajustable S_{10}, la période du signal ayant une valeur de 697...835 μs.

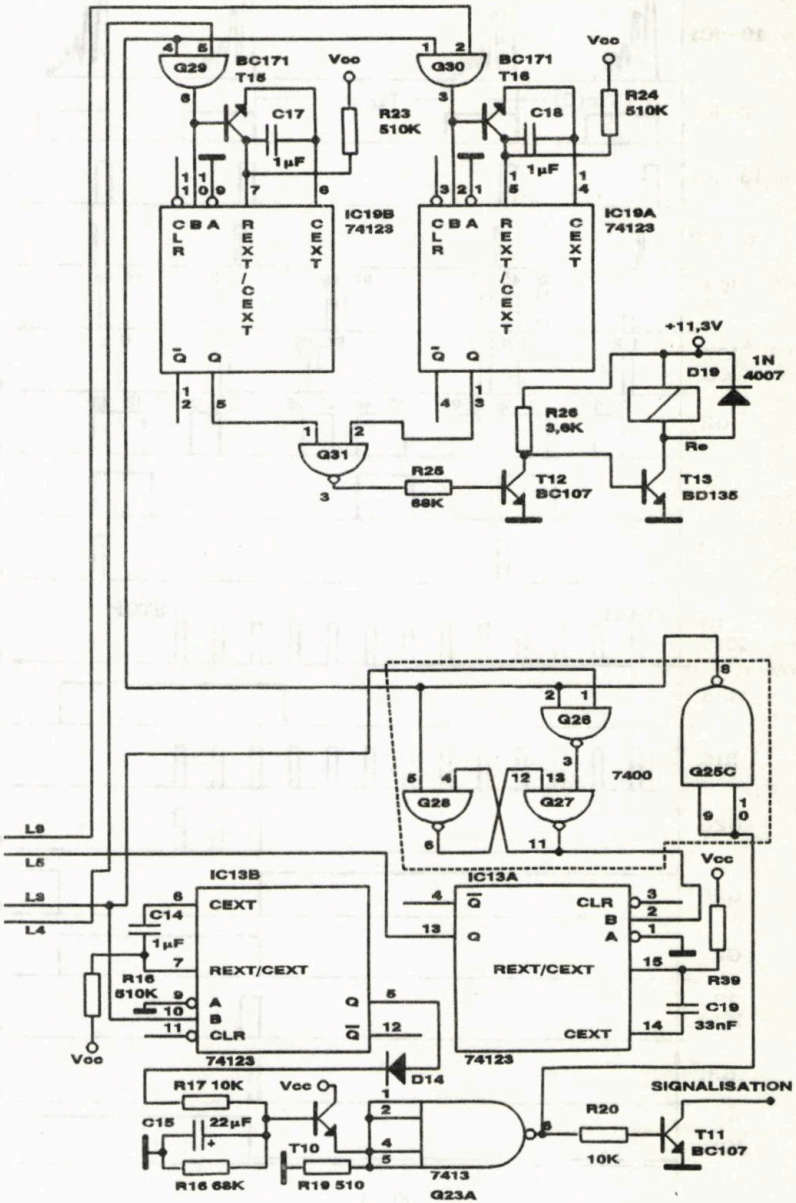

Fig. 3 *c*

Les valeurs centrales des deux périodes pour les bases de temps étalons résul-

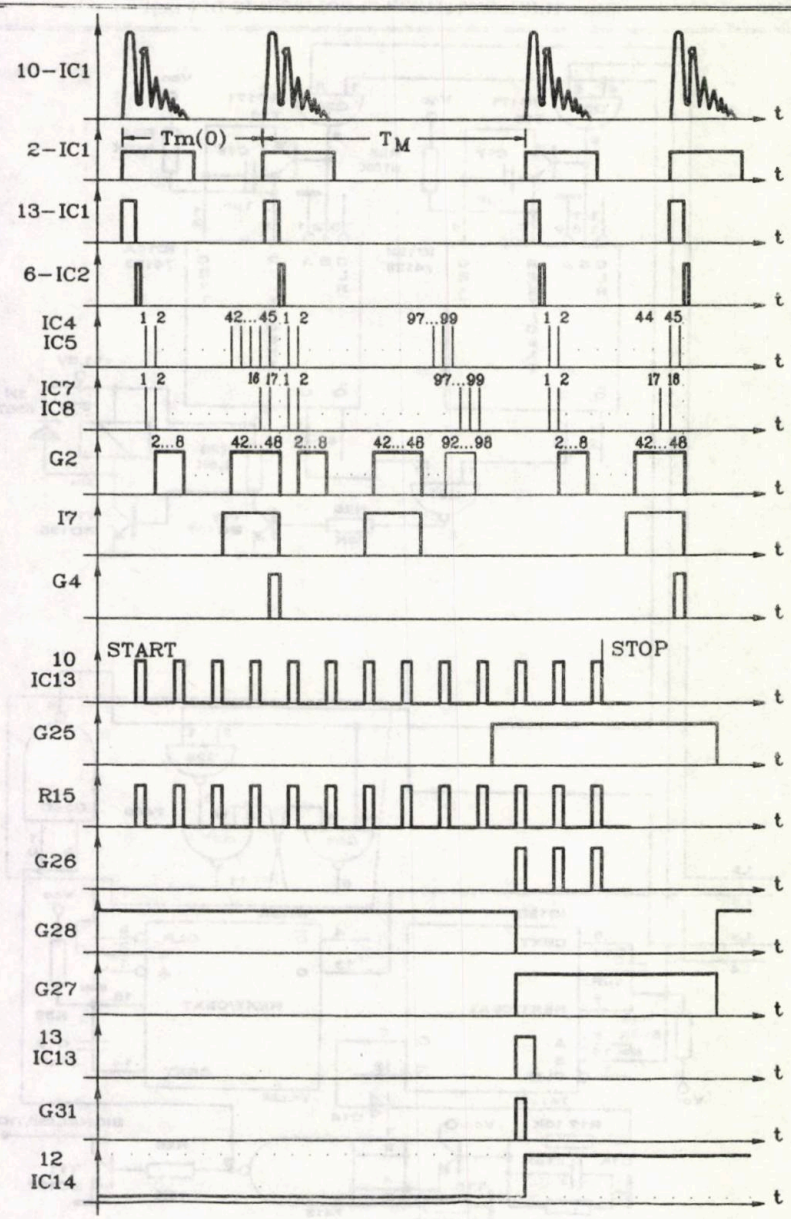

Fig. 4

tent de la condition que les deux durées $T_m(C)$ et $T_M(C)$ du canal C correspondent

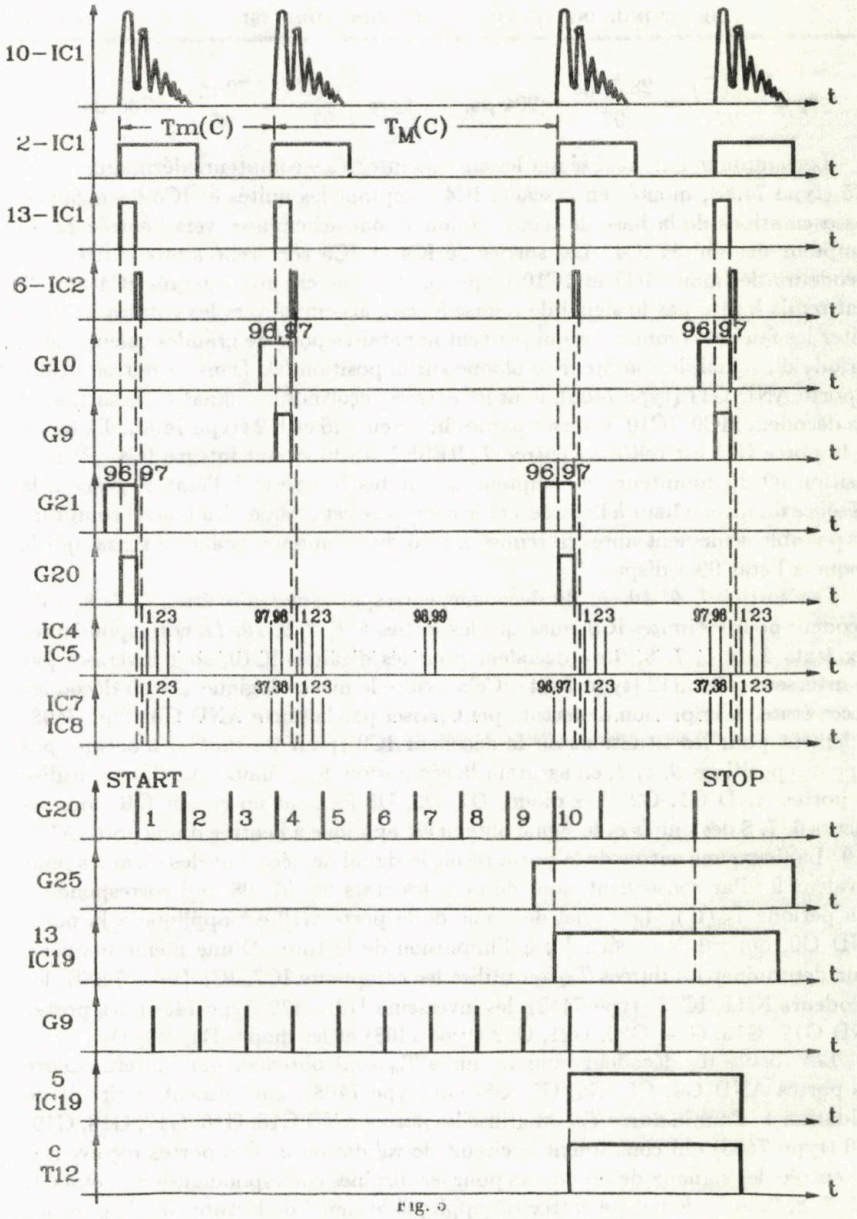

Fig. 5

à 97 périodes t_1 et, respectivement, t_2. Les valeurs 96 et 98 sont aussi correctes, mais on a choisi 97 pour compenser l'instabilité dans le temps. Par conséquent:

$$t_1 = \frac{T_m(C)}{97} = \frac{28.5 \text{ ms}}{97} = 294 \ \mu\text{s}, \qquad t_2 = \frac{T_M(C)}{97} = \frac{72 \text{ ms}}{97} = 736 \ \mu\text{s}.$$

Le compteur *1* est réalisé par les circuits intégrés – compteurs décimaux – IC4, IC5 (type 7490), montés en cascade, IC4 comptant les unités et IC5 les dizaines. Les oscillations de la base de temps étalon *1* sont acheminées vers l'entrée *14* du compteur des unités IC4. Les sorties de IC4 et IC5 sont reliées aux entrées des décodeurs décimaux IC9 et IC10 (type 7442). Les circuits intégrés IC4 et IC5 sont remis à zéro par le signal de remise à zéro, acheminé vers les entrées *2*. Pour éviter les fausses commandes qui peuvent apparaître pour de grandes valeurs de la période du signal, le compteur se bloque sur la position 99. Dans ce but on utilise la porte AND G11 (type 7408), dont les entrées reçoivent les signaux des sorties *11* des décodeurs IC9, IC10, inversés par les inverseurs I6 et I12 (type 7404). La sortie de la porte G11 est reliée à l'entrée *7* (RESET 9) du circuit intégré IC4. Pour la position 99 du compteur, le compteur des unités IC4 reste à l'état *9*, grâce à la présence du niveau haut à l'entrée *7* et le comptage est bloqué. Un nouvel comptage est possible seulement après la remise à zéro du compteur, quand le signal qui le bloque à l'état 99 a disparu.

Les sorties *7, 9, 10, 11* du décodeur, correspondantes aux états 6, 7, 8, 9 du décodeur pour les unités IC9, aussi que les sorties *5, 6, 7, 9, 10, 11*, correspondantes aux états 4, 5, 6, 7, 8, 9 du décodeur pour les dizaines IC10, sont inversées par les inverseurs I3,...,I12 (type 7404). Cela assure le niveau logique „1" au décodage de ces états. L'impulsion de lecture peut passer par la porte AND G3 (type 7408) seulement pour les situations où le décodeur IC9 (pour les unités) n'occupe pas l'une des positions *9, 0, 1*, en assurant la séparation des canaux. A ce fin on utilise les portes AND G1, G2. Les diodes D1, D2, D3 forment un circuit OR pour les valeurs 6, 7, 8 des unités et le signal obtenu est appliqué à l'entrée d'une porte AND G10. La deuxième entrée de la porte reçoit le signal de décodeur des dizaines pour la valeur 9. Par conséquent, sont décodés les états 96, 97, 98, qui correspondent à la période $T_m(C)$. Le signal de sortie de la porte G10 est appliqué à la porte AND G9, qui valide ce signal par l'impulsion de lecture. D'une même manière, pour déterminer les durées T_M on utilise les compteurs IC7, IC8 (type 7490), les décodeurs IC11, IC12 (type 7442), les inverseurs I13,...,I22 (type 7404), les portes AND G12, G13, G14, G20, G21, G22 (type 7408) et les diodes D4, D5, D6.

Les sorties du décodeur pour la durée T_m sont obtenues par l'intermédiaire des portes AND G4, G5, G6, G7, G8, G9 (type 7408), qui forment le circuit de validation *1*. Pour la durée T_M on utilise les portes AND G15, G16, G17, G18, G19, G20 (type 7408) qui constituent le circuit de validation *2*. Ces portes reçoivent à une entrée des signaux de décodeurs pour les dizaines correspondantes aux états 4, 5, 6, 7, 8, 9. À la deuxième entrée est appliqué le signal de lecture, validé pour les états 2, 3, 4, 5, 6, 7, 8, des unités. Les sorties de ces portes sont reliées aux diodes D7, D8, D9, D10, D11, D12, D13, D14, D15, D16, D17 qui forment un circuit OR (le circuit mixer). Les impulsions du circuit OR sont utilisées pour déclencher le monostable IC13 (type 74123), R_{14}, C_{14}. Les impulsions ainsi générées ont une

durée de 143 ms et sont appliquées à un circuit intégrateur R_{17}, C_{15}, R_{18}. Le signal de l'intégrateur est capté par le suivre T10 et appliqué à un Trigger Schmitt G23 (type 7413). Quand les impulsions du circuit mixer sont répétitives, la capacité C_{15} se charge et le niveau de tension dépasse le seuil Schmitt de façon que la sortie du Trigger enregistre un état bas. Dans ce moment le signal est décodé et l'information peut être utilisée. Un LED de signalisation, commandé par le transistor T11, indique cette situation. Cette porte reçoit à une entrée le signal inversé du Trigger et à l'autre entrée le signal du mixer. À la première impulsion du mixer, après avoir dépassé le seuil Schmitt, le bistable $R-S$ passe à l'état haut de la sortie de la porte G27. De cette manière on déclenche le monostable IC13 (type 74123), R_{39}, C_{19} qui délivre une seule impulsion pour un état décodé. Si la touche de l'émetteur est maintenue appuyée, l'intégrateur reçoit d'une manière continuelle des impulsions et l'état du Trigger Schmitt ne se modifie pas. Pour une nouvelle commande il faut renoncer d'appuyer la touche. L'intégrateur ne reçoit pas des impulsions, l'état du Trigger Schmitt se modifié et le bistable $R-S$ revient à l'état bas à la sortie de la porte $G27$. L'impulsion du monostable IC13, R_{39}, C_{19} est appliquée au circuit démultiplexeur réalisé par les portes AND $G31$, $G32,...,G40$ (type 7408). Les sorties de ces portes délivrent une seule impulsion quand un canal *0, 1,...,8, 9* est décodé. Ces impulsions sont utilisées pour actionner les bistables de mémoire IC14, IC15,...,IC18 (type 7473), qui fonctionnent comme diviseurs binaires. À la mise sous tension du montage, les bistables sont remis à zéro par le circuit formé par la résistance R_{22}, la capacité C_{19}, le Trigger Schmitt G_{24} (type 7413) et l'inverseur $I23$ (type 7404). Les états des bistables sont affichés par des LED de signalisation, commandés par les transistors T0, T1,...,T9. Les sorties des bistables peuvent être utilisées pour actionner de différents circuits. Si l'on actionne pour la première fois une touche, le bistable correspondant au canal sélectionné passe à l'état haut et à la deuxième il revient à l'état bas.

La commande C est décodée de la manière suivante: les impulsions correspondantes à la durée $T_M(C)$ sont décodées et validées par la section *2* et appliquées au mixer par la diode D17. Ces impulsions sont utilisées à la commande de l'intégrateur et du trigger Schmitt. Quand la commande C est détectée, la sortie de l'inverseur $G25$ passe à l'état haut et valide les portes AND $G29$, $G30$ (type 7408). La porte $G29$ reçoit sur l'autre entrée le signal de validation 1 pour le signal $T_m(C)$ (la porte $G9$). Les impulsions de sortie sont utilisées pour déclencher le monostable retriggerable IC19 (type 74123), R_{23}, C_{17}. La durée de l'impulsion générée est plus grande que $T_m(C)+T_M(C)$. De cette façon, pour l'entière période d'action de la touche C, la sortie *5* du monostable a un niveau haut. De même façon le monostable retriggerable IC19 (type 74123), R_{24}, C_{28}, délivre à la sortie *13* un niveau haut pour la période d'action de la touche C. Tenant compte que la commande C suppose l'existence d'une manière simultanée des durées $T_m(C)+T_M(C)$, la porte NAND $G31$ (type 7400) fournit à la sortie un niveau bas. Le signal de sortie de la porte $G31$ actionne l'amplificateur réalisé par les transistors T12, T13, les résistances R_{25}, R_{26}, la diode D19. L'amplificateur permet de fermer un relais R_e pendant toute la période que la touche C est appuyée. À la libération de la touche,

après un retard donné par l'intégrateur, le relais est ouvert.

Dans la Fig.3 sont précisées les valeurs des composantes utilisées. Les diodes D1, D2,...,D18 sont du type AA 112.

4. Les problèmes technologiques

Pour la réalisation pratique du décodeur on doit considérer les problèmes suivants:

a) Une bonne stabilité des périodes des signaux des bases de temps étalon. Pour satisfaire à cette demande on a utilisé pour les oscillateurs des résistances à pellicule métallique, des capacités de bonne qualité et très stables dans le temps (mylar) et des ajustables de type CERMET.

b) Un petit courant consommé par le décodeur peut être obtenu en utilisant des circuits intégrés CMOS.

c) La mise au point du décodeur est très simple; en effet on appuis n'importe quelle touche *0, 1, 2, 3, 4,* et on agit le curseur de l'ajustable S_6 pour obtenir à la sortie la confirmation de la commande activée. Puis on vérifie les autres canaux et s'il est nécessaire on refait le réglage. D'une façon similaire, pour les canaux *5, 6, 7, 8, 9* on agit le curseur de l'ajustable S_{10}. Finalement on vérifie le fonctionnement de la commande *C*.

5. Conclusions

En utilisant le schéma de principe, avec les valeurs indiquées dans la Fig.3, on a réalisé un décodeur pour des systèmes de télécommande par rayonnement infrarouge, caractérisé par: a) le contrôle de 11 canaux; b) stabilité excellente dans le temps; c) les sorties compatibles TTL.

Reçue le 15 décembre 1993

Université Technique „Gh.Asachi", Jassy,
Chaire d'Électronique appliquée

BIBLIOGRAPHIE

1. Dimitriu L., Oriţă C., Cârstescu A., *Une méthode de réalisation d'un système multicanal de télécommande par rayonnement infrarouge.* Bul. Inst. polit., Iaşi, **XXXII (XXXVI)**, *1-4*, s.III (1986).
2. Dimitriu L., Oriţă C., Cârstescu A., *Système multicanal de télécommande par rayonnement infrarouge. L'émetteur.* Bul. Inst. polit., Iaşi, **XXXIII (XXXVII)**, *1-4*, s.III (1987).
3. Dimitriu L., Oriţă C., Cârstescu A., *Système multicanal de télécommande par rayonnement infrarouge. Le récepteur.* Bul. Inst. polit., Iaşi, **XXXIV (XXXVIII)**, *1-4*, s.III (1988).

SISTEM DE TELECOMANDĂ MULTICANAL CU RADIAŢIE INFRAROŞIE
Decodorul
(Rezumat)

Se prezintă schema bloc, schema de principiu şi formele de undă pentru un decodor folosit într-un sistem de telecomandă cu radiaţie infraroşie. Se precizează modul de funcţionare şi se indică valorile componentelor. În final se indică modul de reglare a montajului şi căile de rezolvare a principalelor probleme tehnologice sesizate cu ocazia realizării practice a sistemului.

BULETINUL INSTITUTULUI POLITEHNIC DIN IAŞI
Tomul XLI (XLV), Fasc. 1–2, 1995
Secţia III
ELECTROTEHNICĂ. ENERGETICĂ. ELECTRONICĂ

D.C. 621.396.619; 621.313.33

OPTIMAL POWER CONTROL STRATEGIES FOR SPACE VECTOR PWM INVERTERS

BY

M. LUCANU, DORIN NEACŞU and VICTOR DONESCU

1. Introduction

The development of high-frequency power devices and the increase in the computing power of microprocessor-based systems allowed the development of Pulse Width Modulator (PWM) strategies. This ones provide quasisinusoidal output voltages with variable amplitude and frequency and low harmonics content. A strong digital method for three-phase inverter controller synthesis is based on Space Vector Modulation (SVM) [1],...,[5]. A rotating Space Vector is accordingly associated to the three-phase system of the six pulse inverter output and six switching vectors are defined for unmodulated operation (Fig.1).

Any three-phase voltage system could be obtained by switching the inverter between the six active states defining the unmodulated operation and the null ones in order to approximate an uniform rotation of the Space Vector corresponding to the three-phase output voltage system. A desired position of the Space Vector in the complex plane is realized by weighted addition of switching vectors which limit the sector where the desired vector belongs to.

The time constants allocated to the switching vectors correspond to the weights V_{s1}, V_{s2} (Fig.1) yielding:

$$(1)\ t_a = \frac{3U_s}{2U_d}T\left(\cos\alpha - \frac{1}{\sqrt{3}}\sin\alpha\right) = \frac{\sqrt{3}U_s}{U_d}T\sin\left(\frac{\pi}{3}-\alpha\right),\quad (2)\ t_b = \frac{\sqrt{3}U_s}{U_d}T\sin\alpha,$$

where (U_s, α) are the polar coordinates of desired vector, U_d – the dc voltage (Fig.2) and T – the sampling period.

The interval $t_0 = T - t_a - t_b$ must be divided between the two null states so that a minimum number of switching processes may be obtained. The time intervals t_{01} and t_{02} could be easily calculated by software using the equation:

$$(3)\qquad t_{01} = t_{02} = \frac{1}{2}(T - t_a - t_b).$$

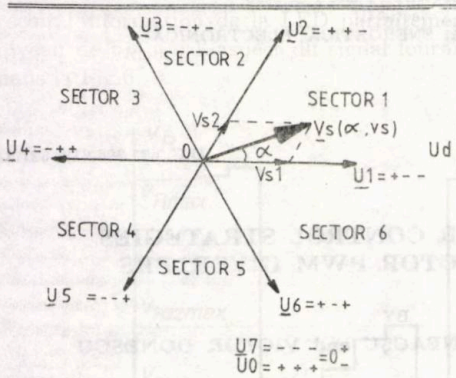

Fig. 1.– Switching vectors.

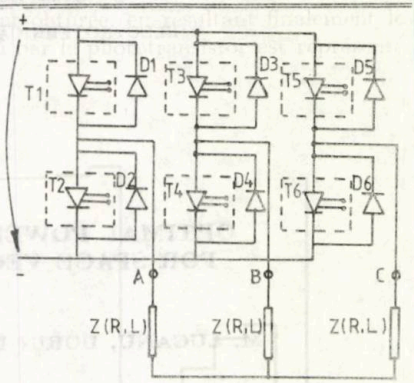

Fig. 2.– Inverter structure.

Moreover, designing a PWM strategy consists in defining the appropriate number of pulses over the inverter output period on the basis of an optimal criterion.

In this paper, optimal power control strategies are presented employing the Space Vector PWM techniques for the following cases: a) variable-voltage variable-frequency inverter for ac motor drive applications (volt/Hertz constant); b) constant-frequency variable-voltage inverter power supply. In fact, these cases are the most common and their optimal control strategies become interesting [8].

2. Proposed Strategy for AC Motor Drives

The most important control strategy for an ac motor drive consists of keeping constantly the ratio.

$$K_1 = \frac{V_1}{f}, \tag{4}$$

where V_1 is the fundamental of the inverter output voltage.

The harmonics of the current in the ac motor due to the n-th voltage harmonic V_n can be approximated as:

$$I_n = \frac{V_n}{2\pi n f L_e}, \tag{5}$$

where L_e is the leakage inductance per phase and n – the harmonic order.

The percentage of the total unwanted harmonic current in the ac motor can be written as:

$$\delta = \frac{100}{I_1}\sqrt{\sum_{n=5}^{\infty} I_n^2} = \frac{K_1}{2\pi L_e I_1}\cdot\frac{100}{V_1}\sqrt{\sum_{n=5}^{\infty}\left(\frac{V_n}{n}\right)^2} = \text{const. HCF}, \tag{6}$$

where I_1 is the motor rated current and HCF represents the harmonic current factor which is to be analyzed in the followings, namely:

$$\text{HCF, } [\%] = \frac{100}{V_1}\sqrt{\sum_{n=5}^{\infty}\left(\frac{V_n}{n}\right)^2}. \tag{7}$$

The aim of the analysis consists of selecting the proper number of pulses for each frequency range in order to maintain the HCF content less than a specified value. Fig.3 shows the computer analysis results for HCF in the cases of 24, 36, 48, 72 and 96 pulses over the output period.

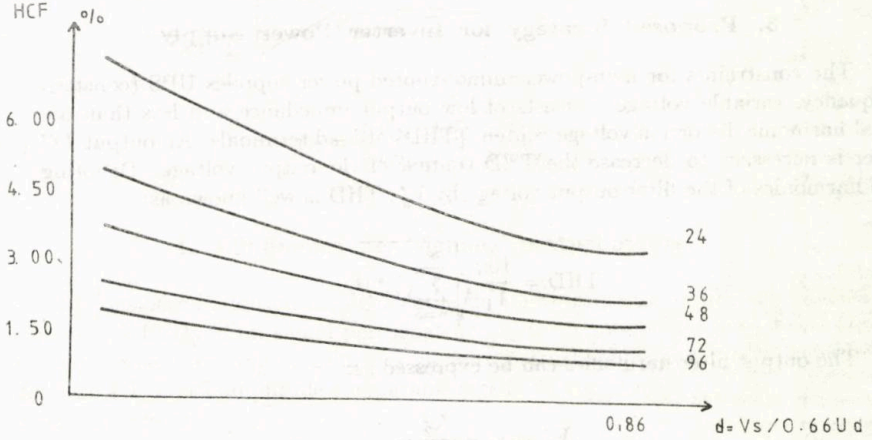

Fig. 3.– HCF content for different numbers of pulses.

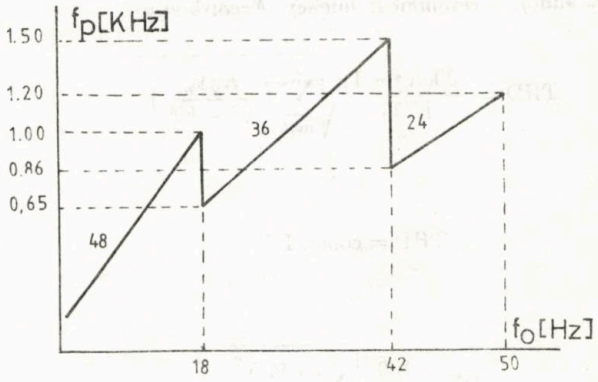

Fig. 4.– Sampling frequency versus output frequency.

Imposing a desired value for the HCF results in a specific share of the frequency range. For instance, when a minimum value of 4% is considered, the maximum switching frequency is about 1.5 kHz.

Since the plots presented in Fig.2 are in different ranges, one can consider with priority to limit the output carrier frequency to less than 800...900 Hz, that is acceptable for the induction machines. Moreover, both conditions could be taken into account for the PWM design. Secondly, a limit of the number of pulses must be assumed in the low speed range in order to simplify the microcomputer implementation. For this reason a relaxation of the HCF constraint will result for modulation duty ratio less than 0.05. The proposed dependence of the sampling frequency f_p on the output frequency f_0 is represented in Fig.4.

3. Proposed Strategy for Inverter Power Supply

The constraints for high-power uninterrupted power supplies UPS (constant frequency, variable voltage) consists of low output impedance and less than 5% total harmonic distortion voltage content (THD) at load terminals. An output LC filter is necessary to decrease the THD content of the output voltage. Denoting the harmonics of the filter output voltage by V_n^*, THD is well-known as:

$$\text{THD} = \frac{100}{V_1}\sqrt{\sum_{n=5}^{\infty}(V_n^*)^2}. \tag{8}$$

The output filter harmonics can be expressed as:

$$V_n^* = V_n \frac{K_2^2}{K_2^2 + n^2}, \tag{9}$$

where $K_2 = f_r/f_p$ and f_r – resonant frequency. Accordingly,

$$\text{THD} = \frac{100(K_2^2 - 1)}{K_2^2 V_1}\sqrt{\sum_{n=5}^{\infty}\left(\frac{K_2^2 V_n}{n^2 - K_2^2}\right)^2} \tag{10}$$

i.e.

$$\text{THD} = \text{const. DF}, \tag{11}$$

where

$$\text{DF} = \frac{100}{V_1}\sqrt{\sum_{n=5}^{\infty}\left(\frac{V_n}{n^2}\right)^2}. \tag{12}$$

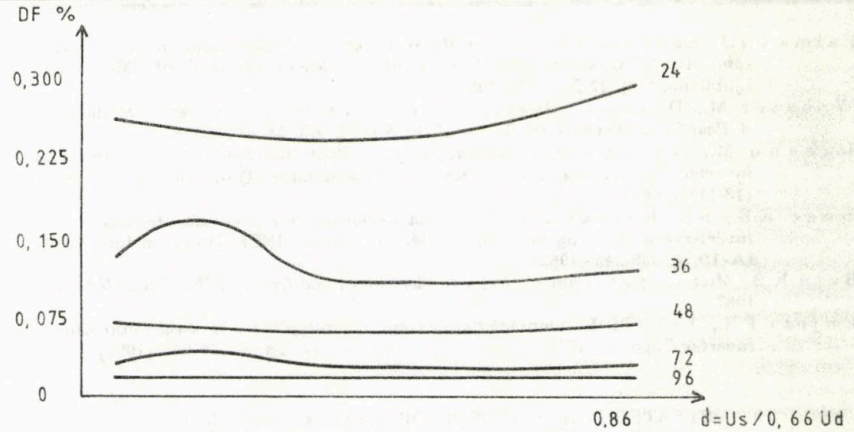

Fig. 5.– DF content for different number of pulses.

Fig.5 shows the computer analysis results for DF in the cases of 24, 36, 48, 72 and 96 pulses over the output period.

If a constant number of pulses is used for all the modulation duty ratio values, the output filter tends to become bulky for a minimum DF in the low voltages range and the output impedance is accordingly increased.

By maintaining a constant value of DF, one can define the proper number of pulses for the desired output frequency. The resulting advantage consists in a simpler controller which would not change the number of pulses for different ranges.

4. Conclusion

An evaluation of proposed harmonic indices for the cases of 24, 36, 48, 72 and 96 pulses Space Vector PWM is presented. On this basis, high-performance optimal power control can be achieved by a Space Vector Modulator.

These strategies are obtained without substantial increase in inverter switching frequency and are proved to result in lower harmonic current in either ac motor drive or power supply cases, lower size and cost of the input and output inverter filters.

Received, December 14, 1993

Technical University "Gh.Asachi", Jassy,
Department of Applied Electronics

REFERENCES

1. van der Broeck, Skudelny H.C., Stanke G., *Analysis and Realisation of a Pulse Width Modulator Based on Voltage Space Vectors*. Conf. Rec. 1986 Annual Meeting IEEE-IAS, Denver, USA, 244-251.

2. Granado J., Harley R.G., Diana G., *Understanding and Designing a Space Vector Pulse-Width-Modulator to Control a Three Phase Inverter*. Trans. of the SAIEE, **80**, 29-37 (1989).

3. Palma C.P.J., Santana J.E.J., *Vectorial PWM Methods, Implementation and Results for some AC-AC Converter Structures.* Conf. Rec. Medit. Electr. Conf. "Melecon'91", Ljubliana, May 22-24, 1991, 1388-1401.
4. Webster M., Diana G., Harley R.G., Levy D.C., *Space Vector Modulation – A Real Time Application.* Trans. of the SAIEE, **80**, 38-42 (1989).
5. Lucanu M., Neacşu D., *Optimization of the Controller Synthesis for Three-Phase Inverter Using Space Vector Pulse-Width Modulator.* Trans. of the SAIEE, 83, 113-117 (1992).
6. Bose K.B., Sutherland A.H., *A High Performance Pulsewidth Modulator for an Inverter-Fed Drive System Using a Microcomputer.* IEEE Trans. on Ind. Applic., **IA-19**, *2*, 235-243 (1983).
7. Bose K.B., *Microcomputer Control of Power Electronics and Drives.* IEEE Press, New York, 1987.
8. Enjeti P.N., Jakkli R., *Optimal Power Control Strategies for Neutral Point Clamped Inverter Topology.* IEEE Trans. on Ind. Applic., **IA-28**, *3*, 558-566 (1992).

STRATEGII DE CONTROL OPTIMAL AL PUTERII PENTRU INVERTOARE CU MID VECTORIALĂ

(Rezumat)

Se prezintă algoritmii de proiectare optimală a unor tehnici de modulaţie vectoriale cu scopul de a menţine coeficienţii de distorsiuni sub anumite valori impuse, în situaţiile controlului unei maşini asincrone sau pentru obţinerea unor surse de alimentare la frecvenţă constantă.

BULETINUL INSTITUTULUI POLITEHNIC DIN IAŞI
Tomul XLI (XLV), Fasc. 1–2, 1995
Secţia III
ELECTROTEHNICĂ. ENERGETICĂ. ELECTRONICĂ

C.D. 535.8; 678

TRADUCTEUR OPTIQUE POUR LE CONTRÔLE DE LA LARGEUR DU FILM DE POLYÉTHYLÈNE DANS LES INSTALLATIONS D'EXTRUSION

PAR
LIVIA COCIU et RADU COCIU

1. Introduction

Pendant le processus de la fabrication du film de polyéthylène il est nécessaire à refroidir le ballon formé après l'extrusion. Outre le refroidissement extérieur du ballon, les procédées modernes utilisent aussi le refroidissement intérieur. En telle circonstance l'air de l'intérieur du ballon est en permanence récirculé. Pour maintenir le diamètre du ballon, respectivement la dimension du film, à la valeur désirée, il faut contrôler en permanence le débit de l'air de refroidissement. Cela nécessite l'emploi des traducteurs de dimensions appropriés.

Dans ce qui suit on propose un tel traducteur, qui fonctionne en se basant sur des principes optiques et qui utilise la modulation en durée d'impulsions.

2. Principe de fonctionnement

Le traducteur est constitué par deux parties principales: l'émetteur des rayonnements optiques E et le récepteur de celles-ci, R. La Fig.1 montre la manière d'emplacement du traducteur optique vis-à-vis du ballon B.

L'émetteur comporte plusieurs LEDs à émission infrarouge, allumées successivement à l'aide des impulsions de commande rectangulaires, de période T.

En fonction du diamètre du ballon, le phototransistor reçoit les signaux lumineux des LEDs activées et non obturées par le ballon. Afin d'obtenir un signal logique, le signal fourni par le phototransistor v_R passe par un bloc de traitement. Il en résulte le signal v_L, en impulsions modulées en durée, comme le montre la Fig.2.

La période de répétition T est la même que celle des impulsions de commande des LEDs; la largeur des impulsions dépend du nombre des LEDs non obturées, c'est-à-dire du diamètre du ballon, Φ. Au moyen d'un filtre passe-bas on sépare la

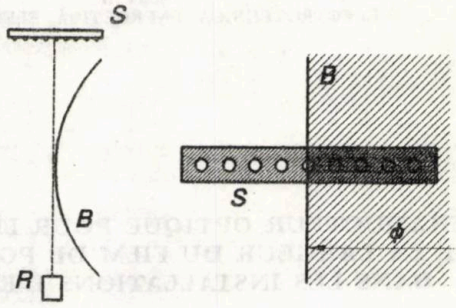

Fig. 1

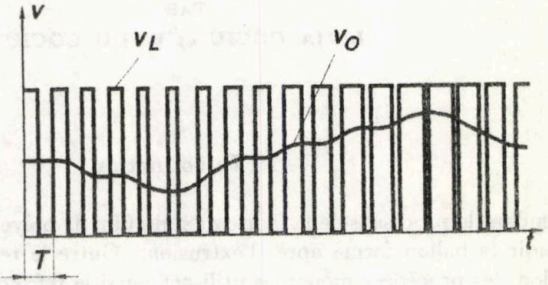

Fig. 2

composante continue de v_L, en fait le signal de sortie du traducteur v_0.

La Fig.3 représente la caractéristique de transfert du traducteur $v_0 = f(\Phi)$; le nombre de paliers est égal au nombre de LEDs de l'émetteur.

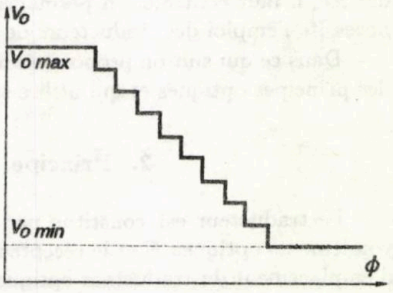

Fig. 3

3. Bloc de traitement du signal du phototransistor

À cause de l'allure du signal v_R il s'avère nécessaire un circuit qui doit décider si la diode allumée à un certain moment est obturée ou non. Afin d'obtenir cette allure on peut considérer le cas de la Fig.4 *a*, où le ballon reste immobile et la source des rayonnements S se déplace le long de l'axe Ox. On obtient alors la caractéristique expérimentale illustrée dans la Fig.4 *b*.

On peut remarquer l'apparition d'une surtension à la proximité du ballon, due à la réflexion de la lumière sur la surface du ballon. De plus, le niveau de la tension de la diode allumée et obturée tend à augmenter le long de l'axe Ox, d'autant plus que le ballon est plus transparent; il y résulte un niveau résiduel de tension, pour les diodes obturées, v_{rez}.

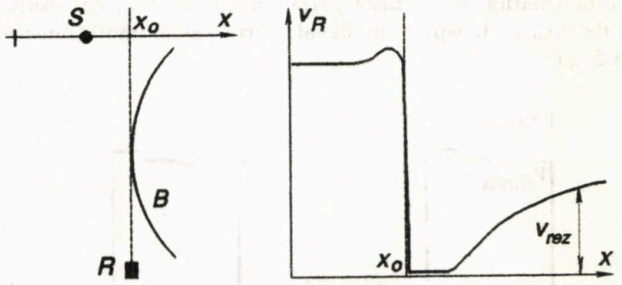

Fig. 4

La valeur de la surtension dépend principalement du diamètre du ballon, mais aussi des caractéristiques du matériel. Sa valeur maxima est de 15...20% par rapport au niveau de référence (le niveau de tension fourni par le phototransistor, dû à une LED allumée, non obturée et située loin de la surface du ballon).

La tension résiduelle dépend des caractéristiques d'opacité du film de polyéthylène, dues à l'épaisseur, à la couleur et à la nature du matériel. Sa valeur maxima est de 70...75%.

Puisque la lumière ambiante se superpose aux rayonnements des LEDs, le signal v_R contient une composante continue. L'information concernant le diamètre du ballon est donnée uniquement par la composante alternative. Donc, la composante continue doit être éliminée, à l'aide d'un filtre passe-haut.

Au cas où toutes les LEDs sont obturées ou non obturées la composante alternative disparait et aussi l'information concernant le diamètre du ballon. Il y résulte la nécessité de maintenir en permanence une diode non obturée, afin d'obtenir le niveau maximum du signal, v_{Rmax}, ce qu'on réalise facilement par le placement de la première diode au-delà d'un limiteur de position du ballon. D'autre part, il est nécessaire de maintenir une LED obturée en permanence, afin d'obtenir le niveau minimum du signal, v_{Rmin}, ce qu'on réalise en utilisant un intervalle de temps, pendant la période T, où aucune LED n'est pas allumée.

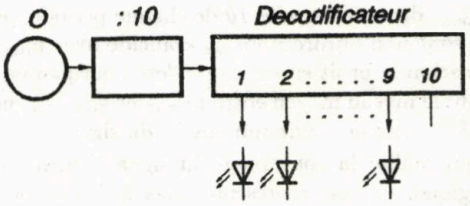

Fig. 5

Le circuit de commande des LEDs est représenté dans la Fig.5. Celui-ci est constitué par un générateur d'impulsions O, à haute fréquence $(10/T)$, qui attaque un compteur par dix; ses quatre sorties sont décodifiées. La sortie *10* n'est pas connectée, de sorte que pendant la durée où celle-ci est activée le phototransistor

reçoit l'information de la LED parfaitement obturée, en résultant finalement le niveau de $v_{R\min}$. L'aspect du signal fourni par le phototransistor est représenté dans la Fig.6.

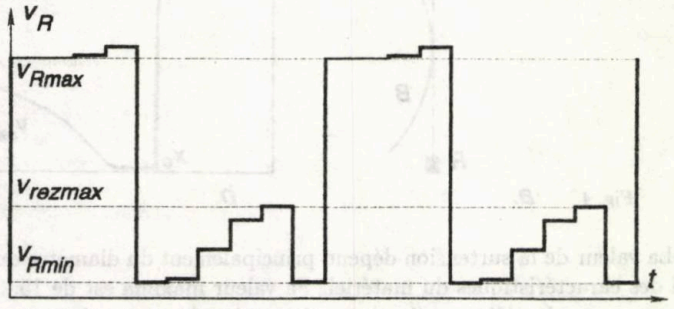

Fig. 6

Comme on a précisé ci-dessus, il est nécessaire d'établir le seuil entre le niveau de tension pour une LED obturée et une autre non obturée. Au moyen de deux circuits échantillonneurs-bloqueurs, activés sur les intervalles *1* et *10* de chaque période, on obtient les niveaux de tension $v_{R\max}$ et $v_{R\min}$.

Afin de couvrir toutes les situations il faut choisir le seuil de comparaison (ou de commutation) à partir du cas le plus défavorable, celui de la tension résiduelle maxima. Compte tenu de sa valeur de 75% par rapport au niveau de référence, on peut choisir le seuil de comparaison à un niveau de 87%. Mais, à cause du rapprochement de celui-ci du niveau maximum de 100%, l'immunité au bruit devient trop faible. Il convient alors qu'on choisisse le seuil de comparaison à partir du niveau minimum réel de tension, pour chaque cas, c'est-à-dire le niveau fourni par le phototransistor dans l'intervalle *9* de chaque période, $v_{\text{rez max}}$.

On introduit, donc, un circuit supplémentaire échantilloneur-bloqueur, actif, dans l'intervalle *9*.

Cependant, on ne doit pas éliminer la nécessité de connaître le niveau minimum absolu, $v_{R\min}$, dans l'intervalle *10* de chaque période, puisque dans le cas où toutes les LEDs sont non obturées $v_{R\max}$ coïncide avec $v_{R\min}$ et la commutation devient aléatoire selon le bruit superposé. C'est pourquoi on a choisi le niveau de commutation comme niveau moyen entre $v_{R\max}$ et $v_{\text{rez max}}$, mais à condition de ne pas dépasser 87% du niveau maximum absolu du signal.

Le circuit qui réalise la conversion du signal fourni par le phototransistor, v_R, en signal logique, v_L, est représenté dans la Fig.7, où v_C est le niveau de comparaison ou de commutation et v_{CL} est le niveau limite de commutation:

$$(1) \qquad v'_C = \frac{v_{R\max} + v_{\text{rez max}}}{2}, \qquad (2) \quad v_{CL} = 0,87 v_{R\max} + 0,13 v_{R\min};$$

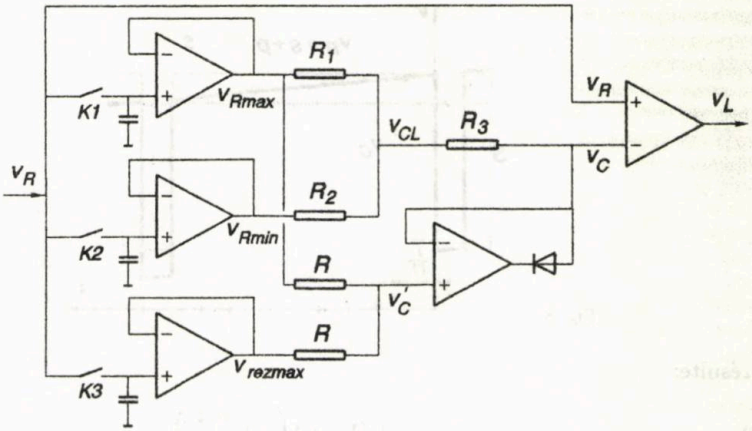

Fig. 7

(3) $$v_C = \begin{cases} v'_C, & v'_C \leq v_{CL}; \\ v_{CL}, & v'_C > v_{CL}. \end{cases}$$

4. L'influence des signaux perturbateurs

On considère l'addition au signal utile du phototransistor, s, dû aux rayonnements des LEDs, d'un signal perturbateur, p. Il est intéressant à analyser un cas fréquemment rencontré, celui des signaux perturbateurs ayant la fréquence inférieure à $1/T$ et l'amplitude comparable à celle du signal utile (par exemple, la lumière artificielle).

On suppose, tout d'abord, que la pente du signal perturbateur, $m = \mathrm{d}p/\mathrm{d}t$, est constante. Dans ce cas il y a le risque de l'apparition des erreurs de commutation. De ce point de vue, le cas le plus défavorable est représenté dans la Fig. 8, où toutes les LEDs sont non obturées et la pente m est négative. On peut écrire alors:

(4) $$v_R = s + p = s + mt,$$

et aussi, en choisissant convenable l'origine des temps:

(5) $$v_R(0_-) = v_{R\min}; \quad v_R(0_+) = v_{R\min} + s;$$

(6) $$v_R\left(\frac{T}{n}\right) = v_{R\min} + s + \frac{mT}{n} = v_{R\max},$$

où n est le nombre des LEDs.

Si on utilise la notation:

(7) $$\alpha = \frac{v_{R\max} - v_C}{v_{R\max} - v_{R\min}},$$

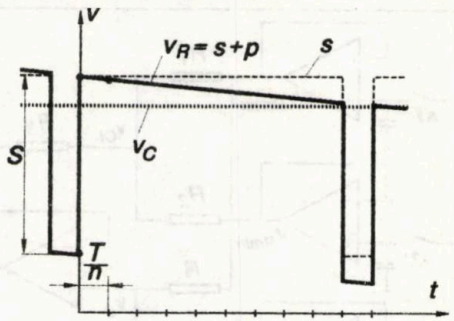

Fig. 8

il résulte:

$$v_C = v_{R\min} + (1-\alpha)\left(s + \frac{mT}{n}\right). \tag{8}$$

La dernière information utile est reçue par le phototransistor à la fin de l'avant-dernière impulsion émise:

$$v_R\left(\frac{n-1}{n}T\right) = v_{R\min} + s + \frac{m(n-1)}{n}T. \tag{9}$$

Pour un bon fonctionnement sa valeur ne doit pas devenir inférieure au seuil de commutation v_C, c'est-à-dire:

$$v_R\left(\frac{n-1}{n}T\right) \geq v_C. \tag{10}$$

On obtient alors:

$$v_{R\min} + s + m\frac{n-1}{n}T \geq v_{R\min} + (1-\alpha)\left(s + \frac{m}{n}T\right), \quad s + m\frac{n-1}{n}T \geq \left(s + \frac{m}{n}T\right)(1-\alpha), \tag{11}$$

d'où on peut déduire:

$$m \geq \frac{-\alpha n s}{T(n-2+\alpha)} = m_{\lim}. \tag{12}$$

Dans le cas d'un signal perturbateur sinusoïdal:

$$p = P\sin\omega_p t, \quad m = \frac{\mathrm{d}p}{\mathrm{d}t} = 2\pi f_p P\cos\omega_p t. \tag{13}$$

Si l'on considère la pente négative maximum, $m_{\min}$, on obtient le cas le plus défavorable:

$$m_{\min} = -2\pi f_p P. \tag{14}$$

Imposant la condition:

$$m_{\min} = m_{\lim} \tag{15}$$

ou:

$$\frac{-\alpha n s}{T(n-2+\alpha)} = -2\pi f_p P, \tag{16}$$

on obtient la valeur maximum du rapport entre l'amplitude du signal perturbateur et le signal utile qui ne conduit pas à des erreurs dans le fonctionnement du traducteur:

$$\frac{P}{s} = \frac{\alpha f n}{2\pi f_p (n-2+\alpha)}. \tag{17}$$

Dans le cas pratique considéré $f = 1/T = 5$ kHz, $n = 10$, $f_p = 100$ Hz (la lumière artificielle), $\alpha = 0,13$. Le rapport maximum bruit/signal (P/s) vaut alors 1,3. Dans des situations plus favorables α peut atteindre 0,5 et $P/s = 5$.

On peut donc obtenir, dans n'importe quelle situation, une très bonne immunité aux perturbations rayonnantes superposées au signal utile.

5. Conclusions

Le traducteur proposé est destiné à déterminer l'écart du diamètre du ballon de polyéthylène de la valeur désirée. Il fonctionne en se basant sur des principes optiques, en évitant la touche du film, donc la dégradation de sa surface. Il est destiné aux installations d'extrusion à refroidissement intérieur, où le diamètre du ballon est maintenu constant par l'intermédiaire d'un système de contrôle automatique du débit de l'air de refroidissement.

Vu que le fonctionnement est basé sur le principe de la modulation en durée des impulsions, on assure l'élimination de l'influence des dérives, une bonne stabilité thermique et une haute immunité aux bruits (rayonnantes ou électromagnétiques). En ce qui concerne la résolution, bien que limitée, elle satisfait aux nécessités de ces applications.

Le traducteur peut être utilisé pour chaque type de film, quel qu'ils soient le matériel, l'épaisseur, la couleur ou la transparence.

Reçue le 15 mars 1993

Université Technique „Gh. Asachi", Jassy,
Chaire d'Électrotechnique
et Machines électriques

BIBLIOGRAPHIE

1. Cociu L., Cociu R., Goraş L., *Procedeu şi instalaţie pentru menţinerea diametrului balonului din polietilenă în instalaţii de extrudere, în cazul răcirii interioare.* Patent Roumanie, *99014* (1989).

2. Cociu L., Goraş L., Cociu R., *Traductor pentru determinarea diametrului balonului din polietilenă în instalaţii de extrudere.* Patent Roumanie, *98996* (1989).

TRADUCTOR OPTIC PENTRU CONTROLUL LĂŢIMII FOLIEI DE POLIETILENĂ ÎN INSTALAŢII DE EXTRUDERE

(Rezumat)

Se prezintă un traductor funcţionând pe principii optice, pentru determinarea abaterii diametrului balonului de polietilenă, în instalaţiile automate de extrudere care folosesc răcirea interioară.

Traductorul este alcătuit dintr-un emiţător de radiaţii infraroşii, format dintr-un şir de LED-uri care se aprind succesiv, şi un receptor (un fototranzistor), care detectează radiaţiile emise de LED-urile activate şi neobturate de către balonul de polietilenă. După prelucrarea semnalului analogic de recepţie rezultă un semnal logic modulat în durată, având factorul de umplere dependent de abaterea diametrului balonului de polietilenă de la valoarea prescrisă.

Performanţele traductorului sunt foarte bune, mai ales din punct de vedere al stabilităţii termice şi al imunităţii la zgomot, fiind apt să lucreze cu orice tip de folie din polietilenă.

BULETINUL INSTITUTULUI POLITEHNIC DIN IAŞI
Tomul XLI (XLV), Fasc. 1-2, 1995
Secţia III
ELECTROTEHNICĂ. ENERGETICĂ. ELECTRONICĂ

C.D. 621.398; 621.3.014; 621.316.1

SUR LA SIGNALISATION À DISTANCE DES COURT-CIRCUITS DANS LES RÉSEAUX DE MOYENNE TENSION

PAR

C. ASAFTEI, MIRCEA GUŞĂ, MARCEL ISTRATE et N. GAVRILAŞ

1. Introduction

À présent, dans les systèmes énergétiques on poursuit d'une façon remarquables l'optimisation de la structure et de l'exploitation des réseaux de distribution de moyenne tension, dans le but d'une meilleure qualité concernant le service des consommateurs d'énergie électrique. Parmi les nombreux problèmes de cet objectif, une attention spéciale est réservée à l'identification automatique des zones dans lesquelles se sont produits des défauts d'isolement, réalité soulignée par le fait qu'au Congrès International des Réseaux Électriques de Distribution CIRED – Liège, 1991, les travaux de la 4-ème section ont été centrés sur ce sujet.

Malhereusement, dans notre pays, jusqu'aux dernières années, l'intêret dans cette direction a été très réduit.

On peut localiser les défauts dans différents moments de temps par rapport à leurs apparition, à savoir: a) avant la manifestation proprement-dite du défaut; b) en même temps où immédiatement après que le défaut a eu lieu; c) avec un certain retardement après l'apparition du défaut.

Une solution intéressante [1] propose la localisation du défaut après la variante c) ci-dessus. On propose à intercaler dans les conducteurs de la ligne, en certains endroits, des circuits LC ayant différentes fréquences de résonance. Le lieu du défaut, toujours situé entre deux tels circuits (LC) consécutifs, est découvert par l'injection d'un signal de fréquence variable à l'entrée de la ligne et l'observation du changement du courant en fonction de la fréquence.

Cette idée ne s'est pas affirmée à cause de certaines difficultés techniques à savoir: le sectionnement des conducteurs, l'utilisation des bobines et des condensateurs pour assurer le fonctionnement à l'extérieur, etc.

Dans ce qui suit on présente, à la suite des recherches effectuées pour F.R.E. de Jassy, un système de localisation à distance des défauts, qui représente une application, facile à implanter, de la variante b) ci-dessus.

2. Considérations concernant un système de localisation à distance qui utilise des indicateurs de défaut

On a élaboré un système de localisation à distance des zones avec défauts d'isolement, qui utilise des indicateurs de défaut dispersés dans le réseau, qu'on va décrire ci-dessous. Chaque indicateur peut transmettre, par suite d'un défaut en

aval de son emplacement, une information vers un récepteur qui se trouve dans la sous-station HT/MT. Ce récepteur reçoit et décodifie l'information (Fig.1).

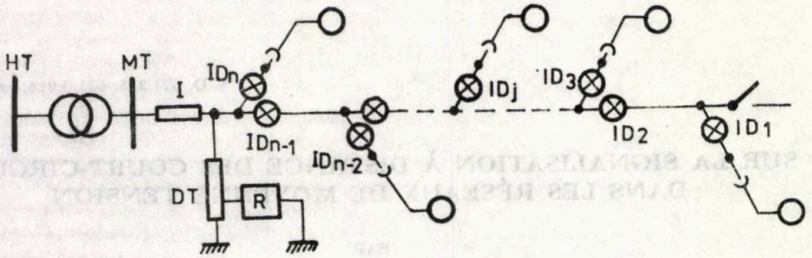

Fig. 1.– Schéma générale de principe d'un système de signalisation centrale des zones à défauts.

Les significations des notations utilisées dans la Fig.1 sont les suivantes: $ID_{1...n}$ – indicateurs de défaut numéro 1,...,n; R – récepteur; DT – diviseur de tension; I – disjoncteur automatique; O – transformateur MT/BT.

Le système de surveillance proposé est destiné aux lignes électriques aériennes de moyenne tension. Il est conçu à partir des caractéristiques du réseau, dont les plus importantes sont:

a) L'architecture en „antenne" du réseau.

b) Le mode d'emploi de l'appareillage de commutation qui suppose un seul disjoncteur automatique dans la sous-station HT/MT pour chaque ligne et des sectionneurs sur l'axe principal et sur les branches, actionnés en absence de la charge.

c) Le régime du neutre dans le réseau; le système proposé est destiné pour les défauts monophasés dans les réseaux dont le neutre est mis à la terre par une impédance réduite. Pour les défauts polyphasés la sensibilité des indicateurs de défaut peut être garantie sans tenir compte du régime du neutre.

d) La configuration du relief dans la région du réseau, qui en Roumanie est plus souvent accidenté.

e) Enfin, la possibilité d'obtenir l'énergie nécessaire pour le fonctionnement de l'indicateur par prélévation de la ligne.

Les dernières deux aspects représentent les difficultés techniques et économiques principales qui concernent l'utilisation des ondes hertziennes comme support des informations dans ce système. Par suite on utilise les conducteurs de la ligne surveillée pour transmettre les signaux emis par les indicateurs de défaut ID_j vers le récepteur R situé dans le poste.

Les indicateurs de défaut peuvent être munis où pas par des éléments pour la signalisation locale du défaut. Par rapport à la solution de signalisation à distance on a étudié deux variantes, l'une monophasée et l'autre triphasée. Dans la Fig.2 sont ilustrées des configurations possibles pour les indicateurs de défaut.

L'indicateur de défaut de la Fig.2*a* est composé par un élément de signalisation locale IL et un émetteur E qui transmet l'information concernant l'apparition

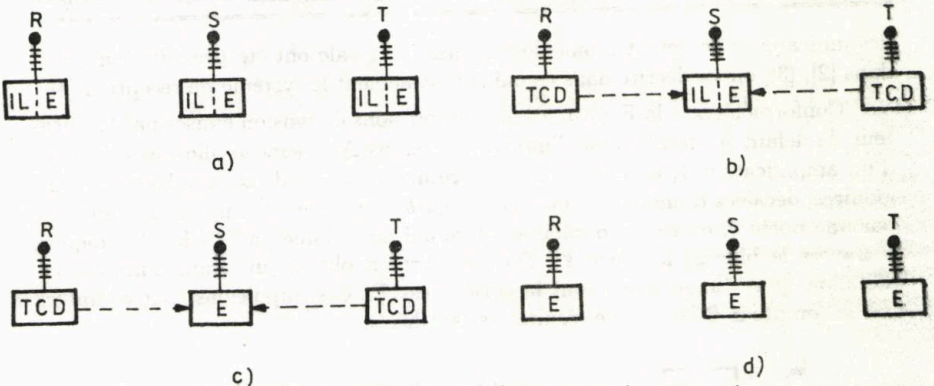

Fig. 2.– Possibilités de réalisation, emplacement et interconnection pour les indicateurs de défaut: IL – indicateur local de signalisation; E – émetteur; TCD – traducteur de courant de défaut; → – interconnection.

d'un court-circuit. La présence de l'indicateur local fournit une confirmation supplémentaire à l'équipe d'intervention qui va s'occuper de séparer le secteur à défaut, en ce qui concerne le fonctionement correcte de la signalisation à distance.

Pour les solutions de la Fig.2 *b* et *c*, les indicateurs de défaut placés sur les phases latérales contiennent seulement des traducteurs de courant de défaut (TCD); dans ce cas le TCD devra exciter l'indicateur de défaut sur la phase moyenne par une liaison d'interconnection (par exemple réalisée en fibre optique). L'utilisation d'une telle liaison peut apporter, en apparence, certaines simplifications pour la réalisation des indicateurs de défaut, mais tenant compte des conditions d'exploitation, ce procédé présente quelques difficultés, surtout pour les réseaux aeriens (Fig.2 *d*).

Comme on a déjà précisé ci-dessus l'information concernant l'apparition d'un défaut en aval de l'endroit de l'indicateur est fournie par son émetteur. Celui-ci transmettra son signal dans la première pause du cycle RAR effectué par le disjoncteur automatique de la sous-station HT/MT. Le signal codifié, qui se propage sur les conducteurs et arrive au poste, sera décodifié par le récepteur de sorte qu'il pourra identifier l'émetteur qui l'a transmis.

Cette solution, de transmettre le signal codifié en absence de la tension de service, présente certaines avantages à savoir: a) un diminution au minimum des signaux parasites; b) une sensibilité accrue à la réception; c) la nécessité de prendre des mesures simples de protection pour le personnel dans le poste.

Pour identifier l'émetteur, le signal transmis par celui-ci contient deux impulsions de tension consécutives séparées par un certain interval de temps, propre pour chaque ensemble d'indicateurs (sur les trois phases, dans un certain endroit).

Les moments où les indicateurs de défaut émettent leurs signaux, par rapport à l'apparition du défaut, sont directement déterminés par la manière de leur emplacement dans le réseau notamment sur les dérivations et sur l'axe principal où seulement sur les dérivations. Compte tenu que ces problèmes ainsi que la réalisation

des indicateurs de défaut munis de signalisation locale ont été présentés en detail dans [2], [3], on va décrire dans ce qui suit seulement le système de réception [4].

Conformément à la Fig.3 *a*, les deux impulsions de tension émises par l'indicateur de défaut n, décalées par l'interval de temps Δt_n, sont appliquées à l'entrée d'un amplificateur *1*, à la sortie du quel résultent autres deux impulsions rectangulaires, décalées d'une même manière (Fig.3 *b*). La première impulsion transmise par une porte *2*, excite un oscillateur *3*, ce qui aura d'une part l'effet de bloquer, à travers le bloc *4*, la porte *2*. D'autre part on obtient un train d'impulsions d'étallonage rectangulaires, dont la période est T. Ces impulsions sont comptées par le compteur BCD *6* et le résultat est affiché.

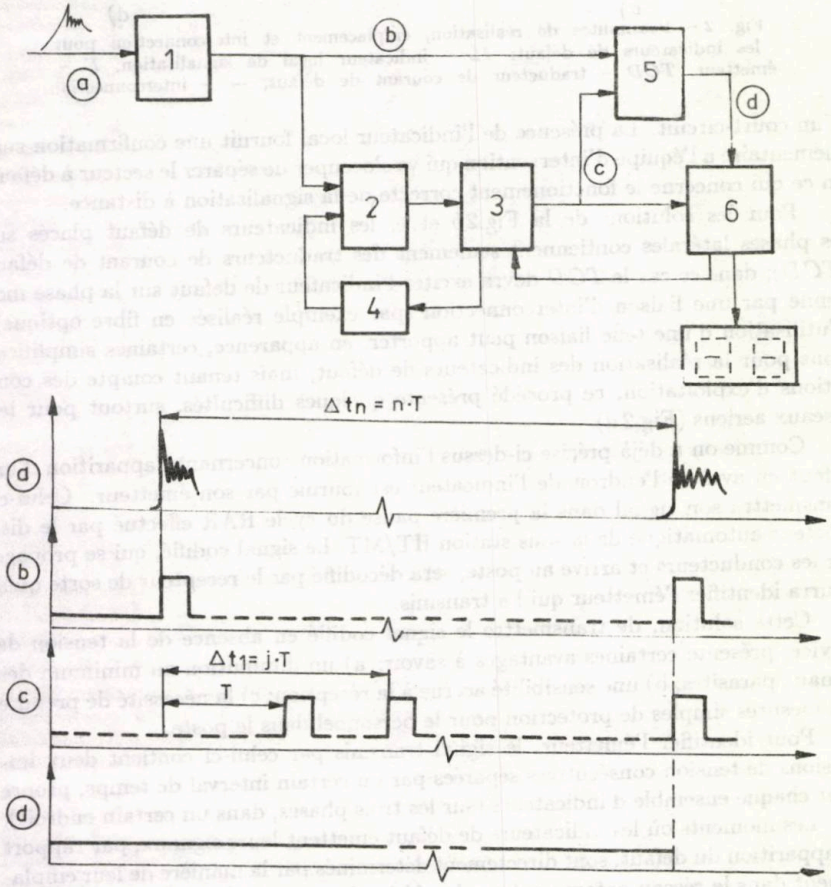

Fig. 3.– Le schéma bloc du récepteur des signaux codifiés et le diagramme des impulsions.

Dans le moment où la deuxième impulsion du signal codifié, qui arrive après un interval de temps Δt_n, multiple de la période T ($\Delta t_n = nT$), se superpose sur l'une des impulsions produites par l'oscillateur *3*, le compteur *6* est bloqué à travers la porte *5*. À ce moment l'affichage présente le nombre des impulsions comptées, n, qui représente aussi le numéro d'ordre de l'indicateur de défaut.

Les essais effectuées dans les réseaux de FRE de Jassy ont confirmé la valabilité de la solution proposée. Les composants du système ont fait preuve de leur simplicité constructive, aussi que de leur robustesse et fiabilité, sans utiliser des matériaux déficitaires.

3. Conclusions

L'utilisation des systèmes de signalisation à distance de l'endroit où s'était produit un court-circuit dans un réseau aerien de moyenne tension, présente une grande importance pour une meilleure exploitation des ces réseaux parce que, sans très grandes dépenses, on peut obtenir une diminution importante des durées d'interruption dans la fourniture d'énergie électrique aux consommateurs, aussi qu'une réduction très importante de l'usure des contacts des disjoncteurs grâce à la baisse du nombre des manoeuvres concernant le défaut.

Les auteurs, en se raliant aux recherches dans ce domaine, présentent quelques idées concernant un système de localisation des court-circuits dans les réseaux de moyenne tension. Ce système contient des indicateurs de défaut dispersés dans le réseau et un récepteur dans la sous-station HT/MT. À l'aide des signaux codifiés transmis par les conducteurs de la ligne, dans la première pause du cycle RAR, on peut identifier l'émetteur le plus proche du défaut. L'éventualité d'une identification fausse n'est pas importante grâce à l'utilisation des impulsions d'étallonage.

Les essais effectués dans le réseau ont validé la solution proposée et ont souligné la nécessité de poursuivre les recherches pour l'optimisation de ce système.

Reçue le 18 mai 1993

Université Technique „Gh. Asachi", Jassy, Chaire d'Energétique

BIBLIOGRAPHIE

1. H ă n g ă n u ţ M. et al., *Procedeu de localizare a defectelor în linii electrice aeriene.* Patent Roumanie, *57053* (1974).

2. G u ş ă M., I s t r a t e M., A s a f t e i C., G a v r i l a ş N., *Semnalizarea centralizată a scurtcircuitelor în reţele aeriene de medie tensiune.* Rapport au III-ème Symp. „Optimisation du développement des installations énergétiques", Jassy, 1991.

3. I s t r a t e M., G u ş ă M., A s a f t e i C., G a v r i l a ş N., *Cu privire la un emiţător de semnale codificate.* Rapport au III-ème Symp. „Optimisation du développement des installations énergétiques", Jassy, 1991.

4. A s a f t e i C., G u ş ă M., I s t r a t e M., G a v r i l a ş N., *Receptor de semnale codificate.* Patent Roumanie, *104849* (1991).

SEMNALIZAREA LA DISTANŢĂ A SCURTCIRCUITELOR ÎN REŢELELE DE MEDIE TENSIUNE

(Rezumat)

Îmbunătaţirea calităţii deservirii consumatorilor de energie electrică constituie o preocupare în plină dezvoltare în numeroase ţări avansate tehnologic. În reţelele de medie tensiune din mediul rural, predominant aeriene, detectarea şi eliminarea defectelor se pot realiza prin mai multe procedee, problema comună a acestora rămânând modul de transmitere la distanţă a informaţiilor aferente. Considerând că transmisia radio implică dificultăţi în unele zone din România, se propune un sistem care foloseşte emiţătoare de semnale codificate, amplasate în reţea, transmisia semnalelor pe conductoarele liniei, recepţia şi decodificarea acestora în staţia de transformare. Semnalul transmis, constituit din două impulsuri decalate cu un interval de timp prescris pentru fiecare emiţător, permite recunoaşterea acestuia de către receptor. Principalele componente ale acestui sistem – emiţătorul şi receptorul – au fost realizate practic şi testate atât în laborator, cât şi în reţele reale.

BULETINUL INSTITUTULUI POLITEHNIC DIN IAŞI
Tomul XLI (XLV), Fasc. 1–2, 1995
Secţia III
ELECTROTEHNICĂ. ENERGETICĂ. ELECTRONICĂ

D.C. 621.316.1

THE OPTIMAL PLANNING OF MEDIUM VOLTAGE POWER DISTRIBUTION NETWORKS

BY
GH. GEORGESCU, M. GAVRILAŞ,
GH. CÂRŢINĂ and VIRGIL ALEXANDRESCU

1. Introduction

In order to achieve an optimal planning of power distribution networks, comprising the actual optimization of networks operating conditions and their optimal development, a great amount of data has to be stored and processed.

Most of the methods proposed so far use algorithms that lead to suitable results only if a compromise between the amount of input data (especially direct measurements in the network), the memory used and the computational time is accepted. Thus, in order to obtain a set of programs dedicated to the optimal planning of power distribution systems a design and, afterwards, a rational use of a data base are necessary. To be efficient these programs have to satisfy several conditions and have to fulfil several functions, namely: the data must be organized in a hierarchical and modular structure; it must be provided a suitable way to facilitate the updating of basic data; the information must be displayed in an adequate way, at the user demand; the protection and security of data base must be ensured, etc.

Recent studies have emphasized new possibilities for the application of load curves in view to optimal planning of the operating conditions of power distribution systems. One of these suggests to use an approximate model developed from a Fourier's series decomposition of the real load curves at the buses of the networks [1]. This method, in association with the modelling of the loads at the networks buses by means of typical load curves [2],...,[4], ensures a substantial decrease of the amount of input data (measurements in the network), a simplification of the algorithms, an important diminution of the number of power flows that have to be calculated and, implicitly, the decrease of computational time, with none sensible implication on the accuracy of the results.

2. Mathematical Model

Daily load curves at the buses (substations) of a medium voltage (MV) distribution network, for different characteristic annual operating conditions (summer/winter or work day/leissure day), are approximated using the typical load curves of consumers supplied from these buses, in association with few other information determined by direct measurements in the network, such as: the current at a certain hour of the day; the electrical energy transmitted within a certain time; the statistical loading coefficients for transformers in substations, etc. [3],[4]. Using this model a load curve at a bus in the distribution network looks like a 24 levels diagram, each level corresponding to the hourly mean load from the daily load curves (24 hours) associated to that bus.

$P_{i,t}$ and $Q_{i,t}$, which represent the load curves for active and reactive powers at bus i of a distribution network, for a period T, could be decomposed in Fourier's series as follows:

$$P_{i,t} = \overline{P_i} + \sum_{k=1}^{N} A_{i,k}^{P} \sin\left(\frac{2k\pi}{T}t\right) + \sum_{k=1}^{N} B_{i,k}^{P} \cos\left(\frac{2k\pi}{T}t\right), \tag{1}$$

$$Q_{i,t} = \overline{Q_i} + \sum_{k=1}^{N} A_{i,k}^{Q} \sin\left(\frac{2k\pi}{T}t\right) + \sum_{k=1}^{N} B_{i,k}^{Q} \cos\left(\frac{2k\pi}{T}t\right), \tag{2}$$

where: N is the number of harmonics taken into consideration; t – number of hourly levels from the daily load curve, ($t = 1, ..., T$, usually $T = 24$); $\overline{P_i}, \overline{Q_i}$ – mean values of the active and reactive powers over period T at bus i; $A_{i,k}^{P}, B_{i,k}^{P}, A_{i,k}^{Q}, B_{i,k}^{Q}$ – Fourier's coefficients corresponding to the k-th harmonic for active and reactive powers, respectively, at bus i. These coefficients could be calculated using their well-known definition formula [1].

The optimization of the operating conditions of a MV distribution network supposes, as a rule, to determine those conditions for which the quality of the energy supplied to consumers (voltage level, supplying continuity) is sufficiently high and, at the same time, the energy losses in the components of the network (MV cables, transformers in substations) are minima.

For those networks that under normal operating conditions have a radial structure the Joule energy losses in element j of the network, characterized by a resistance R_j and a reactance X_j, in a period T, are calculated as:

$$\Delta W_j = \frac{R_j}{U^2}\left(\sum_{t=1}^{T} P_{j,t}^2 + \sum_{t=1}^{T} Q_{j,t}^2\right) \tag{3}$$

and the longitudinal voltage drop across the same element as:

$$\Delta U_{j,t} = \frac{P_{j,t}R_j + Q_{j,t}X_j}{U}, \tag{4}$$

where $P_{j,t} = \sum_i P_{i,t}$ and $Q_{j,t} = \sum_i Q_{i,t}$ are the active and reactive power flows through element j at hour t (the sums $\sum_i$ in equations above and bellow are calculated for all buses i that follow after the element j).

The statistical coefficients used to evaluate the voltage quality at bus i of the distribution network are defined as:

a) the mean deviation of voltage during period T:

$$\overline{\Delta U_i} = \frac{1}{T}\sum_{t=1}^{T} \Delta U_{i,t}; \tag{5}$$

b) the mean square deviation:

$$\overline{\Delta U_i^2} = \frac{1}{T}\sum_{t=1}^{T} \Delta U_{i,t}^2; \tag{6}$$

c) the variance of the voltage:

$$\sigma_i^2 = \frac{1}{T}\sum_{t=1}^{T} (\Delta U_{i,t} - \overline{\Delta U_i})^2, \tag{7}$$

where $U_{i,t} = [(U_{i,t} - U_n)/U_n]100$ is the voltage deviation at bus i and hour t, (U_n – the rated voltage of the network; $U_{i,t}$ – the voltage at bus i and hour t).

If the daily load curves associated to the buses have been decomposed in accordance with Eqs. (1) and (2), the sums in Eq. (3) could be determined using the P a r s e v a l's theorem:

$$\sum_{t=1}^{T} P_{j,t}^2 = \left\{ \overline{P_j}^2 + \sum_{k=1}^{N} \left[\left(\frac{A_{j,k}^P}{\sqrt{2}} \right)^2 + \left(\frac{B_{j,k}^P}{\sqrt{2}} \right)^2 \right] \right\} T + \varepsilon_P^2, \tag{8}$$

$$\sum_{t=1}^{T} Q_{j,t}^2 = \left\{ \overline{Q_j}^2 + \sum_{k=1}^{N} \left[\left(\frac{A_{j,k}^Q}{\sqrt{2}} \right)^2 + \left(\frac{B_{j,k}^Q}{\sqrt{2}} \right)^2 \right] \right\} T + \varepsilon_Q^2, \tag{9}$$

where: $\overline{P_j} = \sum_i \overline{P_i}$, $\overline{Q_j} = \sum_i \overline{Q_i}$ are the mean values of active and reactive power flows through the element j over period T; $A_{j,k}^P, B_{j,k}^P, A_{j,k}^Q, B_{j,k}^Q$ – Fourier's coefficients corresponding to active and reactive power flows through element j over period T,

$$A_{j,k}^P = \sum_i A_{i,k}^P, \quad B_{j,k}^P = \sum_i B_{i,k}^P; \quad A_{j,k}^Q = \sum_i A_{i,k}^Q, \quad B_{j,k}^Q = \sum_i B_{i,k}^Q,$$

$\varepsilon_P^2, \varepsilon_Q^2$ – errors generated as a result of neglecting the harmonics with a rank greater than N.

By substituting (8) and (9) in Eq. (3), it can be find that the energy losses could be calculated using only the mean values of the loads and the Fourier's coefficients corresponding to different harmonics, on the whole $2N+1$ power flows that are to be determined. In fact, instead of calculating T power flows corresponding to the T levels from the daily load curves, someone could determine $2N+1$ power flows associated to the Fourier's series decomposition, following the equation:

$$\Delta W_j = \Delta \overline{P_j} T + \sum_{k=1}^{N} (\Delta P'_{j,k} + \Delta P''_{j,k}) T + \varepsilon_W, \tag{10}$$

where:

$$\Delta \overline{P_j} = \frac{R_j (P_j^2 + Q_j^2)}{U^2}$$

– power losses due to mean active and reactive power flows;

$$\Delta P'_{j,k} = \frac{R_j}{U^2} \left[\left(\frac{A^P_{j,k}}{\sqrt{2}} \right)^2 + \left(\frac{A^Q_{j,k}}{\sqrt{2}} \right)^2 \right]; \quad \Delta P''_{j,k} = \frac{R_j}{U^2} \left[\left(\frac{B^P_{j,k}}{\sqrt{2}} \right)^2 + \left(\frac{B^Q_{j,k}}{\sqrt{2}} \right)^2 \right]$$

– power losses corresponding to the k-th harmonic, determined for two stationary operating conditions, for loads at the buses chosen as:

$$P'_{i,k} = \frac{A^P_{i,k}}{\sqrt{2}}, \quad P''_{i,k} = \frac{B^P_{i,k}}{\sqrt{2}}; \quad Q'_{i,k} = \frac{A^Q_{i,k}}{\sqrt{2}}, \quad Q''_{i,k} = \frac{B^Q_{i,k}}{\sqrt{2}}; \tag{11}$$

ε_W – error due to the omission of those harmonics with a rank greater than N.

In accordance to the above mathematical model, for a network having a radial structure, the analysis of $2N+1$ operating conditions is sufficient in order to determine the energy losses in the network components. Taking into consideration the purpose to be achieved, i.e., the diminution of computational time maintaining the accuracy at an acceptable value, it may be concluded that the use of the method described above is considered to be suitable only in those situations when the inequality $2N+1 < T$ is fulfilled (T is the number of levels from the load curves).

This method was tested for a great number of MV distribution networks with a radial structure [4],[5]. These tests were intended to determine the minimum number of harmonics that have to be considered in the series decompositions (1) and (2) so that the errors induced by these truncations in the values of energy losses and voltage quality statistical coefficients do not exceed an acceptable value.

The results of these tests proved that the errors do not exceed 2% if the load curves at the buses of the distribution network are modelled using typical load

curves for different consumers and the Fourier's decomposition of these curves contain three harmonics. This accuracy is sufficiently high to conclude that considering more harmonics would not lead to further significant improvement. Consequently, to estimate the daily energy losses and the voltage quality statistical coefficients using the mathematical model above, only $2 \cdot 3 + 1 = 7$ power flows are sufficient to be determined, instead of 24 power flows, when using the load curves with hour levels.

3. Programs

Using the mathematical model described, a soft package was written and tested. These programs offer the possibility to develop a complex analysis of the MV distribution networks concerning the optimal planning of their operating conditions. The block diagram of these programs is shown in Fig. 1.

These programs process and store a lot of informations that is organized as a Data Base in files on floppy (hard) disk(s). This information is as follows: the typical load curves of the consumers in the urban and rural distribution networks, for all annual characteristics operating conditions; the specific electrical parameters of the MV cables; the characteristics of transformers from the substations; topological and electrical characteristics of the network; different data obtained by direct measurements in the network.

The main programs that make up this application are meant to: a) the modelling of the load curves from the buses of the network using typical load curves and measurements in the network; b) the Fourier's series decomposition for the daily load curves; c) the calculation of active and reactive power flows in the MV distribution network; d) the calculation of voltage quality statistical coefficients at the buses of the network; e) the calculation of energy losses in the components of the network; f) the calculation of the optimal rated power and optimal displacement of the power sources used for reactive power compensation (shunt capacitors); g) the calculation of optimal sectionalizing points in the MV networks that are designed in a loop configuration, but use a radial one in normal operating conditions.

The set of programs is written in Turbo PASCAL and can be used with any personal computer compatible with IBM-PC and MS-DOS operating system.

4. Conclusions

The mathematical model described in this paper, which consists in modelling the daily load curves from the buses of the MV distribution networks and their decomposition using Fourier's series, could be used to optimal planning of the operating conditions of the networks; this model enjoys the following advantages: a) an important decrease of the amount of input data and especially the number of measurements in the network; b) the algorithms are simpler; c) a significant reduction in the number of power flows that have to be calculated under the cir-

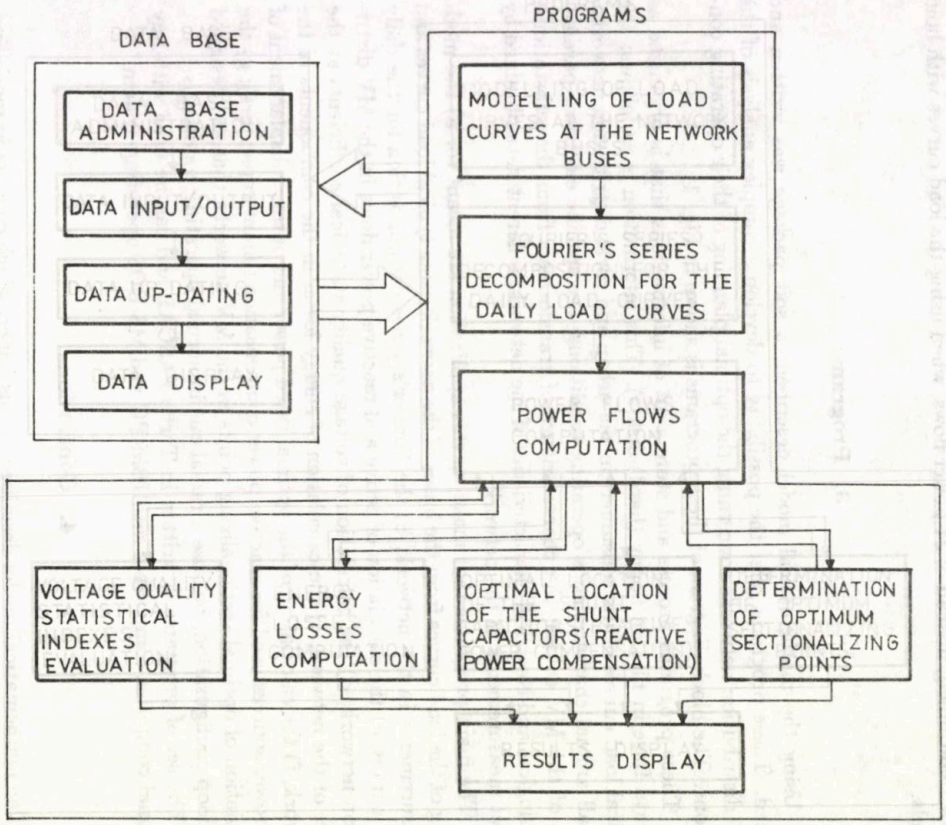

Fig. 1.– Flow chart of the soft package.

cumstances of an acceptable accuracy.

At the same time the set of programs developed on the basis of this model offers useful informations and suggestions to the service staff with the view to optimize the operating conditions of urban and rural MV distribution networks.

Received, February 9, 1994

Technical University "Gh. Asachi", Jassy, Department of Energetics

REFERENCES

1. Potrebič A.A., *Rasčet poteri energyi električeskih setiah s učetom grafikov nagruzok.* Električestvo, *6* (1990).
2. Codiasse A.M., Guillevic M., Giraud D., *Connaissance des charges moyenne tension en vue de leur prise en compte dans les études de planification.* Rev. Gén. de l'Électr., *7-8* (1982).
3. Poeată Al., Georgescu Gh., *Conducerea automată a reţelelor electrice.* ENERG, *3*, 163-180 (1987).
4. Georgescu Gh., Gavrilaş M., *Some Aspects about the Spectral Analysis of Load Curves of Electrical Distribution Networks.* Bul. Inst. polit., Iaşi, **XL (XLIV)**, *1-4*, s.III (1994).
5. Georgescu Gh.,Poeată Al., Gavrilaş M., Cârţină Gh., Alexandrescu V., Bonciu C., *Pachet de programe de calcul în scopul planificării optimale a regimurilor reţelelor de distribuţie de medie tensiune.* Nation. Symp. on Electrical Networks, Suceava, 1994.

PLANIFICAREA OPTIMALĂ A REŢELELOR ELECTRICE DE DISTRIBUŢIE DE MEDIE TENSIUNE

(Rezumat)

Se prezintă un pachet de programe de calcul care include un algoritm îmbunătăţit, bazat pe descompunerea armonică a graficelor de sarcină, în scopul analizei regimurilor optime ale reţelelor de distribuţie de medie tensiune.

BULETINUL INSTITUTULUI POLITEHNIC DIN IAŞI
Tomul XLI (XLV), Fasc. 1–2, 1995
Secţia III
ELECTROTEHNICĂ. ENERGETICĂ. ELECTRONICĂ

RECENZII BOOK REVIEWS

NAUNIN D., *Elektrische Strassenfahrzeuge. Technik, Entwicklungsstand und Einsatzgebiete.* Expert Verlag, Renningen, 1994, 218 S., ISBN 3-8169-1075-0.

Elektrische Strassenfahrzeuge gibt es seit 100 Jahren – und dieser Zeit werden auch ihre Vorteile und Nachteile diskutiert. Unabhängigkeit von der Primärenergie, geringerer Lärm und Abgasfreiheit unmittelbar am Fahrzeug sowie die neuesten Entwicklungen im Batteriebereich und bei den Motorsteuerungen lassen das Elektroauto in bestimmten Verkehrsbereichen attraktiv werden.

Das Buch berichtet über: a) wirtschaftliche und verkehrspolitische Aspekte; b) verschiedene neuartige Batteriesysteme; c) verschiedenartige Motorkonzepte; d) Möglichkeiten und Probleme der Serienfertigung; e) heutige Einsatzbereiche in Kurorten und künftige Verwendungschancen und stellt jeweils den neuesten Stand der Technik und Diskussion dar.

Das Buch wendet sich an Ingenieure in der Fahrzeug- und Batterie-Industrie und an Planer in den Verkehrsabteilungen von privaten, städtischen und staatlichen Einrichtungen, die über den Einsatz neuer Fahrzeuge zu entscheiden haben.

GROH H., *Hochspannungsmesstechnik.* Expert Verlag, Renningen, 1994, 147 S., ISBN 3-8169-1018-1.

Das Buch: a) vermittelt praxisbezogen den neuesten Stand der Teilentladungsmeßtechnik und der Impulsmeßtechnik im Bereich hoher Spannungen und hoher Ströme; b) beschreibt die physikalischen Grundlagen und die technische Realisierung der Meßsysteme; c) stellt die technische Ausführung hochfrequenzdichter und störstrahlungsfester Schirmungen der Sensoren und Impulsgeneratoren vor; d) enthält ein umfangreiches Literaturverzeichnis zu speziellen Problemlösungen auf diesen Gebieten.

Es wendet sich an Ingenieure und Physiker aus Entwicklung und Prüffelderprobung, aus der Grundlagenforschung mit den Schwerpunkten gepulste Lasersysteme und kontrollierte Kernfusion, aus der Schalterentwicklung im Hoch- und Niederspannungbereich, aus der Entwicklung und Prüfung elektrischer Isoliersysteme.

I n h a l t: Grundlagen der Strom- und Spannungsmessung bei transienten Vorgängen – Meßwiderstände – Rogowski-Spule – Faraday-Effekt (magnetorotation) – Hall-Effekt – Ohmsche und kapazitive Spannungsteiler – Messung der Lichtbogenspannung zu Schaltgeräten – Kerr-Effekt – Grundlagen der Teilentladungsmessung (TE-Messung) – Aufbau von TE-Prüffeldern und geschirmten Meßkabinen (Faraday-Käfig) – Synthetische Prüfschaltungen – Chemische Reaktionen in Teilentladungen-Mobile – Prüfspannungsquellen bei TE-Messungen – Kabel als Impulsgeneratoren – Schaltelemente der Hochstromtechnik.

ONDRACEK G., (federführend), *Werkstoffkunde.* Expert Verlag, Renningen, 1994, 305 S., ISBN 3-8169-1169-2.

Das bewährte Lehrbuch stellt die Grundlagen der Werkstoffkunde in vier Teilen dar: a) Aufbau der Werkstoffe; b) Eigenschaften der Werkstoffe; c) Werkstofftechnologie; d) Werkstoffprüfung und -untersuchung und vergleicht dabei zwischen den verschiedenen Werkstoffhauptgruppen: metallische, keramische, polymere und Verbundwerkstoffen.

Es ist für Ingenieure unterschiedlicher Fachrichtungen und für Naturwissenschaftler geschrieben, die im Bereich zwischen Theorie und Praxis stehen und denen es primär nicht um Einzelheiten der Werkstoffwissenschaften einerseits oder der Werkstofftechnik andererseits geht, sondern um das Verständnis des Gebietes und seiner Zusammenhänge anhand einer systematischen, möglichst kompakten Darstellung.

Für den an einer Vertiefung interessierten Leser ist am Ende des Buches deutschsprachige Literatur über Werkstoffkunde und ihre Peripheriegebiete zusammengestellt.

SARKOWSKI H., (federführend), *Dimensionierung von Halbleiterschaltungen.* Expert Verlag, Renningen, 1994, 279 S., ISBN 3-8169-0261-8.

Das mit zahlreichen Schaltbildern, Diagrammen, Beispielen, praxisnahen Formeln und Tabellen ausgestattete Lehr- und Fachbuch gibt eine systematische Anleitung für das Entwerfen, Berechnen und Dimensionieren der wichtigsten elektronischen Schaltungen: Verstärker mit bipolaren Transistoren und Feldeffekt-Transistoren – Kapazitätsdioden – Hochfrequenzschaltungen – Übertraglose NF – Endstufen – Rausch- und klirrarme Verstärker – Differenzverstärker – Operationsverstärker – Aktive Filter – Digitale Schaltungen in integrierter Technik.

RIGOLL G., *Neuronale Netze.* Expert Verlag, Renningen, 1994, 274 S., ISBN 3-8169-0975-2.

Das Buch: a) gibt Einführung in die Grundlagen der neuronalen Netze; b) beschreibt die Funktionsweise der neuronalen Netze aus ingenieurswissenschaftlicher Perspektive, speziell unter dem Aspekt der Musterverarbeitung und der künstlichen Intelligenz; c) vermittelt Ingenieuren, Informatikern und Naturwissenschaften eine detaillierte Übersicht über ca. 20 verschiedene Netzwerktypen und ihre mathematische Beschreibung; d) demonstriert das Anwendungspotential dieser neuen Technologie anhand zahlreicher Anwendungsbeispiele; e) geht auf Implementierungsaspekte und praktische Probleme bei der Realisierung neuronaler Algorithmen ein.

Es wendet sich an: a) Ingenieure, Informatiker und Naturwissenschaftler, die sich mit den Grundlagen und der Anwendung von Methoden der künstlichen Intelligenz beschäftigen; b) Mitglieder des technischen Managements, die die Funktionsweise von neuronalen Netzen und das Anwendungspotential dieser neuen Technologie kennenlernen möchten.

I n h a l t: Allgemeine Einführung – Besondere Eigenschaften neuronaler Netze – Neurobiologische Grundlagen – Mathematische Grundlagen neuronaler Netze – Lernverfahren – Übersicht über verschiedene Paradigmen neuronaler Netze – Anwendungsmöglichkeiten – Implementierungsaspekte.

BĂJENESCU T.I., *Datenkommunikationsnetzwerke, Heute und Morgen.* Expert Verlag, Renningen, 1994, 348 S., ISBN 3-8169-0984-1.

Das Buch: a) vermittelt praxisbezogen den aktuellen (und zukünftigen) Stand der Datenkommunikationsnetzwerke; b) gibt einen Überblick über die geschichtliche Entwicklung und über die Klassifikation von Rechnernetzen; c) informiert über die kennzeichnenden Eigenschaften der lokalen Netzwerke (Ring- und Bussysteme), Basis- und Breitbandtechnik, E-Mail, EDI, ODA, ODIF, EDIFACT, VANS, Teleports, über „Intelligente" Netze, integrierte Informationssysteme, Typisierung von Rechnernetzen (GAN, WAN, LAN, VLAN); d) gibt hinweise zur Informationssicherheit im Gebiet der Datenkommunikation; e) informiert über das neueste Übermittlungsverfahren (ATM) für zukünftige öffentliche Breibanddienste sowie über Pilotnetze in Deutschland und in der Schweiz; f) kann als Nachschlagewerk dienen, auch für Datenübertragung via Funktelefon nach GSM-Standard; g) enthält ein reiches englisches Abkürzungsverzeichnis und ein deutsches Stichwörtverzeichnis; h) definiert in einem alphabetischen Wörterverzeichnis die meistverwendeten Stichwörtverzeichnis; i) definiert in einem alphabetischen Wörterverzeichnis die meistverwendeten Fachbegriffe.

Es wendet sich an alle, die mit Datenkommunikationsnetzwerken – direkt oder indirekt befaßt sind wie: a) Entwicklungs-, Versuchs- und Betriebsingenieure; b) Techniker, Electroniker, Konstrukteure; c) Gutachter, Beratungsfirmen; d) Betreiber von kleinen und mittleren spezialisierten Privatfirmen.

I n h a l t: Einführungskapitel – Lokale Netzwerke – Büroautomationssysteme und Datenkommunikation – Quo Vadis Lan? Integrierte Informationssysteme-X 400; Schlüssel zur weltweiten elektronischen Kommunikation – Einige Gedanken über Datensicherheit und Kryptologie – Informationssicherheit im Gebiet der Datenkommunikation – Datenkommunikationsnetzwerke heute und morgen – Eine neue Übertragungstechnik und gleichzeiting der erste öffentliche Breibanddienste – Intelligente Netze – Datenübertragung via Funktelefon nach GSM-Standard – Die ISDN-Entwicklung in der Schweiz und einige Probleme des Datenschutzes in Deutschland.

SCHOBERT S., *Protokollanalyse in Lokalen Netzen.* Expert Verlag, Renningen, 1994, 278 S., ISBN 3-8169-1149-8.

In diesem Buch werden die verschiedenartigsten Datenprotokolle der heute so interessanten Lokalen Netze mit Meßwerkzeugen (Analysatoren) dargestellt. Es werden neben allgemeinen Hinweisen, Meßbeispielen und Handlungen der Messergebnisse verschiedenen Protokolle bis in die Bit-Ebene erläutert, und es wird deren Bedeutung angegeben. Viele Bildbeispiele veranschaulichen die „trockene" Materie.

Hier sind Informationen verschiedener Hersteller von Datenanalysatoren zusammengetragen worden, und in verschiedenen Kapiteln werden die jeweiligen Möglichkeiten und Darstellung (Bildschirmauszüge) der Ergebnisse und Auswertungen sowie Statistiken einander gegenübergestellt.

Das Buch ist geschrieben für: a) Betreiber von Lokalen Netzen; b) Administratoren in Rechnzentren; c) Entwickler und Planer im Bereich Datenkommunikation; d) Servicedienste von Netzbetreibern; e) Schulungs- und Ausbildungswecke bei Firmen (intern sowie Kundenschulungen), bei der Telekom, bei Fernmeldeschulen und Seminaren für Datentechnik sowie zum Einsatz in Fachbereichen für Informatik und Nachrichtentechnik an Universitäten und Fachhochschulen sowie an Technischen Akademien; f) Abteilungen für Produktförderung in produzierenden Firmen von Komponenten lokaler Netze und Meßtechnik.

Hardware:

- IBM-kompatibler PC bzw. PS/2-System;
- 640 kB Hauptspeicher, davon ca. 350 kB, frei;
- Festplatte mit mindestens 3 MB freiem Platz;
- 3,5″-HD-Floppylaufwerk (Format 5,25″ für DM, -lieferbar);
- Monitor: VGA;
- Drucker: Epson- oder IBM-Propinter-kompatibel oder Laserdrucker.

Software:

- Betriebssystem MS-DOS bzw. PC-DOS, Version 3.3, 4.01, 5.0 oder 6.0;
- Im „DOS-Fenster" unter Windows 3.x lauffähig.

SCHMIDT P.-F., *Praxis der Rasterelektronenmikroskopie und Mikrobereichsanalyse.* Expert Verlag, Renningen, 1994, 810 S., ISBN 3-8169-1038-6.

Der Themenband: a) vermittelt Kenntnisse über den Aufbau und die Funktionsweise von Rasterelelektronenmikroskopen; b) informiert über Vielfalt der Abbildungsmöglichkeiten; c) gibt praxisbezogen Hinweise auf die Optimierung der Geräteeinstellung für eine optimale Abbildung; d) führt in die Verfahren zur qualitativen und quantitativen Mikrobereichsanalyse ein; e) gibt eine Übersicht über Verfahren zur Oberflächenanalytik; f) informiert über alternative Rastermethoden; g) gibt Tops für die Präparation und Beschichtung von Proben; h) zeigt Einsatzmöglichkeiten der Rastelelektronenmikroskopie für Schadensfalluntersuchungen an Metallen, Keramiken und Polymeren; i) informiert über die Möglichkeiten der Rasterelektronenmikroskopie in der Halbleitertechnologie; j) informiert über Zusatzgerate zur Erweiterung des Einsatzbereichs von REM.

Das Buch wendet sich an alle: a) die Kenntnisse über die Methode der Rasterelektronenmikroskopie und Mikrobereichsanalyse gewinnen wollen; b) die sich über den optimalen Betrieb und Einsatz von REM und über die vielfältigen und analytischer Verfahren informieren möchten.

I n h a l t: Einführung in die Rasterelektronenmokroskopie – Aufbau eines Rastelelektronenmikroskops – Signalverarbeitung in einem Rasterelektronenmikroskop – Analog- und Digital REM, Bildspeicherung, Bildverarbeitung und Bildanalyse – Wechselwirkung der Primärelektronen mit der Probenmaterie: Signale im REM – Feldemissions-Rasterelektronenmikroskopie – Abbildung von Oberflächen und Vermeidung von Abbildungsfehlern – Mikroskopiertechnik – Röntgenmikroanalyse mit dem Rasterelektronenmikroskop – Quantitative Elektronenstrahl – Röntgenmikroanalyse – Kathodolumineszenz – Zuordnung von Schäden an keramischen Bauteilen – Ausgewählte Schadensbeispiele – Zuordnung Polymerwerkstoffen mit der Rasterelektronenmikroskopie – Alternative Rastermethoden – Laser-Mikrosonden – Massen-Spektrometrie.

GUTMANN F., *Energietechnik vom Kraftwerk bis zum Verbraucher.* Expert Verlag, Renningen, 1994, 156 S., ISBN 3-8169-1046-7.

Der Themenband: a) zeigt den aktuellen Stand der elektrischen Energietechnik aus der Praxis auf; b) gibt einen umfassenden Überblick (vom Kraftwerk bis zum Verbraucher); c) informiert

über alle wessentlichen Komponenten der Elektrotechnik; d) dient wegen seines Praxisbezugs als Nachschlagewerk für alle, die mit der Elektro-Energietechnik im Berührung kommen; e) zeigt zukunftsorientiert Entwicklungen und Tendenzen auf.

Für alle, die elektrotechnische Anlagen betreuen sowie auslegen und planen, wie Betriebsingenieure, -techniker und -meister, Gutachter und Beratungsfirmen, technisch orientierte Ein- und Verkäufer sowie für in der Ausbildung befindliche Ingenieure und Techniker ist dieses Buch als Nachschlagewerk unverzichtbar.

I n h a l t: Funktion und Einsatzbereiche von Transformatoren – Leistungsschilder elektrischer Maschinen – Anlaß-, Betriebsverhalten und Auslegung elektrischer Motoren – Die Verfügbarkeit der Primär-Energiequellen – Kraftwerksarten, ihre gegenwärtige und zukünftige Bedeutung – Umweltschutz in und um das Kraftwerk – Verteilunssysteme und Netze für den Energietransport – Vergleich der wichtigsten Leuchtmittel – Elektrowärme im industrielen Einsatz.

ZASTROW F., *Messen, Steuern und Regeln mit dem Personal-Computer.* Expert Verlag, Renningen, 1994, 261 S., ISBN 3-8169-1016-5.

Das Buch: a) vermittelt anwendungs- und praxisorientiert, wie analoge und digitale Meßwerte mit Hilfe einer Meßwerterfassungskarte von einem PC gelesen und ausgegeben werden können; b) gibt einen Überblick über die Ansteuerung der Ein-Ausgabekanäle (Ports) von Meßwerterfassungskarten anhand von Base-Adressen; c) macht den Benutzer unabhängig von firmenspezifischer Anwendungssoftware und spart somit Lizenzgebühren; d) führt in die Assembler-Programmierung ein; e) erläutert jeden Befehl ausführlich.

Es wendet sich an: a) Ingenieure und Studenten der Electrotechnik, des Fertigungstechnik, der Verfahrenstechnik, des Betriebs- und Versorgungstechnik und der Schiffsbetriebstechnik; b) Physiker, Chemiker und Biologen.

I n h a l t: Aufbau eines Mikroprozessorsystems – Register der Prozessorfamilie 80286, 80386 und 80486 – AD-Wandler – DA-Wandler – Ein Ausgabetreiber – Einbinden von Assemblerprogrammen in Turbo Pascal – Beispiele aus der Meß-, Steuerungs- und Regelungstechnik wie Invertierer – Zeitschleifen – Maskierung – Logische Verknüpfungen – Alarmverarbeitung – Ventilansteuerung – PID-Regler – Digitale Filter – Kaskadenregelung.

QUANG-HUE VO, (federführend), *Soundeningineering.* Expert Verlag, Renningen, 1994, 277 S., ISBN 3-8169-1177-3.

Namhafte Wissenschaftler von verschiedenen Universitäten und kompetente Fachexperten aus der europäischen Fahrzeugindustrie berichten über die grundlegenden Themen der Psychoakustik, über den Stand der Erforschung des Hörempfindens sowie über die konkreten technischen Maßnahmen am Fahrzeug für ein erwünschtes Geräuschbild.

Verschiedene praktische Wege, Methoden, Meß- und Auswerteverfahren und viele technische Beispiele auf dem Gebiet Soundeningeneering/Geräuschgestaltung sind dargestellt.

Das Buch wendet sich an alle, die mit dem Thema Akustik, Psychoakustik und Kundenmeinung bzgl. Akustikverhalten eines Produktes direkt oder indirekt befaßt sind, wie Kundenmeinungsforscher, Konstrukteure, Entwicklungs- und Versuchsingenieure, Gutacher, Anwendungstechniker und Beratungsfirmen, Fahrzeug-Projektleiter, Meßtechniker, Vertriebsleute und Fahrzeugverkäufer.

I n h a l t: Gütebeurteilung – Psychoakustik und Geräuschbeurteilung – Psychologische und akustische Aspekte der Klangqualität von Fahrzeuggeräuschen – Versuch der Objektivierung von Geräuschen der Verbrennungsmotoren – Geräuschsimulation zur Verbesserung des akustischen Charakters von Verbrennungsmotoren – Entwicklung eines objektiven Beurteilungmaßstabes für die subjektive Lästigkeit von Motorgeräuschen – Angewandte Psychoakustik als Bindeglied zwischen subjektiver Reifengeräuschbeurteilung und klassischer Meßtechnik – Verknüpfung der gehörgerechten Schallmeßtechnik mit einer Mehrkanal – Schwingungsanalyse – Active Noise Cancellation für Kraftfahrzeuge – Konzeption, Auslegung und versuchsgestützte Optimierung der Aggregatelagerung von Fahrzeugen – Möglichkeiten und Grenzen des Soundeningeneerings.

1996 APR 01

ISSN 0258-9109

F 1503/3

F 1503
41. V.
LSZ
9 000004 056691

BULETINUL INSTITUTULUI POLITEHNIC DIN IAŞI

Tomul XLI (XLV)
Fasc. 3-4

Secția III **ELECTROTEHNICĂ**
ENERGETICĂ
ELECTRONICĂ

1995

ORSZÁGOS MŰSZAKI INFORMÁCIÓS KÖZPONT ÉS KÖNYVTÁR 1883

BULETINUL INSTITUTULUI POLITEHNIC DIN IAŞI

Tomul XLI (XLV)
Fasc. 3–4

Secţia III

ELECTROTEHNICĂ. ENERGETICĂ. ELECTRONICĂ

1995

EDITORIAL STAFF

Prof. dr. eng. **VITALIE BELOUSOV** (President)
Prof. dr. eng. **PAULICĂ RĂILEANU** (Secretary)
Prof. dr. eng. **EFTIMIE NIŢESCU**
Prof. dr. doc. **ALFRED BRAIER** (Editor)
Prof. dr. eng. **HUGO ROSMAN** (Editor)
Prof. dr. eng. **MIHAIL VOICU** (Head of the Exchange Service)
Prof. dr. **AUREL BEJANCU**
Prof. dr. eng. **VICTOR BULACOVSCHI**
Prof. dr. eng. **DIMITRIE ALEXA**
Prof. dr. eng. **SPIRIDON CREŢU**
Prof. dr. eng. **ADRIAN RADU**
Prof. dr. eng. **ION GIURMA**
Prof. dr. eng. **MIRCEA MATEESCU**

The **Bulletin of the Polytechnic Institute of Jassy** is edited by
the **Technical University "Gh.Asachi"** (the former Polytechnic Institute), Jassy.

TEXredaction:
B. Grigoriu, A. Rotaru
Technical University of Jassy

BULETINUL INSTITUTULUI POLITEHNIC DIN IAŞI
BULLETIN OF THE POLYTECHNIC INSTITUTE OF JASSY
Tomul XLI (XLV), Fasc. 3–4 1995

Secţia III

ELECTROTEHNICĂ. ENERGETICĂ. ELECTRONICĂ

SUMAR

Pag.

I. TULEAŞCĂ, Asupra propagării undelor electromagnetice în medii neliniare inerţiale (engl., rez. rom.) 7

IRINEL CASIAN-BOTEZ, Asupra echivalenţei dintre metoda TLM şi metoda cu diferenţe finite (franc., rez. rom.) 19

ALFRED BRAIER şi HUGO ROSMAN, Un studiu simbolic al răspunsului sistemelor liniare la semnale de intrare modulate în amplitudine. I. Semnale cu purtătoarea suprimată (engl., rez. rom.) 25

C.E. SAVIN, M.O. AHMAD şi M.N.S. SWAMY, Un nou procedeu pentru formularea programului liniar a cărui soluţie este un filtru stivă de eroare absolută minimă (engl., rez. rom.) 37

ADRIAN LEUCIUC şi DANIEL MIHALACHI, Filtru de urmărire opreşte bandă (engl., rez. rom.) 47

PAUL COTAE şi DANIELA TĂRNICERIU, Comparaţie între performanţele tehnicilor de modulaţie digitale folosind filtre de bandă limitată cauzale (engl., rez. rom.) 53

N.D. ALEXANDRU, O investigaţie a spectrului de putere a codurilor AMSI (engl., rez. rom.) 59

N. DAMEAN, Tehnici de măsurare formulate ca probleme inverse. I. Abordări principale (engl., rez. rom.) 63

MARIANA BUZDUGA, Asupra condiţiilor de apariţie a oscilaţiilor mecanice într-un sistem electromecanic. II. Studiul stabilităţii soluţiilor (franc., rez. rom.) 73

MARIANA BUZDUGA şi CRISTIAN FOŞALĂU, Liniarizarea răspunsului unui convertor analog–numeric pentru măsurarea unor mărimi neelectrice (engl., rez. rom.) 81

ADRIAN BARABOI, Caracteristicile bobinei neliniare cu miez magnetizat pe direcţii ortogonale (franc., rez. rom.) 85

LAURENŢIU DIMITRIU, Câteva consideraţii privind structurile sistemelor de control ale motoarelor cu aprindere prin scânteie (engl., rez. rom.) 91

Pag.

D. ALEXA şi CLARISSA GÎTLAN, Sistem de alimentare cu factor de putere ridicat pentru motoarele electrice de tracţiune de curent continuu ale unei locomotive (germ., rez. rom.) 97

RADU COCIU şi LIVIA COCIU, Consideraţii asupra cuplului electromagnetic al servomotorului asincron bifazat (franc., rez. rom.) 105

MIRCEA GOGU, Funcţionarea motorului asincron bifazat cu rotor în scurtcircuit, comandat de un convertor PWM, luând în considerare efectele armonicilor de curent (engl., rez. rom.) 113

CRISTINA SCHREINER, LORIN CANTEMIR şi MARINEL TEMNEANU, Un nou parametru complex util în caracterizarea regimurilor tranzitorii de mişcare ale motorului asincron liniar (engl., rez. rom.) 123

GH. BĂLUŢĂ, MIRCEA DIACONESCU şi C. CĂCIULEANU, Contribuţii privind comanda fără traductor de poziţie a sistemelor de acţionare electrică cu motoare pas cu pas (franc., rez. rom.) 131

IULIAN GRAUR, GR. TAŞCĂ, ADRIAN GRAUR, DRAGOŞ TAŞCĂ, M. ALBU, MIHAELA MAREŞ, DORIN LUCACHE şi V. HORGA, Model matematic pentru calculul regimului de funcţionare stabilizat al unor sisteme de acţionare electrică utilizate în industria metalurgică (engl., rez. rom.) 137

FLORIN MUNTEANU, D. IVAS şi GERARDUS-CHRISTOFFEL PAAP, De la mentenanţa planificată la mentenanţa oportună (engl., rez. rom.) 145

GH. CÂRŢINĂ, VIRGIL ALEXANDRESCU şi GH. GEORGESCU, Particularităţile modelelor de optimizare în energetică în etapa actuală (franc., rez. rom.) 155

M. GAVRILAŞ şi GH. GEORGESCU, Identificarea categoriei consumatorilor din reţelele electrice de distribuţie folosind reţele neuronale artificiale de tip Hopfield (engl., rez. rom.) 161

DUMITRU BĂRBULESCU 167

RECENZII 169

BULETINUL INSTITUTULUI POLITEHNIC DIN IAŞI
BULLETIN OF THE POLYTECHNIC INSTITUTE OF JASSY
Tome XLI (XLV), Fasc. 3–4 1995

Section III

ELECTROTECHNICS. ENERGETICS. ELECTRONICS

CONTENTS

Pp.

I. TULEAŞCĂ, About Electromagnetic Waves Scattering in Nonlinear Inertial Media (English, Romanian summary) 7

IRINEL CASIAN-BOTEZ, Sur l'équivalence entre la méthode TLM et la méthode des différences finies (French, Romanian summary) 19

ALFRED BRAIER and HUGO ROSMAN, A Symbolic Study of Linear Systems Response to Amplitude Modulated Inputs. I. Inputs with Suppressed Carrier (English, Romanian summary) 25

C.E. SAVIN, M.O. AHMAD and M.N.S. SWAMY, On the Derivation of the Linear Program which Finds a Minimum Mean Absolute Error Stack Filter (English, Romanian summary) 37

ADRIAN LEUCIUC and DANIEL MIHALACHI, Notch Tracking Filter (English, Romanian summary) 47

PAUL COTAE and DANIELA TĂRNICERIU, Comparison of Performances of Digital Modulation Techniques Using Causal Bandlimiting Filters (English, Romanian summary) 53

N.D. ALEXANDRU, An Investigation of the Power Spectrum of the AMSI Codes (English, Romanian summary) 59

N. DAMEAN, Measurement Techniques Formulated as Inverse Problems. I. Main Approaches (English, Romanian summary) 63

MARIANA BUZDUGA, Sur les conditions d'apparition des oscillations mécaniques dans un système électromécanique. II. Étude de la stabilité des solutions (French, Romanian summary) 73

MARIANA BUZDUGA and CRISTIAN FOŞALĂU, Linearisation of the Response of an A/D Converter for Measuring Non-Electrical Variables (English, Romanian summary) 81

ADRIAN BARABOI, Les caractéristiques de la bobine nonlinéaire à noyau magnetisé orthogonalement (French, Romanian summary) 85

LAURENŢIU DIMITRIU, Some Considerations concerning the Structures of Control Systems for Spark Ignition Engines (English, Romanian summary) 91

Pp.

D. ALEXA und CLARISSA GÎTLAN, Speisungssystem mit erhöhtem Leistungsfaktor für elektrische Lokomotiven mit Gleichstrommotoren (German, Romanian summary) .. 97

RADU COCIU et LIVIA COCIU, Considérations sur le couple électromagnétique du servomoteur asynchrone biphasé (French, Romanian summary) 105

MIRCEA GOGU, Two-Phase Squirrel-Cage Induction Machine Working, Driven by a PWM Converter, Considering the Effects of the Current Harmonics (English, Romanian summary) 113

CRISTINA SCHREINER, LORIN CANTEMIR and MARINEL TEMNEANU, A New Complex Parameter in Establishing the Transient Moving Regime of Linear Induction Motors (English, Romanian summary) 123

GH. BĂLUŢĂ, MIRCEA DIACONESCU et C. CĂCIULEANU, Contributions concernant la commande sans capteur de position des systèmes d'entrainement électrique à moteurs pas à pas (French, Romanian summary) 131

IULIAN GRAUR, GR. TAŞCĂ, ADRIAN GRAUR, DRAGOŞ TAŞCĂ, M. ALBU, MIHAELA MAREŞ, DORIN LUCACHE and V. HORGA, Mathematical Model for Stabilized State of Electrical Drive Systems Used in Metallurgical Industry (English, Romanian summary) 137

FLORIN MUNTEANU, D. IVAS and GERARDUS-CHRISTOFFEL PAAP, From Planned Maintenance to Opportune Maintenance (English, Romanian summary) 145

GH. CÂRŢINĂ, VIRGIL ALEXANDRESCU et GH. GEORGESCU, Les particularités des modèles d'optimisation en énergétique dans l'étape actuelle (French, Romanian summary) 155

M. GAVRILAŞ and GH. GEORGESCU, Consumer Category Identification in Distribution Networks Using Hopfield Nets (English, Romanian summary) 161

DUMITRU BĂRBULESCU 167

BOOK REVIEWS 169

BULETINUL INSTITUTULUI POLITEHNIC DIN IAŞI
Tomul XLI (XLV), Fasc. 3–4, 1995
Secţia III
ELECTROTEHNICĂ. ENERGETICĂ. ELECTRONICĂ

D.C. 538.56

ABOUT ELECTROMAGNETIC WAVES SCATTERING IN NONLINEAR INERTIAL MEDIA

BY

I. TULEAŞCĂ

1. Introduction

In order to study the electromagnetic field spreading in nonlinear media it appears the difficulty of solving specific nonlinear equations with partial derivatives.

Following the idea of finding an acceptable analytical solution, it has been made the attempt [5] to take specific nonlinear circuits investigation methods [7] and to adapt them for the electromagnetic waves study. Thus, considering a quasistationary electromagnetic field and a weak nonlinear medium, it was adapted to the medium the *inertial* concept which implies, for the nonlinear circuits, the existence of a linear relation between the instantaneous excitation and response signal values as well as a nonlinear relation between their RMS values. The advantage of the approach consists in the fact that, for a nonlinear inertial circuit, the spectra of the response and excitation signals are identical. Consequently, in the particular situation of such a circuit, excited by a sinusoidal signal, the response is also sinusoidal and the symbolic analytical complex method of representation can be utilized, providing all the advantages known from the harmonic steady state circuit analysis [4].

On the other hand, it has been performed the ferromagnetic materials study using only their fundamental magnetization curve, neglecting the hysterezis phenomenon. From many existing $B(H)$ fundamental curve approximations [3], it has been used the exponential formulation [2], valid for every magnetic material on the whole domain from zero to curvature point and saturation zone. It has been pointed out [2] a remarkable approximation accuracy, with an error less than 5%, associated with the computer's use advantage in the approximation constants determination, regarding both magnetic material with a fast rising $B(H)$ curve (annealed sheet steel) and those with a very slow rising one (cast iron). Taking into account this approximation, it has been extended the procedure for situations that imply the existence of a $H(t)$ sinusoidal excitation signal with the appearance of a $B(t)$ periodic response one.

In this paper it is made the attempt to associate the above described methods in order to obtain the general material constants expression and the electromagnetic field spreading equations in inertial media as well as their particular expressions for a ferromagnetic medium, the semi-infinite slab, determining the electromagnetic field characteristic propagation relations, the magnetic permeability μ and the depth of penetration δ.

2. The "Inertialization" Concept Utilization

From the already mentioned fact regarding the characteristic of a medium considered to be inertial (i.e. the identity of the excitation and response signal spectrum) and from the nonlinear circuit forced steady state definition [7], it appears immediately that the quasistationary electromagnetic field penetration in such a medium means [6] to obtain a forced state solution of the second order differential with partial derivatives equation which characterizes the state variables. Additionally, the employment of the symbolic analytical complex representation for the state vectors simplifies the diffusion equation, which becomes differential, much easier to deal with than with partial derivatives one.

According to what has already been mentioned above. it is extremely adequate to use the simplifying but practically accepted hypothesis of the inertial behaviour of the nonlinear medium in which the electromagnetic field evolves. Thus, the medium will have an inertial behaviour if, while the excitation–response amplitude curve $Y_m(X_m)$ has a nonlinear character, the instantaneous values curve $Y(X)$ can be considered linear.

Therefore, it is admitted that, being given a quasistationary harmonic electromagnetic field, excited by the sinusoidal state vector $\mathbf{X}$ and characterized by the material constant r of the medium, considered to be nonlinear, isotropic, homogeneous, motionless, without permanent polarization and magnetization as well as hereditary properties, it can be defined a response state vector $\mathbf{Y}$, so that

$$\mathbf{Y} = r\mathbf{X}; \quad \mathbf{X} = \mathbf{E}, \mathbf{H}; \quad \mathbf{Y} = \mathbf{J}, \mathbf{B}; \quad r = \varepsilon, \sigma, \mu. \tag{1}$$

The notations are the usual ones and the association of the vectors $\mathbf{E}, \mathbf{H}, \mathbf{J}, \mathbf{B}$ in $\mathbf{Y}=r\mathbf{X}$ relations of type (1) is in accordance with the material equations of the field.

3. The Material Constants Calculus

It is considered that the nonlinear medium is characterized by material constants which are scalar functions of the excitation vector modulus, $r = r(X)$.

Once adopted the inertial concept for the electromagnetic field propagation medium, it can be considered that the nonlinear dependence of the response state vector Y modulus versus the excitation state vector X modulus can be described analytically using a polynomial form

$$Y = \sum_{k=1}^{n} a_k e^{\alpha_k x}, \tag{2}$$

where it is considered a development of the form

$$e^x = 1 + x + \frac{x^2}{2} + \frac{x^3}{6} + \cdots \tag{3}$$

With the notation $\beta = \omega t + \gamma$, the state vector X modulus time variation may be described using the relation:

$$X(t) = X_m \cos\beta = \sqrt{2} X \cos\beta. \tag{4}$$

Considering only the first n terms of the Fourier series based relation obtained for Y, it results the expression written below, whose coefficients are, evidently, dependent from a_k, α_k and X_m:

$$Y(t) = \sum_{k=1}^{n} \sum_{i=0}^{n} a_k \frac{\alpha_k^i X_m^i \cos^i \beta}{i!}. \tag{5}$$

Due to the fact that it has been considered a forced steady state in inertial conditions, the response implies only the presence of the fundamental harmonic of angular frequency ω. Thus, there will be neglected the other harmonics of superior order and it will be imposed for the continuous component the condition:

$$Y_0 = 0, \quad \text{i.e.} \quad \sum_{k=1}^{n} \left(a_k + \frac{a_k \alpha_k^2 X_m^2}{4} \right) = 0. \tag{6}$$

In the expression (5) it will be given to n the value 4, taken thus into consideration only the first four terms from the expansion of e^x and from the polynomial dependence $Y(X)$. In these conditions, it will be calculated [1] the amplitude of the fundamental term of the response state vector modulus, which will be of the form:

$$Y_{1m} = \frac{1}{\pi} \int_0^{2\pi} Y(X) \cos\beta \mathrm{d}\beta = \sum_{k=1}^{4} \left(a_k \alpha_k X_m + \frac{a_k \alpha_k^3}{8} X_m^3 \right). \tag{7}$$

Acting similarly with the case of the nonlinear inertial circuits, the material constant r can be defined as the ratio of the fundamental term of the state vector modulus, $Y_1(t)$ and the excitation vector modulus, $X(t)$:

$$r = \frac{Y_1}{X}, \tag{8}$$

relation used to calculate the value of the material constant:

$$r = \sum_{k=1}^{4} a_k \alpha_k + X_m^2 \sum_{k=1}^{4} \frac{a_k \alpha_k^3}{8} = U + V X_m^2 = U + 2VX^2, \tag{9}$$

where

$$U = \sum_{k=1}^{4} a_k \alpha_k, \quad V = \sum_{k=1}^{4} \frac{a_k \alpha_k^3}{8}, \quad X_m = \sqrt{2} X \tag{10}$$

render evident its dependence from the amplitude (RMS) of the excitation vector modulus.

Accordingly, in the case of inertial media, in harmonic quasistationary state, the electric conductivity, the magnetic permeability and the permitivity may be calculated with the expressions

$$\begin{cases} \sigma = U(\sigma) + V(\sigma) E_m^2 = \sigma(E_m), \\ \mu = U(\mu) + V(\mu) H_m^2 = \mu(H_m), \\ \varepsilon = U(\varepsilon) + V(\varepsilon) E_m^2 = \varepsilon(E_m). \end{cases} \tag{11}$$

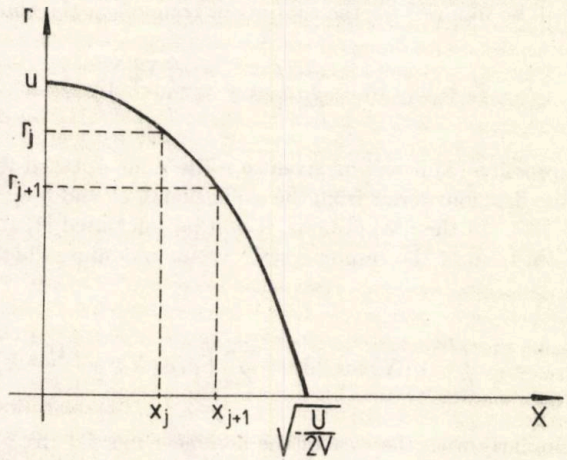

Fig. 1.– The $r(X) = U + 2VX^2$ graphic representation.

Since r, the material constant designated by (9), must be positive ($r > 0$), even in the case of $X = 0$, from $r(0) = U$ it follows that $U > 0$. The subsequent analysis of the function $r(X)$ requires that V must be negative ($V < 0$) so that for $r(X)$ it is obtained the representation in Fig.1, from which it can be inferred

$$X_{j+1} > X_j \quad \text{and} \quad r_{j+1} < r_j. \tag{12}$$

Thus, forming the system

$$r_j = U + 2VX_j^2, \quad r_{j+1} = U + 2VX_{j+1}^2, \tag{13}$$

there are obtained for U and V the expressions:

$$U = \frac{r_j X_{j+1}^2 - r_{j+1} X_j^2}{X_{j+1}^2 - X_j^2}, \quad V = \frac{r_{j+1} - r_j}{2X_{j+1}^2 - 2X_j^2}. \tag{14}$$

4. The Harmonic Quasistationary Electromagnetic Field Equations

Considering the case of a homogeneous electromagnetic field evolving in an internal, isotropic, motionless medium, having no permanent polarization and magnetization as well as hereditary properties, the evolution, state and material equations in harmonic quasistationary state are:

$$\begin{gathered} \operatorname{rot} \underline{\mathbf{E}} = -\mathrm{j}\omega \underline{\mathbf{B}}, \quad \operatorname{rot} \underline{\mathbf{H}} = \underline{\mathbf{J}} + \mathrm{j}\omega \underline{\mathbf{D}}, \quad \operatorname{div} \underline{\mathbf{D}} = 0, \quad \operatorname{div} \underline{\mathbf{B}} = 0, \\ \underline{\mathbf{B}} = \mu \underline{\mathbf{H}}, \quad \underline{\mathbf{D}} = \varepsilon \underline{\mathbf{E}}, \quad \underline{\mathbf{J}} = \sigma \underline{\mathbf{E}}. \end{gathered} \tag{15}$$

If the material constants expressions are taken into account the first two equations become

$$\begin{cases} \operatorname{rot} \underline{\mathbf{H}} = \{U(\sigma) + \mathrm{j}\omega U(\varepsilon) + [V(\sigma) + \mathrm{j}\omega V(\varepsilon)] E_m^2\} \underline{\mathbf{E}}, \\ \operatorname{rot} \underline{\mathbf{E}} = -\mathrm{j}\omega [U(\mu) + V(\mu) H_m^2] \underline{\mathbf{H}}, \end{cases} \tag{16}$$

constituting a nonlinear differential with partial derivatives equations system, whose solutions are difficult to be determined in the general case of media with nonlinear permitivity, conductivity and magnetic permeability. In important particular situations, the system simplifies considerable permitting, relatively easy, its integration under given limit conditions.

Thus, in the case of inertial dielectrics, the equations shape becomes much simple:

$$\operatorname{rot} \underline{\mathbf{H}} = \mathrm{j}\omega [U(\varepsilon) + V(\varepsilon) E_m^2] \underline{\mathbf{E}}, \quad \operatorname{rot} \underline{\mathbf{E}} = -\mathrm{j}\omega \mu \underline{\mathbf{H}}. \tag{17}$$

Taking into consideration that $\operatorname{rot} \operatorname{rot} \underline{\mathbf{E}} = \operatorname{grad} \operatorname{div} \underline{\mathbf{E}} - \Delta \underline{\mathbf{E}}$ and $\operatorname{div} \underline{\mathbf{E}} = 0$, it follows:

$$\Delta \underline{\mathbf{E}} = \omega^2 \mu [U(\varepsilon) + V(\varepsilon) E_m^2] \underline{\mathbf{E}}. \tag{18}$$

In the case of the inertial ferromagnetics, neglecting, of course, the displacement current, the equations (16) become

$$\operatorname{rot} \underline{\mathbf{H}} = \sigma \underline{\mathbf{E}}, \quad \operatorname{rot} \underline{\mathbf{E}} = -\mathrm{j}\omega [U(\mu) + V(\mu) H_m^2] \underline{\mathbf{H}}. \tag{19}$$

Having in view that $\operatorname{rot} \operatorname{rot} \underline{\mathbf{H}} = \operatorname{grad} \operatorname{div} \underline{\mathbf{H}} - \Delta \underline{\mathbf{H}}$ and $\operatorname{div} \underline{\mathbf{H}} = 0$, it results

$$\Delta\underline{\mathbf{H}} = \mathrm{j}\omega\sigma[U(\mu) + V(\mu)H_m^2]\underline{\mathbf{H}}. \tag{20}$$

5. The Harmonic Quasistationary Electromagnetic Field Spreading in the Semi-Infinite Ferromagnetic Conductor Inertial Slab

In what follows it will be studied the electromagnetic field penetration in the semi-infinite conductor ferromagnetic slab, weak nonlinear, inertial, in the case of a harmonic quasistationary evolution. In exterior, at the surface of the semi-infinite slab, it is established a homogeneous magnetic field, directed tangential along Ox axis, whose intensity, $\underline{H}_0(t)$, has a harmonic variation in time, $\underline{\mathbf{H}}_0 = \sqrt{2}\underline{H}_0 \sin(\omega t + \Psi)\mathbf{i}$, consequently $\underline{\mathbf{H}}_0 = \underline{H}_0\mathbf{i}$ with $\underline{H}_0 = H_0 e^{\mathrm{j}\Psi}$.

Taking into consideration the infinite extension of the medium, the uniformity of the inductive magnetic field as well as the continuity of its tangential components at the surface of the conductor, the interior magnetic field, oriented along the Ox axis, is a function of y and t only, as $\underline{\mathbf{E}}$ and $\underline{\mathbf{J}}$ are too. Thus $\underline{\mathbf{H}}$ will have its complex image $\underline{\mathbf{H}} = \underline{H}_x(y)\mathbf{i}$. The waves appear to be plane and the equation

$$\Delta\underline{\mathbf{H}} = \mathrm{j}\omega\sigma[U(\mu) + V(\mu)H_m^2]\underline{\mathbf{H}}, \tag{21}$$

which, considering the medium conductivity σ linear, becomes

$$\frac{\mathrm{d}^2\underline{H}_x}{\mathrm{d}y^2} = \mathrm{j}\omega\sigma[U(\mu) + V(\mu)H_m^2]\underline{H}_x, \tag{22}$$

a differential, nonlinear equation, difficult to be integrated. If, however, in the case of the nonlinear term it is taken into account the complex form of $\underline{H}_x$ namely

$$\underline{H}_x = \frac{H_m}{\sqrt{2}} e^{\mathrm{j}\Psi_H} \tag{23}$$

and it is chosen $\Psi_H = \pi/2$ (22) becomes a Duffing equation, having the form

$$\frac{\mathrm{d}^2\underline{H}_x}{\mathrm{d}y^2} - \mathrm{j}\omega\sigma U(\mu)\underline{H}_x + \mathrm{j}2\omega\sigma V(\mu)\underline{H}_x^3 = 0, \tag{24}$$

whose solution is obtained using the perturbation (small parameter) method. In this respect, in order to be able to use the method, it is made the division by $\mathrm{j}\omega\sigma U(\mu)$ resulting

$$\frac{\mathrm{d}^2\underline{H}_x}{\mathrm{j}\omega\sigma U(\mu)\mathrm{d}y^2} - \underline{H}_x + \frac{2V(\mu)}{U(\mu)}\underline{H}_x^3 = 0. \tag{25}$$

With the notations $\underline{\gamma}^2 = j\omega\sigma U(\mu)$, $\underline{\gamma} y = \tau$, $\lambda = 2V(\mu)/U(\mu)$, (25) becomes:

$$\frac{d^2\underline{H}_x}{d\tau^2} - \underline{H}_x + \lambda \underline{H}_x^3 = 0. \tag{26}$$

The condition for λ to be a small parameter ($|\lambda| \ll 1$) results calculating

$$|\lambda| = \left|\frac{2V(\mu)}{U(\mu)}\right|, \tag{27}$$

which, taking into account (14), is

$$|\lambda| = \left|\frac{\mu_{j+1} - \mu_j}{\mu_j H_{j+1} - \mu_{j+1} H_j^2}\right|. \tag{28}$$

Considering, according to (12), that

$$\left|\frac{\mu_{j+1} - \mu_j}{\mu_j H_{j+1} - \mu_{j+1} H_j^2}\right| = \frac{\mu_j - \mu_{j+1}}{\mu_j H_{j+1}^2 - \mu_{j+1} H_j^2} \tag{29}$$

the condition $|\lambda| \ll 1$ is equivalent with

$$\mu_j(H_{j+1}^2 - 1) - \mu_{j+1}(H_j^2 - 1) \gg 0. \tag{30}$$

The inequality (30) is true for all $H > 1$ and for all μ, which enables the affirmation that

$$\lambda = \frac{2V(\mu)}{U(\mu)} \ll 1, \quad \forall\mu, \quad \forall H > 1. \tag{31}$$

It is admitted as solution of the equation (26) the series

$$\underline{H}_x = \underline{H}_{x0} + \lambda \underline{H}_{x1} + \lambda^2 \underline{H}_{2x} + \cdots, \tag{32}$$

from which, if it converges fast enough, there can be retained, with a satisfactory approximation, only the first three terms. It is imposed that this solution satisfies the equation (26), therefore it will be obtained

$$\begin{aligned} &\frac{d^2\underline{H}_{x0}}{d\tau^2} + \lambda\frac{d^2\underline{H}_{x1}}{d\tau^2} + \lambda^2\frac{d^2\underline{H}_{x2}}{d\tau^2} - (\underline{H}_{x0} + \lambda\underline{H}_{x1} + \lambda^2\underline{H}_{x2}) + \\ &+ \lambda(\underline{H}_{x0} + \lambda\underline{H}_{x1} + \lambda^2\underline{H}_{x2})^3 = 0. \end{aligned} \tag{33}$$

Identifying the terms in λ^0, λ^1 and λ^2 there are obtained linear differential equations. After their integration it is determined the generating solution and the

correction terms. Thus, for $\underline{H}_0 = H_0 e^{j0}$: a) the generating equation, which is differential, linear, homogeneous, with constant coefficients, specific for the linear media, having the form

$$\frac{d^2 \underline{H}_{x0}}{d\tau^2} - \underline{H}_{x0} = 0, \tag{34}$$

with the solution

$$\underline{H}_{x0} = H_0 e^{-\tau}; \tag{35}$$

b) the equation of the first approximation,

$$\frac{d^2 \underline{H}_{x1}}{d\tau^2} - \underline{H}_{x1} + \underline{H}_{x0}^3 = 0, \tag{36}$$

has the solution:

$$\underline{H}_{x1} = \tfrac{1}{8} H_0^3 (e^{-\tau} - e^{-3\tau}), \tag{37}$$

obtained with the method of variation of parameters [1]; c) the equation of the second approximation:

$$\frac{d^2 \underline{H}_{x2}}{d\tau^2} - \underline{H}_{x2} + 3\underline{H}_{x0}^2 \underline{H}_{x1} = 0, \tag{38}$$

admits the solution:

$$\underline{H}_{x2} = \tfrac{1}{64} H_0^5 (2e^{-\tau} - 3e^{-3\tau} + e^{-5\tau}) \tag{39}$$

obtained using the same method.

Consequently, the general solution, with the shape:

$$\underline{H}_x = \underline{H}_{x0} + \lambda \underline{H}_{x1} + \lambda^2 \underline{H}_{x2}, \tag{40}$$

is

$$\underline{H}_x(y) = A H_0 e^{-\tau} - B H_0 e^{-3\tau} + C H_0 e^{-5\tau}, \tag{41}$$

where

$$A = 1 + \tfrac{1}{4} m + \tfrac{1}{8} m^2, \quad B = \tfrac{1}{4} m + \tfrac{3}{16} m^2, \quad C = \tfrac{1}{16} m^2, \quad m = \frac{V(\mu)}{U(\mu)} H_0^2. \tag{42}$$

Resorting to the equation rot $\underline{\mathbf{H}} = \underline{\mathbf{J}}$ and having in view that $\underline{\mathbf{H}} = \underline{H}_x(y)\mathbf{i}$ it results for $\underline{\mathbf{J}}$ an expression of the form

$$\underline{J}_z(y) = -\frac{\mathrm{d}\underline{H}_x}{\mathrm{d}y} = \underline{\gamma}(AH_0\mathrm{e}^{-\tau} - 3BH_0\mathrm{e}^{-3\tau} + 5CH_0\mathrm{e}^{-5\tau}). \tag{43}$$

Also, knowing that $\underline{\mathbf{J}} = \sigma\underline{\mathbf{E}}$, it results immediately that

$$\underline{E}_z(y) = \sigma^{-1}\underline{J}_z(y) = \sigma^{-1}\underline{\gamma}(AH_0\mathrm{e}^{-\tau} - 3BH_0\mathrm{e}^{-3\tau} + 5CH_0\mathrm{e}^{-5\tau}). \tag{44}$$

For the Poynting vector, due to the plane character of the electromagnetic waves penetrating the conductor ferromagnetic space, it results:

$$\underline{\mathbf{S}} = \underline{\mathbf{E}} \times \underline{\mathbf{H}}^* = \mathbf{k}\underline{E}_z \times \mathbf{i}\underline{\mathbf{H}}_x^* = \mathbf{j}\underline{S}_y(y), \tag{45}$$

with

$$\underline{S}_y(0) = \underline{E}_z(0)\underline{H}_x^*(0) = \sigma^{-1}\underline{\gamma}H_0^2\left(1 - \frac{m}{2} - \frac{m^2}{8}\right). \tag{46}$$

From the expression (46), knowing that $\underline{\gamma} = \alpha(1 + \mathrm{j})$ is the propagation constant, where $\alpha = \sqrt{\omega\sigma U(\mu)/2}$ represents the attenuation one, it can be inferred

$$\underline{S}_y(0) = (1 + \mathrm{j})\alpha\sigma^{-1}H_0^2\left(1 - \frac{m}{2} - \frac{m^2}{8}\right) = p + \mathrm{j}q, \tag{47}$$

where p and q are the active, respectively, reactive power, absorbed in the unit of surface area.

Also, for $\underline{H}_x(y)$ it can be written

$$\underline{H}_x(y) = AH_0\mathrm{e}^{-\alpha y}\mathrm{e}^{-\mathrm{j}\alpha y} - BH_0\mathrm{e}^{-3\alpha y}\mathrm{e}^{-\mathrm{j}3\alpha y} + 5CH_0\mathrm{e}^{-5\alpha y}\mathrm{e}^{-\mathrm{j}5\alpha y}, \tag{48}$$

from where it results for the RMS $H_x(y)$ the expression:

$$H_x(y) = \sqrt{A^2H_0^2\mathrm{e}^{-2\alpha y} + B^2H_0^2\mathrm{e}^{-6\alpha y} + C^2H_0^2\mathrm{e}^{-10\alpha y}}. \tag{49}$$

Considering the relation (9) it may be obtained for the magnetic permeability the expression

$$\mu = U(\mu) + 2H_0^2(A^2 + B^2\mathrm{e}^{-4\alpha y} + C^2\mathrm{e}^{-8\alpha y})V(\mu)\mathrm{e}^{-2\alpha y}, \tag{50}$$

with $A, B, C, U(\mu), V(\mu)$ given by (42) and (10).

The electromagnetic field depth of penetration, δ, can be defined, as it is accustomed, like representing the distance from the semi-infinite slab surface in which it would be uniformly distributed the total current for the active power losses to be the same. In order to calculate this parameter, it is applied the Ampère rule

on the curve Γ of the xOy surface, for a dimension equal to l_x along Ox axis, $\oint_\Gamma \mathbf{Hds} = i_{s\Gamma}$, from where it results $\underline{H}_0 l_x = \underline{I}$, $\underline{I}$ being the complex RMS of the total current for a thickness l_x (in the Ox direction) of the semi-infinite slab. So, it is considered a band of thickness l_x (in the Ox direction) in the semi-infinite slab. For the unit of length along Oz axis, $l_z = 1$, the active power loss will be $P = RI^2 = \sigma^{-1} l_z A_1^{-1} H_0^2 l_x^2$ for the case of the uniformly distributed current, with $A_1 = \delta l_x$ and $P = \Re e\, \underline{S}_y(0) A_2 = \Re e\, l_x l_z \underline{S}_y(0)$ for the case in which the power is received through the surface, with $A_2 = l_x l_z$. Equalizing the two expressions, it is obtained for the depth of penetration:

$$\delta = \frac{1}{\alpha} \cdot \frac{1}{1 - m/2 - m^2/8}. \tag{51}$$

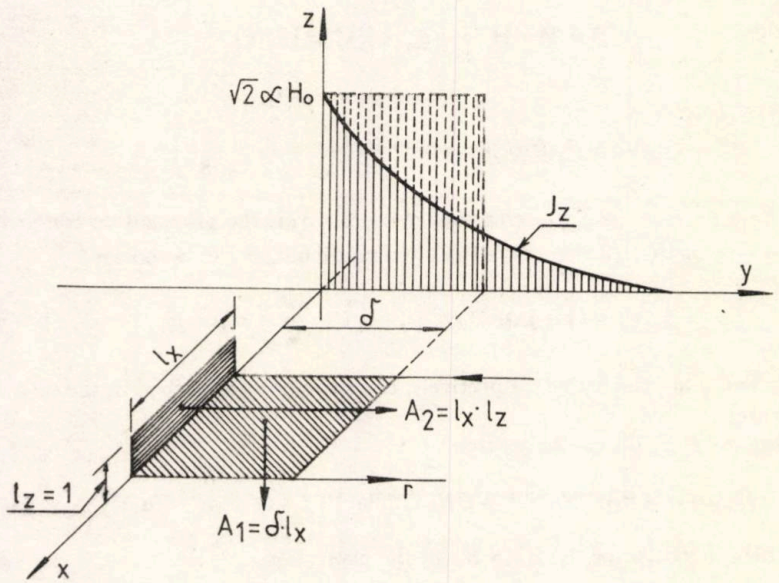

Fig. 2.– The depth of penetration δ calculus.

It is to be noticed that the depth of penetration, δ, depends both of the material characteristics and the exterior magnetic field H_0 amplitude.

6. Conclusions

It has been made the approach of the electromagnetic field spreading in nonlinear media, assigning an inertial character to the medium in study and correlating this procedure with the approximation of the nonlinear dependence of the response state vector Y modulus versus the excitation state vector X one through an exponential polynomial having the form (2), aiming to obtain specific formulations for

the magnetic permeability, μ, electric permitivity, ε and conductivity, σ. In this respect, after finding the general expression of the material constant (9), with the graphic representation in Fig.1, it has been pointed out (11) the nonlinear dependence of the material constants by the square amplitude (RMS) of the excitation state vector modulus, E or H.

After writing the harmonic quasistationary electromagnetic field equations for inertial dielectric and ferromagnetic materials, it has been studied the field spreading in the semi-infinite inertial ferromagnetic conductor slab, demonstrating the possibility of using the small parameter method in solving the Duffing equation which characterizes the field penetration. It has been determined the expressions of the magnetic field intensity, (41), conduction current density, (43), electric field, (44), as well as of the Poynting vector, (45), magnetic permeability, (50) and depth of penetration (51).

Compared to the previous papers dealing with the same subject [5], [6], this one brings an amelioration not only by proving the possibility of using a certain method of solving a Duffing equation, but also in providing new expressions for the magnetic permeability and depth of penetration, which enables a future approach of the topic by considering two complementary directions of study: a) knowing the material used in the application, there are determined the coefficients of the polynomial approximation of the magnetization curve, calculating then the material constant μ and the other terms necessary for the study of the application (meaning by application everything that is in connection with the process of electromagnetic waves scattering in the given material); b) knowing the necessities of the application (from the active power losses per unit area or depth of penetration point of view), it is determined the required material imposing the fulfilment of the given conditions through a system of equations from which there can be determined the coefficients of the polynomial approximation of the magnetization curve.

Received, April 12, 1994

Technical University "Gh.Asachi", Jassy,
Department of General Electrotechnics
and Electrical Machines

REFERENCES

1. D e m i d o v i c h B., *Problems in Mathematical Analysis.* Mir Publ., Moscow, 1976.
2. E l - S h e r b i n y M.K., *Representation of the Magnetization Characteristic by a Sum of Exponentials.* IEEE Trans. Magn., **9**, *1*, 60-62 (1973).
3. M â n d r u Gh., R ă d u l e s c u M., *Analiza numerică a câmpului electromagnetic.* Ed. Dacia, Cluj-Napoca, 1986.
4. M o c a n u C.I., *Teoria câmpului electromagnetic.* EDP, Bucureşti, 1981.
5. R o s m a n H., *Constantele de material ale mediilor electromagnetice cu neliniaritate slabă, inerţiale, în regim cvasistaţionar armonic.* Mem. secţ. şt. Acad. R.S.R., s.IV, **II**, 189-194 (1979).
6. R o s m a n H., *Pătrunderea câmpului electromagnetic în semispaţiul feromagnetic infinit cu neliniaritate slabă, în regim cvasistaţionar armonic.* Mem. secţ. şt. Acad. R.S.R., s.IV, **III**, 331-342 (1980).
7. S a v i n Gh., R o s m a n H., *Circuite electrice neliniare şi parametrice.* Ed. Tehnică, Bucureşti, 1973.

ASUPRA PROPAGĂRII UNDELOR ELECTROMAGNETICE ÎN MEDII NELINIARE INERŢIALE

(Rezumat)

Făcându-se apel la analiza circuitelor neliniare se prezintă o posibilitate de abordare a mediilor cu neliniaritate slabă, atribuindu-se acestora un caracter inerţial. Analiza ulterioară permite obţinerea expresiei constantei de material precum şi a ecuaţiilor câmpului electromagnetic corespunzătoare mediului studiat. Acestea din urmă se particularizează pentru cazul semispaţiului conductor feromagnetic infinit, cu găsirea relaţiilor intensităţii câmpului magnetic şi electric, a permeabilităţii magnetice şi a adâncimii de pătrundere.

BULETINUL INSTITUTULUI POLITEHNIC DIN IAŞI
Tomul XLI (XLV), Fasc. 3-4, 1995
Secţia III
ELECTROTEHNICĂ. ENERGETICĂ. ELECTRONICĂ

C.D. 621.3.029.6

SUR L'ÉQUIVALENCE ENTRE LA MÉTHODE TLM ET LA MÉTHODE DES DIFFÉRENCES FINIES

PAR
IRINEL CASIAN-BOTEZ

1. Introduction

La méthode TLM c'est un modèle physique, fondé sur le principe de Huygens, qui utilise les lignes TEM pendant que la méthode DF c'est un modèle mathématique fondé directement sur les équations de Maxwell. Toutes les deux ont été beaucoup utilisées pour résoudre des problèmes électromagnétiques pareils [1], [2]. Malgré ces applications, le rapport entre les expressions TLM et DF n'a pas été rigoureusement démontré, bien qu'il y a des tentatives en cette direction [3], [4]. Dans ce qui suit on présente une possibilité d'obtenir la méthode TLM à deux dimensions en discrétisant les équations de Maxwell directement dans le domaine temporel, à l'aide d'un schéma aux différences finies.

2. Démonstration

On considère les équations de Maxwell à deux dimensions pour les modes TE_y, dans un milieu parfait ($\mathbf{D} = \varepsilon\mathbf{E}$, $\mathbf{B} = \mu\mathbf{H}$, $\mathbf{J} = 0$):

$$(1) \qquad H_x = H_z = 0,\ E_y = 0, \qquad (2) \quad \frac{\partial H_y}{\partial x} = \varepsilon\frac{\partial E_z}{\partial t},$$

$$(3) \qquad \frac{\partial H_y}{\partial z} = -\varepsilon\frac{\partial E_x}{\partial t}, \qquad (4) \quad \left(\frac{\partial E_x}{\partial z} - \frac{\partial E_z}{\partial x}\right) = -\mu\frac{\partial H_y}{\partial t}.$$

a) La somme des relations (2),...,(4), la dernière étant multipliée par A, une constante à déterminer, conduit à:

$$\frac{\partial}{\partial x}(H_y - AE_z) + \frac{\partial}{\partial z}(H_y + AE_x) = \varepsilon\frac{\partial}{\partial t}\left(E_z - \frac{A\mu}{2\varepsilon}H_y\right) - \varepsilon\frac{\partial}{\partial t}\left(E_x + \frac{A\mu}{2\varepsilon}H_y\right).$$

Si on choisit $A\mu/2\varepsilon = 1/A$ et, par conséquent, $A = \sqrt{2\varepsilon/\mu}$ on obtient, après quelques calculs simples:

$$(5) \qquad \left(\frac{\partial}{\partial x} + \sqrt{\frac{\varepsilon\mu}{2}} \cdot \frac{\partial}{\partial t}\right)(H_y - AE_z) = -\left(\frac{\partial}{\partial z} + \sqrt{\frac{\varepsilon\mu}{2}} \cdot \frac{\partial}{\partial t}\right)(H_y + AE_x).$$

D'une manière similaire on va obtenir: b) en soustrayant les relations (2) et (3) et puis en les additionant avec (4) multipliée par A, la relation:

$$(6) \qquad \left(\frac{\partial}{\partial x} + \sqrt{\frac{\varepsilon\mu}{2}} \cdot \frac{\partial}{\partial t}\right)(H_y - AE_z) = \left(\frac{\partial}{\partial z} - \sqrt{\frac{\varepsilon\mu}{2}} \cdot \frac{\partial}{\partial t}\right)(H_y - AE_x);$$

c) effectuant la somme des relations (2), (3) et, puis, en soustrayant (4) multipliée par A, l'expression:

$$(7) \qquad \left(\frac{\partial}{\partial x} - \sqrt{\frac{\varepsilon\mu}{2}} \cdot \frac{\partial}{\partial t}\right)(H_y + AE_z) = -\left(\frac{\partial}{\partial z} - \sqrt{\frac{\varepsilon\mu}{2}} \cdot \frac{\partial}{\partial t}\right)(H_y - AE_x).$$

Les équations (5),...,(7) suggèrent à chercher des solutions sous la forme d'ondes planes à savoir:

$$H_y - AE_z = A_x(x - vt), \quad H_y + AE_z = B_x(x + vt),$$
$$H_y + AE_x = A_z(z - vt), \quad H_y - AE_x = B_z(z + vt),$$

où

$$v = \sqrt{\frac{2}{\varepsilon\mu}}.$$

On observe que:

$$(8) \qquad A_x + B_x = A_z + B_z.$$

Les ondes incidentes A se propagent en sens positif de l'axe Ox ou Oz, avec la vitesse v, et les ondes réfléchies B se propagent en sens négatif de l'axe Ox ou Oz, avec la même vitesse. Les équations (5),...,(7) deviennent alors:

$$(9) \qquad \left(\frac{\partial}{\partial x} + \sqrt{\frac{\varepsilon\mu}{2}} \cdot \frac{\partial}{\partial t}\right) A_x(x - vt) = -\left(\frac{\partial}{\partial z} + \sqrt{\frac{\varepsilon\mu}{2}} \cdot \frac{\partial}{\partial t}\right) A_z(z - vt),$$

$$(10) \qquad \left(\frac{\partial}{\partial x} + \sqrt{\frac{\varepsilon\mu}{2}} \cdot \frac{\partial}{\partial t}\right) A_x(x - vt) = \left(\frac{\partial}{\partial z} - \sqrt{\frac{\varepsilon\mu}{2}} \cdot \frac{\partial}{\partial t}\right) B_z(z + vt),$$

$$(11) \qquad \left(\frac{\partial}{\partial x} - \sqrt{\frac{\varepsilon\mu}{2}} \cdot \frac{\partial}{\partial t}\right) B_x(x + vt) = -\left(\frac{\partial}{\partial z} - \sqrt{\frac{\varepsilon\mu}{2}} \cdot \frac{\partial}{\partial t}\right) B_z(z + vt).$$

La technique numérique utilisée pour résoudre le système d'équations (8),..., (11) repose sur la méthode des différences finies. Afin de réaliser la discrétisation spatiale, l'espace à deux dimensions est décomposé en mailles élémentaires carrées. Chaque cellule est caractérisée par ses dimensions $(\Delta x, \Delta y)$. Un pas temporel d'incrémentation Δt et défini sous la forme:

$$\Delta t = \frac{h}{v},$$

en considérant $\Delta x = \Delta y = h$. Alors, les opérateurs différentiels du système (9),...,(11) deviennent:

$$\left(\frac{\partial}{\partial x} + \frac{1}{v}\cdot\frac{\partial}{\partial t}\right) A_x(x - vt) \approx$$
$$\approx \frac{A_x\left[x + \frac{h}{2} - v\left(t + \frac{\Delta t}{2}\right)\right] - A_x\left[x - \frac{h}{2} - v\left(t + \frac{\Delta t}{2}\right)\right]}{h}, \tag{12}$$

$$\left(\frac{\partial}{\partial x} - \frac{1}{v}\cdot\frac{\partial}{\partial t}\right) B_x(x + vt) \approx$$
$$\approx \frac{B_x\left[x + \frac{h}{2} + v\left(t - \frac{\Delta t}{2}\right)\right] - B_x\left[x - \frac{h}{2} + v\left(t + \frac{\Delta t}{2}\right)\right]}{h}, \tag{13}$$

$$\left(\frac{\partial}{\partial z} + \frac{1}{v}\cdot\frac{\partial}{\partial t}\right) A_z(z - vt) \approx$$
$$\approx \frac{A_z\left[z + \frac{h}{2} - v\left(t + \frac{\Delta t}{2}\right)\right] - A_z\left[z - \frac{h}{2} - v\left(t + \frac{\Delta t}{2}\right)\right]}{h}, \tag{14}$$

$$\left(\frac{\partial}{\partial z} - \frac{1}{v}\cdot\frac{\partial}{\partial t}\right) B_z(z + vt) \approx$$
$$\approx \frac{B_z\left[z + \frac{h}{2} + v\left(t - \frac{\Delta t}{2}\right)\right] - B_z\left[z - \frac{h}{2} + v\left(t + \frac{\Delta t}{2}\right)\right]}{h}. \tag{15}$$

On voit, par exemple, que $A_x\left(x + \frac{h}{2} - v\left(t + \frac{\Delta t}{2}\right)\right)$ représente une onde qui passe au moment $t + \Delta t/2$ par le point $x + h/2$ dans la direction positive de Ox et $B_x\left(x + \frac{h}{2} + v\left(t - \frac{\Delta t}{2}\right)\right)$ - une onde qui passe par le même point, mais au moment $t - \Delta t/2$ dans la direction négative de Ox. On va noter alors les ondes incidentes au moment $t - \Delta t/2$ par A_1, A_2, A_3, A_4 et, respectivement, les ondes réfléchies au moment $t + \Delta t/2$ par B_1, B_2, B_3, B_4, conformément à la Fig.1. Les ondes du système (12),...,(15) deviennent:

$$A_x\left(x + \frac{h}{2} - v\left(t + \frac{\Delta t}{2}\right)\right) = B_4, \quad A_x\left(x - \frac{h}{2} - v\left(t - \frac{\Delta t}{2}\right)\right) = A_2, \tag{16}$$

$$(17)\qquad B_x\left(x+\frac{h}{2}+v\left(t-\frac{\Delta t}{2}\right)\right)=A_4,\quad B_x\left(x-\frac{h}{2}+v\left(t+\frac{\Delta t}{2}\right)\right)=B_2,$$

$$(18)\qquad A_z\left(z+\frac{h}{2}-v\left(t+\frac{\Delta t}{2}\right)\right)=B_3,\quad A_z\left(z-\frac{h}{2}-v\left(t-\frac{\Delta t}{2}\right)\right)=A_1,$$

$$(19)\qquad B_z\left(z+\frac{h}{2}+v\left(t-\frac{\Delta t}{2}\right)\right)=A_3,\quad B_z\left(z-\frac{h}{2}+v\left(t+\frac{\Delta t}{2}\right)\right)=B_1.$$

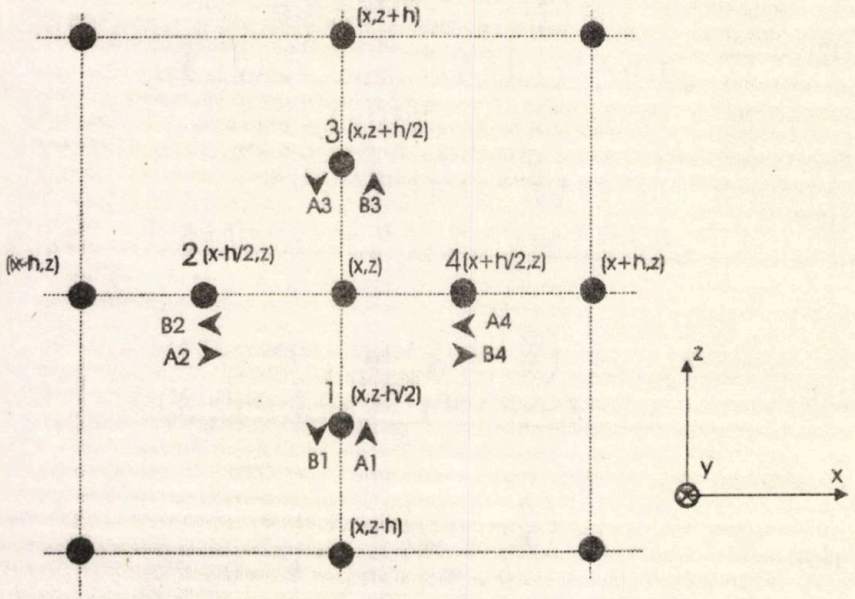

Fig. 1.– Le réseau de lignes de transmission dans le plan xOz.

Remplaçant dans les équations (8),...,(11) les relations (12),...,(19) on obtient:

$$(20)\qquad B_4-A_2=-(B_3-A_1),\qquad (21)\qquad B_4-A_2=A_3-B_1,$$

$$(22)\qquad A_4-B_2=-(A_3-B_1),\qquad (23)\qquad A_2+B_2=A_1+B_1.$$

On peut démontrer facilement que le système (20),...,(23) est équivalent à l'équation matricielle:

$$(24) \qquad \begin{bmatrix} B_1 \\ B_2 \\ B_3 \\ B_4 \end{bmatrix} = \frac{1}{2} \begin{bmatrix} -1 & 1 & 1 & 1 \\ 1 & -1 & 1 & 1 \\ 1 & 1 & -1 & 1 \\ 1 & 1 & 1 & -1 \end{bmatrix} \begin{bmatrix} A_1 \\ A_2 \\ A_3 \\ A_4 \end{bmatrix}.$$

L'équation (24) représente, d'autre part, la définition de la matrice de diffraction pour 4 accès connectés en parallèle. Donc, le processus itératif imposé par la méthode DF (2D) peut être représenté par un réseau de lignes TEM idéaux (impédance d'onde $1\,\Omega$ et exposant de propagation $j\omega/v$), connectées en parallèle, excité par une impulsion; c'est-à-dire la méthode TLM (2D) [5].

3. Conclusion

On propose une démonstration rigoureuse pour établir l'équivalence entre la méthode DF (2D) et la méthode TLM. Elle permet aussi d'obtenir d'une façon claire la liason entre les ondes incidentes et réfléchies d'une part et les grandeurs de champ électromagnétique d'autre part.

Reçue le 6 juillet 1994

Université Technique „Gh. Asachi", Jassy,
Chaire d'Électronique Appliquée

BIBLIOGRAPHIE

1. Zhang X., Mei K., *Time Domain Finite Difference Approach for the Calculation of the Frequency-dependent Characteristic of Microstrip Discontinuities.* IEEE Trans. Microwave Theory Tech., **MTT-36**, *12*, 1775-1787 (1987).
2. Akhtarzad S., Johns P.B., *Three-Dimensional Transmission-Line-Matrix Computer Analysis of Microstrip Resonators.* IEEE Trans. Microwave Theory Tech., **MTT-23**, *12*, 990-997 (1975).
3. Johns P.B., *On the Relationship between TLM and Finite-Difference Methods for Maxwell's Equations.* IEEE Trans. Microwave Theory Tech., **MTT-35**, *1*, 60-61 (1987).
4. Chen Z., Ney M.M., Hoefer W.J.R., *A New Finite-Difference Time-Domain Formulation and its Equivalence with the TLM Symmetrical Condensed Node.* IEEE Trans. Microwave Theory Tech., **MTT-39**, *12*, 2160-2169 (1991).
5. Itoh T. (Ed.), *Numerical Techniques for Microwave and Milimeter-Wave Passive Structures.* J. Wiley & Sons, 501-502, 1988.

ASUPRA ECHIVALENŢEI DINTRE METODA TLM ŞI METODA CU DIFERENŢE FINITE

(Rezumat)

Se propune o demonstraţie riguroasă a echivalenţei dintre metoda TLM (2D) şi metoda cu diferenţe finite. Se pune în evidenţă o legătură mai directă dintre mărimile care intervin în metoda TLM şi mărimile electromagnetice.

BULETINUL INSTITUTULUI POLITEHNIC DIN IAŞI
Tomul XLI (XLV), Fasc. 3–4, 1995
Secţia III
ELECTROTEHNICĂ. ENERGETICĂ. ELECTRONICĂ

D.C. 538.567.4; 538.551

A SYMBOLIC STUDY OF LINEAR SYSTEMS RESPONSE TO AMPLITUDE MODULATED INPUTS

I. INPUTS WITH SUPPRESSED CARRIER

BY

ALFRED BRAIER and HUGO ROSMAN

1. Introduction

The problem of symbolic representation by hypercomplex numbers of some important classes of nonharmonic signals and its subsequent application in studying the passing of such signals through linear passive systems was formulated and solved in [1] and then developed in other works [2], [3] and especially in [4].

In this paper we utilize the mentioned symbolic method, expounded as to directly evidence some significant physical aspects, in order to study the steady-state of linear passive system produced by an amplitude modulated input, with suppressed carrier (AMSC).

2. Symbolic Representation of AMSC Signals

2.1. Distortionated Signals

To the modulated and distortionated signal

$$f(t) = e^{\delta t}[A_1 \sin(pt + \alpha)\sin(\omega t + \beta) + A_2 \cos(pt + \alpha)\cos(\omega t + \beta)] \tag{1}$$

we attach the hypercomplex number

$$\hat{w} = a_1 + ia_2 + ja_3 + ija_4, \quad a_1, ..., a_4 \in \mathbb{R}, \quad i^2 = j^2 = -1, \quad (ij)^2 = (ji)^2 = 1. \tag{2}$$

Such a number is an element of the associative and commutative algebra of IVth order, with unity element, over the real field. This algebra, called $\mathcal{P}$-polynions algebra, is the direct sum and at the same time the direct product of complex algebras.

If $A_2 = 0$, the signal (1) is nondistortionated; if $A_2 = \delta = 0$, it becomes a "true" AMSC signal, such as those frequently involved in telecommunications or in automatics.

The functions corresponding to the basis elements from (2), i.e. to i, j and ij, are:

$$\begin{aligned} f_1(t) &= e^{\delta t}\sin pt \sin \omega t, \quad f_2(t) = e^{\delta t}\cos pt \sin \omega t, \\ f_3(t) &= e^{\delta t}\sin pt \cos \omega t, \quad f_4(t) = e^{\delta t}\cos pt \cos \omega t, \end{aligned} \tag{3}$$

while the components of (2_1) are expressed by

$$(4)\qquad \begin{aligned} a_1 &= A_1\cos\alpha\cos\beta + A_2\sin\alpha\sin\beta, \quad a_2 = A_1\sin\alpha\cos\beta - A_2\cos\alpha\sin\beta,\\ a_3 &= A_1\cos\alpha\sin\beta - A_2\sin\alpha\cos\beta, \quad a_4 = A_1\sin\alpha\sin\beta + A_2\cos\alpha\cos\beta. \end{aligned}$$

The symbolic representation means that to the derivative with respect to time t of $f(t) = \sum_{i=1}^{4} a_i f_i$, given by (1) - derivative presenting the same form, namely $\mathrm{d}f/\mathrm{d}t = \sum_{i=1}^{4} a_i^* f_i$ - corresponds the hypercomplex number

$$(5)\qquad \hat{w}^* = \hat{d}\hat{w}, \quad \text{with} \quad \hat{d} = \delta + \mathrm{i}p + \mathrm{j}\omega.$$

This number is to be obtained directly, by multiplying $\hat{w}$ with the element (5_2), playing the rôle of derivation operator in the $\mathcal{P}$-polynions algebra attached to signals (1).

The correspondence between the function (1) and the elements (2_1), with the derivation operator (5_2), allows to obtain by elementary computation:

$$(6)\qquad \begin{aligned} A_1, A_2 &= \tfrac{1}{2}[\sqrt{(a_1+a_4)^2+(a_2-a_3)^2} \pm \sqrt{(a_1-a_4)^2+(a_2+a_3)^2}],\\ \tan\alpha &= \tfrac{a_4A_1-a_1A_2}{a_3A_1+a_2A_2} = \tfrac{a_2A_1+a_3A_2}{a_1A_1-a_4A_2},\\ \tan\beta &= \tfrac{a_3A_1+a_2A_2}{a_1A_1-a_4A_2} = \tfrac{a_4A_1-a_1A_2}{a_2A_1+a_3A_2},\\ \operatorname{sign}(\tan\alpha\tan\beta) &= \operatorname{sign}[(a_2^2+a_3^2)A_1A_2 + a_2a_3(A_1^2+A_2^2)]. \end{aligned}$$

Let introduce relations (4) in the algebraic expression (2_1); the exponential form

$$(7)\qquad \hat{w} = (A_1 + \mathrm{ij}A_2)\mathrm{e}^{\mathrm{i}\alpha}\mathrm{e}^{\mathrm{j}\beta},$$

is now obtained, where, as usually, $\mathrm{e}^{\mathrm{i}\alpha} = \cos\alpha + \mathrm{i}\sin\alpha$, $\mathrm{e}^{\mathrm{j}\beta} = \cos\beta + \mathrm{j}\sin\beta$. Thus we get also the inverse element

$$(8)\qquad \frac{1}{\hat{w}} = \frac{A_1 - \mathrm{ij}A_2}{A_1^2 - A_2^2}\mathrm{e}^{-\mathrm{i}\alpha}\mathrm{e}^{-\mathrm{j}\beta},$$

with $A_1^2 - A_2^2$ as modulus or norm of element $\hat{w}$. The quantity $A_1 + \mathrm{ij}A_2$ may be denoted as its *hypercomplex modulus*.

The divisors of zero in the $\mathcal{P}$-polynions algebra are those having $A_1 = \pm A_2$, therefore characterized by

$$(9)\qquad a_1 + a_4 = 0, \quad a_2 - a_3 = 0, \quad \text{or} \quad a_1 - a_4 = 0, \quad a_2 + a_3 = 0.$$

2.2. Nondistortionated Signals

For $A_2 = 0$ and $A_1 = A$, the signal changes take place at the level of expressions (4), who become

$$(10)\qquad a_1 = A\cos\alpha\cos\beta, \quad a_2 = A\sin\alpha\cos\beta, \quad a_3 = A\cos\alpha\sin\beta, \quad a_4 = A\sin\alpha\sin\beta.$$

Let underline the important fact that now

$$(11)\qquad a_1a_4 = a_2a_3.$$

It means that the components of the $\mathcal{P}$-polynions attached to nondistortionated AMSC signals are not independent. The hypercomplex numbers of type (11) are called *special elements* or $\mathcal{P}_s$-polynions.

The results (6) become now simpler, namely

$$A = \sqrt{a_1^2 + a_2^2 + a_3^2 + a_4^2}, \quad \tan\alpha = \frac{a_4}{a_3} = \frac{a_2}{a_1}, \quad \tan\beta = \frac{a_3}{a_1} = \frac{a_4}{a_2}, \tag{12}$$

$$\operatorname{sign}(\tan\alpha \tan\beta) = \operatorname{sign}(a_1 a_4).$$

Also

$$\hat{w} = Ae^{i\alpha}e^{j\beta}, \quad \frac{1}{\hat{w}} = \frac{1}{A}e^{-i\alpha}e^{-j\beta}. \tag{13}$$

R e m a r k. The exponential forms (7) and especially (13) show that a special polynion $\mathcal{P}_s$ results only by multiplying or dividing two special ones, as well as by dividing two arbitrary polynions (7), but with proportional "hypercomplexe moduli" $(A_1 + ijA_2 = \lambda(B_1 + ijB_2), \ \lambda \in \mathbb{R})$.

2.3. Polynions as Bicomplex Number

The change of basis in the $\mathcal{P}$-polynions algebra showing the existence of two orthogonal idempotents, simplifies the algebraic aspects and reveals direct physical meanings. With this purpose let introduce the quantities:

$$\alpha_1 = a_1 + a_4, \quad \alpha_2 = a_2 - a_3, \quad \alpha_3 = a_1 - a_4, \quad \alpha_4 = a_2 + a_3, \tag{14}$$

allowing to express the $\mathcal{P}$-polynion components (2_1) as

$$a_1 = \tfrac{1}{2}(\alpha_1 + \alpha_2), \quad a_2 = \tfrac{1}{2}(\alpha_4 + \alpha_2), \quad a_3 = \tfrac{1}{2}(\alpha_4 - \alpha_2), \quad a_4 = \tfrac{1}{2}(\alpha_1 - \alpha_3). \tag{15}$$

By introducing them in (2_1) we get easily that

$$\hat{w} = \alpha_1 E_1 + \alpha_2 F_1 + \alpha_3 E_2 + \alpha_4 F_2,$$

where

$$E_1 = \tfrac{1}{2}(1 + ij), \quad E_2 = \tfrac{1}{2}(i - ij), \quad F_1 = \tfrac{1}{2}(i - j), \quad F_2 = \tfrac{1}{2}(i + j), \tag{16}$$

with

$$E_1^2 = E_1, \quad E_2^2 = E_2, \quad E_1E_2 = E_2E_1, \quad E_1 + E_2 = 1; \quad F_1 = -jE_1, \quad F_2 = jE_2. \tag{17}$$

Then $\hat{w} = (\alpha_1 - j\alpha_2)E_1 + (\alpha_3 + j\alpha_4)E_2$, that is

$$\hat{w} = \underline{z}_1 E_1 + \underline{z}_2 E_2, \tag{18}$$

where, taking in mind (14),

$$\underline{z}_1 = (a_1 + a_4) + j(a_3 - a_2), \quad \underline{z}_2 = (a_1 - a_4) + j(a_3 + a_2). \tag{19}$$

If the $\mathcal{P}$-polynions are considered as a pair of complex numbers connected by the two orthogonal idempotents, E_1 and E_2, is possible to simplify appreciable the computations and to perceive significant physical features concerning the AMSC signals and their passing through passive systems. Thus

$$\begin{aligned} &\hat{w}_1\hat{w}_2 = (\underline{z}_1'E_1 + \underline{z}_2'E_2)(\underline{z}_1''E_1 + \underline{z}_2''E_2) = \underline{z}_1'\underline{z}_2'E_1 + \underline{z}_1''\underline{z}_2''E_2; \\ &\hat{w}^k = (\underline{z}_1E_1 + \underline{z}_2E_2)^k = \underline{z}_1^kE_1 + \underline{z}_2^kE_2, \quad k \in \mathbb{N}; \quad \frac{1}{\hat{w}} = \frac{1}{\underline{z}_1}E_1 + \frac{1}{\underline{z}_2}E_2. \end{aligned} \tag{20}$$

The inverse element exists only for the hypercomplex numbers with $z_1 \neq 0$ or $z_2 \neq 0$, i.e. (s.(19) and (9)) which are not divisors of zero.

With the components (4) of the $\mathcal{P}$-polynions attached to signal (1), the complex numbers (19) become

$$\underline{z}_1 = (A_1 + A_2)e^{j(\beta-\alpha)}, \quad \underline{z}_2 = (A_1 - A_2)e^{j(\beta+\alpha)}. \tag{21}$$

It results also (since $A_2 \leq A_1$)

$$A_1, A_2 = \tfrac{1}{2}(|\underline{z}_1| \pm |\underline{z}_2|), \quad 2\beta = \arg(\underline{z}_1\underline{z}_2), \quad 2\alpha = \arg\frac{\underline{z}_2}{\underline{z}_1}. \tag{22}$$

Element (5_2), playing the rôle of derivation operator, becomes

$$\hat{d} = [\delta + j(\omega - p)]E_1 + [\delta + j(\omega + p)]E_2, \tag{23}$$

underlining clearely the presence of the two lateral circular frequencies typical for the AMSC signals.

The condition (11) assuring that a $\mathcal{P}$-polynion is a special one (which resumes to $A_2 = 0$), takes the simple eloquent form

$$|\underline{z}_1| = |\underline{z}_2|. \tag{24}$$

Also, having in mind that the quantities (14) are the real and respectively imaginary parts of the pair of complex numbers (19) attached to element (2_1) we can write without difficulties the expressions

$$\begin{aligned} &a_1 = \tfrac{1}{2}\Re e(\underline{z}_1 + \underline{z}_2), \; a_2 = -\tfrac{1}{2}\Im m(\underline{z}_1 - \underline{z}_2), \\ &a_3 = \tfrac{1}{2}\Im m(\underline{z}_1 + \underline{z}_2), \; a_4 = \tfrac{1}{2}\Re e(\underline{z}_1 - \underline{z}_2). \end{aligned} \tag{25}$$

Is to be noticed that, generally speaking for the time being, the components a_1, a_4, as otherwise a_2, a_3, are more directly related.

3. The Passing of AMSC Signals Through Linear Systems

The steady-state output of a linear dynamic system with constant parameters (described by ordinary linear differential equations with constant coefficients), corresponding to the input (1), has, in general, the same form as this last signal (being

expressed by the particular solution corresponding to that type of excitation). In virtue of the mechanism associating a $\mathcal{P}$-polynion to the mentioned signal and in full accordance with the very usual frequency response (operating with harmonic signals represented symbolically by complex numbers), we can write

$$\hat{X}_0 = \hat{W}(\hat{d})\hat{X}_1. \tag{26}$$

Here $\hat{X}_1$ and $\hat{X}_0$ are the $\mathcal{P}$-polynions attached to the input and respectively output (steady-state) signals, while $\hat{W}(\hat{d})$ is the *transferance* of the linear system. It is the $\mathcal{P}$-polynion obtained by substituting in the usual transfer function of this system, the current complex variable by element (5_2) playing the rôle of derivation operator, in algebra attached to functions (1). The result holds in general, whatever are the signals symbolically represented by elements of algebras over the real field [3], [4].

For the systems considered here, the usual transfer function is a rational one, and accordingly the transferance is:

$$\hat{W}(\hat{d}) = \frac{\hat{F}(\hat{d})}{\hat{G}(\hat{d})} = \frac{b_m\hat{d}^m + b_{m-1}\hat{d}^{m-1} + \cdots + b_1\hat{d} + b_0}{c_n\hat{d}^n + c_{n-1}\hat{d}^{n-1} + \cdots + c_1\hat{d} + c_0}, \tag{27}$$

where $b_h,\ c_k \in \mathbb{R},\ (h = 1,...,m;\ k = 1,...,n)$, depend only of the system characteristic elements.

Let consider now an undamped AMSC signal (1), i.e. with $\delta = 0$; derivation operator (5_1) or (23) becomes

$$\hat{d} = \mathrm{i}p + \mathrm{j}\omega \quad \text{or} \quad \hat{d} = \mathrm{j}\omega^{-}\mathrm{E}_1 + \mathrm{j}\omega^{+}\mathrm{E}_2 \quad \text{with} \quad \omega^{\mp} = \omega \mp p. \tag{28}$$

If $\hat{G}(\hat{d})$ is not a divisor of zero or the null element of the $\mathcal{P}$-polynion algebra, with $\hat{d}$ given by (28_1), the transferance acquires finally the algebraic form:

$$\hat{W}(\hat{d}) = W_1 + \mathrm{i}W_2 + \mathrm{j}W_3 + \mathrm{ij}W_4, \quad W_k = W_k(p,\omega), \quad (k = 1,...,4). \tag{29}$$

In accordance with (26) we get the $\mathcal{P}$-polynion attached to the output signal and the relations (6) allow to obtain all the quantities occurring in (1). Such a function describes now (with $\delta = 0$) the time dependence of the output signal.

The plotting of the components (29_2) versus ω and p leads to new types of frequency characteristics, typical for a system excited by an AMSC input signal (s. also [3], [4]).

If now we resort to the form (28_2) of the derivation operator and compute the numerator of (27) accordingly to the simple rules (20) (taking into account that $\hat{d}^0 = 1 = \mathrm{E}_1 + \mathrm{E}_2$), then

$$\begin{gathered} b_m\hat{d}^m + b_{m-1}\hat{d}^{m-1} + ... + b_1\hat{d} + b_0\hat{d}^0 = \\ = [b_m(\mathrm{j}\omega^{-})^m + b_{m-1}(\mathrm{j}\omega^{-})^{m-1} + ... + b_1(\mathrm{j}\omega^{-}) + b_0]\mathrm{E}_1 + \\ + [b_m(\mathrm{j}\omega^{+})^m + b_{m-1}(\mathrm{j}\omega^{+})^{m-1} + ... + b_1(\mathrm{j}\omega^{+}) + b_0]\mathrm{E}_2 = \\ = \underline{F}(\mathrm{j}\omega^{-})\mathrm{E}_1 + \underline{F}(\mathrm{j}\omega^{+})\mathrm{E}_2. \end{gathered}$$

A similar result comes from the denominator, and if $\hat{G}(\hat{d})$ is not a divisor of zero or the null element, the transferance (27) has the expression

$$\hat{W}(\hat{d}) = \frac{\underline{F}(j\omega^-)}{\underline{G}(j\omega^-)}E_1 + \frac{\underline{F}(j\omega^+)}{\underline{G}(j\omega^+)}E_2 = \underline{W}(j\omega^-)E_1 + \underline{W}(j\omega^+)E_2. \tag{30}$$

This very significant result shows that the two components of the bicomplex number attached to transferance (27), written as in (30), are the usual transfer functions giving the system response to the pure harmonic inputs corresponding to the two components (with the lateral frequencies ω^-, ω^+) coexisting in signal (1).

The relations between the more compact expression (30) and the individual behaviour of the two components with frequencies $\omega^{\pm}$ are given by (19), (21), (22), (25).

4. Application to Linear Electric Networks

4.1. General Aspects

Let be an electric linear, passive, oneport (LPO), supplied by an AMSC nondistortionated voltage

$$u(t) = U_0 \sin(\Omega t + \Phi)\sin(\omega_0 t + \varphi). \tag{31}$$

On the basis of the above presented correspondence, we associate to (31) (s.(10), (11)) the $\mathcal{P}$-polynion:

$$\begin{aligned}\hat{U} = U_0\cos\Phi\cos\varphi_0 + iU_0\sin\Phi\cos\varphi_0 + jU_0\cos\Phi\sin\varphi_0 + ijU_0\sin\Phi\sin\varphi_0 = \\ = U_0 e^{i\Phi}e^{j\varphi_0},\end{aligned} \tag{32}$$

with the derivation operator

$$\hat{d} = i\Omega + j\omega_0 = j\omega^- E_1 + j\omega^+ E_2, \quad \omega^{\mp} = \omega_0 \mp \Omega. \tag{33}$$

The usual impedance, $\underline{Z}(j\omega)$, of the LPO allows to write the transferance of the same LPO when feeded with a modulated voltage like (31). The derivation operator being obviously (33), the transferance (impedance) results

$$\begin{aligned}\hat{Z}(\hat{d}) = R_1 + iX_1 + jX_2 + ijR_2 = \underline{Z}(j\omega^-)E_1 + \underline{Z}(j\omega^+)E_2 = \\ = \underline{Z}_1 E_1 + \underline{Z}_2 E_2 = (Z_1 + ijZ_2)e^{i\Phi^*}e^{j\varphi_0^*}.\end{aligned} \tag{34}$$

It is useful to individualize the equivalent resistances and reactances, corresponding to the two components with lateral frequencies, but "mixed" in transferance. They are the real and imaginary parts of $\underline{Z}(j\omega^{\mp})$ from (34_2), namely

$$\underline{Z}(j\omega^-) = R'(\omega^-) + jX'(\omega^-), \quad \underline{Z}(j\omega^+) = R''(\omega^+) + jX''(\omega^+). \tag{35}$$

In accordance with Eqs.(25) we get the expressions and especially the meaning of the $\mathcal{P}$-polynion (34) components:

$$R_1 = \tfrac{1}{2}(R' + R''), \quad X_1 = -\tfrac{1}{2}(X' - X''),$$
$$X_2 = \tfrac{1}{2}(X' + X''), \quad R_2 = \tfrac{1}{2}(R' - R''). \tag{36}$$

In this way it is clear that the extreme components of the transferance (34) have the caracter of resistances, the remaining two being both reactances. It is also obvious that a single component is always nonnegative, namely $R_1 \geq 0$.

The transferance is a special element ((11) or (24)) if

$$R_1 R_2 = X_1 X_2 \text{ or } R'^2 + X'^2 = R''^2 + X''^2 \text{ or } |\underline{Z}(\mathrm{j}\omega^-)| = |\underline{Z}(\mathrm{j}\omega^+)|. \tag{37}$$

The connection (26) between the input and output signals becomes now at the level of LPO:

$$\hat{I} = \frac{\hat{U}}{\hat{Z}} = \hat{Y}\hat{U}, \tag{38}$$

which may be considered as *Ohm's law in symbolic form*, where $\hat{Y}\,(= 1/\hat{Z})$ is the *hypercomplex admittance*. With the help of (7), (34) and (20_3) we have

$$\hat{Y}(\hat{d}) = \frac{1}{\hat{Z}(\hat{d})} = \underline{Y}(\mathrm{j}\omega^-)\mathrm{E}_1 + \underline{Y}(\mathrm{j}\omega^+)\mathrm{E}_2 =$$
$$= \underline{y}_1\mathrm{E}_1 + \underline{y}_2\mathrm{E}_2 = \frac{1}{\underline{Z}(\mathrm{j}\omega^-)}\mathrm{E}_1 + \frac{1}{\underline{Z}(\mathrm{j}\omega^+)}\mathrm{E}_2 = \tag{39}$$
$$= \frac{1}{\underline{z}_1}\mathrm{E}_1 + \frac{1}{\underline{z}_2}\mathrm{E}_2 = G_1 - \mathrm{i}B_1 - \mathrm{j}B_2 + \mathrm{ij}G_2 = (Y_1 + \mathrm{ij}Y_2)\mathrm{e}^{-\mathrm{i}\Phi^*}\mathrm{e}^{-\mathrm{j}\varphi_0^*}.$$

It is obvious also that

$$\underline{Y}(\mathrm{j}\omega^-) = G'(\omega^-) - \mathrm{j}B'(\omega^-), \quad \underline{Y}(\mathrm{j}\omega^+) = G''(\omega^+) - \mathrm{j}B''(\omega^+);$$
$$G_1 = \tfrac{1}{2}(G' + G''), \quad B_1 = -\tfrac{1}{2}(B' - B''), \tag{40}$$
$$B_2 = \tfrac{1}{2}(B' + B''), \quad G_2 = \tfrac{1}{2}(G' - G'').$$

The admittance becomes a $\mathcal{P}$-polynion if

$$G_1 G_2 = B_1 B_2 \text{ or } G'^2 + B'^2 = G''^2 + B''^2 \text{ or } |\underline{Y}(\mathrm{j}\omega^-)| = |\underline{Y}(\mathrm{j}\omega^+)|. \tag{41}$$

Bearing in mind (32) and (30), the $\mathcal{P}$-polynion attached to the current is

$$\hat{I} = U_0\mathrm{e}^{\mathrm{i}\Phi}\mathrm{e}^{\mathrm{j}\varphi_0}(Y_1 + \mathrm{ij}Y_2)\mathrm{e}^{-\mathrm{i}\Phi^*}\mathrm{e}^{-\mathrm{j}\varphi_0^*} = (I_1 + \mathrm{ij}I_2)\mathrm{e}^{\mathrm{i}(\Phi - \Phi^*)}\mathrm{e}^{\mathrm{j}(\varphi_0 - \varphi_0^*)}, \tag{42}$$

which means that the output signal may be written as

$$(43)\qquad \begin{aligned} i(t) &= I_1 \sin(\Omega t + \Phi - \Phi^*)\sin(\omega_0 t + \varphi_0 - \varphi_0^*) + \\ &+ I_2 \cos(\Omega t + \Phi - \Phi^*)\cos(\omega_0 t + \varphi_0 - \varphi_0^*), \quad (I_1 = U_0 Y_1,\ I_2 = U_0 Y_2). \end{aligned}$$

We conclude that, in general, the current presents a parasite phase distortion; indeed, putting

$$(44)\qquad I_1 \sin(\Omega t + \Phi - \Phi^*) = \mathcal{A}(t)\cos\Theta(t), \quad I_2 \cos(\Omega t + \Phi - \Phi^*) = \mathcal{A}(t)\sin\Theta(t),$$

we get

$$(45)\qquad \begin{aligned} \mathcal{A}(t) &= \sqrt{I_1^2 \sin^2(\Omega t + \Phi - \Phi^*) + I_2^2 \cos^2(\Omega t + \Phi - \Phi^*)}, \\ \tan\Theta(t) &= \frac{I_2}{I_1}\operatorname{cotan}(\Omega t + \Phi - \Phi^*). \end{aligned}$$

The output signal (43) becomes then

$$(46)\qquad i(t) = \mathcal{A}(t)\sin[\omega_0 t + \varphi_0 - \varphi_0^* + \Theta(t)].$$

Only if LPO presents the property expressed by (37) (or (41)), the electric network does not introduce distortion.

R e m a r k s. 1. If the input signal is from the beginning distortionated, belonging to the family (1), the attached $\mathcal{P}$-polynion has the general form (7), being $\hat{U} = (U_1 + \mathrm{i}\mathrm{j}U_2)e^{\mathrm{i}\Phi}e^{\mathrm{j}\varphi_0}$. The element attached to the current retains the expression (42_2), but with

$$(47)\qquad I_1 = Y_1 U_1 + Y_2 U_2, \quad I_2 = Y_1 U_2 + Y_2 U_1.$$

The condition that in this case the LPO be able to correct the distortion carried by the input voltage is obviously $I_2 = 0$ (or $I_1 = 0$).

2. If we intend that the LPO act as a pure resistance when excited by an AMSC input, i.e. (s.(34)) $\hat{Z}(\hat{d}) = R$, according to (35) and (36) it is necessary and sufficient that

$$(48)\qquad \Re e\,\underline{Z}(\mathrm{j}\omega^-) = \Re e\,\underline{Z}(\mathrm{j}\omega^+) \quad \text{and} \quad \Im m\,\underline{Z}(\mathrm{j}\omega^-) = \Im m\,\underline{Z}(\mathrm{j}\omega^+) = 0.$$

More informations about such *resonance regimes* are given in [5].

4.2. The R, L Series Network

Having in mind the usual impedance $\underline{Z} = R + \mathrm{j}L\omega$, by using (34) and (39) we get

$$(49)\qquad \underline{z}_1 = \frac{1}{\underline{y}_1} = \underline{Z}(\mathrm{j}\omega^-) = R + \mathrm{j}L(\omega_0 - \Omega), \quad \underline{z}_2 = \frac{1}{\underline{y}_2} = \underline{Z}(\mathrm{j}\omega^+) = R + \mathrm{j}L(\omega_0 + \Omega),$$

while (22_1) and (39) allow to write

$$Y_1, Y_2 = \frac{1}{2}\left[\frac{1}{\sqrt{R^2 + L^2(\omega_0 - \Omega)^2}} \pm \frac{1}{\sqrt{R^2 + L^2(\omega_0 + \Omega)^2}}\right]. \tag{50}$$

We conclude that always $Y_2 \neq 0$, which means that the R, L series networks introduces an unavoidable parasite phase distortion.

The phase angles (s.$(22_{2,3})$) are

$$2\varphi_0^* = \arg\{[R^2 - L^2(\omega_0^2 - \Omega^2)] + \mathrm{j}2RL\omega_0\}, \quad 2\Phi^* = \arg\frac{R + \mathrm{j}L(\omega_0 + \Omega)}{R + \mathrm{j}L(\omega_0 - \Omega)}, \tag{51}$$

leading by elementary computing to

$$\begin{gathered}\cos 2\varphi_0^* = \frac{1}{N}[R^2 - L^2(\omega_0^2 - \Omega^2)], \quad \cos 2\Phi^* = \frac{1}{N}[R^2 + L^2(\omega_0^2 - \Omega^2)], \\ \sin 2\varphi_0^* = \frac{2}{N}RL\omega_0, \quad \sin 2\Phi^* = \frac{2}{N}RL\Omega,\end{gathered} \tag{52}$$

with

$$N = \sqrt{R^4 + 2R^2L^2(\omega_0^2 + \Omega^2) + L^4(\omega_0^2 - \Omega^2)^2}.$$

One can see that $\varphi_0^* \in (0, \pi/2)$ and $\Phi^* \in (0, \pi/4)$. If

$$\frac{R}{L} = \sqrt{\omega_0^2 - \Omega^2}\,(= \sqrt{\omega^-\omega^+}), \tag{53}$$

the obtained results become simpler, namely

$$Y_1, Y_2 = \frac{1}{2R\sqrt{2\omega_0}}(\sqrt{\omega_0 + \Omega} \pm \sqrt{\omega_0 - \Omega}), \quad \varphi_0^* = \frac{\pi}{4}, \quad \Phi^* = \frac{1}{2}\tan^{-1}\frac{\Omega}{\omega_0}. \tag{54}$$

R e m a r k. The components (36) of the hypercomplex impedance (34_1) are

$$R_1 = R, \quad X_1 = L\Omega, \quad X_2 = L\omega_0, \quad R_2 = 0, \tag{55}$$

while those (s.(40)) of the hypercomplex admittance (39) result

$$\begin{gathered}G_1 = \frac{R}{N^2}R^2 + L^2(\omega_0^2 + \Omega^2), \quad B_1 = \frac{1}{N^2}L\Omega[R^2 - L^2(\omega_0^2 - \Omega^2)], \\ B_2 = \frac{1}{N^2}L\omega_0[R^2 + L^2(\omega_0^2 + \Omega^2)], \quad G_2 = \frac{R}{N^2}L^2(\omega_0^2 + \Omega^2),\end{gathered} \tag{56}$$

where N is expressed by (52_3).

When condition (53) is fulfilled,

$$G_1 = \frac{1}{2R}, \quad B_1 = 0, \quad B_2 = \frac{1}{2L\omega_0}, \quad G_2 = \frac{1}{4R}\left(1 + \frac{\Omega^2}{\omega_0^2}\right). \tag{57}$$

4.3. Parallel Network

With the usual admittance $\underline{Y} = 1/R - \mathrm{j}/L\omega_0$, (39) allows to write

$$\underline{y}_1 = \underline{Y}(\mathrm{j}\omega^-) = \frac{1}{R} - \frac{\mathrm{j}}{L(\omega_0 - \Omega)}, \quad \underline{y}_2 = \underline{Y}(\mathrm{j}\omega^+) = \frac{1}{R} - \frac{\mathrm{j}}{L(\omega_0 + \Omega)}, \tag{58}$$

and then to obtain

$$Y_1, Y_2 = \frac{1}{2RL}\left[\frac{\sqrt{R^2 + L^2(\omega_0 - \Omega)^2}}{\omega_0 - \Omega} \pm \frac{\sqrt{R^2 + L^2(\omega_0 + \Omega)^2}}{\omega_0 + \Omega}\right]. \tag{59}$$

As $Y_2 \neq 0$, the R, L parallel network always introduces a parasite phase distortion.

The phase angles are expressed by

$$\cos\varphi_0^* = -\frac{1}{N}[R^2 - L^2(\omega_0^2 - \Omega^2)], \quad \cos\Phi^* = \frac{1}{N}[R^2 + L^2(\omega_0^2 - \Omega^2)],$$
$$\sin 2\varphi_0 = \frac{2}{N}RL\omega_0, \quad \sin 2\Phi^* = -\frac{2}{N}RL\Omega, \tag{60}$$

where N has the meaning (52_3). Comparing with (52) we see that the phase angles introduced by the R, L series and respective parallel networks, are complementary at the oscillation level, and directly opposed at the harmonic modulation level.

When the "accord" condition (53) is fulfilled

$$Y_1, Y_2 = \frac{L}{R^2}\sqrt{\frac{\omega_0}{2}}(\sqrt{\omega_0 + \Omega} \pm \sqrt{\omega_0 - \Omega}), \quad \varphi_0^* = \frac{\pi}{4}, \quad \Phi^* = -\frac{1}{2}\tan^{-1}\frac{\Omega}{\omega_0}. \tag{61}$$

R e m a r k. The components of the hypercomplex admittance ($40_{3\ldots6}$) become

$$G_1 = \frac{1}{R}, \quad B_1 = -\frac{1}{L}\cdot\frac{\Omega}{\omega_0^2 - \Omega^2}, \quad B_2 = \frac{1}{L}\cdot\frac{\omega_0}{\omega_0^2 - \Omega^2}, \quad G_2 = 0, \tag{62}$$

those of the hypercomplex impedance being

$$R_1 = \frac{1}{N^2}RL^2[R^2(\omega_0^2 + \Omega^2) + L^2(\omega_0^2 - \Omega^2)], \quad X_1 = \frac{1}{N^2}R^2L\Omega[R^2 - L^2(\omega_0^2 - \Omega^2)],$$
$$X_2 = \frac{1}{N^2}R^2L\omega_0[R^2 + L^2(\omega_0^2 - \Omega^2)], \quad R_2 = -\frac{2}{N^2}R^3L^2\omega_0\Omega, \tag{63}$$

with the same N given by (52_3). If condition (53) holds, then

$$G_1 = \frac{1}{R}, \quad B_1 = -\frac{L\omega}{R^2}, \quad B_2 = \frac{L\omega_0}{R^2}, \quad G_2 = 0 \tag{64}$$

and

$$R_1 = \frac{1}{2}R, \quad X_1 = 0, \quad X_2 = \frac{1}{2}\cdot\frac{R^2}{L\omega_0}, \quad R_2 = -\frac{1}{2}R\frac{\Omega}{\omega_0}. \tag{65}$$

5. Conclusions

1. One proves that in a suitable symbolic representation, to a signal like (1) can be attached the hypercomplex number (2), (4). This means that to the derivative with respect to time of functions (1) correspond hypercomplex numbers

(5_1) obtained by multiplying those attached to (1) with a single one (5_2), playing the rôle of derivation operator.

2. The hypercomplex numbers utilized are elements of an associative and commutative algebra of IVth order, with unity element, over the real field. Called $\mathcal{P}$-polynions algebra, we utilize it in the most simple basis, with the multiplication table ($2_{2,3}$). The correspondence between signals (1) and the elements of this algebra is assured by (4) and (6).

3. By means of the algebra's two orthogonal idempotents, the hypercomplex numbers result as a pair of usual complex numbers. This reveals directly significant physical aspects concerning the amplitude modulated signals with suppressed carrier (AMSC), especially those regarding their passing through passive systems. At the same time, the computations reduce to current operations involving only complex numbers.

4. The steady-state study of a linear passive dynamic system excited by an AMSC input signal reveals that all the response peculiarities are contained by the system's transferance. It is the $\mathcal{P}$-polynion resulting after substituting the current variable in the usual transfer function by element (5_2) playing the rôle of derivation operator.

A significant result shows that each of the two components of the hypercomplex number attached to the transferance is the usual system transfer function related to the pure harmonic inputs whose frequencies equals the two lateral ones (sum and difference, (28_2)), coexisting in an AMSC signal like (1).

5. An electric linear passive oneport (LPO) supplied with an AMSC nondistortionated voltage (31) produces a current presenting, in general, a parasite phase distortion (s. (43),...,(46)). Such distortion does not appear only if (37) takes place, meaning equal moduli of the impedances corresponding to the above mentioned two components with lateral frequencies.

6. Two examples illustrating the method consider the R, L series (s. (50), (52)) and paralel (s. (59), (60)) LPO. Both always introduce parasite phase distortion.

7. Other types of modulated signals with application to electric networks, including also a power balance, will be further considered.

Received, March 15, 1995

Technical University "Gh.Asachi", Jassy,
Department of Theoretical Mechanics
and
Department of Electrotechnics

REFERENCES

1. Braier A., *Sur la représentation par des nombres hypercomplexes des fonctions réeles d'une variable.* Bul. Inst. polit., Iaşi, **XI (XV)**, *1-2*, 89-96 (1965); *La représentation symbolique des fonctions qui vérifient des équations différentielles linéaires à coefficients constants.* Ibid., **XI (XV)**, *3-4*, 93-100 (1965).
2. Braier A., Rosman H., *Mişcarea forţată a oscilatorului liniar supus la perturbaţii modulate armonic în amplitudine.* Bul. Inst. polit., Iaşi, **XII (XVI)**, *1-2*, 315-325 (1966).

3. Braier A., *Exponential Form of the Elements of Some Algebras.* Bul. Inst. polit., Iaşi, **XIII (XVII)**, *1-2*, 115-122 (1967); *The Transferance of a System.* Ibid., **XV (XIX)**, *3-4*, s.I, 59-69 (1969); *Frequency Response of First Order Systems to Amplitude Modulated Inputs (I).* Ibid., **XVI (XX)**, *3-4*, s.IV, 7-14 (1970); *Frequency Response of Second Order Systems to Amplitude Modulated Inputs.* Ibid., **XIX (XXIII)**, *1-2*, s.IV, 9-12 (1973).
4. Braier A., *New Algebraic Method in Dynamic Systems.* International Center for Mechanical Sciences, Udine, 1972, 120 pp.
5. Rosman H., Braier A., *Sur les régimes de résonance dans les circuits électriques excités par des signaux modulés en amplitude.* Rev. Roum. Sci. Techn., s. Électrot. et Énerg. (in print).

UN STUDIU SIMBOLIC AL RĂSPUNSULUI SISTEMELOR LINIARE LA SEMNALE DE INTRARE MODULATE ÎN AMPLITUDINE

I. Semnale cu purtătoarea suprimată

(Rezumat)

Un procedeu simbolic asociază numere hipercomplexe (elemente de algebre reale de ordinul IV) semnalelor modulate armonic în amplitudine, cu purtătoarea suprimată (MAPS). Se utilizează cei doi idempotenţi ortogonali ai algebrei pentru a scrie un element ca pereche de numere complexe, obţinând semnificaţii fizice directe. Se studiază trecerea unor astfel de semnale prin sisteme liniare pasive, în particular circuite electrice, punând în evidenţă, printre altele, conexiunile dintre impedanţele uzuale corespunzătoare componentelor cu frecvenţele laterale, ce „alcătuiesc" semnalul MAPS. De pildă, când modulii acestor impedanţe coincid, circuitul electric nu introduce distorsiuni parazite de fază. Se exemplifică procedeul pentru două circuite simple, R, L serie şi paralel.

BULETINUL INSTITUTULUI POLITEHNIC DIN IAŞI
Tomul XLI (XLV), Fasc. 3–4, 1995
Secţia III
ELECTROTEHNICĂ. ENERGETICĂ. ELECTRONICĂ

D.C. 621.318.7

ON THE DERIVATION OF THE LINEAR PROGRAM WHICH FINDS A MINIMUM MEAN ABSOLUTE ERROR STACK FILTER

BY

C.E. SAVIN*), M.O. AHMAD and M.N.S. SWAMY

1. Introduction

Linear filters have long been considered as primary tools for signal and image processing. They are easy to implement and analyze, and well-suited for the design under the mathematically tractable mean square error criterion. However, this design can be used only when the input signal is corrupted with additive Gaussian noise. It has been experimentally observed that even a small deviation from the Gaussian assumption may sometimes lead to severe deteriorations in the performance of linear filters [1].

Currently, in view of the increasing technological demand, better and more specialized tools are needed, for processing signals which are severely corrupted with different types of non-Gaussian noise, such as speckle noise and salt and pepper noise. It has been shown that in this type of applications, nonlinear filters constitute a much better alternative than linear ones [1]. Specifically, when the input signal is corrupted by speckle noise or by salt and pepper noise, rank-order-based filters (ROBF) have proved to be especially attractive [6]. However, there are several classes of ROBF, and the task of choosing the right one is by itself a challenge.

Two main types of ROBF have been traditionally given a special attention. The first type includes filters in which rank order operations are combined with linear ones in some fashion. It has been shown, in [6] and [9], that this type of ROBF has a major drawback, in that the optimization over such classes of filters is mainly reduced to optimizing the linear part of the filter. The class of stack filters is

*) C.E. S a v i n is currently working towards his Ph.D. degree at Concordia University, Montreal, Canada.

the second major type of ROBF. They perform purely nonlinear rank-order-based operations, and have been introduced in an effort to correct the drawback of the first type of filters [3].

In 1985, a very powerful theoretical tool for analyzing rank order filters was developed by F i t c h *et al.* [2]. They showed that these filters possess a limited superposition property, which states that the rank order filtering of an arbitrary multilevel sequence is equivalent to decomposing the signal into binary sequences by thresholding, filtering each binary sequence by a binary rank order filter, and then reversing the decomposition process. This equivalence, reduces the analysis of multilevel sequences to that of binary sequences. The configuration in which a multilevel sequence is reduced to binary sequences is called *threshold decomposition architecture.*

In addition to the above mentioned limited superposition property of rank order filters in the threshold decomposition architecture, another property, called *stacking property*, was identified by W e n d t *et al.* [3]. Stacking property is an ordering one which referes to the outputs of the binary rank order filters. Precisely, the binary outputs at each instant n have a structure in which a stack of 0's is piled on top of a stack of 1's.

The definition of stack filters was given by abstracting the properties of rank order filters in the threshold decomposition configuration [3]. Specifically, in a stack filter architecture, the binary rank-order-based operator is characterized by an arbitrary positive Boolean function (PBF)[1]. An optimality theory for the design of stack filters under the MMAE criterion was later developed by C o y l e and L i n [4]. Based on this theory, it is possible to determine a stack filter which minimizes the mean absolute error (MAE) between its output and a desired signal, given a noise-corrupted observation of the latter. This optimality theory for nonlinear ROBF is as analytically tractable as the theory of optimal linear filtering, and it is based on using an LP formulation of the optimization problem. The LP which finds an MMAE stack filter has been derived by C o y l e and L i n in [4], by employing an artificial estimation error defined as a weighted mean absolute error function. A direct approach for the formulation of this LP is proposed in this paper which offers an increased insight into the physical interpretation of the optimization problem.

2. MAE Criterion and Stacking Property of PBFs

The estimation problem for the class of stack filters can be stated using Fig.1. The process R(n) which is received at the input of a stack filter S_f is assumed to be

[1] A Boolean function $f(x)$, for which there exists a disjunctive form such that the variable $\overline{x}_j$ does not appear in any term of this form, is said to be positive in $\overline{x}_j$. A PBF is a Boolean function which is positive in all its variables [7]. As an example, the binary function $f(x_0, x_1, x_2) = x_0x_1 + x_1x_2 + x_2x_0$ is a PBF. Note that a stack filter characterized by this PBF performs a median filtering operation.

a corrupted version of some desired process $S(n)$ through an operation $g(\cdot,\cdot)$. The corruption may be caused either by a noise process $N(n)$ or by some intentional operation, such as a modulation scheme. The stack filter $\mathcal{S}_f$ is characterized by the PBF f. At each time instant n, the stack filter output is an estimate, called $\hat{S}(n)$, of the desired process $S(n)$. This estimate is based on the sequence $\mathbf{R}_M(n)$ observed in the input window of the stack filter

$$\hat{S}(n) = \mathcal{S}_f(\mathbf{R}_M(n)). \tag{1}$$

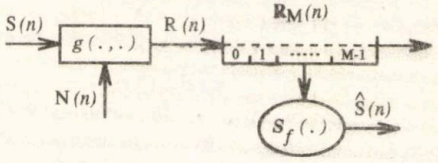

Fig. 1.– The structure of the estimation problem for the class of stack filters.

The MAE between the desired signal, $S(n)$, and the estimated one, $\hat{S}(n)$, at time instant n, is defined to be the cost of using the stack filter $\mathcal{S}_f$ at time n, and it can be expressed as

$$C_n(\mathcal{S}_f) = E\left[\left|S(n) - \mathcal{S}_f(\mathbf{R}_M(n))\right|\right]. \tag{2}$$

If we make the assumption that the signal and noise processes are jointly stationary, then the cost function $C_n(\mathcal{S}_f)$ has the same value at all time instants n. Therefore, in the subsequent discussion, the subscript n is not used for the cost function. The optimal stack filter for estimation under MAE criterion is the filter for which $C(\mathcal{S}_f)$ is minimum.

The rationale of choosing the MAE criterion for the design of a stack filter is that it allows to express the estimation error of a stack filter as the sum of the decision errors incurred by the Boolean filter at each level of the stack filter architecture. By decomposing the desired and estimated signals by thresholding, (2) becomes

$$\begin{aligned} C_n(\mathcal{S}_f) = E\left[\left|S(n) - \mathcal{S}_f(\mathbf{R}_M(n))\right|\right] &= E\left[\left|\sum_{\ell=1}^{L-1} s_\ell(n) - \sum_{\ell=1}^{L-1} f(\mathbf{t}_\ell(\mathbf{R}_M(n)))\right|\right] = \\ &= E\left[\left|\sum_{\ell=1}^{L-1} [s_\ell(n) - f(\mathbf{t}_\ell(\mathbf{R}_M(n)))]\right|\right]. \end{aligned} \tag{3}$$

In (3), $s_\ell(n)$ and $\mathbf{t}_\ell(\mathbf{R}_M(n))$ denote the binary sequences in the threshold decomposition of $S(n)$ and $\mathcal{S}_f(\mathbf{R}_M(n))$, respectively. Due to the stacking property of the binary operator f, all the nonzero terms of the sum in (3) have the same sign,

and therefore, the operations of summation and taking the absolute value may be interchanged as

$$C(\mathcal{S}_f) = E\left[\sum_{\ell=1}^{L-1} \left| s_\ell(n) - f(\mathbf{t}_\ell(\mathbf{R}_M(n))) \right| \right]. \tag{4}$$

The operations of finding the expected value and summation in (4) can also be interchanged, since the mean value of a sum of random variables equals the sum of their mean values [8]. Thus, (4) becomes

$$C(\mathcal{S}_f) = \sum_{\ell=1}^{L-1} \left[E\left| s_\ell(n) - f(\mathbf{t}_\ell(\mathbf{R}_M(n))) \right| \right] = \sum_{\ell=1}^{L-1} \left[E\left| s_\ell(n) - f(\mathbf{r}_\ell(n)) \right| \right], \tag{5}$$

where we have used the notation $\mathbf{r}_\ell(n) = \mathbf{t}_\ell(\mathbf{R}_M(n))$.

The ℓth term of the summation in (5) is the mean absolute error incurred at level ℓ, $E[|e_\ell(n)|]$, when the Boolean operator f is used at that level. Therefore, (5) can be written as

$$C(\mathcal{S}_f) = \sum_{\ell=1}^{L-1} E[|e_\ell(n)|], \tag{6}$$

where $e_\ell(n)$ is given by

$$e_\ell(n) = s_\ell(n) - f(\mathbf{t}_\ell(\mathbf{R}_M(n))). \tag{7}$$

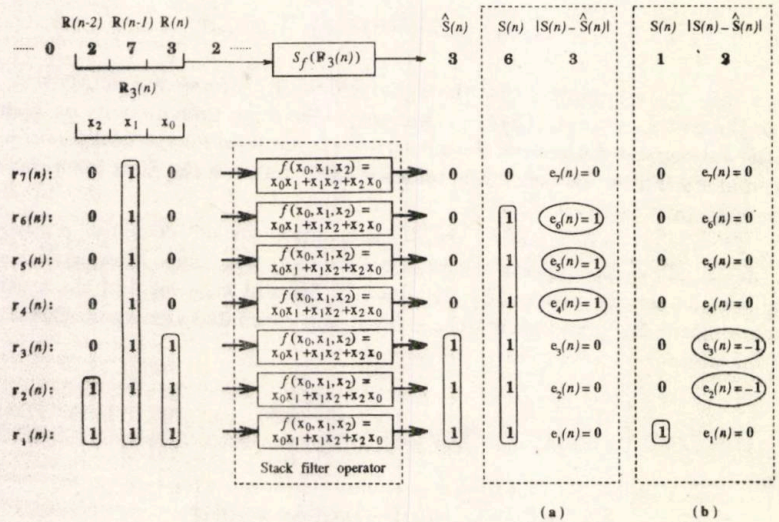

Fig. 2.– An illustration of the errors incurred between the desired and estimated samples in a stack filter architecture, for the two possible cases ($\hat{S}(n) \leq S(n)$ and $\hat{S}(n) > S(n)$): (a) when the desired sample is greater than the estimated one, the binary errors at the various threshold levels can assume only the values 0 or 1; (b) when the desired sample is less than the estimated one, they can be only 0 or −1.

Fig. 2 illustrates the errors incurred in signal estimation using a stack filter architecture, for two possible cases, $\hat{S}(n) \leq S(n)$ and $\hat{S}(n) > S(n)$. In conclusion, the mean absolute error estimation using a stack filter architecture is equivalent to a massively parallel decision making process, in which, at each level ℓ, it is determined whether or not the estimated signal is less than ℓ, when these decisions are constrained to be consistent with each other as required by the stacking property [4].

3. The Optimization Problem to Determine an MMAE Stack Filter

As shown in § **2**, when f is restricted to be a PBF (i.e., when f satisfies the stacking property), the cost function $C(S_f)$ defined by (3) can be expressed as in (5). The problem of designing a stack filter which is optimal for estimation under the MAE criterion is concerned with minimizing this cost function, and this problem can be formally stated as follows:

O p t i m i z a t i o n P r o b l e m. *Determine a Boolean filter* $\tilde{f} \in \mathcal{F}_M$, *where* $\mathcal{F}_M$ *is the set of all Boolean filters of window size* M, *which achieves*

$$C(S_{\tilde{f}}) = \min_{f \in \mathcal{F}_M} \sum_{\ell=1}^{L-1} E[|s_\ell(n) - f(\mathbf{r}_\ell(n))|], \tag{8}$$

subject to the constraint that f *should satisfy the stacking property.*

Note that the total number of Boolean filters of window size M is 2^{2^M}, while the total number of PBFs with M variables is known to be approximatively $2^{2^{M/2}}$ [4].

A Boolean filter f of window size M is completely determined by the vector

$$\mathbf{F} = (f(\mathbf{b}_1), f(\mathbf{b}_2), ..., f(\mathbf{b}_j), ..., f(\mathbf{b}_{2^M})), \tag{9}$$

where $\{\mathbf{b}_j | j = 1, 2, ..., 2^M\}$ is an ordered sequence of all Boolean vectors of size M. The jth entry in (9) represents the output of the filter, when the binary vector in the filter's input window is $\mathbf{b}_j$. Therefore, in order to solve the optimization problem as formulated above, we have to first find an explicit expression for $E[|s_\ell(n) - f(\mathbf{r}_\ell(n))|]$ as a function of the variables $f(\mathbf{b}_j) \in \{0, 1\}$, $(j = 1, 2, ..., 2^M)$.

Let us consider the experiment of observing different realizations of the desired threshold process at level ℓ of a stack filter architecture at the time instant n, $s_\ell(n) \in \{0, 1\}$, and the corresponding realizations of the binary input vector process to the Boolean filter f at level $\ell, \mathbf{r}_\ell(n) \in \{\mathbf{b}_1, \mathbf{b}_2, ..., \mathbf{b}_{2^M}\}$. The sample space (i.e., the set of all possible outcomes) of this experiment is given by

$$\{(0, \mathbf{b}_1), (0, \mathbf{b}_2), ..., (0, \mathbf{b}_{2^M}), (1, \mathbf{b}_1), (1, \mathbf{b}_2), ..., (1, \mathbf{b}_{2^M})\}, \tag{10}$$

where a pair $(0, \mathbf{b}_j)$ denotes the outcome $(s_\ell(n) = 0, \mathbf{r}_\ell(n) = \mathbf{b}_j)$, while a pair $(1, \mathbf{b}_j)$ corresponds to $(s_\ell(n) = 1, \mathbf{r}_\ell(n) = \mathbf{b}_j)$. The expected value of an arbitrary

discrete random variable Y, defined on a sample space with K possible outcomes, is given by

$$E[\mathrm{Y}] = \sum_{j=1}^{\mathrm{K}} y_j P(y_j), \tag{11}$$

where y_j denotes a particular value of Y, having the probability of occurence $P(y_j)$ [8]. Therefore, for the expected value of the random variable $|e_\ell(n)| = |\mathrm{s}_\ell(n) - f(\mathbf{r}_\ell(n))|$ (which is a real function of the elements in the sample space (10)), we have

$$\begin{aligned} E[|e_\ell(n)|] &= \sum_{j=1}^{2^{\mathrm{M}}} (|0 - f(\mathbf{b}_j)| P[\mathrm{s}_\ell(n) = 0, \mathbf{r}_\ell(n) = \mathbf{b}_j] + \\ &\quad + |1 - f(\mathbf{b}_j)| P[\mathrm{s}_\ell(n) = 1, \mathbf{r}_\ell(n) = \mathbf{b}_j]) = \\ &= \sum_{j=1}^{2^{\mathrm{M}}} \left(P(0, \mathbf{b}_j|\ell) f(\mathbf{b}_j) + P(1, \mathbf{b}_j|\ell) \overline{f}(\mathbf{b}_j) \right) = \\ &= \sum_{j=1}^{2^{\mathrm{M}}} [(P(0, \mathbf{b}_j|\ell) - P(1, \mathbf{b}_j|\ell)) f(\mathbf{b}_j) + P(1, \mathbf{b}_j|\ell)], \end{aligned} \tag{12}$$

where the notations $P(0, \mathbf{b}_j|\ell)$ and $P(1, \mathbf{b}_j|\ell)$ imply, respectively, $P[\mathrm{s}_\ell(n) = 0, \mathbf{r}_\ell(n) = \mathbf{b}_j]$ and $P[\mathrm{s}_\ell(n) = 1, \mathbf{r}_\ell(n) = \mathbf{b}_j]$. Therefore, the decision error $E[|e_\ell(n)|]$ at each level ℓ of a stack filter architecture is a linear function of the variables $f(\mathbf{b}_j), (j = 1, 2, ..., 2^{\mathrm{M}})$. Using (12), the cost function $\mathrm{C}(\mathcal{S}_f)$ in (5) becomes

$$\begin{aligned} \mathrm{C}(\mathcal{S}_f) &= \sum_{j=1}^{2^{\mathrm{M}}} \left[f(\mathbf{b}_j) \left(\sum_{\ell=1}^{\mathrm{L}-1} P(0, \mathbf{b}_j|\ell) \right) + \overline{f}(\mathbf{b}_j) \left(\sum_{\ell=1}^{\mathrm{L}-1} P(1, \mathbf{b}_j|\ell) \right) \right] = \\ &= \sum_{j=1}^{2^{\mathrm{M}}} [\alpha_j f(\mathbf{b}_j) + \beta_j \overline{f}(\mathbf{b}_j)], \end{aligned} \tag{13}$$

where $\alpha_j = \sum_{\ell=1}^{\mathrm{L}-1} P(0, \mathbf{b}_j|\ell)$ and $\beta_j = \sum_{\ell=1}^{\mathrm{L}-1} P(1, \mathbf{b}_j|\ell)$. Denoting $\gamma_j = \alpha_j - \beta_j$, (13) can alternately be written as

$$\mathrm{C}(\mathcal{S}_f) = \sum_{j=1}^{2^{\mathrm{M}}} [\gamma_j f(\mathbf{b}_j) + \beta_j]. \tag{14}$$

Finally, the optimization problem can be stated as:

Zero-One LP Optimization Procedure. *Determine a Boolean filter* $\tilde{f}$ *of window size* M, *which achieves*

$$C(\mathcal{S}_{\tilde{f}}) = \min_{f \in \mathcal{F}_M} \sum_{j=1}^{2^M} [\gamma_j f(\mathbf{b}_j) + \beta_j], \tag{15}$$

subject to the following constraints: a) *for each vector* $\mathbf{b}_j$:

$$f(\mathbf{b}_j) \in \{0,1\}, \tag{16}$$

and b) *for each pair of vectors* $[(\mathbf{p},0,\mathbf{q}),(\mathbf{p},1,\mathbf{q})]$:

$$f(\mathbf{p},1,\mathbf{q}) \geq f(\mathbf{p},0,\mathbf{q}). \tag{17}$$

The set of inequalities (17) imposes the constraint that f should satisfy the stacking property, that is, be a PBF.

Assuming that the probability models of the signal and noise processes are given, one can determine the joint probabilities $P(0,\mathbf{b}_j|\ell)$ and $P(1,\mathbf{b}_j|\ell)$, and then calculate the constant coefficients α_j's and β_j's. In general, it is a difficult task to determine the joint probabilities $P(0,\mathbf{b}_j|\ell)$ and $P(1,\mathbf{b}_j|\ell)$. However, in [4], Coyle and Lin have discussed this problem in the context of the specific case when the signal and noise are independent Markov chains, and they have developed some techniques which might be helpful when other modelling assumptions are considered. As a more practical alternative, an algorithm for the adaptive design of stack filters has been proposed [5]. In this algorithm, an optimal filter is determined by applying a training procedure given a reference (desired) signal and its noise corrupted version, and counting the probabilities $P(0,\mathbf{b}_j|\ell)$ and $P(1,\mathbf{b}_j|\ell)$.

4. The Solution to the Optimization Problem Using a Linear Program

A Boolean stack filter obtained through the solution to the zero-one LP optimization problem discussed in § 3 can be determined more efficiently by transforming the integer LP into a regular LP. In order to give a physical interpretation to this transformation, we define the concept of a randomizing Boolean vector function and introduce its stacking property.

Definition. A randomizing Boolean vector function, $\mathbf{P}_f$, of a vector Boolean variable $\mathbf{b}$ of size M is defined as

$$\mathbf{P}_f = (P_f(\mathbf{b}_1), P_f(\mathbf{b}_2), ..., P_f(\mathbf{b}_j), ..., P_f(\mathbf{b}_{2^M})),$$

in which $P_f(\mathbf{b}_j) \in [0,1], \forall j = 1,2,...,2^M$.

Given a randomizing Boolean vector function $\mathbf{P}_f$, a Boolean function (which, in this context, can be designated as nonrandomizing Boolean function) f can be determined by

$$f(\mathbf{b}_j) = \begin{cases} 1 \text{ if } P_f(\mathbf{b}_j) \geq \mathrm{T}_j, \\ \\ 0 \text{ if } P_f(\mathbf{b}_j) < \mathrm{T}_j, \end{cases} \qquad \forall j = 1, 2, ..., 2^{\mathrm{M}}, \tag{18}$$

where $\mathrm{T}_j \in (0,1)$. For instance, a simple correspondence from $\mathbf{P}_f$ to f can be defined by taking $\mathrm{T}_j = 0.5, \forall j = 1, 2, ..., 2^{\mathrm{M}}$.

P r o p e r t y. A randomizing Boolean vector function $\mathbf{P}_f$ is said to satisfy a stacking property if and only if

$$P_f(\mathbf{b}_\alpha) \geq P_f(\mathbf{b}_\beta) \text{ whenever } \mathbf{b}_\alpha \geq \mathbf{b}_\beta, \quad \forall \alpha, \beta \in \{1, 2, ..., 2^{\mathrm{M}}\}.$$

Let us now consider a cost function

$$\mathrm{C}' = \sum_{j=1}^{2^{\mathrm{M}}} [\gamma_j P_f(\mathbf{b}_j) + \beta_j], \tag{19}$$

and observe that $\mathrm{C}' \equiv \mathrm{C}(\mathcal{S}_f)$ in the special case when $P_f(\mathbf{b}_j) \in \{0,1\}, \forall j = 1, 2, ..., 2^{\mathrm{M}}$ (see (14)). Based on the concept of a randomizing Boolean vector function, and employing the cost function C', we now formulate the following

L P O p t i m i z a t i o n P r o c e d u r e. *Determine a function* $\mathbf{P}_{\tilde{f}}$ *which achieves the following*:

$$\textit{minimize} \quad \sum_{j=1}^{2^{\mathrm{M}}} [\gamma_j P_f(\mathbf{b}_j) + \beta_j] \tag{20}$$

subject to the constraints: a) *for each vector* $\mathbf{b}_j$:

$$0 \leq P_f(\mathbf{b}_j) \leq 1, \tag{21}$$

and b) *for each pair of vectors* $[(\mathbf{p}, 0, \mathbf{q}), (\mathbf{p}, 1, \mathbf{q})]$:

$$P_f(\mathbf{p}, 1, q) \geq P_f(\mathbf{p}, 0, \mathbf{q}). \tag{22}$$

It has been shown in [4] that all the solutions to the LP optimization problem (Eqns.(20),...,(22)) are integers. Besides, as 0 and 1 are the only possible integer solutions, each variable $P_f(\mathbf{b}_j)$ will assume values of either 0 or 1. Therefore, any solution using the LP optimization procedure is a nonrandomizing Boolean filter, and consequently, the LP optimization procedure gives the solution to the original optimization problem (8) for designing an MMAE stack filter.

5. Conclusion

A new approach for the derivation of the LP which finds an MMAE stack filter has been presented. In this approach, a zero-one LP has been constructed by

deriving an expression for the expected value of the binary decision error at the level ℓ of a stack filter architecture. Then, it has been indicated that the solution to this zero-one LP can be obtained more efficiently by transforming the integer LP into a regular LP.

Received, November 18, 1993

Concordia University, Montreal, Canada,
Centre for Signal Processing
and Communications,
Department of Electrical
and Computer Engineering

REFERENCES

1. Gallagher N.C., Wise G.L., *A Theoretical Analysis of the Properties of Median Filters.* IEEE Trans. Acoust., Speech, Signal Processing, 29, 1136-1141 (1981).
2. Fitch J.P., *Threshold Decomposition of Multidimensional Ranked Order Operations.* IEEE Trans., Circuits and Syst., 32, 445-450 (1985).
3. Wendt P.D., Coyle E.J., Gallagher N.C., *Stack Filters.* IEEE Trans. Acoust., Speech, Signal Processing, **34**, 898-911 (1986).
4. Coyle E.J., Lin J.H., *Stack Filters and the Mean Absolute Error Criterion.* IEEE Trans. Acoust., Speech, Signal Processing, **36**, 1244-1254 (1988).
5. Lin J.H., Sellke T.M., Coyle E.J., *Adaptive Stack Filtering under the Mean Absolute Error Criterion.* IEEE Trans. Acoust., Speech, Signal Processing, **38**, 938-954 (1990).
6. Gabbouj M., Coyle E.J., Gallagher N.C., *An Overview of Median and Stack Filtering.* Circuits, Systems and Signal Process., **11**, 7-45 (1992).
7. Muroga S., *Threshold Logic and Its Applications.* J. Wiley, New York, 1971.
8. Peebles P.Z., *Probability, Random Variables, and Random Signal Principles.* McGraw-Hill, New York, 1980.
9. Gabbouj M., *Estimation and Structural-Based Approach for the Design of Optimal Stack Filters.* Ph.D. Thesis, Purdue University, West Lafayette, 1989.

UN NOU PROCEDEU PENTRU FORMULAREA PROGRAMULUI LINIAR A CĂRUI SOLUŢIE ESTE UN FILTRU STIVĂ DE EROARE ABSOLUTĂ MINIMĂ

(Rezumat)

Se propune un nou procedeu pentru formularea programului liniar a cărui soluţie este un filtru stivă de eroare absolută minimă. În cadrul acestui procedeu se elaborează o expresie matematică simplă pentru eroarea absolută binară la nivelul ℓ al unui filtru stivă şi se construieşte un program liniar în numere binare pentru determinarea unui filtru stivă optimal (în sensul erorii absolute minime). În final se observă că programul în numere binare poate fi transformat într-un program liniar ordinar, ceea ce aduce avantajul unor metode eficiente pentru determinarea soluţiilor.

BULETINUL INSTITUTULUI POLITEHNIC DIN IAŞI
Tomul XLI (XLV), Fasc. 3-4, 1995
Secţia III
ELECTROTEHNICĂ. ENERGETICĂ. ELECTRONICĂ

D.C. 621.318.7

NOTCH TRACKING FILTER

BY
ADRIAN LEUCIUC and DANIEL MIHALACHI

1. Introduction

In this paper a second order notch tracking filter is presented. The proposed structure is based on a previously reported voltage-controlled notch biquad realization [1] and compared with other techniques the tracking loop does not contain a phase comparator block. The op-amp based structure of the proposed circuit makes it suitable for low frequency applications, but the employed tracking technique can be easily extended to high frequency configurations.

2. Voltage-Controlled Biquads

As it is well known the general second order transfer function of a biquad is given by:

$$H(s) = \frac{P(s)}{s^2 + B_p s + \omega_n^2}, \tag{1}$$

where $P(s)$ is a polynomial of second order in s, B_p – the angular pole bandwidth and ω_n – the undamped natural angular frequency. A most versatile structure used to obtain different types of second order filters is the A n t o n i o u's General Immittance Convertor (GIC) [2], [3] (Fig. 1) with Z_2 capacitive and Z_1, Z_3, Z_4 and Z_5 resistive.

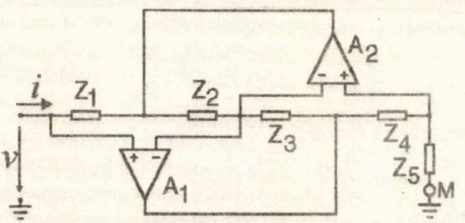

Fig. 1

In order to control ω_n, a voltage-controlled GIC configuration has been used (Fig. 2). In this structure the resistance R_3 was replaced by a JFET operating in the nonsaturated region as a voltage-controlled resistance. The functioning of the JFET in the nonsaturated region is described by the nonlinear relationship:

(2) $$I_D = \frac{I_{DSS}}{V_P^2}[2(V_P - V_{GS})V_{DS} - V_{DS}^2].$$

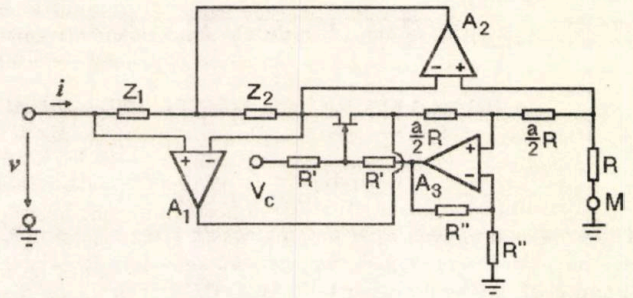

Fig. 2

This relation can be approximated with a linear one only for drain-to-source voltages up to 100 mV. The extension of the linear range is possible by either of the following conditions: a) ensuring an appropriate voltage to the gate of the JFET:

(3) $$V_{GS} = \frac{V_C + V_{DS}}{2}$$

to convert the nonlinear relation (2) into a linear one:

(4) $$I_D = \frac{I_{DSS}}{V_P^2}(V_C - 2V_P)V_{DS} = \frac{V_{DS}}{R_{\text{JFET}}};$$

b) reducing the drain-to-source voltage to a fraction $a \ll 1$ of the input voltage v to keep the JFET in the nonsaturated region.

The above conditions a) and b) are both satisfied by the circuit presented in Fig.2 by means of the supplementary op-amp A_3, the resistances R' and R'' and the appropriate values of $R_4 = aR$ (composed of two equal resistances $aR/2$) and $R_5 = R$. Indeed:

(5) $$V_{DS} = \frac{R_4}{R_5}V = aV.$$

The experiments carried out with this structure confirmed its wide dynamic range and low distortion properties and it was successfully used in voltage-controlled active filter synthesis and voltage-controlled impedance simulation [4], [5]. Four GIC-based biquads and their corresponding transfer functions are given in Fig.3.

3. The Tracking Loop

From the expressions of the transfer functions of the biquads presented in Fig.3 one can easily observe that the control voltage, by means of the JFET resistance,

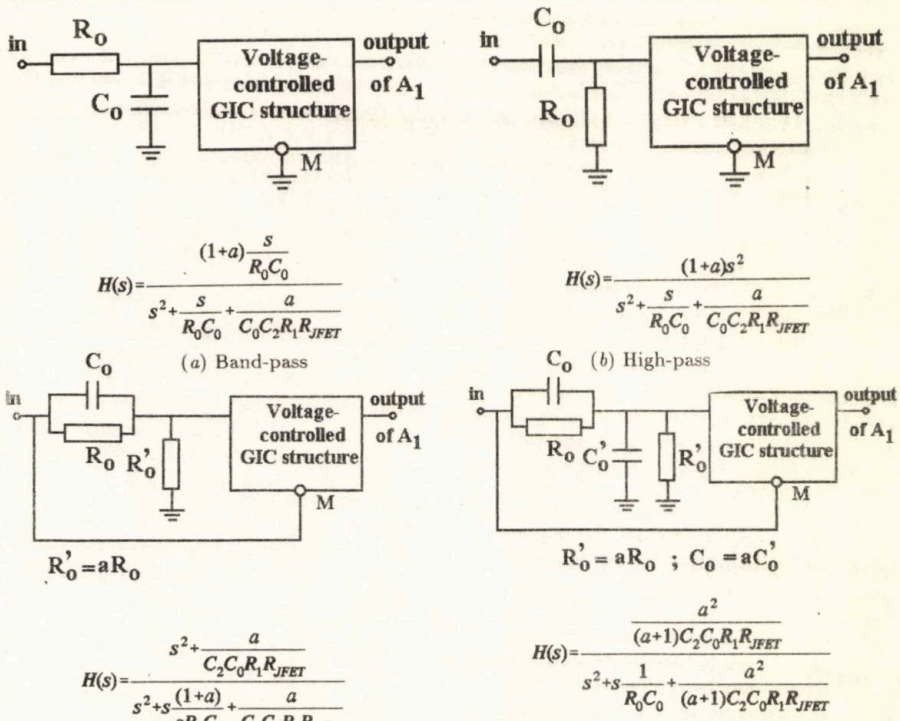

Fig. 3

affects only the ω_n parameter. This type of controlled filters is suitable for tracking filtering applications but most of the tracking filter structures reported in literature make use of a phase lock loop (PLL).

In Fig.4 a PLL-less tracking system is presented, the notch filter from its structure being realized with the basic scheme from Fig.3 *c*. The phasorial diagram describing the functioning of the proposed system is given in Fig.5.

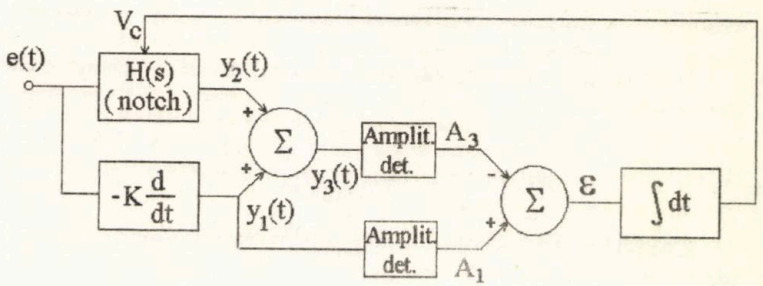

Fig. 4

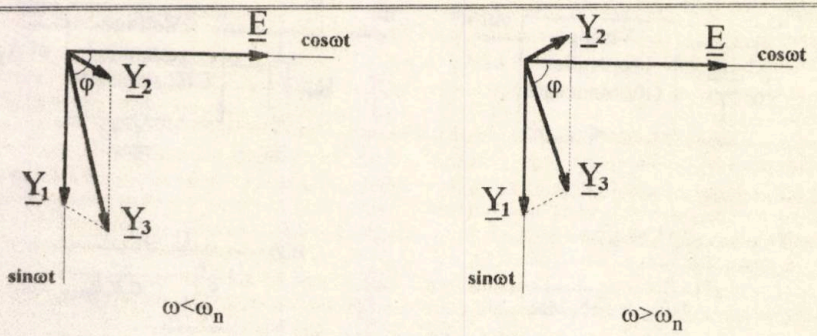

Fig. 5

$$H(s) = \frac{s^2 + \omega_n^2}{s^2 + B_p s + \omega_n^2} \tag{6}$$

and for a harmonic input signal:

$$e(t) = A\cos\omega t, \tag{7}$$

the following relations can be written:

$$y_1(t) = \omega K A \sin\omega t, \tag{8}$$

$$y_2(t) = A|H(\omega)|\cos[\omega t + \arg(H(\omega))], \tag{9}$$

$$y_3(t) = A\sqrt{|H(\omega)|^2 + \omega^2 K^2 - 2\omega K|H(\omega)|\sin[\arg(H(\omega))]}\,\sin(\omega t + \varphi), \tag{10}$$

where

$$|H(\omega)| = \frac{|\omega_n^2 - \omega^2|}{\sqrt{(\omega_n^2 - \omega^2)^2 + B_p^2\omega^2}}, \quad \arg(H(\omega)) = \arctan\frac{B_p\omega}{\omega^2 - \omega_n^2}. \tag{11}$$

For a proper tracking, the error ε (which is given by the difference of the amplitudes of $y_1(t)$ and $y_3(t)$) must be negative for $\omega < \omega_n$, positive for $\omega > \omega_n$ and zero for and only for $\omega = \omega_n$.

Since $|H(\omega_n)| = 0$ it results that $\varepsilon = 0$ for $\omega = \omega_n$. The other two conditions from above yield:

$$\begin{cases} |H(\omega)| - 2\omega K \sin[\arg(H(\omega))] > 0, & \text{if} \quad \omega < \omega_n, \\ |H(\omega)| - 2\omega K \sin[\arg(H(\omega))] < 0, & \text{if} \quad \omega > \omega_n. \end{cases} \tag{12}$$

The first of these relations is obviously fulfilled since $\arg(H(\omega)) < 0$ for $\omega < \omega_n$, while the second one leads to:

$$\omega^2(1 - 2KB_p) - \omega_n^2 < 0, \tag{13}$$

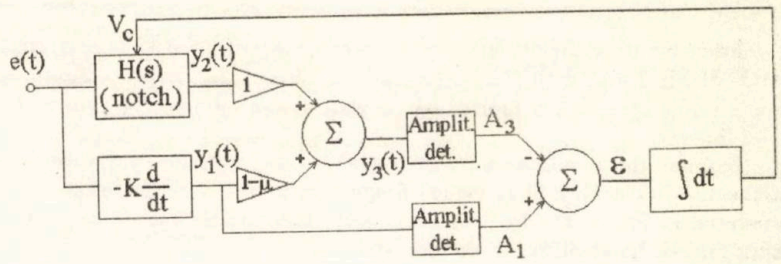

Fig. 6

for any $\omega < \omega_n$. This condition is satisfied if $K > 1/2B_p$.

The physical realization of a notch filter has a transfer function different from (6), of the form:

$$H(s) = \frac{s^2 + B_z s + \omega_n^2}{s^2 + B_p s + \omega_n^2}, \tag{14}$$

with $B_z \ll B_p$. In these conditions $|H(\omega_n)| = B_z/B_p \neq 0$ and obviously $\varepsilon \neq 0$ for $\omega = \omega_n$. To avoid this inconvenience the scheme of Fig.4 was slighty modified as it is shown in Fig.6.

The μ parameter results from the condition that $\varepsilon = 0$ for $\omega = \omega_n$. A simple mathematical calculus yields:

$$\mu = 1 - \sqrt{1 - \frac{B_z^2}{B_p^2 K^2 \omega_n^2}}. \tag{15}$$

As μ depends on ω_n, the error ε vanishes for a single value of the tracking frequency. In order to minimize this error over the entire tracking range (defined by $\omega_{\max} - \omega_{\min}$), the following condition has to be fulfilled:

$$|\varepsilon(\omega_{\max})| = |\varepsilon(\omega_{\min})|. \tag{16}$$

After a simple algebraic calculus, the value ω_n to be considered in (15) is given by:

$$\omega_n = \frac{1}{\sqrt{2}} \sqrt{\omega_{\min}\omega_{\max} + \sqrt{\omega_{\min}^2 \omega_{\max}^2 + \frac{B_z^2}{B_p^2 K^2}(\omega_{\min} + \omega_{\max})^2}}. \tag{17}$$

4. Results and Conclusions

The block scheme of Fig. 6 was practically realized using the voltage-controlled structure of Fig. 2 and the classical op-amp based configurations for the differentiator, adders and integrator. There have been used LM201 type op-amp in the GIC structure and MAX414 type op-amps in the tracking loop.

Intensive experiments have been carried out with the voltage-controlled biquads of Fig.3 and with the notch tracking filter. The circuit exhibits wide dynamic range (practically limited by the saturation voltage of op-amps) and very good linearity.

From all the acquired results, the steady state rms value of the output voltage of the notch tracking filter versus frequency (at 0.5 V rms harmonic input) is presented in Fig.7. For frequencies greater than 20 kHz the influence of the op-amps limited bandwidth can be observed.

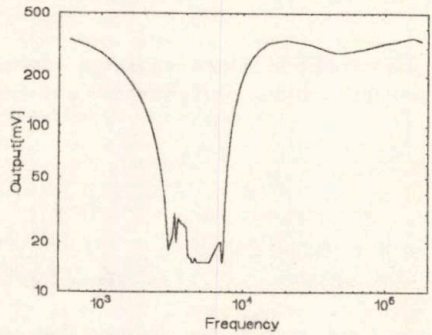

Fig. 7

The advantage of the proposed tracking technique is represented by the elimination of the phase lock loop (which is a circuit rather complex) and can be used with any type of voltage-controlled second order notch filter. A high frequency version of the presented structure is now under investigation.

Received, June 24, 1994

Technical University "Gh.Asachi", Jassy,
Department of Electronics

REFERENCES

1. L e u c i u c A., G o r a ş L., *New GIC-JFET Voltage-controlled Impedances and their Application to Voltage-controlled Biquads Synthesis.* IEEE Trans. Circuits and Syst. (submitted).
2. A n t o n i o u A., *Gyrator Using Operational Amplifier.* Electron. Lett., **3**, 350-352 (1967).
3. A n t o n i o u A., *Realization of Gyrators Using Operational Amplifiers and their Use in RC-active Networks.* Proc. Inst. Elec. Eng., **116**, 1838-1850 (1969).
4. G o r a ş L., L e u c i u c A., *GIC-JFET Voltage-controlled Impedances.* Proc. of 1993 ECCTD, Davos, Switzerland, **2**, 1579-1582 (1993).
5. L e u c i u c A., G o r a ş L., *High-Q Voltage-controlled Inductance.* Proc. of the Internat. Symp. on Signals, Circuits and Systems, Jassy, Romania, **1**, 74-77 (1993).

FILTRU DE URMĂRIRE OPREŞTE BANDĂ

(Rezumat)

Se prezintă o structură de filtru de urmărire de tip opreşte bandă (FOB) care, spre deosebire de alte realizări prezentate în literatură, nu foloseşte o buclă de calare pe fază. Circuitul propus se bazează pe utilizarea filtrelor de ordinul doi realizate cu ajutorul Convertorului General de Impedanţă (GIC) [2], [3]. Posibilitatea de control al frecvenţei centrale a FOB a fost obţinută folosind o variantă modificată a GIC ce conţine un tranzistor cu efect de câmp lucrând în regim de rezistenţă controlată în tensiune [1], [4], [5].

BULETINUL INSTITUTULUI POLITEHNIC DIN IAŞI
Tomul XLI (XLV), Fasc. 3–4, 1995
Secţia III
ELECTROTEHNICĂ. ENERGETICĂ. ELECTRONICĂ

D.C. 621.318.7; 621.396.619

COMPARISON OF PERFORMANCES OF DIGITAL MODULATION TECHNIQUES USING CAUSAL BANDLIMITING FILTERS

BY
PAUL COTAE and DANIELA TĂRNICERIU

1. Introduction

In a transmitting system the distortions depend on the filter bandwidth. Since the bandwidth is large, the matched filter is the best; since the bandwidth is narrow, a simple detector which takes decisions based directly on the received sample leads to a smaller error then the matched filter.

In order to realize the above comparison, two facts have to be consider: a) the impulse response of the whole transmission system, obtained by convolution product of all filter impulse responses from transmission chain; b) the noise variance, obtained at the detection filter output and defined as follows:

$$\sigma_n^2 = \overline{n^2(t)} = \frac{N_0}{2}\int_{-\infty}^{\infty} |H_R(f)H_D(f)|^2 \mathrm{d}f. \tag{1}$$

2. Impulse Response Computation

In Table 1 there are presented the system name, the type of the transmitter and receiver filter and the type of the detector.

A first verification consists in the comparison of the obtained results and the other already before obtained one.

Due to this fact, the established notations are maintained namely.

$$h(t) = \begin{cases} h_N(t) = u(t) - u(t-T), & \text{NRZ;} \\ h_H(t) = \sin\left(\frac{\pi t}{T}\right) u(t) + \sin\left[\frac{\pi(t-T)}{T}\right] u(t-T), & \text{HS;} \\ h_{SP}(t) = u(t) - 2u\left(t - \frac{T}{2}\right) + u(t-T), & \text{SP.} \end{cases} \tag{2}$$

Table 1

System	$h_F(t)$	$h_D(t)$	Detection type
NN	$h_N(t)$	$h_N(t)$	Matched filter
NS	$h_N(t)$	$\delta(t)$	Sample detection
HH	$h_H(t)$	$h_H(t)$	Matched filter
HS	$h_H(t)$	$\delta(t)$	Sample detection
HN	$h_N(t)$	$h_N(t)$	Sample add hold
SPSP	$h_N(t)$	$h_{SP}(t)$	Matched filter
SPS	$h_N(t)$	$\delta(t)$	Sample detection
HR	$h_N(t)$	$U_{T/2}(t)$	Sample and hold of $T/2$ duration

The system name depends on the type of the transmitter and receiver filter.

If $n_R(t)$ denotes the noise in the received signal at the input of receiver filter, then the noise after the receiver filter is:

$$n(t) = n_R(t) * h_D(t) = \int_0^\infty n_R(t-\tau)h_D(\tau)\mathrm{d}\tau. \tag{3}$$

If the detection filter is missing, the noise variance follows:

$$\sigma_n^2 = \overline{n^2(t)} = \overline{n_R^2(t)} = R_{nR}(0), \tag{4}$$

where $R_{nR}(\tau)$ is the autocorrelation function of the noise. Thus, (4) is true for HS, NRZ and SPS cases. For the other cases the noise variance is given by:

$$\sigma_n^2 = \overline{n^2(t)} = \int_0^T \int_0^T \overline{n_R(t-\tau_1)n_R(t-\tau_2)}h_D(\tau_1)h_D(\tau_2)\mathrm{d}\tau_1\mathrm{d}\tau_2. \tag{5}$$

Denoting $\tau = \tau_2 - \tau_1$, (5) becomes:

$$\sigma_n^2 = \int_0^T R_{nR}(\tau)R_D(\tau)\mathrm{d}\tau, \tag{6}$$

where $R_D(\tau)$ is the autocorrelation function filter.

In Table 2 the autocorrelation functions for different type of detection filters are computed.

Table 2

Detector type	Autocorrelation function $R_D(\tau)$, $0 \le \tau \le T$
$h_N(t)$	$2(T-\tau)$
$h_{T/2}(t)$	$(T-2\tau)U_{T/2}(t)$
$h_{SP}(t)$	$2(T-3\tau)U_{T/2}(\tau) - 2(T-\tau)U_{T/2}(\tau - T/2)$
$h_H(t)$	$(T-\tau)\cos(\pi\tau/T) - (T/\pi)\sin(\pi\tau)$

In order to compute the system impulse response, the impulse response behind the detection filter, denoted by $g_R(t)$, will be first determined:

$$g_R(t) = h_F(t) * h_E(t) * h_R(t). \tag{7}$$

With the aim to determine $g_R(t)$, the response to each element from (2) will be consider, so that, according to this relation, it results:

$$g_R(t) = \begin{cases} g_N(t) - g_N(t-T), \\ g_N(t) + g_N(t-T), \\ g_N(t) - 2g_N\left(t - \frac{T}{2}\right) + g_N(t-T). \end{cases} \tag{8}$$

In order to determine $g(t)$ the convolution product between $g_R(t)$ and $h_D(t)$ is considered:

$$g(t) = g_R(t) * h_D(t), \tag{9}$$

where $h_D(t)$ is given in Table 1.

Using the computed values for $g(t)$ and σ_n the $g(t)/\sigma_n$ ratio which intervenes in the error probability computation can be determined.

3. Noise Variance Calculus

Let E the energy of a signal of impulse response $h(t)$, according to (10) and the transfer function defined in [2], namely

$$E = \int_0^T h_F^2(t)\mathrm{d}t. \tag{10}$$

The average energy per bit is:

$$E_b = \frac{(M^2-1)\alpha T}{3\log_2 M}, \tag{11}$$

where $\alpha = 1$ for NRZ and $\alpha = 1/2$ for SP and T/N_0 ratio is:

$$\frac{T}{N_0} = \frac{3\log_2 M}{\alpha(M^2-1)} \cdot \frac{E_b}{N}. \tag{12}$$

In Fig.1 it is shown the bit error probability for a Butterworth filter of order 2, 3 and 4, for a NSR of 10 dB.

In Fig.1 binary symbols are used ($M = 2$) and in Fig.2 one chooses $M = 4$, quaternary symbols being used.

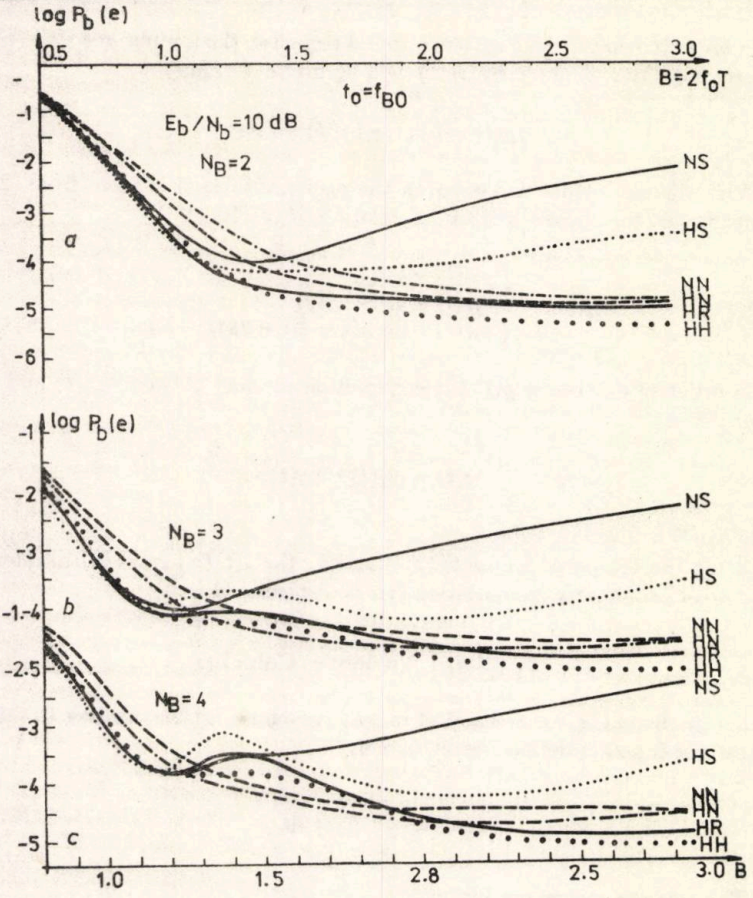

Fig. 1.– $P(e)$ for a binary ASK system.

The above presented pattern may be generalized for other type of filters, which bandwidth will be normalized at 3 dB.

4. Conclusions

According to type of the received signal and the transmitter and receiver filters, the following problem obviously appears: what is the best receiver filter so that, the received signal have the minimum error probability? If we consider only the receiver filter, the answer comes easy. If we consider the whole communication chain, the distortions introduced by the sender filter, channel and receiver filter have to be consider.

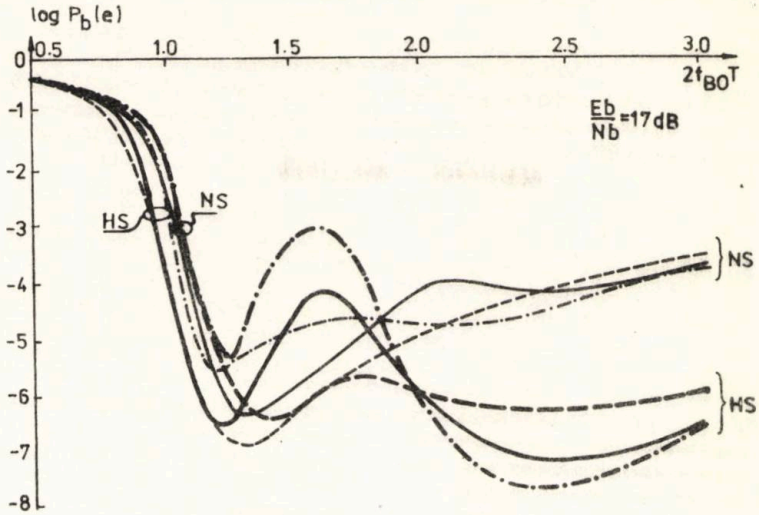

Fig. 2.– $P(e)$ for a QASK system.

The above case is emphasized by the figures obtained by computer simulation.

Received, April 30, 1992

Technical University "Gh. Asachi", Jassy, Department of Telecommunications

REFERENCES

1. Cotae P., *Contributions to the Improving of the Modulation Techniques for High Speed Data Transmission.* Ph.D. Diss., Technical University "Politehnica", Bucharest, 1992.
2. Cotae P., *Digital Communication. I. Digital Modulation.* Technical University "Gh. Asachi", Jassy, 1992.
3. Taub H., Schilling D.L., *Principles of Communications Systems.* McGraw Hill, N.Y., 1987.

COMPARAŢIE ÎNTRE PERFORMANŢELE TEHNICILOR DE MODULAŢIE DIGITALE FOLOSIND FILTRE DE BANDĂ LIMITATĂ CAUZALE

(Rezumat)

Se compară eficacitatea spectrală şi probabilitatea de eroare pentru diferite funcţii pondere ale filtrului formator. Compararea eficacităţii spectrale a fost făcută în [1] când s-au calculat DSP ale semnalelor modulate şi s-au făcut referiri numai asupra emiţătorului. Se studiază receptorul şi anume efectul filtrului de recepţie asupra probabilităţii de eroare.

BULETINUL INSTITUTULUI POLITEHNIC DIN IAŞI
Tomul XLI (XLV), Fasc. 3-4, 1995
Secţia III
ELECTROTEHNICĂ. ENERGETICĂ. ELECTRONICĂ

D.C. 621.394.9

AN INVESTIGATION OF THE POWER SPECTRUM OF THE AMSI CODES

BY

N.D. ALEXANDRU

1. Introduction

The Alternate Mark/Space Inversion (AMSI) codes were introduced by P r u c n a l [1]. They possess very attractive properties, such as: zero d.c. content, data-rate-transparent decoding and synchronization, self-clocking capability as well as bandwidth conservation. The AMSI code generates two binary data streams, denoted by $S1$ and $S2$ and the coding rules are: a) an input data bit "1" ("0") is encoded as the same (opposite) symbol in $S1$ and $S2$; b) each subsequent occurence of a "1" ("0") is encoded with the symbol opposite of the previous symbol representing a "1" ("0") in both $S1$ and $S2$.

A coding example is represented in Fig.1.

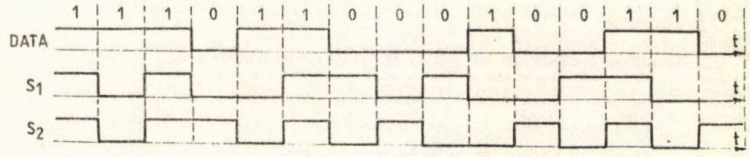

Fig. 1

2. Derivation of the P.S.D. of AMSI Code

The transition diagram of the AMSI code is represented in Fig.2. The coding law is similar to AMAZI code [2]. The matrix of the state transition probabilities, extracted from Fig.2, is

$$(1) \qquad P = \begin{bmatrix} 0 & 0 & 0 & 1-p & 0 & p & 0 & 0 \\ p & 0 & 0 & 0 & 0 & 0 & 1-p & 0 \\ 0 & 1-p & 0 & 0 & 0 & 0 & 0 & p \\ 0 & 0 & p & 0 & 1-p & 0 & 0 & 0 \\ 0 & 0 & 0 & 1-p & 0 & p & 0 & 0 \\ p & 0 & 0 & 0 & 0 & 0 & 1-p & 0 \\ 0 & 1-p & 0 & 0 & 0 & 0 & 0 & 0 \\ 0 & 0 & p & 0 & 1-p & 0 & 0 & 0 \end{bmatrix},$$

where p is the probability of a mark at the input of the coder.

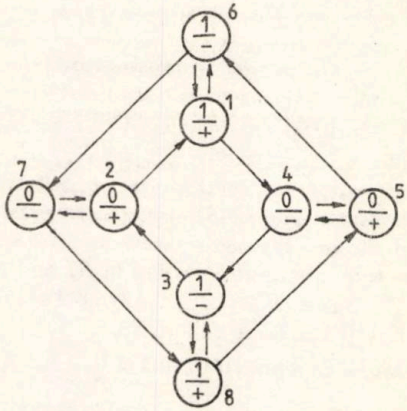

Fig. 2

The steady state probability distribution matrix is

$$(2) \qquad \Pi = \begin{bmatrix} p/4 & 0 & 0 & 0 & 0 & 0 & 0 & 0 \\ 0 & (1-p)/4 & 0 & 0 & 0 & 0 & 0 & 0 \\ 0 & 0 & p/4 & 0 & 0 & 0 & 0 & 0 \\ 0 & 0 & 0 & (1-p)/4 & 0 & 0 & 0 & 0 \\ 0 & 0 & 0 & 0 & (1-p)/4 & 0 & 0 & 0 \\ 0 & 0 & 0 & 0 & 0 & p/4 & 0 & 0 \\ 0 & 0 & 0 & 0 & 0 & 0 & (1-p)/4 & 0 \\ 0 & 0 & 0 & 0 & 0 & 0 & 0 & p/4 \end{bmatrix},$$

satisfying the relation

$$(3) \qquad \Pi P = \Pi.$$

The autocorrelation matrix Z (full bit interval) is given by

$$Z = \begin{bmatrix} +1 & +1 & -1 & -1 & +1 & -1 & -1 & +1 \\ +1 & +1 & -1 & -1 & +1 & -1 & -1 & +1 \\ -1 & -1 & +1 & +1 & -1 & +1 & +1 & -1 \\ -1 & -1 & +1 & +1 & -1 & +1 & +1 & -1 \\ +1 & +1 & -1 & -1 & +1 & -1 & -1 & +1 \\ -1 & -1 & +1 & +1 & -1 & +1 & +1 & -1 \\ -1 & -1 & +1 & +1 & -1 & +1 & +1 & -1 \\ +1 & +1 & -1 & -1 & +1 & -1 & -1 & +1 \end{bmatrix}. \tag{4}$$

Using the approach from [4] and [5], we get for $p = 0.5$:

$$R(0) = 1, \quad R(1) = -\frac{1}{2}, \quad R(i) = 0, \quad i \neq 0, 1. \tag{5}$$

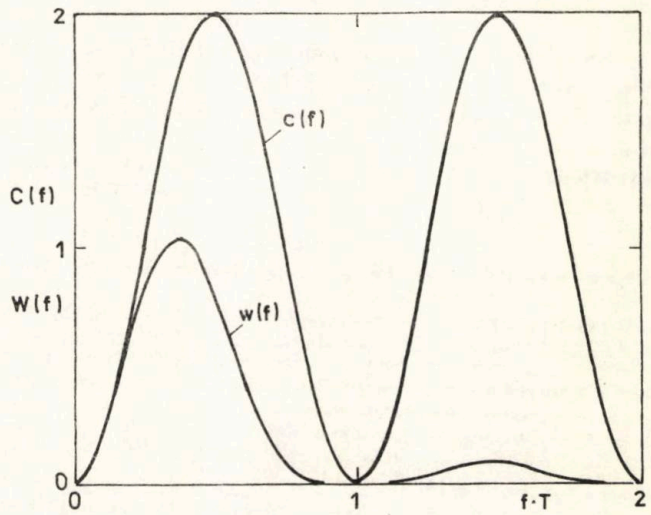

Fig. 3

Then, using B e n n e t t's formula

$$W(f) = \left(\frac{m_1}{T}\right)^2 |G(f)|^2 \delta\left(f - \frac{m}{T}\right) + \frac{1}{T}|G(f)|^2 \left\{ R(0) - \right.$$
$$\left. - m_1^2 + 2\sum_{k=1}^{\infty} [R(k) - m_1^2] \cos 2\pi k f T \right\} \tag{6}$$

and considering

(7) $$m_1 = 0$$

we get

(8) $$W(f) = \frac{1}{T}\left|\frac{\sin(x/2)}{x/2}\right|^2 (1 - \cos 2\pi fT),$$

where

(9) $$x = 2\pi fT,$$

with the shape factor

(10) $$C(f) = 1 - \cos 2\pi fT = 2\sin^2 \pi fT.$$

The p.s.d. $W(f)$ and the shape factor $C(f)$ of the AMSI codes are represented in Fig.3.

3. Conclusions

An original transition diagram was derived for the AMSI codes. Based on it, it was shown that for the equiprobable case $p = 1 - p = 0.5$, the shape factor varies as the sine squared of y, where $y = \pi fT$. Also it was shown that the p.s.d. is zero at d.c.

Received, April 13, 1992

Technical University "Gh.Asachi", Jassy, Department of Telecommunications

REFERENCES

1. P r u c n a l P.R., P e r r i e r L., *A Rate-Transparent Self-Clocking Line Code.* Proc. IEEE, **75**, *8*, 1123-1125 (1987).
2. M o r g e n s t e r n G., *Schrittspaltungs-Codes. Eine systematische Übersicht über bekannte und neue Codes nebst den Autokorrelationsfolgen und Spektren ihrer codierten Signale.* Laborbericht des Forschungsinstitut der DBP beim FTZ, *26/21*, Febr. 1987.
3. A l e x a n d r u N.D., I m a d F.M., *About Alcovem Coding.* COMCONEL 90, Dec. 16-20, 1990, Cairo, Egipt, 101.
4. H e c h t M., G u i d a A., *Delay Modulation.* Proc. IEEE, **57**, 1314-1316 (1969).
5. C a r i o l a r o G.L., T r o n c a G.P., *Spectra of Block Coded Digital Signals.* IEEE Trans. on Comm., **Com-22**, 1555-1556 (1974).
6. A l e x a n d r u N.D., B o a r i u A., *Power Spectral Density of a Delay-Modulation Coded Random Data Sequence.* COMCONEL 90, Dec. 16-20, 1990, Cairo, Egipt, 83.
7. K o r n I., *Digital Communications.* Van Nostrand Reinhold, N.Y., 1985.
8. V a l i n J., *Codes d'impulsions pour transmission d'informations binaires.* Revue Technique Thomson-CSF, **11**, *2*, 359-401 (1979).
9. L i n d s e y W.C., *Telecommunication Systems Engineering.* Prentice Hall, Englewood Cliffs, New Jersey, 1973, ch.1.

O INVESTIGAŢIE A SPECTRULUI DE PUTERE A CODURILOR AMSI

(Rezumat)

Se deduce densitatea spectrală de putere a codurilor AMSI (Alternate Mark/Space Inversion), introduse de P r u c n a l, arătându-se că în adevăr posedă componenta de c.c. nulă. Densitatea spectrală de putere este dedusă pe baza funcţiei de autocorelaţie şi a formulei lui B e n n e t t, plecând de la diagrama de tranziţii a codului.

BULETINUL INSTITUTULUI POLITEHNIC DIN IAŞI
Tomul XLI (XLV), Fasc. 3–4, 1995
Secţia III
ELECTROTEHNICĂ. ENERGETICĂ. ELECTRONICĂ

D.C. 621.3.083

MEASUREMENT TECHNIQUES FORMULATED AS INVERSE PROBLEMS

I. MAIN APPROACHES

BY

N. DAMEAN

1. Introduction

There are many examples when physical parameters f cannot be determined using direct measurements. Sometimes, in these cases, only the effect g produced against the measurement instruments by f is the measurable size. Between f and g are relations based on physical laws. They can be formally expressed as $Af = g$, where f is going to be determined through calculus, while A is the known model of the measurement instrument.

The *direct problem* consists in calculus of Af when f is a known size. The *inverse problem* consists in finding of size f using relation $Af = g$, when g is a known size. Only solution of the inverse problem represents the way to explore entirely the experimental observations.

In studying of inverse problems we often face a lack of information. Sometimes internal parameters of the analysed system, inaccessible to measurement, cannot be uniquely determined. Additional *a priori* information is necessary to be verified by experiments.

The solution of the inverse problem involves a complex approach, the solution of the direct problem playing an important part [1].

The aim of this paper is to present the principal aspects appeared at numerical approximations of measurement problem formulated as an inverse problem. Finally a practical problem is enunciated. This is modelled by a parabolic equation and inverse problem consists in determination of the coefficient term source knowing overspecified boundary data.

The problem to solve stationary inverse problem can be independently approached. In the same time the result of this problem can be considered as a limiting value of a nonstationary inverse problem when time variable tends to infinite. It is considered the stationary problem:

$$A\varphi = f,$$

where $A > 0$, $\varphi \in \phi$ and $f \in B$.

In this relation A is a linear operator defined on B a n a c h space $\phi \subset L^2(D)$, while $D \subset R^n$ is a L e b e s g u e measurable set, $L^2(D)$ is space of the functions 2-summable on D and B is a B a n a c h space.

Instead of this problem, the nonstationary one is studied:

$$\frac{\partial \psi}{\partial t} + A\psi = f \quad \text{if} \quad t \neq 0; \qquad \psi = 0 \quad \text{if} \quad t = 0.$$

Further, it will not be specially showed the domain of the operators.

Let $\{u_n\}$ and $\{u_n^*\}$ the sets of eigenvectors of operator A and its selfadjoined A^* respectively. It is considered that either set makes a complete system and the eigenvectors are normed. Therefore:

$$\varphi = \sum_{n=1}^{\infty} \varphi_n u_n, \quad \psi = \sum_{n=1}^{\infty} \psi_n u_n, \quad f = \sum_{n=1}^{\infty} f_n u_n,$$

where $Au_n = \lambda_n u_n, A^* u_n^* = \lambda_n u_n^*, \varphi_n = < \varphi, u_n^* >, \psi_n = < \psi, u_n^* >, f_n = < f, u_n >$, $\forall n \in \mathbb{N}^*$, and

$$< u_n, u_m^* > = \begin{cases} 1 & \text{if} \quad n = m, \\ 0 & \text{if} \quad n \neq m \end{cases} \qquad \forall n, m \in \mathbb{N}^*.$$

The following two problems for F o u r i e r coefficients λ_n are obtained:

$$\lambda_n \varphi_n = f_n \quad \text{and} \quad \frac{\partial \psi_n}{\partial t} + \lambda_n \psi_n = f_n \quad \text{if} \quad t \neq 0, \quad \psi_n(0) = 0.$$

The solutions of these problems are:

$$\varphi = \sum_{n=1}^{\infty} \frac{f_n}{\lambda_n} u_n \quad \text{and} \quad \psi = \sum_{n=1}^{\infty} \frac{f_n}{\lambda_n} (1 - e^{-\lambda_n t}) u_n.$$

If the spectrum of operator A is real then $\lim_{n \to \infty} \psi = \varphi$.

The nonstationary problem can be solved using an iterative method. A way is to use the finite difference method:

$$\frac{\psi^{j+1} - \psi^j}{\tau} + A\psi^j = f,$$

where j is iteration number and τ is time step.

According to H a d a m a r d's definition, there are known the three conditions so that a stationary inverse problem to be *well-posed*. If one of these three conditions is not fulfilled, the problem is called *not well-posed, ill-posed* or *improperly-posed* [2].

2. Case of Accurate Initial Data

In the following it is considered that A and f are known exactly and all matrices and vectors used are real. In addition, operator A is a square invertible matrix. Consequently the following system must be solved:

$$A\varphi = f, \tag{1}$$

where A is a matrix, φ and f are vectors.

Many iterative methods used to solve linear systems as (1) can be formulated in the following manner:

$$B_j \frac{\varphi^{j+1} - \varphi^j}{\tau_j} = -(A\varphi^j - f), \tag{2}$$

where $\{B_j\}$ is a sequence of invertible matrices and $\{\tau_j\}$ is a sequence of real parameters. Using notation $H_j = \tau_j B_j^{-1}$, relation (2) may be rewritten as:

$$\varphi^{j+1} = \varphi^j - H_j(A\varphi^j - f). \tag{3}$$

Vectors $\xi^j = A\varphi^j - f$ are the residue vectors of relation (2) and vectors $\zeta^j = \varphi^j - \varphi^*$, ($\varphi^* = A^{-1}f$ is the solution of linear system (1)) are the error vectors of the same relation.

Using (3) one gets:

$$\zeta^{j+1} = T_j \zeta^j, \tag{4}$$

where

$$T_j = E - H_j A \tag{5}$$

is the operator of step j of relation (2).

An analogue relation for residue vectors is also obtained:

$$\xi^{j+1} = (E - AH_j)\xi^j, \tag{6}$$

where E is the unit matrix.

Relations (3),...,(6) prove that the method based on relation (2) is convergent if and only if sequences $\{\zeta^j\}$ or $\{\xi^j\}$ converge to zero vector.

For an efficient calculus it is necessary to choose a sequence of matrices $\{H_j\}$ from a given class so that to be minimized the objective function which represents the required number of arithmetical and logical operations to solve system (1) with a known precision $\varepsilon \in (0,1)$.

It is considered that each iteration of the method based on relation (3) involves the same number W_0 of arithmetical and logical operations, for any H_j from the given class. The total number of operations is:

$$W = W_0 N(\{H_j\}, \varepsilon), \tag{7}$$

where $N(\{H_j\}, \varepsilon)$ is the number of iterations required for decreasing the norm of initial error vector ζ^0 by $1/\varepsilon$ times.

Particularly, it is considered that A is positive definite, symmetrical, and the extremes of the spectrum are $\alpha = \alpha(A)$, $\beta = \beta(A)$ so that $0 < \alpha \leq \beta$.

An iterative method to solve (1) based on relation:

$$\varphi^{j+1} = \varphi^j - \tau(A\varphi^j - b), \tag{8}$$

is used, where φ^0 is an initial vector and τ is a real parameter.

There is the following relation for error vectors ζ^j:

$$\zeta^{j+1} = T_\tau \zeta^j, \tag{9}$$

where

$$T_\tau = E - \tau A. \tag{10}$$

Using (9), (10) and the development of vectors $[\zeta^j]$ relating to orthonormal basis $\{u_n\}$, it gets:

$$\zeta_n^{j+1} = (1 - \tau\lambda_n)\zeta_n^j.$$

The above relation implies:

$$\lim_{j\to\infty} \zeta_n^j = 0 \quad \text{for} \quad \forall \zeta^0, \text{ equivalent to } |1 - \tau\lambda_n| < 1, \quad \forall n \in \mathbb{N}^*$$

and

$$\lim_{j\to\infty} \|\zeta^j\|_2 = 0 \text{ equivalent to } q(\tau) = \beta(T) = \max|1 - \tau\lambda_n|_{n\in N^*} < 1, \tag{11}$$

because if λ_n is an eigenvalue of matrix A then $1 - \tau\lambda_n$ is an eigenvalue of matrix T_τ. Relation (11) gets that iterative method based on relation (8) is convergent for $\tau \in (0, 2/\beta)$.

In what follows it will be deal with the efficiency of the above mentionated method.

The compatibility relation among Euclidian, matricial and vectorial norms is:

$$\|\psi^j\| \leq \|T_\tau^j\| \|\zeta^0\|, \tag{12}$$

where

$$\|T_\tau^j\| = (\beta(T_\tau))^j = (q(\tau))^j, \tag{13}$$

because T_τ is a symmetric matrix.

From (12) it is obtained that sufficient number N of iterations required for decreasing of vectorial norm $\|\zeta^0\|$ by $1/\varepsilon$ times $(0 < \varepsilon < 1)$ is the solution of equation:

$$\|T_\tau^N\| = \varepsilon. \tag{14}$$

Relations (13), (14) get:

$$N = \left[\frac{\ln \varepsilon}{\ln q(\tau)}\right] + 1. \tag{15}$$

where, here and in what follows, [...] denotes entire part.

Number of arithmetical and logical operations W_0 for an iteration does not depend on τ and it is supposed, for realising convergence, that $\tau \in (0, 2/\beta)$. In this case (7) and (15) lead to:

$$W = W_0 \left(\left[\frac{\ln \varepsilon}{\ln q(\tau)}\right] + 1 \right). \tag{16}$$

From (16) it is observed that the optimization problem (namely the minimization of W depending on τ) consists in minimization of $q(\tau)$ depending on $\tau \in (0, 2/\beta)$.

Using (11) and $\lambda_n \in [\alpha, \beta]$, one gets:

$$\tau_{\text{opt}} = \frac{2}{\alpha + \beta}, \qquad q_{\text{opt}} = q(\tau_{\text{opt}}) = \frac{\beta - \alpha}{\beta + \alpha}.$$

3. Case of Approximative Initial Data

There are many practical situations when initial data are no exactly known. When they are known approximately, instead of equation (1) the equation

$$A^h \varphi^h = f^h \tag{17}$$

must be solved, where index h shows that initial data depend on error of approximation, some statistic errors or accidental mistakes.

It is supposed that the errors of approximation for operator A and vector f are known. Namely *a priori* estimations are given:

$$\|(A - A^h)\varphi\| \leq \rho(h), \quad \|f - f^h\| \leq \eta(h). \tag{18}$$

The following iterative process to solve (17) when relations (18) are given, analogous to (8), is developed:

$$(\varphi^h)^{j+1} = (\varphi^h)^j - \tau(A^h(\varphi^h)^j - f^h), \quad (\varphi^h)^0 = 0, \tag{19}$$

where parameter τ satisfies condition:

$$q = \|E - \tau A^h\| < 1 \tag{20}$$

analogous to (11).

Concerning optimal number of iterations, it is supossed naturally that the iterative process (19) must continue till the error of iterative process is about equal with the error caused by approximative knowledge of initial data.

Solving formally equations (1) and (18) it results:

$$\varphi = A^{-1}f, \quad \varphi^h = (A^h)^{-1}f^h.$$

From (1), (18) and (19) it gets:

$$\|\varphi^h - \varphi\| \leq \|(A^h)^{-1}\|(\rho(h) + \eta(h)). \tag{21}$$

From (17), (19) and (20) it results:

$$\|\varphi^j - (\varphi^h)^j\| \leq q^j\|(A^h)^{-1}\|\|f^h\|. \tag{22}$$

Using (21), (22), the following relation is obtained:

$$\|\varphi - (\varphi^h)^j\| \leq q^j\|(A^h)^{-1}\|\|f^h\| + \|(A^h)^{-1}\|(\rho(h) + \eta(h)).$$

The former term of r.h.s. of above inequality represents the error introduced by iterative process and the second term is the error caused by vague knowledge of initial data. Imposing that two errors to be equal, the optimal number of iterations for iterative process (19) is obtained:

$$N = \left[\frac{1}{\ln q} \ln \frac{\rho(h) + \eta(h)}{\|f^h\|}\right].$$

4. Example

One practical problem will be enunciated, using above considerations. A similar problem was formulated and solved in [3] utilizing an optimal control technique.

It is considered a resistor made by a metallic wire covered with a material which is good a conductor of heat. The ends of this resistor are maintained at the constant temperature G of medium. This resistor, in equilibrium with medium at initial moment, is passed by a constant dc. The problem is to determine temperature of each point of the wire, electric resistance versus time and to evaluate the measurement error of a resistance caused by thermic effect.

The thermic behaviour of resistor is described by the following equation [4]:

$$U_t(x,t) - aU_{xx}(x,t) + \gamma(U(x,t) - U(x,0)) = q(x,t), \quad x > 0, \quad t > 0, \tag{23}$$

where

$$\gamma = \frac{dp}{c\rho_m A} = \frac{2d}{c\rho_m r}, \tag{24}$$

$$g(x,t) = \frac{E}{c\rho_m Vt} = \frac{RI^2}{c\rho_m Al} = \frac{\rho_e^0(1 + \alpha_\rho(U(x,t) - U(x,0)))I^2}{A^2 c\rho_m}. \tag{25}$$

Equation (23) will be associated with the following boundary and initial conditions:

(26) $$U(0,t) = G, \quad t > 0, \qquad (27) \qquad U(x,0) = G, \quad x > 0.$$

Using relations (22)...(27) it results:

(28) $$U_t(x,t) - aU_{xx}(x,t) = \left(\frac{\rho_e^0 \alpha_\rho I^2}{A^2 c \rho_m} - \gamma\right) U(x,t) + \frac{\rho_e^0 (1 - \alpha_\rho G)}{A^2 c \rho_m} I^2 + \gamma G.$$

To simplify the calculus, the condition:

(29) $$\frac{\rho_e^0 (1 - \alpha_\rho G)}{A^2 c \rho_m} I^2 + \gamma G = 0$$

is imposed. This condition does not effect the generality of the above problem.

If (29) is not satisfied using initial data, a translation of temperature could be performed. Thus the following condition is achieved:

(30) $$G = \frac{\rho_e^0 I^2}{\rho_e^0 \alpha_\rho I^2 - 2d\pi^2 r^3}.$$

Using (24), notation

(31) $$\alpha = \frac{\rho_e^0 \alpha_\rho I^2}{A^2 c \rho_m} - \gamma = \frac{\rho_e^0 \alpha_\rho I^2}{A^2 c \rho_m} - \frac{2d}{c \rho_m r}$$

and relation (29), equation (28) is equivalent to:

(32) $$U_t(x,t) - aU_{xx}(x,t) = \alpha U(x,t), \quad x > 0, \quad t > 0.$$

As it is shown in (31), coefficient α depends on many constants which are not well known generally. Thus one considers that coefficient α is unknown.

Consequently the proposed problem is modelled by parabolic equation (32), boundary condition (26) and initial condition (27).

Because equation (32) contains unknown coefficient α, the enunciated problem cannot be solved, therefore it is *ill-posed*. It is necessary to know a (some) supplementary data as initial problem to be transformed in a *well-posed* one. A possibility to pass over this difficulty is to add the following boundary condition at moment t_0:

(33) $$U_r(0,t_0) = g_0.$$

This relation signifies that spatial temperature gradient of an end wire is known at a named moment.

Therefore the original problem is modelled by parabolic equation (32), boundary conditions (26), (33) and initial condition (27).

Generality of this problem is not affected by the assumptions $a = 1$ and $t_0 = 1$. Therefore this problem is modelled by the following equation associated with boundary and initial conditions:

$$(P)\quad \begin{cases} U_t(x,t) - U_{xx}(x,t) = \alpha U(x,t), \quad x > 0, \quad t > 0, \ (P1), \\ U(0,t) = G, \ t > 0 \ (P2), \quad U(x,0) = G, \ x > 0 \ (P3), \ U_x(0,1) = g_0 \ (P4). \end{cases}$$

This is an evolutive problem with a nonlinear operator having overspecified boundary data.

Solution of this problem and some applications of it will be displayed in a future paper.

5. Conclusions

Some specific aspects of inverse problems used in measurement techniques are presented. Main approaches detailed above show that these techniques can improve traditional methods. In the same time they can be considered as alternative methods when traditional methods are unusable.

A practical problem was proposed to be solved using these techniques. It concerns with dynamic behaviour of a resistor made by a metallic wire which is passed by a constant dc.

Appendix

A – area of cross section of the wire, [m^2];
a – thermal diffusivity of the wire, [$m^2 s^{-1}$];
c – specific heat at constant pressure, [J $kg^{-1} K^{-1}$];
d – heat transfer coefficient between wire and medium, [kg $s^{-3} K^{-1}$];
E – energy consumed by resistor, [W s];
G – temperature of medium, [K];
I – constant dc which passes the resistor, [A];
l_0 – length of the wire at temperature of medium, [m];
p – perimeter of cross section of the wire, [m];
R – electric resistance of the resistor at temperature of medium, [Ω];
r – radius of wire, [m];
R_t – electric resistance of the resistor at the moment t, [Ω];
t – time, [s];
t_0 – moment when an additional boundary measurement is achieved, [s];
V – volume of the wire, [m^3];
$U(x,t)$ – temperature of wire in the point x at the moment t, [K];
x – distance on the wire from an end, [mm];
α_ρ – variation coefficient of ρ_e^0, [K^{-1}];
ω – linear variation coefficient of the wire, [K^{-1}];
ρ_e^0 – electric resistivity of the wire at temperature of medium, [Ω m];
ρ_m – density of the wire, [kg m^{-3}].

Received, May 18, 1994

Technical University "Gh.Asachi", Jassy,
Department of Electric Measurements

REFERENCES

1. Borkowski J., Matuszewski B., *Investigations of Signal Processors Applications in the Real-time Combined Measurements Regarding Spectral Analysis Reconstruction.* In: Finkelstein L., Grattan K.T.V. (Eds.), *State and Advances in Measurement and Instrumentation Education.* City University, London, 1993, 354-359.
2. Anger G. (Ed.), *Inverse Problems in Differential Equations.* Akademie-Verlag, Berlin, 1990.
3. Anita S., Damean N., *A Problem of Measurement of Temperature Solved Using the One-dimensional Heat Equation.* Int. J. Heat Mass Transfer, **4**, *36*, 1043-1048 (1993).
4. Barták J., Herrnsann L., Lovicar V., Vejvoda O. (Eds.), *Partial Differential Equations of Evolution.* Ellis Horwood, Chichester, 1991.

TEHNICI DE MĂSURARE FORMULATE CA PROBLEME INVERSE
I. Abordări principale

(Rezumat)

Se prezintă aspecte specifice ale problemelor inverse utilizate în tehnicile de măsurare. Principalele abordări detaliate arată că aceste tehnici pot îmbunătăţi metodele tradiţionale. În acelaşi timp ele pot fi folosite atunci când metodele tradiţionale sunt inutilizabile. Se propune spre rezolvare o problemă practică care constă în studiul comportării dinamice a unui rezistor confecţionat dintr-un fir metalic, atunci când el este parcurs de un curent continuu şi constant.

BULETINUL INSTITUTULUI POLITEHNIC DIN IAŞI
Tomul XLI (XLV), Fasc. 3–4, 1995
Secţia III
ELECTROTEHNICĂ. ENERGETICĂ. ELECTRONICĂ

C.D. 621.3.016.35

SUR LES CONDITIONS D'APPARITION DES OSCILLATIONS MÉCANIQUES DANS UN SYSTÈME ÉLECTROMÉCANIQUE

II. ÉTUDE DE LA STABILITÉ DES SOLUTIONS

PAR
MARIANA BUZDUGA

1. Introduction

Pour un système hybride électromécanique constitué par un circuit électrique qui contient une diode Tunel et un instrument magnétoélectrique,ont été établies, dans une Note précédente [5], les équations différentielles qui décrivent le comportement du système et leurs domaines de valabilité.

L'analyse a été effectuée dans l'hypothèse que le point de fonctionement du système se trouve au centre de la zone de pente négative de la caractéristique de la diode Tunel et que la condition d'existence des oscillations dans le circuit électrique est satisfaite (la résistance R' du circuit extérieur à la diode est moindre que la pente de la caractéristique (en forme de N) dans le point de fonctionnement) [1].

On a constaté qu'en fonction des valeurs de R' la forme des équations différentielles est différente et les propriétés du circuit aussi.

Dans ce qui suit on analyse la stabilité du fonctionnement du système dans les cas évalués dans la première partie [5].

2. Stabilité du fonctionnement pour $R' \in (0; 2|R_d|/3)$

Dans cette situation le coefficient A' de la relation (14) de [5] est positif et

$$A' \in [0, 1/N\phi_0), \tag{1}$$

le coefficient B' étant positif quelque soit R'.

Les graphiques des fonctions $\mathrm{d}\alpha'(u')/\mathrm{d}t$, respectivement $u'(\mathrm{d}\alpha/\mathrm{d}t)$ sont présentés dans les Fig.1 et 2.

L'équation différentielle qui décrit le comportement du système électromécanique a la forme [5]:

$$J\frac{\mathrm{d}^2\alpha'}{\mathrm{d}t^2} + B\frac{\mathrm{d}\alpha'}{\mathrm{d}t} + C\alpha' = \\ = -\frac{N\phi_0}{R'}\left[N\phi_0\frac{\mathrm{d}\alpha'}{\mathrm{d}t} + \sqrt[3]{-F + \sqrt{F^2+G^3}} + \sqrt[3]{-F - \sqrt{F^2+G^3}}\right], \tag{2}$$

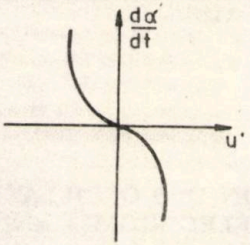

Fig. 1

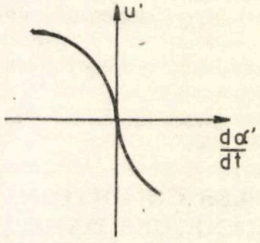

Fig. 2

où:

$$F = \frac{d\alpha'/dt}{2B'}, \quad G = \frac{A'}{3B'}. \tag{3}$$

Si on utilise les notations:

$$\frac{d\alpha'}{dt} = z, \quad \frac{d^2\alpha'}{dt^2} = \frac{dz}{dt} = \frac{dz}{d\alpha'} \cdot \frac{d\alpha'}{dt} = z\frac{dz}{d\alpha'}, \tag{4}$$

il résulte

$$z\frac{dz}{d\alpha'} + \frac{B}{J}z + \frac{(N\phi_0)^2}{JR'}z + \\ + \frac{N\phi_0}{R'J}\left(\sqrt[3]{-\frac{z}{2B'} + \sqrt{z^2 + G^3}} + \sqrt[3]{-\frac{z}{2B'} + \sqrt{-\frac{z^2}{4B'^2} + G^3}}\right) + \frac{C}{J}\alpha' = 0 \tag{5}$$

ou sous la forme équivalente

$$\frac{dz}{d\alpha'} = \frac{-\frac{B}{J}z - \frac{(N\phi_0)^2}{JR'}z}{z} - \\ - \frac{\frac{N\phi_0}{R'J}\left(\sqrt[3]{-\frac{z}{2B'} + \sqrt{\frac{z^2}{4B'^2} + G^3}} + \sqrt[3]{-\frac{z}{2B'} - \sqrt{-\frac{z^2}{4B'^2} + G^3}}\right) - \frac{C}{J}\alpha'}{z} = \frac{Q(z,\alpha')}{P(z,\alpha')}. \tag{6}$$

Le point singulier de l'équation (6) est situé à $\alpha' = 0,\ z = 0$.

Dans le cas des systèmes stables du point de vue structurel il est possible de négliger la nonliniarité autour du point singulier, conformément à la première approximation de Lyapounoff, dans le but de transformer l'équation (6) qui devient

$$\frac{dz}{d\alpha'} = \frac{c\alpha' + dz}{a\alpha' + bz}, \tag{7}$$

permettant assez facilement l'étude de la stabilité locale. Dans ce but on remplace la fonction

$$u'(z) = \sqrt[3]{-\frac{z}{2B'} + \sqrt{\frac{z^2}{4B'^2} + G^3}} + \sqrt[3]{-\frac{z}{2B'} - \sqrt{\frac{z^2}{4B'^2} + G^3}}, \tag{8}$$

qui correspond au terme nonlinéaire, par son approximation linéaire autour du point $z = 0$, c'est-à-dire:

$$u'(z) \simeq \frac{\mathrm{d}u'(z)}{\mathrm{d}z}\Big|_{z=0} z. \tag{9}$$

La pente de la droite d'approximation résulte:

$$\frac{\mathrm{d}u'(z)}{\mathrm{d}z}\Big|_{z=0} = -\frac{1}{A'} < 0 \tag{10}$$

et la relation (6) devient:

$$\frac{\mathrm{d}z}{\mathrm{d}\alpha'} \simeq \frac{-\frac{C}{J}\alpha' - \frac{B}{J}z - \frac{(N\phi_0)^2}{JR'}z + \frac{N\phi_0}{R'J}\cdot\frac{1}{A'}z}{z}. \tag{11}$$

Les coefficients $a, ..., d$ de la relation (6) ont les valeurs ci-dessous:

$$a = 0,\ b = 1,\ c = -\frac{C}{J},\ d = \frac{N\phi_0}{R'J}\cdot\frac{1}{A'} - \frac{B}{J} - \frac{(N\phi_0)^2}{R'J}. \tag{12}$$

Le signe du coefficient d établit le caractère stable ($d < 0$) ou instable ($d > 0$) de la solution du système dans le point respectif.

Le coefficient d est une fonction monotone de R', donc il faut analyser les valeurs aux extrémités de l'intervalle de variation de R':

$$\lim_{R'\to 0} d(R') = \frac{3}{2}\cdot\frac{(N\phi_0)^2}{J}\cdot\frac{1}{|R_d|} - \frac{B}{J}, \tag{13}$$

dont le signe, pour des mécanismes à faible coefficient d'amortissement, est positif. Vu que

$$\lim_{R'\to 2|R_d|/3} d(R') = \infty \tag{14}$$

il résulte que dans tout l'intervalle $R' \in (0; 2|R_d|/3]$ le coefficient d est positif, donc le fonctionement est instable.

Pour vérifier la possibilité de l'existence d'un cycle limite on applique la première proposition de B e n d i x s o n [4] qui établit que si la fonction $\partial P/\partial\alpha' + \partial Q/\partial z$ garde le même signe il n'y a pas de cycle limite.

Pour le cas étudié:

$$\frac{\partial P}{\partial \alpha'} = 0; \quad \frac{\partial Q}{\partial z} = -\frac{B}{J} - \frac{(N\phi_0)^2}{JR'} - \frac{N\phi_0}{R'J} \cdot \frac{\partial u'(z)}{\partial z} = -\frac{B}{J} - \frac{(N\phi_0)^2}{JR'} -$$

$$(15) \quad - \frac{N\phi_0}{R'J} \left[\frac{-\frac{1}{2B'} + \frac{z}{4B'\sqrt{\frac{z^2}{4B'^2}+G^3}}}{3\sqrt[3]{\left[-\frac{z^2}{4B'^2} + \sqrt{\frac{z^2}{4B'^2}+G^3}\right]^2}} + \frac{-\frac{1}{2B'} - \frac{z}{4B'^2\sqrt{\frac{z^2}{4B'^2}+G^3}}}{3\sqrt[3]{\left[-\frac{z^2}{4B'^2} - \sqrt{\frac{z^2}{4B'^2}+G^3}\right]^2}} \right].$$

De l'analyse de la forme de la fonction $u'(z)$ il résulte que $\mathrm{d}u'(z)/\mathrm{d}z$ a une valeur extrême pour $z = 0$, conformément à la relation (10); elle est symétrique par rapport à l'axe Oy, monotone dans les intervalles $z < 0$ et $z > 0$ et ses limites pour $z \to +\infty$ ou $z \to -\infty$ sont zéro.

Le signe de la fonction $\partial Q/\partial z$ change seulement si la fonction s'annule dans l'intervalle respectif, c'est-à-dire si:

$$(16) \quad \frac{B}{J} + \frac{(N\phi_0)^2}{JR'} = -\frac{N\phi_0}{R'J} \cdot \frac{\mathrm{d}u'(z)}{\mathrm{d}z},$$

relation qui est représentée dans la Fig.3.

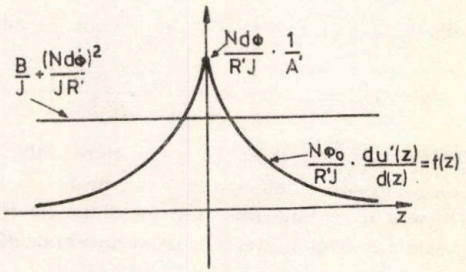

Fig. 3

On connaît que pour $z = 0$, quelque soit R' le coefficient d est positif, donc la droite horizontale a l'ordonnée dans l'origine située au dessous de l'extrémité de la fonction $f(z)$. On observe que pour $R' \to 0$ la valeur extrême de la fonction $f(z)$ tend vers infini, en restant toujours au dessus de la droite horizontale dont l'ordonnée tend elle aussi vers infini. Dans ce cas on a la certitude de l'existence des points d'intersection entre les deux graphiques, dans un domaine très proche de $z = 0$.

Pour $R' \to 2|R_d|/3$, la limite du domaine étudié, le point d'extrémum situé sur l'axe vertical tend vers infini et l'ordonnée de l'horizontale baisse presqu'à la valeur $B/J + N\phi_0/(2J|R_d|/3)$ en existant aussi la certitude de l'existence du point d'intersection.

Pour conclure, dans le domaine $R' \in (0, 2|R_d|/3]$ on n'élimine pas la possibilité de l'existence d'un cycle limite, donc de l'apparition des oscillations mécaniques entretenues.

Pour un circuit concret contenant une diode Tunel type TD716GE pour laquelle les coefficients de la fonction d'approximation ont les valeurs $a_1 = 0.0202$, $a_3 = -0.263$ et $|R_d| = 74\ \Omega$ et un miliampèremetre magnétoélectrique ayant les parametres [1]: $J = 5.10^{-7}$ kgm^2, $B = 8.4.10^{-11}$ Nms/rad, $N = 80$ spires, $C = 10^{-5}$, $\phi_0 = 7.10^{-5}$ Wb, on a essayé de resoudre l'équation de mouvement (4), pour différentes valeurs de R' dans le domaine en discussion (par exemple $R' = 40\ \Omega$, $R' = 20\ \Omega$, $R' = 10\ \Omega$). On a utilisé le programme MATEMATICA qui permet l'approximation numérique de la solution par la méthode R u n g e - K u t t a et qui fournit aussi le diagramme dans le plan des phases.

Chaque fois on a obtenu un cycle limite dans le plan des phases et une oscillation permanente pour le cadre de l'instrument, comme indique l'exemple donné dans les Fig.4 *a* et *b*.

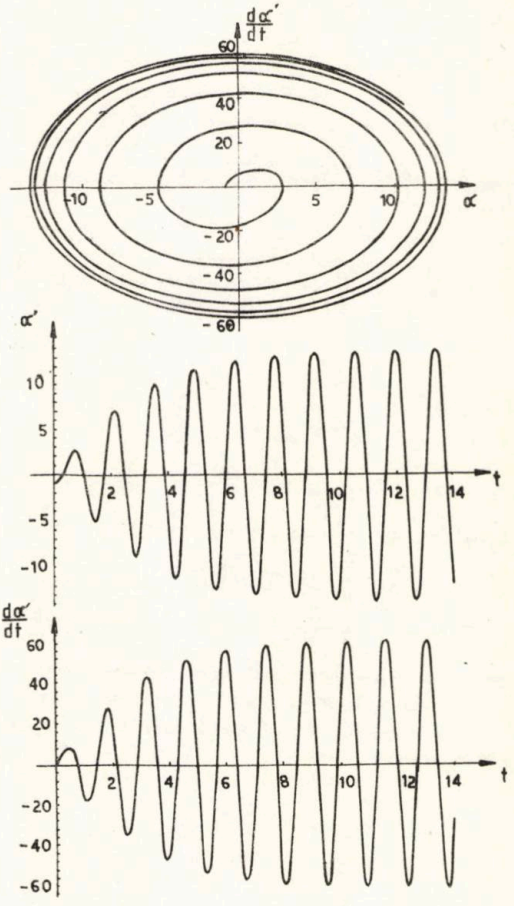

Fig. 4

3. Stabilité du fonctionement du système pour $R' \in (2|R_d|/3, R_d)$

Dans ce cas le signe du coefficient A' de la relation (14) de [5] est négatif et $A' \in (-1/(2N\phi_0), 0]$. Les graphiques des fonctions $\mathrm{d}\alpha'(u')/\mathrm{d}t$, respectif $u'(\mathrm{d}\alpha'/\mathrm{d}t)$, ont la forme présentée dans les Figs.5 et 6.

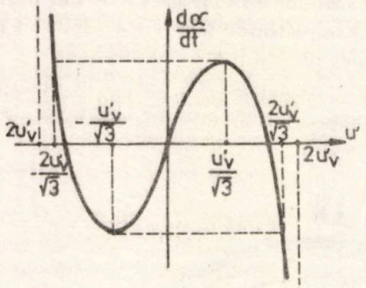

Fig. 5

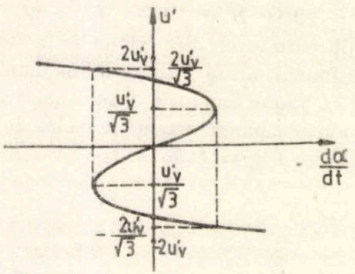

Fig. 6

L'équation différentielle qui décrit le comportement du système électromécanique devient:

$$J\frac{\mathrm{d}^2\alpha'}{\mathrm{d}t^2} + B\frac{\mathrm{d}\alpha'}{\mathrm{d}t} + \frac{(N\phi_0)^2}{R'}\cdot\frac{\mathrm{d}\alpha'}{\mathrm{d}t} + \frac{N\phi_0}{R'}u'\left(\frac{\mathrm{d}\alpha'}{\mathrm{d}t}\right) + C\alpha' = 0, \tag{17}$$

où:

$$u' = \begin{cases} u'_1 = \sqrt[3]{-F+\sqrt{F^2+G^3}} + \sqrt[3]{-F-\sqrt{F^2+G^3}}, & \text{pour } u' \in \left[-2u'_v, -\frac{2u'_v}{\sqrt{3}}\right], \\ u'_b = 2\sqrt{|G|}\cos\left[\frac{1}{3}\mathrm{arctg}\frac{\sqrt{-F^2-G^3}}{-F} + \frac{2\pi}{3}\right], & \text{pour } u' \in \left[-\frac{2u'_v}{\sqrt{3}}, -\frac{u'_v}{\sqrt{3}}\right]; \\ u'_c = 2\sqrt{|G|}\cos\left[\frac{1}{3}\mathrm{arctg}\frac{\sqrt{-F^2-G^3}}{-F} + \frac{4\pi}{3}\right], & \text{pour } u' \in \left[-\frac{u'_v}{\sqrt{3}}, \frac{u'_v}{\sqrt{3}}\right]; \\ u'_a = 2\sqrt{|G|}\cos\left[\frac{1}{3}\mathrm{arctg}\frac{\sqrt{-F^2-G^3}}{-F}\right], & \text{pour } u' \in \left[\frac{u'_v}{\sqrt{3}}, \frac{2u'_v}{\sqrt{3}}\right]; \\ u'_1 = \sqrt[3]{-F+\sqrt{F^2+G^3}} + \sqrt[3]{-F-\sqrt{F^2+G^3}}, & \text{pour } u' \in \left[\frac{2u'_v}{\sqrt{3}}, 2u'_v\right]. \end{cases} \tag{18}$$

Le point singulier de l'équation est situé à $\alpha' = 0$, $z = 0$. On étudie ci-dessous la stabilité locale autour de celui-là. On introduit la notation (4) et on amène l'équation à la forme (7), en utilisant pour $u'(z)$ l'expression u'_c de la relation (18). Il résulte:

$$\frac{\mathrm{d}z}{\mathrm{d}\alpha'} = \frac{Q(\alpha', z)}{P(\alpha', z)} = \frac{-\frac{C}{J}\alpha' - \frac{B}{J}z - \frac{(N\phi_0)^2}{R'J}z - 2\frac{N\phi_0}{R'z}\sqrt{|G|}\cos\left[\frac{1}{3}\mathrm{arctg}\frac{\sqrt{-F^2-G^3}}{-F} + \frac{4\pi}{3}\right]}{z}. \tag{19}$$

Compte tenu que la fonction $u'_c(z)$ correspond aux termes nonlinéaires, elle est remplacée par son approximation linéaire autour de l'origine, c'est-à-dire:

$$(20) \qquad u'_c(z) = \frac{\mathrm{d}u'_c(z)}{\mathrm{d}z}\Big|_{z=0} z \quad \text{où} \qquad (21) \quad \frac{\mathrm{d}u'_c(z)}{\mathrm{d}z}\Big|_{z=0} = \frac{1}{A},$$

donc positive, ce qu'on pouvait déduire par l'analyse de la pente dans l'origine de la fonction directe (A'). On a alors:

$$(22) \qquad \frac{\mathrm{d}z}{\mathrm{d}\alpha'} \simeq \frac{-\frac{C}{J}\alpha' - \frac{B}{J}z - \frac{(N\phi_0)^2}{R'J}z - \frac{N\phi_0}{R'} \cdot \frac{1}{|A'|}z}{z}.$$

Les coefficients $a, ..., d$ ont maintenant les expressions:

$$(23) \qquad a = 0, \quad b = 1, \quad c = -\frac{C}{J}, \quad d = -\frac{B}{J} - \frac{(N\phi_0)^2}{R'J} - \frac{N\phi_0}{R'J} \cdot \frac{1}{|A'|}.$$

En conséquence, le coefficient d garde le signe négatif dans ce domaine de variation de R', en indiquant que le système a un comportement local stable.

4. Conclusions

Pour les équations différentielles qui décrivent le mouvement du cadre mobile d'un instrument magnétoélectrique branché à un circuit électrique qui contient une diode Tunel (équations établies en [5]) on a étudié la stabilité des solutions. On a mis en évidence un fonctionnement stable quand la résistance R' du circuit électrique extérieur à la diode est contenue dans l'intervalle $R' \in [2|R_d|/3, |R_d|)$ et un fonctionnement instable pour $R' \in (2|R_d|/3, 0)$.

Dans le second cas on n'élimine pas la possibilité de l'existence d'un cycle limite, donc de l'apparition des oscillations mécaniques entretenues de l'enroulement cadre de l'instrument.

Reçue le 25 juillet 1994

Université Technique „Gh. Asachi", Jassy,
Chaire de Mesures électriques

BIBLIOGRAPHIE

1. Savin Gh., Grovu M., *Elektromechanishe Schwingungen, die mit nichtlinearen aktiven Netzwerken selbsterregt werden.* Archiv für Elektrotechnik, **62**, 5-12 (1980).
2. Fitzgerald S., *Electric Machinery.* McGraw-Hill, 1971.
3. Gibson J.E., *Sisteme automate neliniare* (trad. de l'anglais). Ed. Tehn., Bucureşti, 1967.
4. Savin Gh., Rosman H., *Circuite electrice neliniare şi parametrice.* Ed. Tehn., Bucureşti, 1973.
5. Buzduga M., *Sur les conditions d'apparition des oscillations mécaniques dans un système électromécanique. I. Établissement des équations de mouvement.* Bul. Inst. polit., Iaşi, **XL (XLIV)**, *1-4*, s.III (1994).

ASUPRA CONDIŢIILOR DE APARIŢIE A OSCILAŢIILOR MECANICE ÎNTR-UN SISTEM ELECTROMECANIC

II. Studiul stabilităţii soluţiilor

(Rezumat)

Pentru un circuit hibrid, conţinând o diodă Tunel şi un instrument magnetoelectric, ale cărui ecuaţii diferenţiale ce descriu mişcarea organului mobil al instrumentului au fost deduse în [5], se determină domeniile de funcţionare stabilă, respectiv cele unde există posibilitatea apariţiei de oscilaţii întreţinute de joasă frecvenţă ale bobinei cadru a instrumentului.

BULETINUL INSTITUTULUI POLITEHNIC DIN IAŞI
Tomul XLI (XLV), Fasc. 3–4, 1995
Secţia III
ELECTROTEHNICĂ. ENERGETICĂ. ELECTRONICĂ

D.C. 621.317.39

LINEARISATION OF THE RESPONSE OF AN A/D CONVERTER FOR MEASURING NON-ELECTRICAL VARIABLES

BY
MARIANA BUZDUGA and CRISTIAN FOŞALĂU

1. Introduction

The non-linearity of some sensors, otherwise cheap, reliable and sensitive is often a strong drawback in the using in the conception of apparatus whose desired quality is like to be the accuracy and the width of range. A circuit which is capable to linearise any transducer having an exponential relationship between input and output signals or to obtain an output signal proportional to the logarithm of any input voltage signal (that is, proportional to the input signal in dB) is presented.

2. Principle of the Method

The proposed scheme is derived from that of a voltage-to-frequency (time) converter, represented in Fig.1. Let be a non-linear function $U_m(x)$, where x is the quantity to be measured. If the function generator provides a function $U_0(t)$, where t is the time variable and

$$U_m(t) \equiv U_0(t), \tag{1}$$

then one can deduce the equality between the two variables:

$$t = x \tag{2}$$

for every particular value of them.

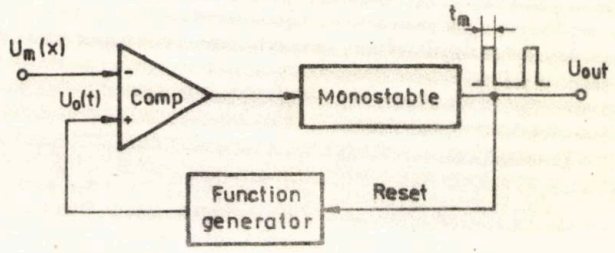

Fig. 1

The period of the output signal of the converter results as a linear function versus the quantity to be measured, x:

$$T = t + t_m = x + t_m, \tag{3}$$

where t_m is the reseting period of the function generator, provided by the monostable.

3. Pecularities

As an example we consider a sort of characteristic with a strong non-linearity, which is presented by the temperature resistive sensors with negative coefficient (thermistors), non-linear active elements (diodes, transistors, etc.). These characteristics have an exponential shape, with an expression as:

$$R_t(T) = Ae^{B/T}. \tag{4}$$

Based on the above trends, we will analyse two cases, depending on the type of the function generator used.

a) Considering the scheme presented in Fig.2 *a*, the output voltage U_m is related on the temperature T by the following relationship:

$$U_m(t) = U_{\text{ref}} \frac{R_1}{R_t(T)} = U_{\text{ref}} \frac{R_1}{A} e^{-B/T}. \tag{5}$$

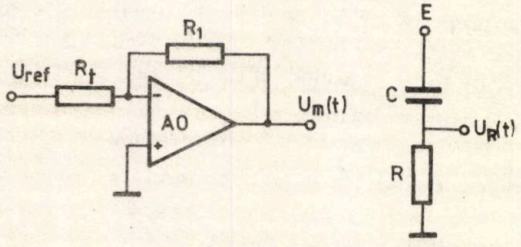

Fig. 2 *a)* *b)*

So, the output voltage of the function generator must be of the form:

$$U_0(t) = K_1 e^{-K_2 t}.$$

This voltage can be obtained using the exponential voltage–time relationship of a capacitor C being charged through a resistor R, as shown in Fig.2 *b*. The voltage U_0 on the terminals of the resistor varies with time t as

$$U_0(t) = Ee^{-t/(RC)}, \tag{6}$$

with E – the supply voltage. From (1), (5) and (6), it results:

$$t = -RC \ln \frac{U_0}{E} = -RC \ln \frac{U_{\text{ref}} R_1}{EA} + \frac{RCB}{T}, \tag{7}$$

and the frequency f, which is picked-up from the output, is:

$$f = (t + t_m)^{-1} = \left(-RC \ln \frac{U_{\text{ref}} R_1}{EA} + \frac{RCB}{T} + t_m \right)^{-1}. \tag{8}$$

We can therefore choose $t_m = RC \ln[U_{\text{ref}} R_1/(EA)]$ to obtain the linear dependence of the frequency versus the temperature:

$$f = \frac{T}{RCB}. \tag{9}$$

b) The scheme shown in Fig.3 *a* presents the second type converter for which the function generated is carried out by a low-pass filter (Fig.3 *b*). The non-inverting input of the comparator is:

$$U_m(t) = K \left[1 - \frac{R_1}{R_t(T)} \right] = K \left(1 - \frac{R_1}{A} e^{-B/T} \right) \tag{10}$$

and the voltage reference given by the function generator is:

$$U_0(t) = E \left[1 - e^{-t/(RC)} \right]. \tag{11}$$

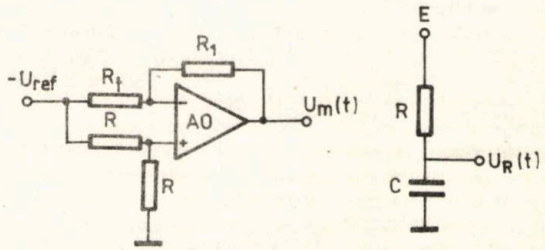

Fig. 3

Finally, taking $K = E$ and $t_m = RC \ln(R_1/A)$, one can obtain the expression (9) for the output frequency of the converter. So, for both cases, this frequency is, theoretically, directly proportional to absolute temperature and the scale factor $1/(RCB)$ can be chosen as any convenient number by varying RC.

4. Sources of Errors

To study the real behaviour of the converter, we used the following standard components: the operational amplifier βM301, the comparator βM399 and the

monostable type βM555E. The maximum useful temperature range is determined by the maximum ratio E/U_0. We can take E_{max}=15 V, but to obtain a minimum value of U_0 we must take into account the offset voltage of the amplifier and the comparator and the possible temperature drift. So, U_0 must be above 200 mV, which is two orders of magnitude above the offset voltage.

The main source of errors consists in the fact that the expression (4) is only an approximation of the true resistance–temperature behaviour for the thermistor. Usually the coefficient B is stated to be temperature dependent. The most difficult problem is to find out the coefficients A and B, i.e. to fit the real curve into an exponential one as well as possible.

Another source of errors is the drift of the function generator, but it might be eliminated using good quality components.

Our experiments were carried out using a disc type thermistor with 50 Ω the nominal resistance at 25°C. The data were taken over a range of 50°...150°C. Using the curve fitting procedures provided by the program MATLAB, we have find the coefficients A=2.22 Ω and B=139°C with a maximum error of 2%. The converter has a sensitivity of 10 Hz/°C and the maximum output frequency is 10 kHz. The accuracy obtained for the 100°C range, between 50°C and 150°C, is ±2.5°C and the linearity is of 2%. It is possible to improve both the linearity and the accuracy paying tribute to the width of the range.

5. Conclusions

The proposed linearising circuit is cheap and relative performant, providing the best results for sensors having a strong non-linear characteristic such thermistors, diodes, transistors. The circuit offers a wideness of the width of the range and an improvement of the linearity, making these sensors able to be used in a larger variety of applications.

Received, July 22, 1994

Technical University "Gh.Asachi", Jassy,
Department of Electric Measurements

REFERENCES

1. White D.R., *The Linearisation of the Resistance Thermometers.* J. of Phys., E: Sci. Instrum., **17**, 381-385 (1984).
2. Bodea M., *Aparate electrice de măsură şi control.* EDP, Bucureşti, 1985.

LINIARIZAREA RĂSPUNSULUI UNUI CONVERTOR ANALOG-NUMERIC PENTRU MĂSURAREA UNOR MĂRIMI NEELECTRICE

(Rezumat)

Se prezintă o metodă simplă şi ieftină pentru liniarizarea răspunsului unui convertor A/D folosit în scopuri generale, cu particularizare pentru elemente sensibile termic cu coeficient negativ de temperatură şi caracteristică puternic neliniară, de tip termistor. Câteva aspecte constructive şi rezultate privitoare la aprecierea erorilor sunt, de asemenea, discutate.

BULETINUL INSTITUTULUI POLITEHNIC DIN IAŞI
Tomul XLI (XLV), Fasc. 3–4, 1995
Secţia III
ELECTROTEHNICĂ. ENERGETICĂ. ELECTRONICĂ

C.D. 538.533

LES CARACTÉRISTIQUES DE LA BOBINE NONLINÉAIRE À NOYAU MAGNETISÉ ORTHOGONALEMENT

PAR
ADRIAN BARABOI

1. Les recherches concernant le comportement des matériaux ferromagnétiques sous l'action des champs magnétiques orthogonaux, dont l'initiateur, à l'Université de Jassy, a été le savant Ştefan P r o c o p i u, ont conduit à la découverte d'un nouvel effet, dénommé „l'effet P r o c o p i u".

Il y a une vingtaine années, sous la coordination du regretté professeur Gheorghe V a s i l i u, qui a été l'un des plus remarquables collaborateurs et continuateurs de Ştefan P r o c o p i u, l'auteur de cette Note a élaboré sa thèse de doctorat, consacrée à l'étude de la bobine nonlinéaire à noyau magnétisé orthogonalement (BNNMO), assimilée par un dispositif électromagnétique et un élément nonlinéaire de circuit dont le fonctionnement est basé sur l'effet P r o c o p i u.

Cet article représente un modeste hommage à la mémoire du savant Ştefan P r o c o p i u et de ses collaborateurs, illustres précurseurs de l'école d'électrotechnique nonlinéaire de Jassy.

2. La bobine nonlinéaire ayant le noyau magnétisé orthogonalement (BNNMO) représente un dispositif électromagnétique constitué par un noyau ferromagnétique muni de deux enroulements, l'un d'excitation et l'autre de commande, dont les axes sont perpendiculaires.

Pour déterminer par voie analytique les expressions des caractéristiques $\theta(\psi, \psi_C)$, $\theta_C(\psi, \psi_C)$ d'une BNNMO, où avec θ, θ_C et ψ, ψ_C on a noté les f.m.m. et les flux magnétiques d'excitation, respectivement de commande, on accepte les hypothèses ci-dessous: a) on considère comme isotrope le matériau du noyau ferromagnétique de la bobine; b) on néglige l'hystérésis magnétique du noyau et les résistances électriques des enroulements.

Compte tenu des hypothèses ci-dessus on fait appel à la courbe fondamentale d'aimantation, exprimée analytiquement par la fonction [1]:

$$H_{k\Sigma} = b_k \operatorname{sh}(b'_k B_{k\Sigma}), \tag{1}$$

où $B_{k\Sigma}$ et $H_{k\Sigma}$ représentent des grandeurs résultantes (sommes vectorielles) des inductions magnétiques orthogonales d'excitation, B_k et de commande, B_{Ck}, respectivement, des champs magnétiques orthogonaux d'excitation, H_k et de commande, H_{Ck}, rapportées à la partie homogène k du noyau ferromagnétique; par b_k, b'_k on a noté les coefficients de la fonction d'approximation.

Entre les grandeurs magnétiques d'excitation (B_k, H_k) et de commande (B_{Ck}, H_{Ck}), rapportées à la partie homogène et isotrope, k, du noyau, on peut écrire encore les relations [1]:

$$\frac{B_{k\Sigma}}{H_{k\Sigma}} = \frac{B_k}{H_k} = \frac{B_{Ck}}{H_{Ck}}, \tag{2}$$

où:

$$B_{k\Sigma}^2 = B_k^2 + B_{Ck}^2, \quad H_{k\Sigma}^2 = H_k^2 + H_{Ck}^2. \tag{3}$$

Par développement en série dans la relation (1) on obtient:

$$H_{k\Sigma} = b_k \sum_{n=0}^{\infty} \frac{(b_k' B_{k\Sigma})^{2n+1}}{(2n+1)!}, \tag{4}$$

et, pour les champs magnétiques H_k, H_{Ck}, orthogonaux dans la partie k du noyau, compte tenu de (2), (3) il en résulte:

$$\begin{cases} H_k = \sum\limits_{i=0}^{\infty} \sum\limits_{j=0}^{\infty} b''_{k,2i+1,2j} B_k^{2i+1} B_{Ck}^{2j}, \\ H_{Ck} = \sum\limits_{i=0}^{\infty} \sum\limits_{j=0}^{\infty} b''_{k,2i+1,2j} B_{Ck}^{2i+1} B_k^{2j}, \end{cases} \tag{5}$$

où:

$$b''_{k,2i+1,2j} = \frac{b_k b_k'^{2(i+j)+1} C_{i+j}^j}{[2(i+j)+1]!}. \tag{6}$$

En appliquant aux contours e et c, des circuits magnétiques orthogonaux d'excitation, respectivement de commande, la loi du circuit magnétique en régime permanent, on peut écrire:

$$\sum_{k \in e} H_k L_k = \theta, \quad \sum_{k \in c} H_{Ck} L_{Ck} = \theta_C, \tag{7}$$

où L_k, L_{Ck} représentent les longueurs de la partie k au long des directions orthogonales e, respectivement c.

Compte tenu de (5), les relations (7) deviennent:

$$\begin{cases} \theta = \sum\limits_{k \in e} \sum\limits_{i=0}^{\infty} \sum\limits_{j=0}^{\infty} b''_{k,2i+1,2j} L_k B_k^{2i+1} B_{Ck}^{2j}, \\ \theta_C = \sum\limits_{k \in c} \sum\limits_{i=0}^{\infty} \sum\limits_{j=0}^{\infty} b''_{k,2i+1,2j} L_{Ck} B_{Ck}^{2i+1} B_k^{2j}. \end{cases} \tag{8}$$

Ayant en vue que:

$$B_k = \frac{\psi}{N S_k}, \quad B_{Ck} = \frac{\psi_c}{N_C S_{Ck}}, \tag{9}$$

où N, N_C représentent, respectivement, les nombres de spires des enroulements d'excitation et de commande et S_k, S_{Ck} les surfaces transversales de la partie k du noyau, traversées par les flux magnétiques ψ, ψ_c, les relations (8) résultent finalement de la forme:

$$(10)\qquad \begin{cases} \theta = \sum\limits_{k\in e}\sum\limits_{i=0}^{\infty}\sum\limits_{j=0}^{\infty} \frac{b''_{k,2i+1,2j} L_k \psi^{2i+1}\psi_C^{2j}}{(NS_k)^{2i+1}(N_C S_{Ck})^{2j}}, \\ \theta_C = \sum\limits_{k\in e}\sum\limits_{i=0}^{\infty}\sum\limits_{j=0}^{\infty} \frac{b''_{k,2i+1,2j} L_{Ck} \psi_C^{2i+1}\psi^{2j}}{(N_C S_{Ck})^{2i+1}(NS_k)^{2j}}. \end{cases}$$

L'utilisation pratique des expressions (10) s'avère assez difficile de sorte que, spécialement pour des analyses qualitatives, une approximation satisfaisante est donnée par des polynômes de troisième où cinquième degré en ψ et ψ_C, à savoir:

$$(11)\qquad \begin{cases} \theta(\psi,\psi_C) = b_{10}\psi + b_{30}\psi^3 + b_{12}\psi\psi_C^2, \\ \theta_C(\psi,\psi_C) = b_{10}^C\psi_C + b_{30}^C\psi_C^3 + b_{12}^C\psi_C\psi^2, \end{cases}$$

où, compte tenu de (6):

$$(12)\qquad \begin{cases} b_{10} = \sum\limits_{k\in e}\frac{b_k b'_k L_k}{NS_k},\ b_{30} = \sum\limits_{k\in e}\frac{b_k b_k'^3 L_k}{6(NS_k)^3},\ b_{12} = \sum\limits_{k\in e}\frac{b_k b_k'^3 L_k}{6NS_k(N_C S_{Ck})^2}, \\ b_{10}^C = \sum\limits_{k\in c}\frac{b_k b'_k L_{Ck}}{NS_{Ck}},\ b_{30}^C = \sum\limits_{k\in c}\frac{b_k b_k'^3 L_{Ck}}{6(N_C S_{Ck})^3},\ b_{12}^C = \sum\limits_{k\in c}\frac{b_k b_k'^3 L_{Ck}}{6N_C S_{Ck}(NS_k)^2}. \end{cases}$$

Pour un noyau ferromagnétique entièrement homogène et isotrope, dont les circuits magnétiques d'excitation et de commande ont respectivement les dimensions L, S, et L_C, S_C, les coefficients (12) deviennent de la forme:

$$(13)\qquad \begin{cases} b_{10} = \frac{bb'L_C}{NS},\ b_{30} = \frac{bb'^3 L}{6(NS)^3},\ b_{12} = \frac{bb'^3 L}{6NS(N_C S_C)^2}, \\ b_{10}^C = \frac{bb'L_C}{N_C S_C},\ b_{30}^C = \frac{bb'^3 L_C}{6(N_C S_C)^3},\ b_{12}^C = \frac{bb'^3 L_C}{6N_C S_C(NS)^2}. \end{cases}$$

Outre cela si les conditions:

$$(14)\qquad NS = N_C S_C,\quad L = L_C$$

sont satisfaites, on obtient, pour les expressions des coefficients (13), les valeurs:

$$(15)\qquad b_{10} = b_{10}^C,\quad b_{30} = b_{30}^C = b_{12} = b_{12}^C.$$

Les fonctions initiales, choisies en vue d'approximer analytiquement les caractéristiques d'une BNNMO, peuvent être de n'importe quel type, à la condition qu'elles soient capables à approximer très précisément la courbe fondamentale d'aimantation du matériau ferromagnétique utilisé dans la construction du noyau.

3. On peut obtenir des conclusions intéressantes concernant les caractéristiques $\theta(\psi, \psi_C)$, $\theta_C(\psi, \psi_C)$, à partir de l'étude du fonctionnement en régime permanent d'une BNNMO, excitée et commandée par des flux magnétiques harmoniques, qui oscillent en quadrature, ayant la même pulsation:

$$\psi(\alpha) = \psi_m \cos\alpha, \quad \psi_C(\alpha) = \psi_{Cm} \sin\alpha, \quad \alpha = \omega t. \tag{16}$$

Par la substitution des expressions (16) dans (11) il résulte:

$$\theta(\alpha) = \theta_{1m} \cos\alpha + \theta_{3m} \cos 3\alpha, \quad \theta_C(\alpha) = \theta_{C1m} \sin\alpha + \theta_{C3m} \sin 3\alpha, \tag{17}$$

où, compte tenu de (13), on a utilisé les notations ci-dessous:

$$\begin{cases} \theta_{1m} = b_{10}\psi_m + 0,75 b_{30}\psi_m^3 + 0,25 b_{12}\psi_m \psi_{Cm}^2, \\ \theta_{3m} = 0,25 b_{12}\psi_m \psi_{Cm}^2 (m-1), \quad m = \frac{b_{30}\psi_m^2}{b_{12}\psi_{Cm}^2} \\ \theta_{C1m} = b_{10}^C \psi_{cm} + 0,75 b_{30}^C \psi_{cm}^3 + 0,25 b_{12}^C \psi_{Cm} \psi_m^2, \\ \theta_{C3m} = 0,25 b_{12}^C \psi_{Cm} \psi_m^2 \frac{m-1}{m}. \end{cases} \tag{18}$$

Les relations (17), (18) mettent en évidence le fait qu'une BNNMO peut se comporter comme un élément linéaire de circuit; vraiment, afin que le circuit d'excitation soit linéaire il est nécessaire à considérer $\theta_{3m} = \theta$, ce que conduit à la condition:

$$m = 1. \tag{19}$$

Conformément aux relations (17), (18), la condition (19) assure simultanément et la linéarité du circuit de commande, c'est-à-dire le comportement linéaire d'un seul circuit de la BNNMO assure entièrement la linéarité du dispositif.

Si par la construction de la BNNMO les relations (14) et donc (15) sont satisfaites, à partir de (16) et compte tenu de (17),...,(19), on obtient pour le flux magnétique résultant:

$$\psi_\Sigma = \psi_m = \psi_{Cm} = \text{const.} \tag{20}$$

Dans les mêmes conditions la f.m.m. résultante, θ_Σ, a l'expression:

$$\theta_\Sigma = b_{10}\psi_m + b_{30}\psi_m^3 = \text{const.} \tag{21}$$

Les relations (20), (21) mettent en évidence le caractère tournant des grandeurs magnétiques ψ_Σ, θ_Σ; D o r o ž k o et L i b k i n d [2] proposent l'utilisation d'une telle sorte de dispositif comme réacteur commandé dans les réseaux électriques.

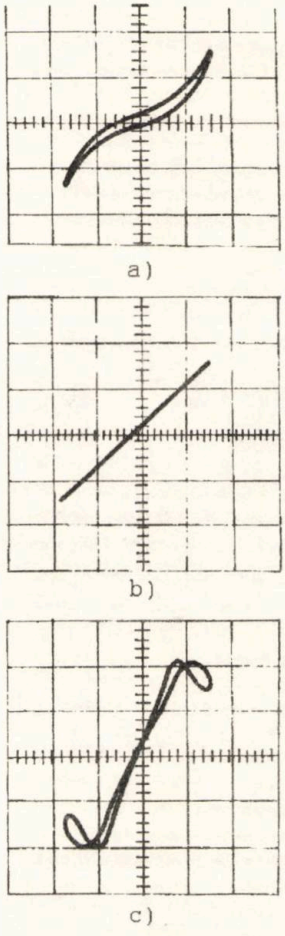

Fig. 1

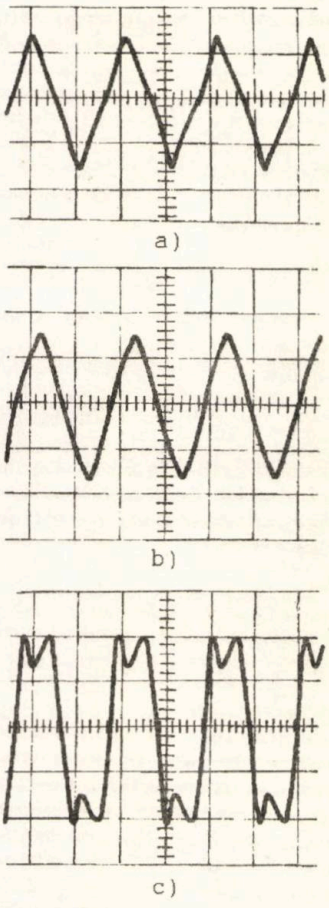

Fig. 2

Pour des valeurs du rapport m différentes de l'unité résultent deux phases initiales distinctes des harmoniques de troisième degré contenues dans les spectres

des f.m.m $\theta(\alpha)$, $\theta_C(\alpha)$. Ainsi, conformément aux relations (17), (18), pour $m > 1$ les harmoniques de troisième degré oscillent respectivement en phase par rapport aux composantes fondamentales, tandis que, pour $m < 1$, les oscillations des ceux-ci ont lieu en opposition de phase.

Les particularités concernant le régime permanent de fonctionnement d'une BNNMO sont mises en évidence et par l'allure de la caractéristique $\theta(\psi, \psi_C)$. Dans la Fig.1 on présente des oscillogrammes de celle-ci, obtenues à l'aide d'une BNNMO fonctionnant dans les hypothèses des cas analysés ci-dessus; les oscillogrammes correspondantes du signal $\theta(\alpha)$ sont presentées dans la Fig.2.

Les résultats théoriques obtenus ont été utilisés dans l'analyse du fonctionnement de quelques dispositifs électromagnétiques [3],...,[5] contenant une BNNMO.

Conclusions

1. On établit les expressions analytiques des caractéristiques $\theta(\psi, \psi_C)$, $\theta_C(\psi, \psi_C)$ d'une BNNMO dont le noyau ferromagnétique est constitué par des portions isotropes et homogènes.

2. On analyse le fonctionnement en régime permanent d'une BNNMO excitée et commandée par des flux magnétiques harmoniques, ayant la même fréquence et oscillant en quadrature. On met en évidence l'influence du paramètre m sur l'allure des caractéristiques de la BNNMO.

3. On étudie par voie expérimentale le fonctionnement en régime permanent d'une BNNMO et on confirme, de cette façon, les résultats théoriques obtenus.

Reçue le 10 juin 1994

Université Technique „Gh. Asachi", Jassy, Chaire d'Énergétique

BIBLIOGRAPHIE

1. Savin Gh., Rosman H., *Circuite electrice neliniare şi parametrice.* Ed. Tehn., Bucureşti, 1973.
2. Dorožko L.I., Libkind M.S., *Reaktory s poperečnym podmagničivaniem.* Izd. Energia, Moskva, 1977.
3. Baraboi A., *Triplor de frecvenţă monofazat cu bobină neliniară cu miez magnetizat pe direcţii ortogonale.* Patent Rom., *70637* (1978).
4. Baraboi A., *L'utilisation d'une bobine nonlinéaire à noyau magnétisé orthogonalement pour la limitation des courants continus de court-circuit.* Bul. Inst. polit., Iaşi, **XXVIII (XXXII)**, *1-4*, s.III, 83 (1982).
5. Baraboi A., Hnatiuc E., Furnică E., *Reactive Power Statical Source with Reactor Using Crossed Magnetic Fields.* Internat. Sci. Conf. on "Quality of Electrical Energy", Spala, Poland, **II**, 81 (1991).

CARACTERISTICILE BOBINEI NELINIARE CU MIEZ MAGNETIZAT PE DIRECŢII ORTOGONALE

(Rezumat)

Se studiază posibilităţile de aproximare a caracteristicilor unei bobine neliniare cu miezul magnetizat pe direcţii ortogonale (BNNMO), utilizând funcţiile de aproximare propuse şi verificate experimental; se evidenţiază unele particularităţi privind regimul permanent de funcţionare a BNNMO.

BULETINUL INSTITUTULUI POLITEHNIC DIN IAŞI
Tomul XLI (XLV), Fasc. 3-4, 1995
Secţia III
ELECTROTEHNICĂ. ENERGETICĂ. ELECTRONICĂ

D.C. 621.43.044; 621-52

SOME CONSIDERATIONS CONCERNING THE STRUCTURES OF CONTROL SYSTEMS FOR SPARK IGNITION ENGINES

BY
LAURENŢIU DIMITRIU

1. Introduction

Today's traffic puts great demands on an automobile. Automotive electronics plays a decisive rôle in the areas of ignition and fuel management. The economical or improved use of fuel in conjunction with low pollutant combustion can also be achieved with the help of electronics.

To improve the features of fuel injection and ignition control systems a preliminary analysis of existing solution is necessary.

2. Classic Control System Structure

The first structure of control systems used in engine management is shown in the Fig.1

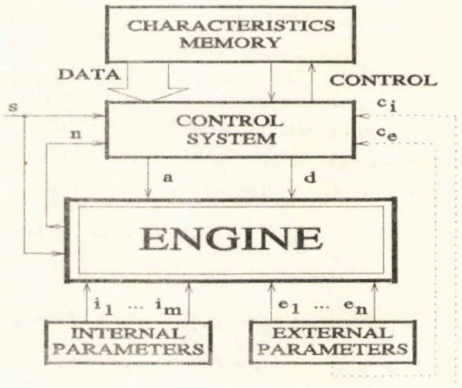

Fig. 1

Such a structure characterizes: carburetor, mechanical injection and open loop electronic fuel injection equipped engines.

The variables of the system are: s – engine load, n – engine speed, a – ignition angle, d – air–fuel mixture ratio, p – pollutants (in exhaust gas), v – knock vibrations, $i_1, ..., i_m$ – internal parameters, $e_1, ..., e_n$ – external parameters.

In stationary and standard working conditions, the advance angle and the air–fuel mixture ratio are formally matrixes memorized. These are A and D matrixes, and they have $n_1 \times s_1$, respectively $n_2 \times s_2$ dimensions:

$$A = \begin{bmatrix} a_{11} & a_{12} & \dots & a_{1s_1} \\ a_{21} & a_{22} & \dots & a_{2s_1} \\ \dots & \dots & \dots & \dots \\ a_{n_1 1} & a_{n_1 2} & \dots & a_{n_1 s_1} \end{bmatrix}, \quad D = \begin{bmatrix} d_{11} & d_{12} & \dots & d_{1s_2} \\ d_{21} & d_{22} & \dots & d_{2s_2} \\ \dots & \dots & \dots & \dots \\ d_{n_2 1} & d_{n_2 2} & \dots & d_{n_2 s_2} \end{bmatrix}.$$

The values of the matrixes are quantified, and they satisfy the following condition:

$$a_{ij},\ d_{ij} \in \mathbb{N}.$$

The control values, used in engine driving, are a_c and d_c. They respects the following relationships:

$$a_c = a_m U_a, \qquad d_c = d_m U_d,$$

where U_a and U_d are specific unitary values of the management system, a_c and d_c being, from dimensional point of view, advance angle, and respectively mixture ratio (fuel quantity).

For stationary conditions, but for different values of internal and external parameters (non-standard), corrections are necessary [1]. Using the same mathematically formalism, these corrections can be expressed using two correction matrixes:

$$C_a = \begin{bmatrix} ca_{11} & ca_{12} & \dots & ca_{1s_1} \\ ca_{21} & ca_{22} & \dots & ca_{2s_1} \\ \dots & \dots & \dots & \dots \\ ca_{n_1 1} & ca_{n_1 2} & \dots & ca_{n_1 s_1} \end{bmatrix}, \quad C_d = \begin{bmatrix} cd_{11} & cd_{12} & \dots & cd_{1s_2} \\ cd_{21} & cd_{22} & \dots & cd_{2s_2} \\ \dots & \dots & \dots & \dots \\ cd_{n_2 1} & cd_{n_2 2} & \dots & cd_{n_2 s_2} \end{bmatrix}.$$

These correction matrixes should be used to generate the final control values of management system. In this way, two matrixes with final values A_f and D_f are obtained. They have the following form:

$$A_f = A + C_a, \qquad D_f = D + C_d.$$

Therefore:

$$a_f = (a_m + c_a)U_a, \qquad d_f = (d_m + c_d)U_d.$$

The values of matrixes are functions having the following forms:

$$c_a = f_{ca}(s, n, i_1, i_2, ..., i_m, e_1, e_2, ..., e_n), \quad c_d = f_{cd}(s, n, i_1, i_2, ..., i_m, e_1, e_2, ..., e_n).$$

For a high quality of corrections, the parameters describing internal and external factors are quantified in a proper number of levels, from practical criterions. If q is this number, N_c possible combinations of parameters appear, where:

$$N_c = C_{q(n+p)}^{n+p}.$$

Therefore a necessary of memory for the corrections of advance angle using N_a values, respectively of mixture ratio using N_d values is imposed:

$$N_a = n_1 s_1 C_{q(n+p)}^{n+p}, \quad N_d = n_2 s_2 C_{q(n+p)}^{n+p}.$$

Taking into account the practical values of memory capacities used (for characteristic maps in stationary standard conditions): $n_1 s_1$ locations for advance angle and $n_2 s_2$ locations for mixture ratio, finally results extremely large necessities of memory to keep all control values in all possible combinations of parameters.

The values used in these memories impose an extremely large number of experimental results. The experiments using proper test beds take place sometimes in extremely difficult to achieve conditions, corresponding to certain combinations of parameters, possible to appear during engine working, but very difficult to maintain for a proper length in artificial medium.

Finally, based on these control principles for all possible stationary conditions, the used values for engine management take the form:

$$a_{sf_{ij}} = a_{sf_{ij}}(s, n, i_1, i_2, ..., i_m, e_1, e_2, ..., e_n), \ (i = 1, 2, ..., n_1; \ j = 1, 2, ..., s_1),$$

$$d_{sf_{ij}} = d_{sf_{ij}}(s, n, i_1, i_2, ..., i_m, e_1, e_2, ..., e_n), \ (i = 1, 2, ..., n_2; \ j = 1, 2, ..., s_2).$$

The block diagram from Fig.1 corresponds to an open loop system, but a feedback can be take into consideration by periodical manual tunings (such as air–fuel mixture ratio and initial advance angle). These operations are effectuated outside from the system. They improve the engine performances, but they are, in a strict sense, of conjucture. The drift of performances will be into technological limits of manufacture. In stationary and standard conditions, the differences between the different solutions depend only from technological dispersion in engines and control systems manufacturing.

3. Modern Control System Structure

For higher performances of engines, the control system structure of Fig.2 was imposed. This structure can be implemented only in electronic control form (electronic carburetor or electronic injection). Moreover than the structure shown in Fig.1, two new signals appear: λ – Lambda sensor signal; z – knock signal.

The superiority of this structure is specially distinguished when the working conditions are different from the standard ones. Consequently of state parameters

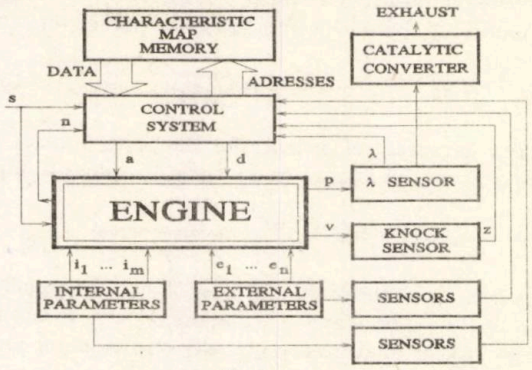

Fig. 2

changes, the response of management system will change. The changes will be put into evidence using Lambda and knock sensors. The Lambda sensor is used to measure the oxygen content in the exhaust gas (excess-air factor λ). The signals from these sensors are included into closed loops and they determine compensatory variations. Thus, the control signals used in the management system take the values to satisfy the following criterions [2],...,[4]: a) excess-air factor: $\lambda = 1 \pm 1\%$ (for reduction in pollutant emission using catalytic converter); b) ignition point: to the engine knock limit.

The changes of control values are step by step effected, incrementing or decrementing the start values a and d. It results step variations of advance ignition angle and air–fuel mixture ratio, of U_a and, respectively, U_d size.

To help the stability of engine well working, these correction values could act directly in the characteristic maps memory. In this way an adaptive structure system is obtained. They assure a decreasing in closed loops "effort". In stationary conditions, an adaptive system will converge to the real necessary values, and will evolve inside quantifying error limits ($\pm U_a, \pm U_d$).

4. Conclusions

Analyzing the stationary response of the studied structures, some conclusions could be obtained:

a) in stationary standard conditions there are not essential differences between the structures, concerning the performances and the behaviour;

b) in stationary, but non-standard conditions, the closed loop systems are better, thanks to stabilizing effect of the feedback.

Received, November 21, 1994

Technical University "Gh.Asachi", Iassy,
Department of Applied Electronics

REFERENCES

1. A r a m ă C., G r ü n w a l d B., *Motoare cu ardere internă. Procese şi caracteristici.* Ed. Tehn., Bucureşti, 1966.
2. D i m i t r i u L., R ă d u c a n u I., T o d e r e a n A.R.P., *An Electronic Engine Management System.* Proc. of the Internat. Symp. on Signals, Circuits and Systems, Jassy, Romania, November 4-5, 1993, 280-284.
3. D i m i t r i u L., *Injection Control Circuit in a Computer Controlled Spark Ignition Engine Test Bed.* Proc. of the Internat. Symp. on Signals, Circuits and Systems, Jassy, Romania, November 4-5, 1993, 285-289.
4. D i m i t r i u L., *Ignition Control Circuit in a Computer Controlled Spark Ignition Engine Test Bed.* Proc. of the Internat. Symp. on Signals, Circuits and Systems, Jassy, Romania, November 4-5, 1993, 290-293.

CÂTEVA CONSIDERAŢII PRIVIND STRUCTURILE SISTEMELOR DE CONTROL ALE MOTOARELOR CU APRINDERE PRIN SCÂNTEIE

(Rezumat)

Se prezintă principalele caracteristici ale structurilor de control pentru motoarele cu aprindere prin scânteie disponibile în prezent pentru echiparea motoarelor de automobil. Se efectuează un studiu comparativ al răspunsului în regim staţionar al acestor tipuri de sisteme de control şi se trag concluzii privind performanţele ce pot fi obţinute, conturând principalele soluţii ce pot satisface condiţiile de funcţionare din ce în ce mai restrictive impuse de normele tehnice antipoluare.

BULETINUL INSTITUTULUI POLITEHNIC DIN IAŞI
Tomul XLI (XLV), Fasc. 3–4, 1995
Secţia III
ELECTROTEHNICĂ. ENERGETICĂ. ELECTRONICĂ

D.K. 621.335.2; 621.313.2; 621.3.018.14

SPEISUNGSSYSTEM MIT ERHÖHTEM LEISTUNGSFAKTOR FÜR ELEKTRISCHE LOKOMOTIVEN MIT GLEICHSTROMMOTOREN

VON

D. ALEXA und CLARISSA GÎTLAN

1. Einleitung

In den letzten Jahren wuchs beträchtlich das Interesse für den Einsatz von elektrischen Lokomotiven, die von Einphasennetzen mit einer Frequenz von 50 Hz gespeist werden und dadurch gekennzeichnet sind, daß sie keine Blindleistung der Netze beanspruchen, wenn ihre Wirkleistungen in weiten Grenzen variieren [1],...,[7].

Alle netzgeführten Stromrichter in Einphasen-Brückenschaltung, die am Eingang der Speisesysteme der Lokomotiven installiert sind, um variable Gleichspannungen zu erzeugen, weisen folgende Nachteile auf: a) sie erzeugen in den Netzen bedeutende Werte von oberen Stromharmonischen; b) sie beanspruchen große Blindleistungen von diesen Netzen.

In Abb.1 *a* ist die Speisungsvariante eines einzelnen Gleichstrommotors mit zwei halbgesteuerten Einphasen-Brückenschaltungen dargestellt. Die zwei Stromrichter in Einphasen-Brückenschaltung sind folgegesteuert und reduzieren die vom Netz beanspruchte Blindleistung um die Hälfte gegenüber dem Gleichstrommotor, der von nur einem halbgesteuerten Stromrichter gespeist wird. Diese Variante reduziert jedoch nicht die im Netz erzeugten Stromoberschwingungen [8],...,[10].

In Abb.1 *b* ist ebenfalls das Schema der Speisung eines einzigen Gleichstrommotors durch zwei halbgesteuerte Stromrichter in Einphasen-Brückenschaltung wiedergegeben. Ein Stromrichter arbeitet mit Zwangskommutierung und erzeugt im Netz Blindleistung; der andere ist netzgeführt, nimmt also Blindleistung auf. Folglich wird bei dieser Variante die vom Netz beanspruchte Blindleistung auf ein Minimum reduziert, aber nicht auch die in diesem Netz erzeugte Verzerrungsleistung. Im Falle der Varianten aus den Abb.1 *a* und 1 *b* müssen, wenn mehrere Antriebsmotoren existieren, für jeden Motor solche Stromrichter vorgesehen werden [8],...,[10].

Schließlich zeigt Abb.1 *c* die Variante mit Gleichstrommotoren, die durch Gleichstromsteller mit GTO-Thyristoren gespeist werden. Diese Lösung macht einen L_1C_1-Filter großen Ausmaßes am Eingangs nötig, ohne daß dadurch eine akzeptable Verkleinerung der im Netz erzeugten Stromoberschwingungen erhalten wird. Die GTO-Thyristoren arbeiten nach dem PWM-Prinzip, wobei ihre Schaltfrequenz zehn- oder zwölfmal größer ist als die Netzfrequenz. Die Einschaltdauer dieser GTO-Thyristoren wird somit für Speisespannungen sehr kleiner Motoren zu klein als daß man sie akzeptieren könnte. Ein anderer Nachteil dieser Lösung besteht darin, daß der totale Leistungsfaktor vom Eingang sich sehr verringert, wenn der Gleichstrom I_d, der durch die Motoren ließt, sich verkleinert [11], [12].

Weiter wird eine Steuermethode für Traktiongleichstrommotoren beschrieben. Durch diese Methode erhält man einen erhöhten Leistungsfaktor am Eingang, ohne daß Filterschaltungen oder statische Blindleistungskompensatoren nötig wären.

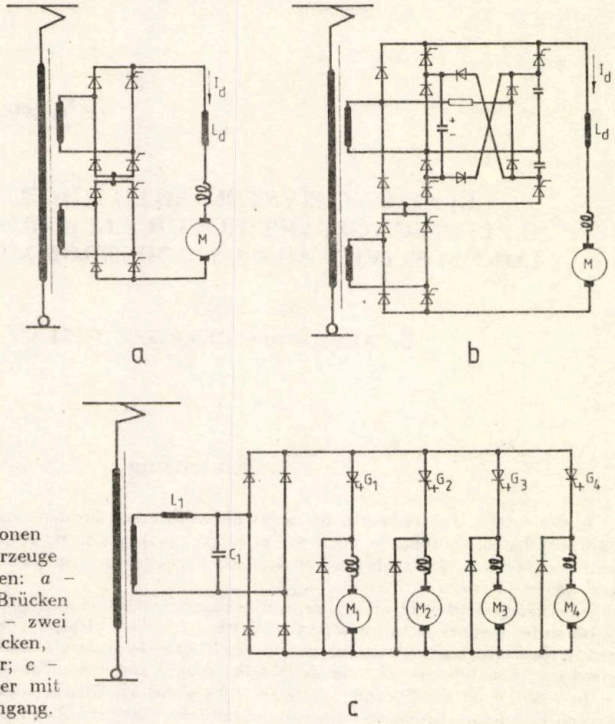

Abb. 1.– Antriebskonfigurationen elektrischer Triebfahrzeuge mit Gleichstrommotoren: *a* – zwei halbsteuerbare Brücken in Folgesteuerung; *b* – zwei halbsteuerbare Brücken, eine Brücke löschbar; c – vier Gleichstromsteller mit L_1C_1-Filter am Eingang.

2. Steuerprinzip der Antriebsmotoren

In Abb.2 ist das Prinzipschaltbild für das Speisungssystem variabler Spannung für vier Gleichstrommotoren auf einer Lokomotive dargestellt. Diese Variante kann auch für Lokomotiven angepaßt werden, die mit einer geradzahligen Anzahl von Motoren, größer als vier, (z.B. 6 oder 8) bestückt sind, aber man stellt fest, daß die meisten Lokomotiven mit 4 Motoren ausgerüstet sind.

Das Speisungssystem besteht aus einem Transformator mit zwei Sekundärwicklungen, zwei Stromrichter in Einphasen-Brückenschaltung mit Dioden, den Kondensatoren C_1 und C_2, den GTO-Thyristoren G_1 – G_4 und den Dioden D_1 – D_4. Wegen der Induktanzen L_1 – L_4, die mit den vier Motoren M_1 – M_4 in Reihe geschaltet sind, können die Ströme, die durch die Motoren fliessen, während einer Frequenzperiode des Speisenetzes als konstant angenommen werden, wobei sie den Wert I_d haben. Es ist besser, wenn diese Frequenz den Wert 50 Hz hat und nicht $16\frac{2}{3}$ Hz, damit man für die Induktanzen L_1 – L_4 kleinere Werte erhält.

Die GTO-Thyristoren werden so gesteuert, daß der Eingangsstrom i einen möglichst kleinen Oberschwingungsgehalt besitzt und keine Blindkomponente enthält.

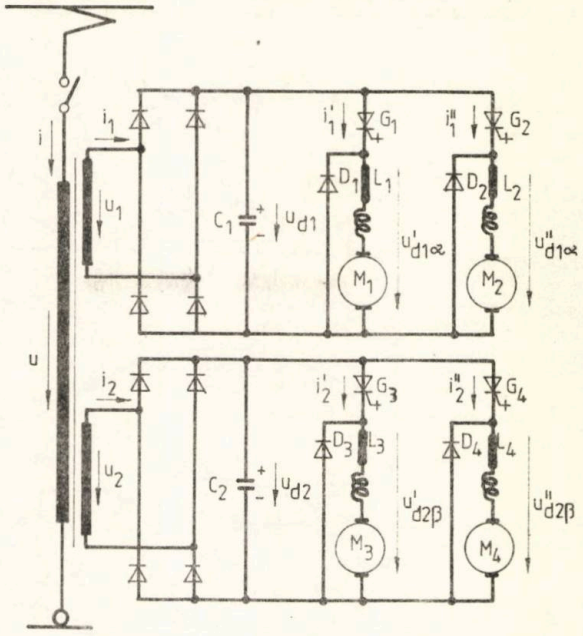

Abb. 2.– Prinzipielles Schema des neuen Antriebssystem mit vier Gleichstromsteller.

Wenn die von der Lokomotive vom Netz geforderte Wirkleistung P zwischen 50% und 100% der maximalen Leistung $P_{\max}$ schwankt, ist die Steuermethode der Thyristoren in Abb.3 veranschaulicht. In dieser Abbildung wird die Einschaltdauer der GTO-Thyristoren, die Spannungen u_{d1} und u_{d2} an den Klemmen der Kondensatoren C_1 und C_2, die Teilströme i'_1, i''_1, i'_2, i''_2, die Ströme i_1 und i_2 am Eingang der Stromrichter in Einphasen-Brückenschaltung, sowie der Gesamtstrom i wiedergegeben. Für die Thyristoren G_1 und G_2 ist der Winkel α_1 konstant, aber $\alpha^{(1)}$ ist zwischen α_2 und $\pi/2$ veränderlich. Bei den Winkeln $\pi - \alpha^{(1)}$ und $2\pi - \alpha^{(1)}$ wird der Thyristor G_1 blockiert und die Diode D_1 eingeschaltet, während bei den Winkeln $\pi - \alpha_1$ und $2\pi - \alpha_1$ der Thyristor G_2 blockiert und die Diode D_2 eingeschaltet wird. Durch diese Steuermethode erhält man die zwei Ausgangsspannungen $u'_{d1\alpha}$ und $u''_{d1\alpha}$, deren Gleichspannungskomponenten $U'_{d1\alpha}$ und $U''_{d1\alpha}$ untereinander gleich sein sollten. Was die Thyristoren G_3 und G_4 anbetrifft, diese werden so gesteuert, daß der Winkel β_1 konstant gehalten wird, und der Winkel $\beta^{(1)}$ zwischen β_2 und $\pi/2$ variiert. Bei den Winkeln $\pi - \beta^{(1)}$ und $2\pi - \beta^{(1)}$ wird der Thyristor G_3 blockiert und die Diode D_3 wird eingeschaltet. Bei den Winkeln $\pi - \beta_1$ und $2\pi - \beta_1$ blockiert G_4 und D_4 schaltet sich ein. Auf diese Art und Weise erhält man die zwei Ausgangsspannungen $u'_{d2\beta}$ und $u''_{d2\beta}$, für deren Gleichspannungskomponenten $U'_{d2\beta}$ und $U''_{d2\beta}$ folgende Bedingungen gelten:

$$U'_{d1\alpha} = U''_{d1\alpha} = U'_{d2\beta} = U''_{d2\beta}. \tag{1}$$

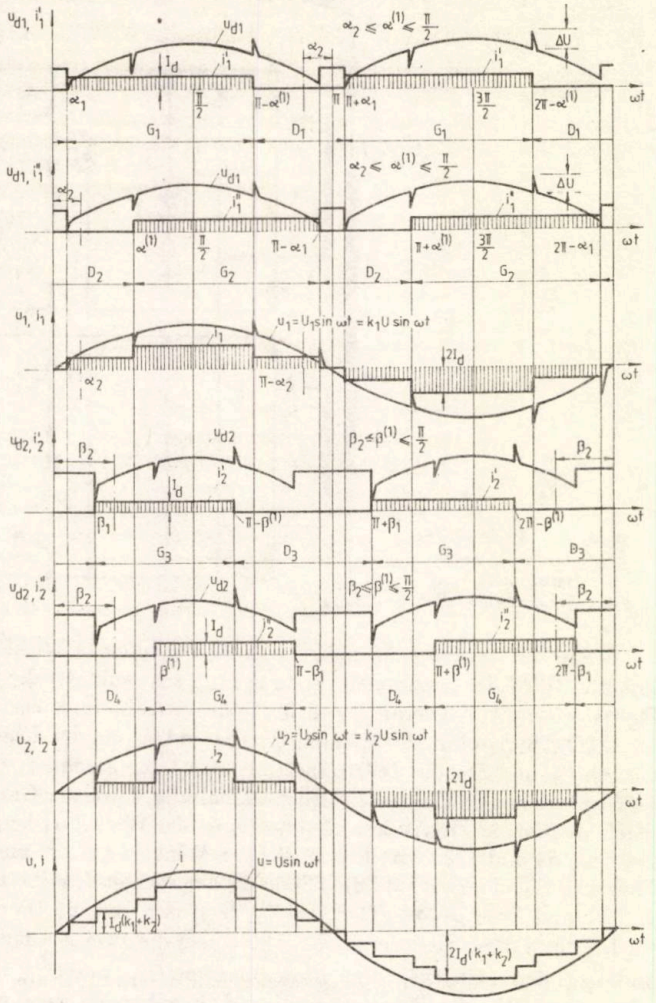

Abb. 3.– Steuerungsmethode für $0,514 \leq P/P_{max} \leq 1$.

Um diese Bedingung zu erfüllen, besteht zwischen den regelbaren Steuerwinkeln $\alpha^{(1)}$ und $\beta^{(1)}$ die Beziehung:

$$U_1(\cos\alpha_1 + \cos\alpha^{(1)}) = U_2(\cos\beta_1 + \cos\beta^{(1)}). \tag{2}$$

Durch Aufsummierung der beiden Eingangsströme i_1 und i_2 ergibt sich ein Gesamtstrom i, deren Grundschwingungsgehalt zwischen den Grenzen 0,97 und 0,986 schwankt (Kurve *1* in Abb.6), wenn für die Wirkleistung P folgende Ungleichung gilt:

(3) $$\frac{\cos\beta_1}{\cos\beta_1+\cos\beta_2}P_{max} \leq P \leq P_{max}.$$

Für diese optimale Situation wurden die Werte $\alpha_1 = 10°$, $\alpha_2 = 20°$, $\beta_1 = 30°$, $\beta_2 = 35°$ und $k_2/k_1 = 1,142$ angenommen.

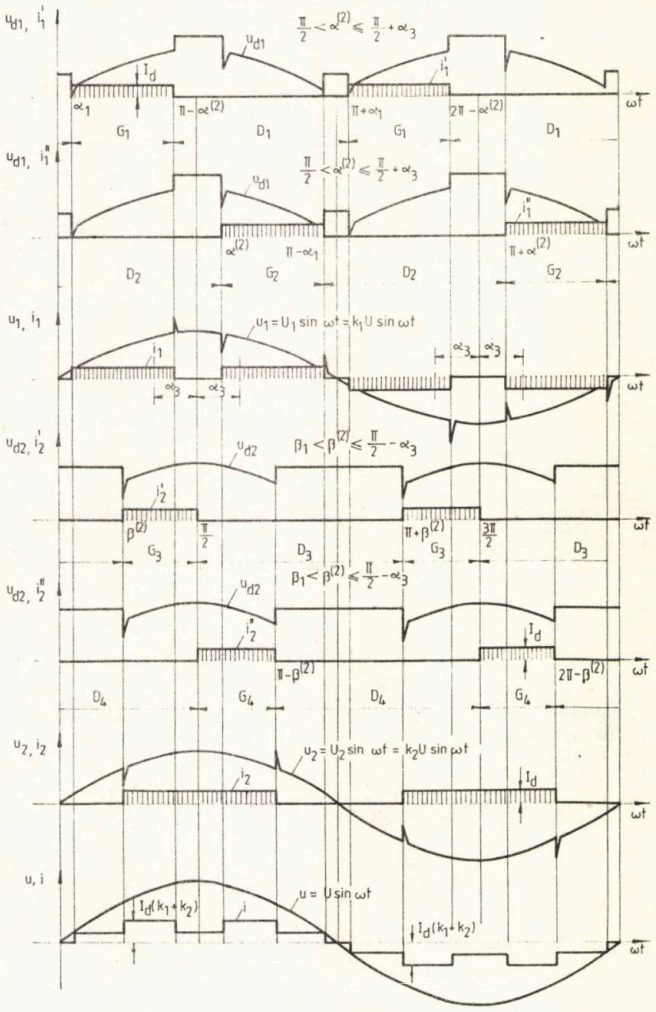

Abb. 4.– Steuerungsmethode für $0,273 \leq P/P_{max} < 0,514$.

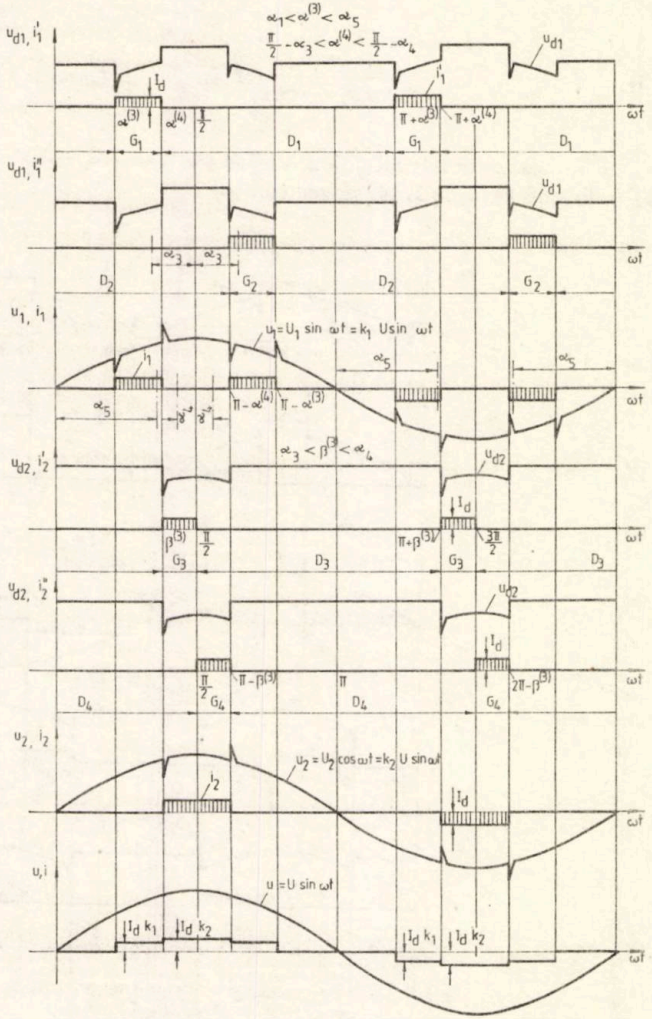

Abb. 5.– Steuerungsmethode für $0,1 \leq P/P_{max} < 0,273$.

Wenn die Wirkleistung in den Grenzen:

$$\frac{\sin \alpha_3}{\cos \beta_1 + \cos \beta_2} P_{max} \leq P < \frac{\cos \beta_1}{\cos \beta_1 + \cos \beta_2} P_{max} \tag{4}$$

variiert, wird die in Abb.4 wiedergegebene Steuermethode angewendet, in der der Winkel α_3 folgender Gleichung genügt:

$$U_1(\cos \alpha_1 - \sin \alpha_3) = U_2 \sin \alpha_3. \tag{5}$$

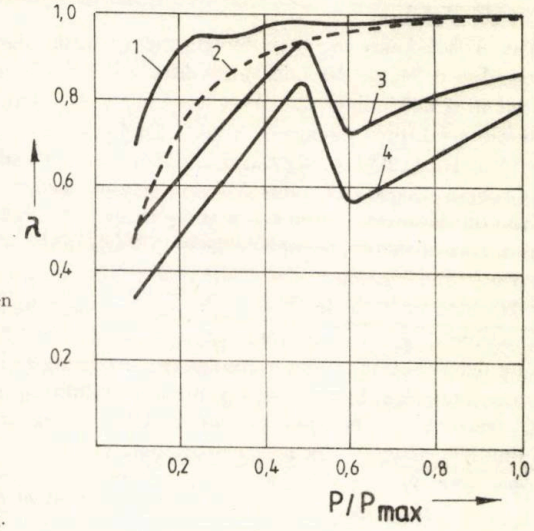

Abb. 6.– Totaler Leistungsfaktor verschiedenen Antriebskonfigurationen: *1* – Antriebssystem nach Abb.2; *2* – vier Gleichstromsteller mit L_1C_1-Filter am Eingang, nach Abb.1 *c*; *3* – zwei halbsteuerbare Brücken, eine Brücke löschbar; *4* – zwei halbsteuerbare Brücken in Folgesteuerung.

Unter Berücksichtigung der oben angenommenen Werte für α_1 und k_2/k_1 erhält man $\alpha_3 = 27,37°$. Für diesen Wert des Winkels α_3 setzt sich der Gesamtstrom i praktisch aus zwei rechtwinkligen Stromblöcken zusammen, die den Winkeln $\pi - 2\alpha_1$ entsprechen. Um eine Veränderung der Wirkleistung entsprechend der Beziehung (4) zu erhalten, schwanken die Winkel $\alpha^{(2)}$ und $\beta^{(2)}$ zwischen den Grenzen:

$$\frac{\pi}{2} < \alpha^{(2)} \leq \frac{\pi}{2} + \alpha_3, \quad \beta_1 < \beta^{(2)} \leq \frac{\pi}{2} - \alpha_3.$$

Im Falle der in Abb.4 veranschaulichten Steuermethode wird ebenfalls die Bedingung (1) eingehalten. Damit diese Bedingung erfüllt wird, genügen die regelbaren Winkel $\alpha^{(2)}$ und $\beta^{(2)}$ der Gleichung:

$$U_1(\cos\alpha_1 + \cos\alpha^{(2)}) = U_2 \cos\beta^{(2)} \tag{6}$$

erfüllen.

Wenn die Wirkleistung in den Grenzen:

$$\frac{\sin\alpha_4}{\cos\beta_1 + \cos\beta_2} P_{\max} \leq P < \frac{\sin\alpha_3}{\cos\beta_1 + \cos\beta_2} P_{\max} \tag{7}$$

variiert, wird die in Abb.5 wiedergegebene Steuermethode angewendet, bei der die Grenzwinkel α_4 und α_5 die Gleichung:

$$U_1(\cos\alpha_5 - \sin\alpha_4) = U_2 \sin\alpha_4 \tag{8}$$

erfüllen.

Wenn eine minimale Grenze von 10% $P_{\max}$ für die von der elektrischen Lokomotive beanspruchten Wirkleistung angenommen wird dann erhält man $\alpha_4 = 9,7°$ und $\alpha_5 = 68,84°$.

Aus Abb.6 kann die Schlußfolgerung gezogen werden, daß bei einer Wirkleistung über $0,2P_{max}$ der Leistungsfaktor λ des Speisungssystem aus Abb.2 einen erhöhten und befriedigenden Wert besitzt. Unter dem Wert von $0,2P_{max}$ sinkt der Leistungsfaktor λ bis auf 0,73 bei einer Leistung von $0,1P_{max}$. Zum Vergleich wurden im selben Abbildung durch die Kurven *2*, *3* und *4* die Veränderungen von λ für die Speisungssysteme aus Abb.1 *c*, *b* und *a* gezeichnet.

Was die Kondensatoren C_1 und C_2 in Abb.2 anbetrifft, so haben diese keine erhöhten Kapazitätswerte, weil sie keine Filterkondensatoren der gerichteten Spannungen u_{d1} und u_{d2} sind. Die Rolle dieser Kondensatoren besteht im Schutz der GTO-Thyristoren und der Dioden in der Stromrichterkomponente in Einphasen-Brückenschaltung bei Überspannungen. Diese Überspannungen treten bei der Blockierung der GTO-Thyristoren infolge der Streuungsinduktanz des Speisetransformators und der dem Speisenetz zugehörigen Induktanz auf. Die Kondensatoren C_1 und C_2 werden so dimensioniert, daß die Überspannungen ΔU (Abb.3) bestimmte angenommene Grenzen nicht überschreiten.

Eingegangen am 29. November 1994

Technische Universität „Gh.Asachi", Jassy, Lehrstuhl für Angewandte Elektronik

LITERATURVERZEICHNIS

1. Eggenberger H.P., *Renaissance der Eisenbahn.* Bull. SEV, **77**, *5*, 229-230 (1986).
2. Depenbrock M., *Einphasen-Stromrichter mit sinusförmigen Netzstrom und gut geglätteten Gleichgrössen.* ETZ-A, Elektrotech. Z., **94**, *8*, 466-471 (1973).
3. Gemmeke K., *Supression of Narow-Band Harmonics in the Input Current of Traction Vehicles.* 3 IFAC Sympos. „Control in Power Electronics and Electrical Drives", Lausanne, 1983, Konf. Bd., 627-634.
4. Appun P., Lienau W., *Der Vierquadrantensteller bei induktivem und kapazitivem Betrieb.* etzArchiv, 6, *1*, 3-8 (1984).
5. Holtz J., Krah J., *Adaptive Optimal Pulse Width Modulation for the Line-Side Converter of Electric Locomotives.* 3rd Eur. Conf. on Power Electron. a. Appl., Aachen, 1989, Konf.-Bd., 567-572.
6. Alexa D., *GTO-Frequenzumrichter mit Wechselrichtern mit zwei Abzweigungen für elektrische Hochgeschwindigkeits Lokomotiven.* Bull. SEV, **82**, *19*, 43-48 (1991).
7. Kemp R.J., *GTO Choppers for Rail Vehicles.* GEC Review, **5**, *1*, 18-21 (1989).
8. Steimel A., *Netzbelastung durch Wechselstrom-Triebfahrzeuge mit leistungselektronischer Steuerung.* etzArchiv, **12**, *3*, 69-79 (1990).
9. Heumann K., *Basic Principles of Power Electronics.* Springer, Berlin–Heidelberg–New-York–London–Paris–Tokyo, 1986.
10. Leonhard W., *Control of Electrical Drives.* Springer, Berlin–Heidelberg–New-York–Tokyo, 1985.
11. Destobbeleer E., Seguier G., Castelain A., *AC-DC Converter Minimizing Induced Harmonics in Industrial Power Systems.* Proc. of the 16th Annual IEEE Power Electronics Specialists Conf., Toulouse, June 24-28, 1985, 573-580.

SISTEM DE ALIMENTARE CU FACTOR DE PUTERE RIDICAT PENTRU MOTOARELE ELECTRICE DE TRACŢIUNE DE CURENT CONTINUU ALE UNEI LOCOMOTIVE

(Rezumat)

Se prezintă o nouă schemă de principiu pentru sistemul de alimentare cu tensiune variabilă a motoarelor de tracţiune de c.c. plasate pe o locomotivă, precum şi o nouă metodă de comandă. Comanda succesivă aplicată dispozitivelor GTO din componenţă, de tip asimetric, permite obţinerea unui factor de putere ridicat la intrare, fără să necesite circuite de filtrare sau compensatoare statice de putere reactivă. Rezultatele obţinute sunt comparate cu performanţele sistemelor de alimentare pentru motoarele de c.c. de tracţiune cunoscute.

BULETINUL INSTITUTULUI POLITEHNIC DIN IAŞI
Tomul XLI (XLV), Fasc. 3-4, 1995
Secţia III
ELECTROTEHNICĂ. ENERGETICĂ. ELECTRONICĂ

C.D. 621.313.333.021.2; 621.3.016.1

CONSIDÉRATIONS SUR LE COUPLE ÉLECTROMAGNÉTIQUE DU SERVOMOTEUR ASYNCHRONE BIPHASÉ

PAR
RADU COCIU et LIVIA COCIU

1. Introduction

L'utilisation du servomoteur asynchrone biphasé (SAB) dans les systèmes de réglage automatique est fort convenable. Le SAB possède les qualités d'un moteur d'induction et, en outre, des multiples moyens de commande (en fréquence, en amplitude et en phase) et aussi la séparation électrique entre les enroulements statoriques.

Pour mettre en valeur ses qualités il faut connaître, tant bien que possible, ses caractéristiques mécaniques et de réglage. En ce que suit on propose l'établissement d'une expression plus précise pour le couple électromagnétique, en gardant une forme acceptable que l'on peut facilement utiliser dans l'étude des systèmes automatiques basés sur le SAB.

2. Expression du couple électromagnétique du SAB

On utilise le schéma électrique équivalent (Fig.1), représentant une machine électrique généralisée type $DQ - dq$. Les enroulements statoriques d'excitation (e) et de commande (d) sont placés à travers les axes D et Q; le rotor possède deux enroulements identiques, mis en court-circuit par des balais, placés à travers les axes d et q.

On suppose la machine non-saturée. Le rotor tourne avec une vitesse angulaire ω_R, liée à la vitesse angulaire du champ tournant statorique ω_s par la relation:

$$\omega_R = \omega_s(1 - s), \tag{1}$$

où s représente le glissement. On utilise les notations: R_e, R_c, R pour les résistances des enroulements d'excitation, de commande et rotoriques équivalentes; L_e, L_c, $L_r = L_d = L_q$ et $M = M_{er} = M_{cr}$, pour les inductances propres et celles mutuelles entre les enroulements. On suppose tous les enroulements ayant le même nombre de spires; sinon, on considère les valeurs rapportées au nombre de spires de l'enroulement d'excitation. Dans ce cas toutes les inductances mutuelles ont la même

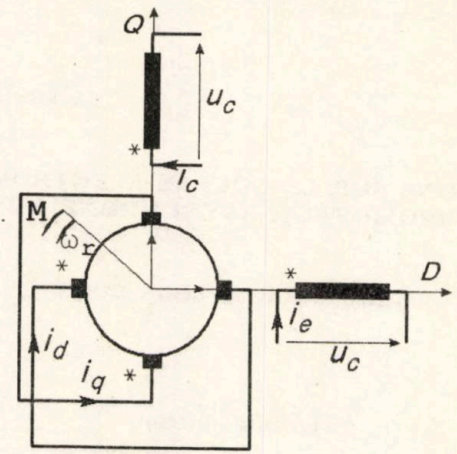

Fig. 1

valeur, M. On introduit les notations: $L_{\sigma e}, L_{\sigma c}$ et $L_{\sigma r}$ pour les inductances de fuites des enroulements d'excitation, de commande et rotorique. Les équations qui caractérisent le fonctionnement du SAB ont la forme:

$$\begin{bmatrix} u_e \\ u_c \\ 0 \\ 0 \end{bmatrix} =$$

$$(2) \quad = \begin{bmatrix} R_e + (L_{\sigma e} + M)\frac{\mathrm{d}}{\mathrm{d}t} & 0 & 0 & M\frac{\mathrm{d}}{\mathrm{d}t} \\ 0 & R_c + (L_{\sigma c} + M)\frac{\mathrm{d}}{\mathrm{d}t} & M\frac{\mathrm{d}}{\mathrm{d}t} & 0 \\ -\omega_R M & M\frac{\mathrm{d}}{\mathrm{d}t} & R + (L_{\sigma r} + M)\frac{\mathrm{d}}{\mathrm{d}t} & -\omega_R(L_{\sigma r} + M) \\ M\frac{\mathrm{d}}{\mathrm{d}t} & \omega_R M & \omega_R(L_{\sigma r} + M) & R + (L_{\sigma r} + M)\frac{\mathrm{d}}{\mathrm{d}t} \end{bmatrix} \times$$

$$\times \begin{bmatrix} i_e \\ i_c \\ i_q \\ i_d \end{bmatrix}.$$

On suppose l'alimentation des enroulements statoriques avec des tensions sinusoïdales. Dans ce cas tous les courants sont aussi sinuisoïdaux et on peut passer à la représentation en complexe. Par conséquent à $M\mathrm{d}/\mathrm{d}t$ correspond $\mathrm{j}\omega_s M = \mathrm{j}X_m$; de même $\omega_R M = \nu X_m$, où $\nu = \omega_R/\omega_s$ est la vitesse angulaire relative de rotation du rotor (par rapport à la vitesse du champ tournant). On suppose les deux enroulements statoriques identiques, donc $R_e = R_c = R_1, L_{\sigma e} = L_{\sigma c} = L_{\sigma 1}$. On introduit les notations: $X_1 = X_{\sigma 1} + X_m = \omega_s L_{\sigma 1} + \omega_s M$ et $X_2 = X_{\sigma 2} + X_m = \omega_s L_{\sigma 2} + \omega_s M$.

On obtient:

$$(3)\qquad \begin{bmatrix} \underline{U}_e \\ \underline{U}_c \\ 0 \\ 0 \end{bmatrix} = \begin{bmatrix} R_1 + \mathrm{j}X_1 & 0 & 0 & \mathrm{j}X_m \\ 0 & R_1 + \mathrm{j}X_1 & \mathrm{j}X_m & 0 \\ -\nu X_m & \mathrm{j}X_m & R + \mathrm{j}X_2 & -\nu X_2 \\ \mathrm{j}X_m & \nu X_m & \nu X_2 & R + \mathrm{j}X_2 \end{bmatrix} \begin{bmatrix} \underline{I}_e \\ \underline{I}_c \\ \underline{I}_q \\ \underline{I}_d \end{bmatrix}.$$

La valeur instantanée du couple, pour la machine multipolaire, est:

$$(4)\qquad \mathcal{M}e = \frac{p_m}{\Omega} = \frac{p_m}{\omega_R/p} = \frac{p}{\omega_R}\dot{\theta}[I]_t[G][I] = p[I]_t[I],$$

où p est le nombre de paires de pôles, $\dot{\theta} = \omega_R, p_m$ – la puissance électrique convertie en puissance mécanique. La valeur moyenne du couple pour la machine multipolaire a la forme:

$$(5)\qquad M_e = p\Re e\{[I]_t^*[G][I]\}.$$

Pour les machines qui ne possèdent pas des pôles saillants on a:

$$(6)\qquad M_e = p\Re e[M(\underline{I}_Q\underline{I}_d - \underline{I}_D\underline{I}_q] = p\frac{X_m}{\omega_R}\Re e(\underline{I}_c\underline{I}_d^* - \underline{I}_e\underline{I}_q^*).$$

Pour simplifier les calculs on utilise les notations suivantes, pour les impédances normalisées par rapport à X_m:

$$(7)\qquad a = \frac{R_1}{X_M},\quad b = \frac{X_1}{X_M},\quad c = \frac{R}{X_m},\quad d = \frac{X_2}{X_m}.$$

En utilisant ces notations, le déterminant principal du système d'équations (3) prend la forme:

$$(8)\qquad \begin{aligned} \underline{\Delta} &= \begin{vmatrix} X_m(a+\mathrm{j}b) & 0 & 0 & \mathrm{j}X_m \\ 0 & X_m(a+\mathrm{j}B) & \mathrm{j}X_m & 0 \\ -\nu X_m & \mathrm{j}X_m & X_m(c+\mathrm{j}d) & -\nu d X_m \\ \mathrm{j}X_m & \nu X_m & \nu d X_m & X_m(c+\mathrm{j}d) \end{vmatrix} = \\ &= X_m^4 \begin{vmatrix} a+\mathrm{j}b & 0 & 0 & \mathrm{j} \\ 0 & a+\mathrm{j}b & \mathrm{j} & 0 \\ -\nu & \mathrm{j} & c+\mathrm{j}d & -\nu d \\ \mathrm{j} & \nu & \nu d & c+\mathrm{j}d \end{vmatrix} = X_m^4\underline{\Delta}'. \end{aligned}$$

On peut déterminer les expressions des courants:

$$(9)\qquad \begin{aligned} \underline{I}_e &= \frac{\underline{U}_e\underline{A} - \underline{U}_c\underline{B}}{X_m\underline{\Delta}'},\quad \underline{I}_c = \frac{\underline{U}_e\underline{B} - \underline{U}_c\underline{A}}{X_m\underline{\Delta}'}, \\ \underline{I}_q &= \frac{\underline{U}_e\underline{C} - \underline{U}_c\underline{D}}{X_m\underline{\Delta}'},\quad \underline{I}_d = \frac{\underline{U}_e\underline{D} - \underline{U}_c\underline{C}}{X_m\underline{\Delta}'}, \end{aligned}$$

où on a utilisé les notations:

$$\begin{aligned}
&\underline{A} = ac^2 - ad^2 - 2bcd + c + ad^2\nu^2 + \mathrm{j}(bc^2 - bd^2 + 2acd + d + bd^2\nu^2 - d\nu^2),\\
&\underline{B} = -\mathrm{j}c\nu, \quad \underline{C} = ac\nu + \mathrm{j}bc\nu,\\
&\underline{D} = -bc - ad + ad\nu^2 + \mathrm{j}(ac - bd + 1 - \nu^2 + bd\nu^2).
\end{aligned} \tag{10}$$

Tous calculs effectués on obtient:

$$\Re e(\underline{I}_c\underline{I}_d^* - \underline{I}_e\underline{I}_q^*) = -\frac{\Re e}{X_m^2\underline{\Delta}'^2}[-(U_e^2 + U_c^2)\mathrm{j}2\Im m(\underline{U}_e\underline{U}_c^*)(\underline{AD}^* - \underline{BC}^*)]. \tag{11}$$

Les deux enroulements statoriques sont alimentés avec des tensions sinusoïdales déphasées d'un angle ψ, ayant des amplitudes différentes:

$$\underline{U}_e = U_e\mathrm{e}^{\mathrm{j}0}, \qquad \underline{U}_c = \lambda U_e\mathrm{e}^{-\mathrm{j}\psi}, \tag{12}$$

où $\lambda = U_c/U_e$ représente le coefficient du signal. En ces conditions (11) devient:

$$\begin{aligned}
&\Re e(\underline{I}_c\underline{I}_d^* - \underline{I}_e\underline{I}_q^*) =\\
&= -\frac{U_e^2(1+\lambda^2)c\nu}{X_m^2\Delta'^2}\{(a^2+b^2)(c^2+d^2) + 2bd - 1 + \nu^2[d^2(a^2+b^2) - 2bd + 1]\} +\\
&\quad + 2c\lambda U_e^2\sin\psi\{[(a^2+b^2)(c^2+d^2) + 2ac - 2bd + 1] -\\
&\quad - \nu^2[(a^2+b^2)d^2 + 2ac - 2bd + 1]\}.
\end{aligned} \tag{13}$$

Le déterminant $\underline{\Delta}'$ a l'expression:

$$\underline{\Delta}' = E + F\nu^2 + \mathrm{j}(G + H\nu^2), \tag{14}$$

où on a utilisé les notations:

$$\begin{aligned}
&E = (a^2 - b^2)(c^2 - d^2) + (1 - 2bd)(1 + 2ac), \quad F = (a^2 - b^2)d^2 + 2bd - 1,\\
&G = 2(ad + bc)(ac - bd + 1), \quad H = 2ad(bd - 1).
\end{aligned} \tag{15}$$

Dans ces circonstances on peut obtenir:

$$\Delta'^2 = E^2 + G^2 + 2\nu^2(EF + GH) + \nu^4(F^2 + H^2). \tag{16}$$

L'expression du couple électromagnétique moyen, M_e, possède deux composants à savoir:

$$\begin{aligned}
M_e = &-\frac{pU_e^2(1+\lambda^2)\nu c}{\omega_s x_m}\cdot\frac{(a^2+b^2)(c^2-d^2) + 2bd - 1 + \nu^2[(a^2+b^2)d^2 - 2bd + 1]}{E^2 + G^2 + 2\nu^2(EF+GH) + \nu^4(F^2+H^2)} +\\
&+\frac{2pU_e^2\lambda c\sin\psi}{\omega_s x_m}\cdot\frac{(a^2+b^2)(d^2+c^2) + 2ac - 2bd + 1 - \nu^2[(a^2+b^2)d^2 + 2ac - 2bd + 1]}{E^2 + G^2 + 2\nu^2(EF+GH) + \nu^4(F^2+H^2)}.
\end{aligned} \tag{17}$$

On peut obtenir le couple de démarrage pour la valeur $\nu = 0$:

$$M_{ep} = \frac{2pU_e^2 \lambda c \sin\psi}{\omega_s x_m} \cdot \frac{(a^2+b^2)(d^2+c^2)+2ac-2bd+1}{E^2+G^2}. \tag{18}$$

Il résulte la valeur maximum pour un champ tournant circulaire ($\lambda = 1$, $\sin\psi = 1$):

$$M_{epm} = \frac{2pU_e^2 c}{\omega_s x_m} \cdot \frac{(a^2+b^2)(d^2+c^2)+2ac-2bd+1}{E^2+G^2}. \tag{19}$$

En passant à la normalisation du couple moyen par rapport à la valeur maximum du couple de démarrage, on obtient:

$$m_e = \frac{M_e}{M_{epm}} = \frac{\lambda \sin\psi(1-\nu^2 a_1) - \frac{\nu(1+\lambda^2)}{2}(a_2+\nu^2 a_3)}{1+\nu^2 b_1+\nu^4 b_2}, \tag{20}$$

où:

$$\begin{aligned} a_1 &= \frac{(a^2+b^2)d^2+2ac-2bd+1}{(a^2+b^2)(c^2+d^2)+2ac-2bd+1}, \\ a_2 &= \frac{(a^2+b^2)(c^2-d^2)+2bd-1}{(a^2+b^2)(c^2+d^2)+2ac-2bd+1}, \\ a_3 &= \frac{(a^2+b^2)d^2-2bd+1}{(a^2+b^2)(c^2+d^2)+2ac-2bd+1}, \\ b_1 &= \frac{2(EF+GH)}{E^2+G^2}, \qquad b_2 = \frac{F^2+H^2}{E^2+G^2}. \end{aligned} \tag{21}$$

L'expression du couple relatif (20) du SAB présente un très haut degré de généralité, mais sa forme est assez compliquée. En utilisant les relations (8), (14) et (20) et en les substituant en (19), on peut obtenir la valeur normalisée du couple en fonction du coefficient du signal λ, du déphasage ψ et de la vitesse relative du rotor ν. Les coefficients a_1, a_2 et a_3 ne sont pas indépendants, étant liés par la relation:

$$a_1 + a_2 + a_3 = 1. \tag{22}$$

Pour les SAB réels, les inductances de fuites sont beaucoup plus faibles que celles mutuelles ($x_{\sigma_1} \ll x_m$, $x_{\sigma_2} \ll x_M$) et on peut donc, en première approximation, les négliger; on peut aussi négliger la résistance des enroulements statoriques ($R_1 \approx 0$). La résistance du rotor a, par construction, une valeur assez grande qu'on ne peut pas la négliger. Par conséquent:

$$x_1 \simeq x_m, \qquad x_2 \simeq x_m. \tag{23}$$

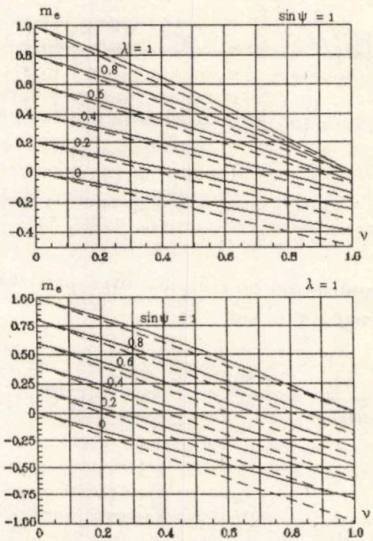

Fig. 2

En ces circonstances on trouve:

$$(24) \qquad a = 0, \quad b = 1, \quad d = 1; \qquad E = -c^2, \quad F = 0, \quad G = 0, \quad H = 0$$

et pour les coefficients:

$$(25) \qquad a_1 = 0, \quad a_2 = 1, \quad a_3 = 0, \quad b_1 = 0, \quad b_2 = 0.$$

En ce cas l'expression du couple est beaucoup plus simple et bien connue:

$$(26) \qquad m_e = \lambda \sin\psi - \frac{\nu(1+\lambda^2)}{2}.$$

La caractéristique mécanique représente la dépendance $\nu = f(m_e)$ pour différentes valeurs constantes des paramètres λ et $\sin\psi$. Dans la Fig.2 on représente la forme de la caractéristique mécanique pour $\sin\psi = 1$ et λ variable et aussi pour $\lambda = 1$ et $\sin\psi$ variable; les lignes épaisses représentent les caractéristiques établies à l'aide de l'équation (20) d'un SAB ayant les paramètres suivants: $a = 0,13, b = 1,2, c = 1,55, d = 1,2$. En utilisant ces données on obtient:

$$(27) \qquad \begin{gathered} E = -4,007, \quad F = -0,1693, \quad G = -0,9616, \quad H = 0,1373; \\ a_1 = 0,15067, \; a_2 = 0,7964, \; a_3 = 0,05288; \quad b_1 = 0,06433, \; b_2 = 0,00279. \end{gathered}$$

Les caractéristique obtenues en négligeant les inductances de fuites et les résistances statoriques sont représentées par des lignes interrompues. On peut remarquer la similitude des caractéristiques, ce que justifie l'utilisation de l'équation (26), beaucoup plus simple. Mais, pour les applications de grande précision, l'équation (20) est bien plus exacte. On peut constater une erreur de 20%, surtout en freinage, ce que n'est pas du tout négligeable.

3. Conclusions

On établit l'équation du couple électromagnétique d'un SAB en tenant compte, non seulement de la résistance rotorique et de l'inductance mutuelle, comme d'habitude, mais aussi de la résistance statorique et des inductances de fuites statorique et rotorique. L'équation est plus complexe et utilise cinq coefficients calculés à partir des paramètres du SAB. La caractéristique mécanique obtenue en utilisant cette équation est beaucoup plus précise surtout en régime de freinage. L'équation met en évidence des particularités de la caractéristique mécanique qu'on les perd en ignorant la résistance statorique et les inductances de fuites.

Reçue le 17 mars 1994

Université Technique „Gh. Asachi", Jassy,
Chaire d'Électrotechnique
et Machines électriques

BIBLIOGRAPHIE

1. B o l d e a I., *Identificarea parametrilor maşinilor electrice.* Ed. Acad. Române, Bucureşti, 1991.
2. M ă g u r e a n u R., V a s i l e N., *Servomotoare fără perii de tip sincron.* Ed. Tehn., Bucureşti, 1990.
3. S i m i o n A., *Maşini electrice speciale.* Inst. polit., Iaşi, 1992.

CONSIDERAŢII ASUPRA CUPLULUI ELECTROMAGNETIC AL SERVOMOTORULUI ASINCRON BIFAZAT

(Rezumat)

Se prezintă modul de stabilire a ecuaţiei cuplului electromagnetic al servomotorului asincron bifazat, ţinând cont nu numai de rezistenţa rotorică şi de inductanţa mutuală, ci şi de rezistenţa statorică şi inductanţele de dispersie ale înfăşurărilor. Ecuaţia cuplului electromagnetic, normată în raport cu valoarea de pornire a cuplului, este mai complexă, conţinând cinci coeficienţi ai servomotorului. Rezultatele obţinute prin utilizarea acestei ecuaţii sunt mai precise, punând în evidenţă aspecte pe care ecuaţia clasică, stabilită pe baza neglijării rezistenţei statorice şi a inductanţelor de dispersie, nu le poate semnala.

Deşi stabilită pentru servomotorul asincron bifazat, ţinând cont de faptul că se bazează pe modelul unei maşini electrice generalizate tip $DQ - dq$, ecuaţia poate fi utilizată şi în cazul maşinilor asincrone monofazate sau trifazate, prezentând deci un ridicat grad de generalitate.

BULETINUL INSTITUTULUI POLITEHNIC DIN IAŞI
Tomul XLI (XLV), Fasc. 3–4, 1995
Secţia III
ELECTROTEHNICĂ. ENERGETICĂ. ELECTRONICĂ

D.C. 621.313.333.021.2; 621.3.018.3

TWO-PHASE SQUIRREL-CAGE INDUCTION MACHINE WORKING, DRIVEN BY A PWM CONVERTER, CONSIDERING THE EFFECTS OF THE CURRENT HARMONICS

BY

MIRCEA GOGU

1. Introduction

The study of the MMF effects in the asynchronous machine working began early, at the same time with the machine theory, because the torque-speed characteristic presents some irregularities in the low speed domain.

The obtained results presented in [1],..,[3] correspond to a balanced configuration machine and don't include the cases of unbalanced or single-phase induction machines. In [4] a study of MMF of the even and odd harmonics effects in single-phase squirrel cage induction machine working is presented.

Moreover, most of these studies refer to the odd harmonics effects, since halfcycle symmetry is imposed. Because in the last time the PWM converters are very used to command asynchronous machines in variable speed drivers, the study of current harmonics effects in the induction machine working is imposed.

In what follows the coupled circuit method is used. The differential equations describing the induction machine working are obtained. These equations are mathematically manipulated, so that the obtained model describes in a simple manner the steady-state behaviour of the induction machine.

2. Simplifying Assumptions

1. The MMF has a uniform space distribution. So, the space harmonics, obtained from the real form of the winding function $w = w(\theta)$ and those due to the permeance variation by slot openings are neglected.

2. The airgap is uniform.

3. The magnetic circuit saturation is neglected.

4. The windings are identically and have their fundamental components orthogonal in space.

5. The rotor cage is considered to be ideally, yielding a flux of the same form as that which is impressed upon it.

3. Basic Equations

The two statoric windings have the folowing equations:

$$(1) \qquad w_a(\theta) = w_s \cos\theta, \quad w_b(\theta) = w_s \cos\left(\theta - \frac{\pi}{2}\right).$$

The windings of the rotor cage are not readily defined. It must posses a set of orthogonal windings, described by the equations:

$$(2) \qquad w_x(\theta) = w_r \cos(\theta - \theta_r), \quad w_y(\theta) = w_r \sin(\theta - \theta_r).$$

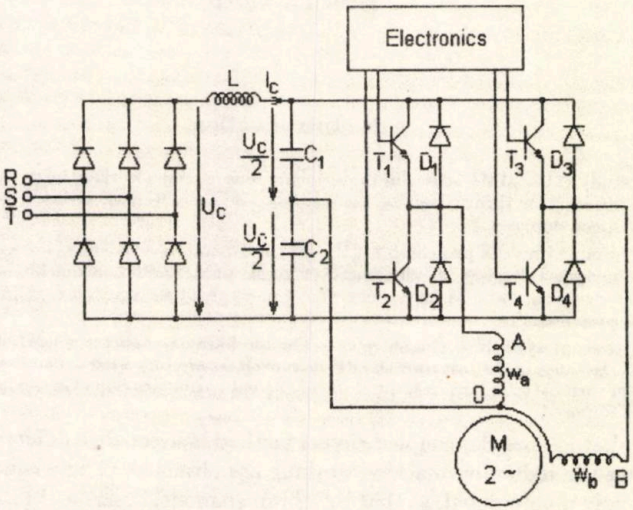

Fig. 1

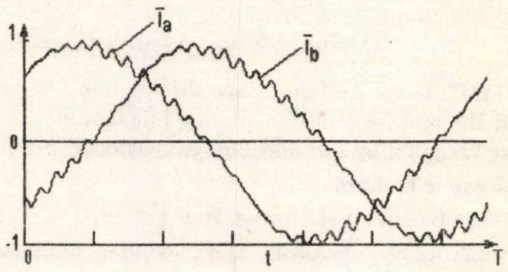

Fig. 2

According to Fig.2, the currents $i_a = i_a(t)$ and $i_b = i_b(t)$ are obtained from the voltages $v_a = v_a(t)$ and $v_b = v_b(t)$, which are applied on the machine windings in Fig.1.

The induction machine is described by the following equations:

$$[v] = [R][i] + \mathrm{d}([L][i]) \tag{3}$$

or

$$\begin{bmatrix} v_{a\nu} \\ v_{b\nu} \\ v_{x\nu} \\ v_{y\nu} \end{bmatrix} = \begin{bmatrix} R_{a\nu} & 0 & 0 & 0 \\ 0 & R_{b\nu} & 0 & 0 \\ 0 & 0 & R_{r\nu} & 0 \\ 0 & 0 & 0 & R_{r\nu} \end{bmatrix} \begin{bmatrix} i_{a\nu} \\ i_{b\nu} \\ i_{x\nu} \\ i_{y\nu} \end{bmatrix} + \mathrm{d} \begin{bmatrix} L_{aa\nu} & L_{ab\nu} & L_{ax\nu} & L_{ay\nu} \\ L_{ab\nu} & L_{bb\nu} & L_{bx\nu} & L_{by\nu} \\ L_{ax\nu} & L_{bx\nu} & L_{xx\nu} & L_{xy\nu} \\ L_{ay\nu} & L_{by\nu} & L_{xy\nu} & L_{yy\nu} \end{bmatrix} \begin{bmatrix} i_{a\nu} \\ i_{b\nu} \\ i_{x\nu} \\ i_{y\nu} \end{bmatrix}. \tag{4}$$

The inductances of the harmonic machine may be evaluated in terms of the winding equations by the method illustrated in [6] and given in Appendix; consequently Eq.(4) may be written:

$$\begin{bmatrix} v_{a\nu} \\ v_{b\nu} \\ v_{x\nu} \\ v_{y\nu} \end{bmatrix} = \begin{bmatrix} R_{a\nu} & 0 & 0 & 0 \\ 0 & R_{b\nu} & 0 & 0 \\ 0 & 0 & R_{r\nu} & 0 \\ 0 & 0 & 0 & R_{r\nu} \end{bmatrix} \begin{bmatrix} i_{a\nu} \\ i_{b\nu} \\ i_{x\nu} \\ i_{y\nu} \end{bmatrix} + \tag{5}$$

$$+\mathrm{d} \begin{bmatrix} L_s & 0 & L_{sr}\cos\theta_r & -L_{sr}\sin\theta_r \\ 0 & L_s & L_{sr}\sin\theta_r & L_{sr}\cos\theta_r \\ L_{sr}\cos\theta_r & L_{sr}\sin\theta_r & L_r & 0 \\ -L_{sr}\sin\theta_r & L_{sr}\cos\theta_r & 0 & L_r \end{bmatrix} \begin{bmatrix} i_{a\nu} \\ i_{b\nu} \\ i_{x\nu} \\ i_{y\nu} \end{bmatrix}.$$

The transformation from rotating to stationary axes is effected by assuming a pair of stationary harmonic windings with new independent currents that will produce the same airgap MMF as the rotating harmonic rotor windings with their currents. The stationary α and β coils have the following winding equations:

$$w_\alpha(\theta) = w_r \cos\theta, \quad w_\beta(\theta) = w_r \sin\theta, \tag{6}$$

where currents $i_{\alpha\nu}$ and $i_{\beta\nu}$, respectively, are postulated as being able to provide the necessary equivalent MMF:

$$w_x(\theta) i_{x\nu} + w_y(\theta) i_{y\nu} = w_\alpha(\theta) i_{\alpha h} + w_\beta(\theta) i_{\beta h}. \tag{7}$$

Substituting (2) in (7), it results:

$$w_r i_{x\nu} \cos\theta_r - w_r i_{y\nu} \sin\theta_r = w_\alpha i_{\alpha\nu}, \quad w_r i_{x\nu} \sin\theta_r + w_r i_{y\nu} \cos\theta_r = w_\beta i_{\beta\nu}. \tag{8}$$

These equations define an orthogonal transformation if $w_\alpha = w_\beta = w_r$, and power invariant if the same transformation is used for the voltage variables as well as the current ones.

One defines the matrix transformation:

$$[C] = \begin{bmatrix} 1 & 0 & 0 & 0 \\ 0 & 1 & 0 & 0 \\ 0 & 0 & \cos\theta_r & -\sin\theta_r \\ 0 & 0 & \sin\theta_r & \cos\theta_r \end{bmatrix}. \tag{9}$$

Finally the harmonic machine is described by the following transformed $v-i$ equations:

$$[v_{\alpha\beta}] = [R_{\alpha\beta}]\mathrm{d}[i_{\alpha\beta}] + \dot{\theta}_r[S_{\alpha\beta}][i_{\alpha\beta}], \tag{10}$$

where:

$$[v_{\alpha\beta}] = [C][v] = \begin{bmatrix} v_{a\nu} \\ v_{b\nu} \\ v_{\alpha\nu} \\ v_{\beta\nu} \end{bmatrix}, \quad [i_{\alpha\beta}] = [C][i] = \begin{bmatrix} i_{a\nu} \\ i_{b\nu} \\ i_{\alpha\nu} \\ i_{\beta\nu} \end{bmatrix}; \tag{11}$$

$$[R_{\alpha\beta}] = [C][R][C]^{-1} = \begin{bmatrix} R_{a\nu} & 0 & 0 & 0 \\ 0 & R_{b\nu} & 0 & 0 \\ 0 & 0 & R_{r\nu} & 0 \\ 0 & 0 & 0 & R_{r\nu} \end{bmatrix}, \tag{12}$$

$$[L_{\alpha\beta}] = [C][L][C]^{-1} = \begin{bmatrix} L_s & 0 & L_{sr} & 0 \\ 0 & L_s & 0 & L_{sr} \\ L_{sr} & 0 & L_r & 0 \\ 0 & L_{sr} & 0 & L_r \end{bmatrix}, \tag{13}$$

$$[S_{\alpha\beta}] = [C]\frac{\mathrm{d}}{\mathrm{d}\theta_r}([L][C]^{-1}) = \begin{bmatrix} 0 & 0 & 0 & 0 \\ 0 & 0 & 0 & 0 \\ 0 & L_{sr} & 0 & L_r \\ -L_{sr} & 0 & -L_r & 0 \end{bmatrix}. \tag{14}$$

The steady-state case is carried out by recasting the equation variables as phasors and setting $\mathrm{d} = \mathrm{j}\nu\omega t$ and $\theta_r = (1-s)\nu\omega$:

$$\begin{cases} \underline{V}_{a\nu} = (R_s + \mathrm{j}X_{a\nu})\underline{I}_{a\nu} + \mathrm{j}X_{m\nu}\underline{I}_{\alpha\nu}, \\ 0 = \mathrm{j}X_{m\nu}\underline{I}_{a\nu} + (R_r + \mathrm{j}X_{r\nu})\underline{I}_{\alpha\nu} + (1-s)X_{m\nu}\underline{I}_{b\nu} + (1-s)X_{r\nu}\underline{I}_{\beta\nu}, \\ 0 = -(1-s)X_{m\nu}\underline{I}_{a\nu} - (1-s)X_{r\nu}\underline{I}_{\alpha\nu} + \mathrm{j}X_{m\nu}\underline{I}_{b\nu} + (R_r + \mathrm{j}X_{r\nu})\underline{I}_{\beta\nu}, \\ \underline{V}_{b\nu} = (R_s + \mathrm{j}X_{b\nu})\underline{I}_{\beta\nu} + \mathrm{j}X_{m\nu}\underline{I}_{\beta\nu}, \end{cases} \tag{15}$$

where: $X_{a\nu} = \nu\omega L_s = X_{b\nu} = X_{s\nu}$, $X_{m\nu} = \nu\omega L_{sr}$, $X_{r\nu} = \nu\omega L_r$, $X_{\sigma s\nu} = X_{s\nu} - -X_{m\nu}$, $X_{\sigma r\nu} = X_{r\nu} - X_{m\nu}$. Where appropriate, the harmonic self- and mutual

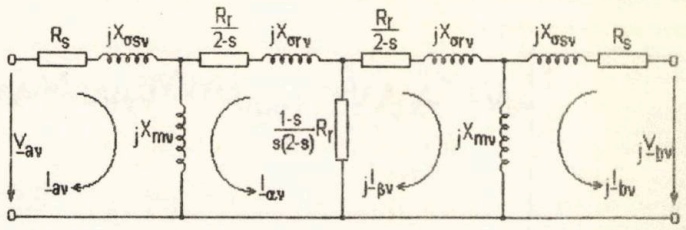

Fig. 3

inductance parameters have been combined to yield leakage inductances. The relations are summarized in the Notations at the end of the paper.

The equivalent circuit is presented in Fig.3.

The formula used to calculate L_{ss}, $L_{as\nu} = L_{bb\nu} = L_s$, $L_{ar\nu}$, $L_{sy\nu}$, $L_{ab\nu}$, $L_{br\nu}$, $L_{by\nu}$, $L_{rr\nu} = L_r$, $L_{ry\nu}$, $R_{a\nu} = R_{b\nu}$, $R_{r\nu}$ may be finded in Appendix.

4. Computer Simulation

This simulation takes into account the exact PWM and uses the equivalent circuit shown in Fig.3. We have considered a two-phase induction machine with the following parameters: $U_N = 80$ V, $I_N = 5$ A, $n_N = 1,430$ rot/min.

Using SPWM technique [7] to command the switches $T_1, ..., T_4$ from Fig.1, the machine windings will be delivered with a voltage waveform presented in Fig.4.

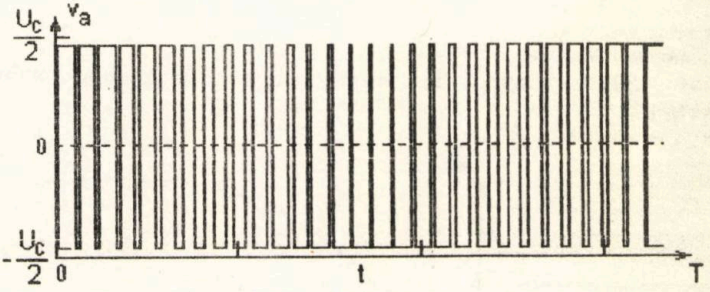

Fig. 4

For $f = 30$ Hz, $r = f_t/f = 30$ and $m = 1$, the electromagnetic torque waveform is presented in Fig.5, where one can observe the influence of the current harmonics on the electromagnetic torque waveform.

Since f has a variation range between 1 Hz and 35 Hz, the magnitude of the first 35 harmonics evolve versus frequency according to Fig.6.

For r=const. (=30) at low frequencies, the fundamental component is smaller than the 29-th harmonic order. In this frequency range the induction machine cannot work, because a significant harmonic torque drives on the rotor.

Once with the frequency increasing, the upper harmonics components decrease, the harmonic torque decreases too, and the induction machine approaches the

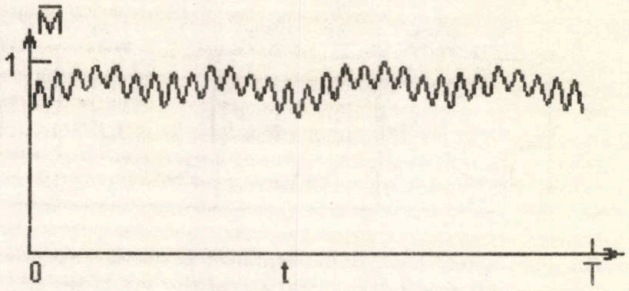

Fig. 5

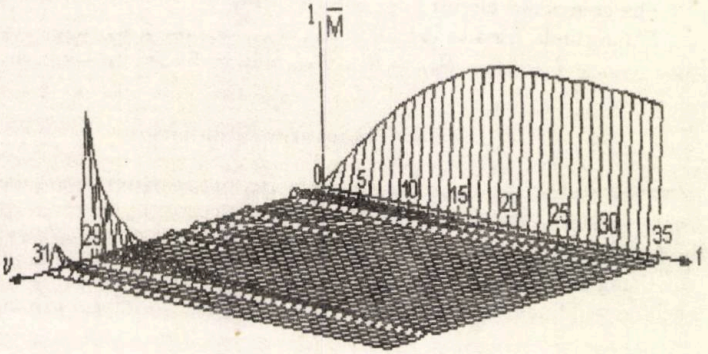

Fig. 6

normal working.

The variation of the average torque value in the above conditions is presented in Fig.7.

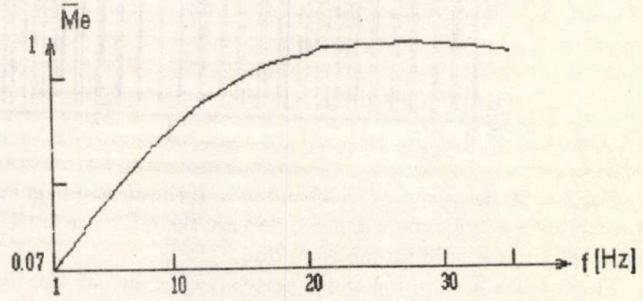

Fig. 7

The evolving of the maximum current value in the D.C. range, I_{cm}, and the average torque value versus r, at $f = 1$, $m = 1$, is presented in Figs.8 and 9.

At lower frequencies, for small values of r, the current I_{cm} increases significantly, fact that can be dangereous for the switches $T_1, ..., T_4$ or the induction machine windings. Because of the above reason, it is necessary that $r > 195$.

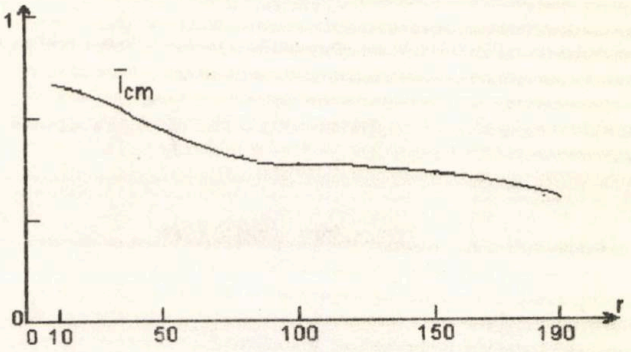

Fig. 8

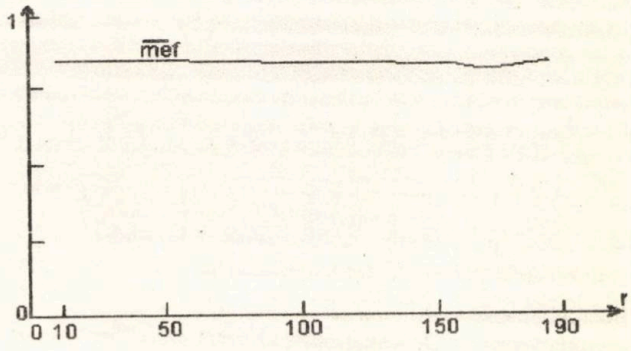

Fig. 9

According to Fig.9 the average torque value isn't significantly influenced by the parameter value r.

At upper values for r, the torque harmonics are of high frequency and they cannot yield mechanic rotor vibrations.

5. Conclusions

The primary result of this paper is the formulation of general equations and the development of an equivalent circuit to describe a two-phase machine with sinusoidal MMF and arbitrary harmonic current content.

The equivalent circuit are of practical value in predicting the starting performances and the steady-state behaviour of the machine at several tension frequencies (several working speed values).

At low speed (low frequencies of the delivery voltage), the electronic drive circuit of PWM converter have to contain algorithms which are necessary to eliminate the low frequency torque harmonics, because they provide mechanic vibration and irregularities in torque-speed characteristic.

Appendix

General formula presented in [6] and adapted for the followed goal in this paper are as follows:

(A.1) $$L_{ss} = \frac{\mu_0 rl}{\delta}\int_0^{2\pi} w_s^2(\theta)\mathrm{d}\theta, \quad L_{sr} = \frac{\mu_0 rl}{\delta}\int_0^{2\pi} w_a(\theta)w_r(\theta)\mathrm{d}\theta;$$

(A.2) $$L_{aa\nu} = \frac{\mu_0 rl}{\delta}\int_0^{2\pi} w_a^2(\theta)\mathrm{d}\theta = \frac{\mu_0 rl}{\delta}\int_0^{2\pi} (w_s\cos\theta)^2\mathrm{d}\theta = \frac{\mu_0 rl}{\delta}\pi w_s^2 = L_{bb\nu} = L_s;$$

(A.3) $$L_{ax\nu} = \frac{\mu_0 rl}{\delta}\int_0^{2\pi} w_a(\theta)w_x(\theta)\mathrm{d}\theta = \frac{\mu_0 rl}{\delta}\int_0^{2\pi} w_s w_r\cos\theta\cos(\theta-\theta_r)\mathrm{d}\theta =$$
$$= \frac{\mu_0 rl}{\delta}\pi w_s w_r\cos\theta_r = L_{sr}\cos\theta_r;$$

(A.4) $$L_{ay\nu} = \frac{\mu_0 rl}{\delta}\pi w_s w_r\sin\theta_r = -L_{sr}\sin\theta_r; \qquad \text{(A.5)} \quad L_{ab\nu} = 0;$$

(A.6) $$L_{bx\nu} = \frac{\mu_0 rl}{\delta}\pi w_s w_r\sin\theta_r = L_{sr}\sin\theta_r;$$

(A.7) $$L_{by\nu} = \frac{\mu_0 rl}{\delta}\pi w_s w_r\cos\theta_r = L_{sr}\cos\theta_r;$$

(A.8) $$L_{xx\nu} = \frac{\mu_0 rl}{\delta}\pi w_r^2 = L_{yy\nu} = L_r; \qquad \text{(A.9)} \quad L_{xy\nu} = 0;$$

(A.10) $$R_{a\nu} = R_{b\nu} = R_s; \quad R_{r\nu} = R_r.$$

Notations

$[C]$ – rotor transformation matrix;
$\mathrm{d} = \mathrm{d}/\mathrm{d}t$ – rate of change;
f – fundamental frequency;
i – instantaneous current, [A];
$[i]$ – instantaneous current matrix;
I – current (rms value), [A];
I_{cm} – D.C. link maximum current value;
$\mathrm{j} = \sqrt{-1}$ – operator;
l – rotor length, [m];
L – inductance, [H];
$[L]$ – inductance matrix;
m – modulation factor;
M – torque, [Nm];
R – resistance, [Ω];
$[R]$ – resistance matrix;
s – fundamental slip;
t – time;
T – fundamental period;
v – instantaneous voltage, [V];
$[v]$ – instantaneous voltage matrix;
w – number of turns;
X – reactance, [Ω];
δ – airgap, [m];
μ_0 – permeability of free space, [H/m];
ω – angular velocity or frequency, [rad/sec];
$\dot{\theta}$ – angular velocity, [rad/sec];

M_e – fundamental torque value;
m_{ef} – average torque value;
r – rotor radius, [m];
θ – angular displacement, [rad];
ν – order of harmonic.

Subscripts

a – stator winding a;
b – stator winding b;
c – D.C. parameter;
m – mutual reactance;
N – nominal parameter;
r – rotor;
s – stator;
t – triangular wave;
x – physical rotor x winding;
y – physical rotor y winding;
α – stationary rotor α winding;
β – stationary rotor β winding;
ν – order of harmonic;
σ – leakage.

Superscripts

-1 – inverse of matrix;
"–" – normalized value.

Received, May 6, 1994

Technical University "Gh.Asachi", Jassy,
Department of General Electrotechnics
and Electrical Machines

REFERENCES

1. Kron G., *Equivalent Circuits of Electric Machinery.* J. Wiley, New York, 1951.
2. Alger P.L., Ku T.H., Pan C.H.T., *Speed-Torque Calculations for Induction Motors with Part Windings.* AIEE Trans., **PAS-73**, 151-1660 (1954).
3. Buchnan L.W., *An Equivalent Circuit for a Single-Phase Motor Having Space Harmonics in its Magnetic Field.* IEEE Trans., **PAS-84**, 999-1007 (1965).
4. Davis J.H., Novotny D.W., *Equivalent Circuits for Single-Phase Squirrel-Cage Induction Machines with both Odd and Even Order MMF Harmonics.* IEEE Trans., **PAS-88**, 1080-1086 (1969).
5. Alexa D., Hrubaru O., *Applications of the Static Power Convertors* (in Romanian). Ed. Tehn., Bucureşti, 1989.
6. Schmitz N.L., Novotny D.W., *Introductory Electromechanics.* Ronald, New York, 1965.
7. Boost M., Ziogas P.D., *State of the Art of PWM Techniques: a Critical Evaluation.* IEEE Trans., **II** (1986).

FUNCŢIONAREA MOTORULUI ASINCRON BIFAZAT CU ROTOR ÎN SCURTCIRCUIT, COMANDAT DE UN CONVERTOR PWM, LUÂND ÎN CONSIDERARE EFECTELE ARMONICILOR DE CURENT

(Rezumat)

Se stabilesc ecuaţiile de funcţionare ale motorului asincron bifazat cu rotor în scurtcircuit, comandat printr-un convertor PWM. Ecuaţiile au fost deduse considerând că forţa magnetomotoare are o distribuţie spaţială sinusoidală, iar curentul prin înfăşurările maşinii are un conţinut de armonici determinat de tehnica PWM utilizată. Schema electrică echivalentă, corespunzătoare ecuaţiilor deduse, corespunde regimului static de funcţionare. Studiul funcţionării motorului asincron bifazat cu rotorul în scurtcircuit, în condiţiile precizate, a fost efectuat prin simulare pe calculator.

BULETINUL INSTITUTULUI POLITEHNIC DIN IAŞI
Tomul XLI (XLV), Fasc. 3–4, 1995
Secţia III
ELECTROTEHNICĂ. ENERGETICĂ. ELECTRONICĂ

D.C. 621.313.333

A NEW COMPLEX PARAMETER IN ESTABLISHING THE TRANSIENT MOVING REGIME OF LINEAR INDUCTION MOTORS

BY

CRISTINA SCHREINER, LORIN CANTEMIR and MARINEL TEMNEANU

1. Introduction

In the special electrical feeding parameters study for linear induction motor oscillators, the U/f=const. condition was reanalysed [1], [2], regarding the following aspects: a) the considered movement is composed by starts, stops and/or sense changings, being characterized by specific slip values (in the proximity of 1), much greater than the nominal ones; b) for the linear induction motor oscillators, the working manner is based on the transient behaviour and so, the dynamic equation of moving (that presumes a stable regime [1]) can not be used in classical form.

The estimation of moving parameters must also begin from the electrical equivalent circuit and according to the electrical feeding parameters.

2. Theoretical Considerations

The electrical equivalent circuit of a linear induction motor [4] is presented in Fig.1, where: R_1 is the phase inductor windings resistance; X_1 – the loss reactance; X_m – the magnetising reactance; R'_2 – the corrected value of armature resistance, all calculated for industrial frequency value.

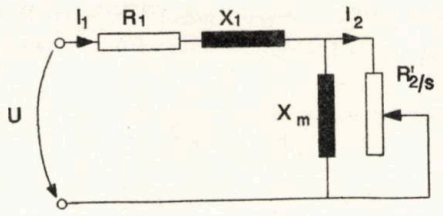

Fig. 1

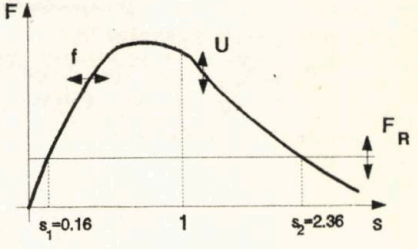

Fig. 2

The useful dissipated power in R_2' is:

$$P = Fv = 3X_m(I_{1r}I_{2a} - I_{1a}I_{2r}) \tag{1}$$

and the expression of the force is:

$$F = \frac{3U^2R_2'X_m^2}{V_s s\left[\left(\frac{R_2'}{s}\right)^2(R_1^2 + X_1^2 + X_m^2 + 2X_1X_m) + \frac{2R_1X_m^2R_2'}{s} + X_m^2(X_1^2 + R_1^2)\right]}. \tag{2}$$

Having in view the synchronism speed value:

$$v_s = 2f\tau_p, \tag{3}$$

the force reduced expression may be obtained:

$$F = \frac{KU^2 s}{f(\alpha s^2 + \beta s + \gamma)}, \tag{4}$$

with:

$$K = \frac{3R_2'X_m^2}{2\tau_p}. \tag{5}$$

The electric command field of motor speed using voltage and/or frequency was widelly presented in [2] and also the best characteristics and physical existing limits were determined.

The limit values of resistant force were established according to the voltage feeding value.

The dynamic equation in "slip"-variable becomes:

$$F(s) - F_R = ma = m\frac{\mathrm{d}v}{\mathrm{d}t} = -mv_s\frac{\mathrm{d}s}{\mathrm{d}t}. \tag{6}$$

Establishing the best frequency conditions of the control characteristic (e.g. $f = f_{\text{nom}}$=const.) the expression (4) is well determined and from equation (6) results the time of moving:

$$t = -mv_s\int_1^s \frac{\mathrm{d}s}{F(s) - F_R} = \frac{v_s}{g}\int_1^s \frac{\left(s^2 + \frac{\beta}{\alpha}s + \frac{\gamma}{\alpha}\right)\mathrm{d}s}{\left[s^2 + \left(\frac{\beta}{\alpha} - \frac{KU^2}{\alpha f F_R}\right)s + \frac{\gamma}{\alpha}\right]}. \tag{7}$$

The denominator admits two distinct positive roots, corresponding to the slip values for which the motor force is at least equal to the resistant force value ($F = F_R$ – Fig.2).

The roots values depend only on K – a constructive parameter, the electrical control characteristics (U, f) and armature resistant force, so the limits of electrical control field determined in [2] have now new theoretical significances.

With the roots s_1 and s_2, the expression of moving time is:

$$t = \frac{v_s}{g}\left(s - 1 + A\ln\frac{s - s_1}{1 - s_1} + B\ln\frac{s - s_2}{1 - s_2}\right). \tag{8}$$

The value of moving space results:

$$L = \int_0^t v\mathrm{d}t = -mv_s^2\int_1^s \frac{(1 - s)\mathrm{d}s}{F(s) - F_r},$$

i.e.

$$L = \frac{V_s^2}{g}\left[\frac{1 - s^2}{2} + (1 - A - B)(s - 1) + \right.$$
$$\left. + A(1 - s_1)\ln\frac{s - s_1}{1 - s_1} + B(1 - s_2)\ln\frac{s - s_2}{1 - s_2}\right]. \tag{9}$$

Under these circumstances there was observed that the same transient moving regime is obtained keeping constant the KU^2/fF_R term (generally speaking about a linear motor) or the U^2/fF_R term for a certain linear motor with a certain F_R-armature resistant force. A particular form is obtained for vertical oscillators, namely F_R=const. (armature weight), leading to U^2/f=const., according to the results obtained in [2].

Under these circumstances a new theoretical parameter is proposed, namely $P_C = KU^2/fF_R$, that describes the transient moving regime of any linear induction motor.

The real moving parameters and characteristics analyse of a linear motor oscillator must consider the P_C variable in determining the best transient regime and then, using the best found P_C value, the practical constructive (K, F_R) and command (U, f) conditions are well determined. The classical method which use a separate analyse for P_C complex parameter components is so avoided, beeing uneconomical.

3. Numerical Application

For the linear motor described in [4],...,[6], having the following parameters:

$R_1 = 0.452\ \Omega$, $R_2' = 0.264\ \Omega$, $X_m = 0.762\ \Omega$, $X_1 = 0.790\ \Omega$, $U_{\mathrm{nom}} = 37.60$ V, $f_{\mathrm{nom}} = 50$ Hz,

a vertical oscillation low-frequency regime (hammer purpose) was tested, with the following stages: a) motor regime of accelerated vertical climbing, on an imposed $L = 0.450$ m distance, followed by motor feeding cuting; b) extra vertical climbing, braked by the gravity effect; c) accelerated free

descending only under gravity effect (without motor feeding); d) final (instantaneous considered) stopping by inferior point hitting/refeeding the motor.

The resistant force is represented by the armature weight, $F_R = 80.5$, N=const. and the physical limits, as shown in Fig.2, are determined using the following values:

$$\alpha = 0.4810,\ \beta = 0.1386,\ \gamma = 0.1821,$$

(e.g. $s_1 = 2.36$ and $s_2 = 0.16$ for $U = U_{\text{nom}}$ and $f = f_{\text{nom}}$, corresponding to the $P_{C\text{nom}} = 1.35$ value).

The moving dynamic equations become:

$$t = 0.61\left(s - 1 + 3.014\ln\frac{2.36 - s}{1.36} - 0.204\ln\frac{s - 0.16}{0.84}\right),\ \text{[s]}; \tag{10}$$

$$L = 3.66\left[\frac{1 - s^2}{2} - 1.81(s - 1) - 4.1\ln\frac{2.36 - s}{1.36} - 0.17\ln\frac{s - 0.16}{0.84}\right],\ \text{[m]}. \tag{11}$$

The $F/F_R(s)$, $s(t)$ and $L(t)$ characteristics at different P_C values are represented in Figs.3,...,5, refering to the first accelerated stage. The real $s_1(P_C)$, $s_2(P_C)$ values are represented in Table 1 and Figs.6, 7. The constructive coefficient value is $K = 3.83$.

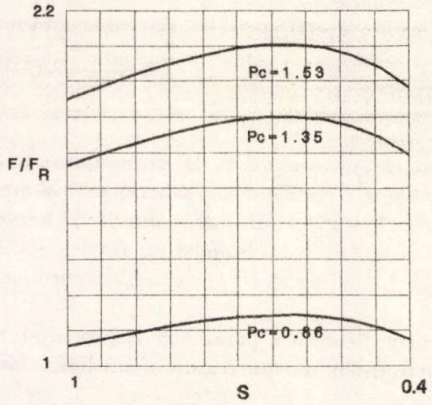

Fig. 3

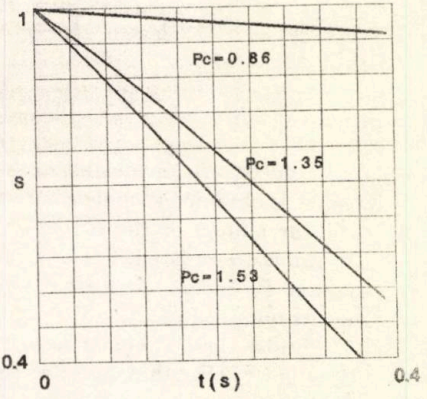

Fig. 4

Table 1

P_C	s_1	s_2	Observations
0.6	0.4796	0.4796	$F = F_{\max}$
0.7	0.4757	0.7954	$F < F_R$
0.8	0.3800	1.0001	Start. cond.
1	0.2447	1.5461	$F > F_R$
1.2	0.1873	2.0192	–
1.4	0.1532	2.4692	–
1.6	0.1301	2.9081	–
2	0.1003	3.7694	–
3	0.0643	5.8845	–
5	0.0375	10.069	Theor. value
9	0.0205	18.402	–

Table 2

Voltage, [V]	30	37.6	40
P_C	0.861	1.352	1.53
s_{fin}	0.84	0.55	0.48

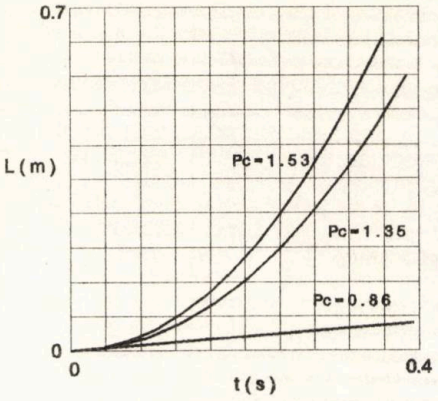

Fig. 5

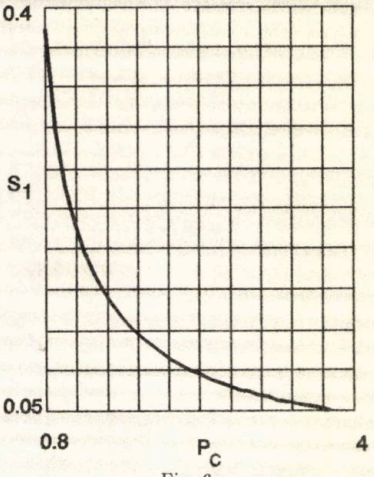

Fig. 6

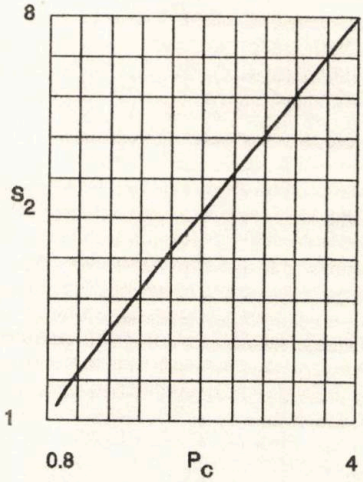

Fig. 7

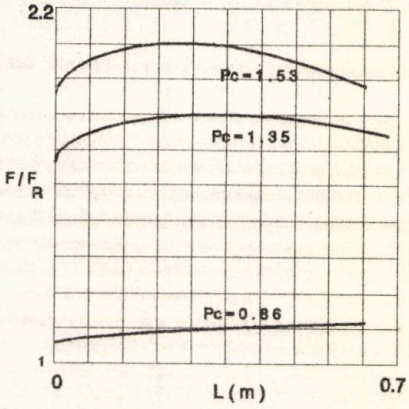

Fig. 8

The final slip values corresponding to imposed $L = 0.450$ m are presented in Table 2 for different P_C values (obtained by modifying the voltage value) and some transient moving characteristics are represented in Figs.8,...,10. The final slip values are remote from nominal $s_{nom} = 0.15$ one, so that this way of dynamic equation studying is fully justified.

The theoretical permitted interval for P_C values is comprised between $P_{C\,min} = 0.8$ (from $s_2 = 1$ starting condition) and $P_{C\,max} = 3$ (determined as $KU^2_{max}/F_{R\,min}f_{min}$, like in [2]).

At the same imposed moving amplitude the final oscillation frequencies are presented in Table 3, for different P_C values.

A desired value of mechanical oscillation frequency imposes, as expected, a sharp P_C value and, regarding the imposed F_R value, the corresponding U value can be calculated.

The founded variants, at P_C=const., are corresponding to very close intervals, and there are no major modifications of the mechanical oscillation value, because the transient regime of the motor depends, mainly, on the (K, F_R) construction parameters and destination (e.g. a optimum of 1 Hz was identified for the presented application variant).

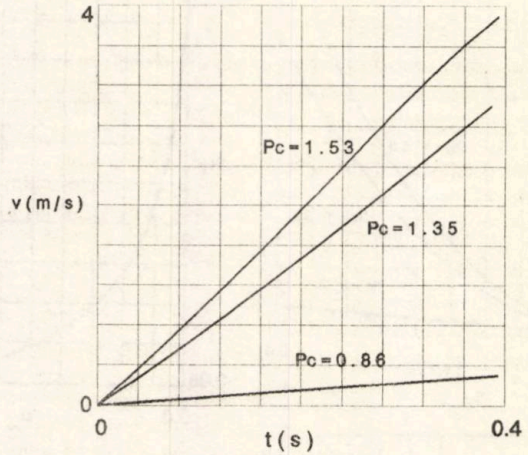

Fig. 9

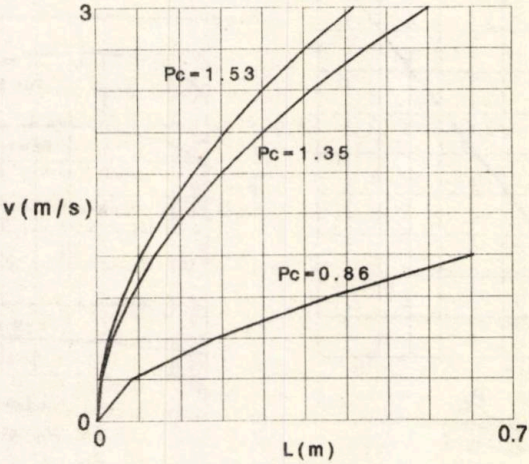

Fig. 10

If the hitting dynamic force must be increased without affecting oscillation parameters, the F_R value must be also increased and correlated to a new U value (or f value) at constant P_C complex parameter value.

The impossibility of obtaining higher frequency values using the same motor construction (K=const.) must be noticed, as there are electrical restriction in increasing the U/f values and mechanical ones in diminishing the F_R or L values. Regarding these working regimes, no continuously (moving) electrical control proceedings are indicated because of low values of t (regarding control elements critical time).

Some lower values of mechanical oscillation frequency can be obtained by reducing the U value. Regarding the $F(v)$ and $F(L)$ characteristics, the electrical control of moving is also unuseful for these working regimes.

The tests made in the Laboratory, using the linear motor test stand, showed an approach to these theoretical estimations with maximum 7% errors (due to the specific frictions and inferior point interraction effect).

Table 3

P_C	0.60	0.80	1.0	1.345	1.5	2.0
Climbing time, [s]	–	3.45	0.57	0.322	0.3	0.23
Final speed, [m/s]	–	0.42	1.72	2.52	3.0	3.85
Extra climbing time, [s]	–	0.04	0.175	0.256	0.31	0.39
Descend. total space, [m]	–	0.46	0.603	0.75	0.92	1.21
Descend. time, [s]	–	0.31	0.35	0.39	0.43	0.50
Oscillation period, [s]	–	3.8	1.1	0.97	1.04	1.13
Oscillation frequency, [Hz]	–	0.26	0.91	1.03	0.96	0.89
Observations	I	N	N	N_m	O	O

We used the following abreviations: I – impossible; N – normal; N_m – nominal; O – overvoltage.

Regarding the fact that the transient moving regime of a linear motor is determined mainly by the constructive parameters, in linear motor design the attention will be major focussed on the motor dimensioning and less on the electrical command variants.

4. Conclusions

A theoretical method in vertical moving equation evaluation for the transient regime of linear induction motors is proposed.

A new complex parameter, P_C, was introduced in order to characterise any transient regime and to identify properly the best possibilities in motor construction and electrical parameters command for a requested oscillation frequency value of armature.

There are some limits in obtaining (using the same linear motor) higher mechanical oscillation frequency values.

For a construction variant of a linear motor the transient behaviour determine a close interval of oscillation frequencies, in spite of any electrical or mechanical parameters adapting.

Regarding the few possibilities of oscillation moving, no electrical continuous control of parameters is indicated in reliable power applications.

Received, June 21, 1994

Technical University "Gh. Asachi", Jassy,
Department of Utilizations,
Electric Drives and Automations
and
Department of Electrical Measurements
and Electrotechnical Materials

REFERENCES

1. Boţan N., *Reglarea vitezei sistemelor de acţionare electrică.* Ed. Tehnică, Bucureşti, 1974.
2. Cantemir L., Schreiner C., *The Parameter and Control Characteristics Analyse for Linear Motors Oscillators.* ICATE'93, Craiova, Session C, 59.
3. Laithwaite E.R., *Induction Machines for Special Purpose.* G. Newness Ltd., London, 1966.

4. Şindrilar D., B.S. Thesis, Polyt. Inst., Jassy, 1991.
5. Cantemir L., *Oscillator Regime of Linear Induction Motors*. Electrotehnica 80-CNAE, Iaşi, 1992, A.12.1.
6. Schreiner C., Cantemir L., *Estimation of Moving Parameters and Dynamic Equation for Linear Induction Motors*. The 4th Int. Conf. ICOEEE, Braşov, May 12-14, 1994, 209.

UN NOU PARAMETRU COMPLEX UTIL ÎN CARACTERIZAREA REGIMURILOR TRANZITORII DE MIŞCARE ALE MOTORULUI ASINCRON LINIAR

(Rezumat)

Regimul tranzitoriu de funcţionare al motorului de inducţie, destinat unor aplicaţii speciale (de exemplu, oscilatoare verticale pentru forje, fierăstraie), nu poate fi caracterizat pe baza ecuaţiilor dinamice clasice. Se propune o ecuaţie integrală exactă, bine fundamentată din punct de vedere fizic, bazată pe caracteristicile electromecanice de control al mişcării, care permite identificarea unui nou parametru complex (P_C) necesar în descrierea regimurilor tranzitorii ale oricărui tip constructiv de motor liniar de inducţie.

Pe baza unui program de calcul numeric s-au analizat caracteristicile dinamice şi s-a demonstrat imposibilitatea obţinerii, pe baza aceleiaşi soluţii constructive, a unui interval de frecvenţă a oscilaţiei mecanice.

BULETINUL INSTITUTULUI POLITEHNIC DIN IAŞI
Tomul XLI (XLV), Fasc. 3-4, 1995
Secţia III
ELECTROTEHNICĂ. ENERGETICĂ. ELECTRONICĂ

C.D. 621-83

CONTRIBUTIONS CONCERNANT LA COMMANDE SANS CAPTEUR DE POSITION DES SYSTÈMES D'ENTRAINEMENT ÉLECTRIQUE À MOTEURS PAS À PAS

PAR
GH. BĂLUŢĂ, MIRCEA DIACONESCU et C. CĂCIULEANU

1. Introduction

Les performances d'un moteur pas à pas (MPP) commandé en boucle ouverte sont réduites, parce que dans l'absence d'une boucle de réaction il n'existe aucun moyen à connaître si le moteur a perdu un pas ou si la vitesse est trop oscillante [1]. Très souvent, si la fréquence des impulsions de commande est trop élevée, le MPP pert totalement le synchronisme avec ces impulsions et, simplement, il s'arrête.

En général, dans les systèmes de commande en circuit ouvert, la position du champ est imposée de l'extérieur et le synchronisme du roteur se maintient ou non, en fonction des charges statiques et dynamiques et des caractéristiques du moteur.

Ainsi, le système est très sensible aux perturbations, en particulier à celles du couple résistant. Les résonances représentant un problème et le comportement du MPP à la variation du couple d'inertie du mécanisme entrainé est déficitaire aussi.

Si on réussit par un moyen quelconque de réaliser, de même, la liaison de la position du champ de la position du roteur (c'est-à-dire, conférer à cette liaison un caractère biunivoque), les problèmes ci-dessus sont pour la plupart résolus, ce que signifie la réalisation d'un feedback local, par lequel la position du roteur peut influencer la position du champ (boucle mineure).

Évidemment, la première solution pour mesurer la position rotorique serait le codeur incrémental de position placé sur l'arbre. Les impulsions fournies par le codeur ont une double utilité: elles assurent la commande qui dépend de l'angle du MPP et, de même, constituent une information concernant la position du roteur, étant créée la possibilité de compter les pas effectués par le moteur. Mais cette solution est chère (le codeur incrémental est souvent plus cher que le moteur même) et elle a le désavantage d'être dépendante des erreurs géometriques du moteur, qui doivent être minimales.

Il existe encore la possibilité d'utiliser seulement le système électrique du moteur pour obtenir des informations concernant la position du roteur. Il est connu que la forme d'onde des courants dans les phases du MPP, notamment pour les moteurs à réluctance variable, présente des points d'extrémum, pour certains domaines de vitesse [1],[2].

Les impulsions de réaction pour la commande en boucle fermée du MPP peuvent être obtenues par détection de ces points d'extrémum, qui dépendent de la tension d'alimentation, du circuit suppreseur, de la vitesse du moteur, de la résistance de la phase et de la variation de l'inductivité avec l'angle à l'arbre.

C'est difficile de trouver le point d'extrémum du courant à la connection, parce que le modèle mathématique conduit à une équation différentielle non-linéaire,

difficile à resoudre par voie analytique. Par conséquence, on présente ci-dessous la solution numérique, à l'aide de l'ordinateur, de cette équation différentielle.

2. L'étude à l'aide de l'ordinateur numérique du système converteur–moteur

Les performances d'un système d'entrainement à moteur pas à pas déterminent le mode d'alimentation et les paramètres du schéma de commande. Le calcul de ces paramètres, basé sur des grandeurs mécaniques données, impose le traitement du moteur, du converteur statique et de la charge comme un système unitaire.

Pour l'analyse du système on a choisi un moteur tetraphasé à réluctance variable, alimenté par un converteur à double tension. Pour la simulation on a utilisé le modèle mathématique linéaire, en coordonnées réeles, du MPP. Le modèle mathématique constitué par les équations des tensions et l'équation de mouvement est de la forme:

$$(1) \qquad \begin{cases} [u_k] = [i_k][R] + \frac{\mathrm{d}[\psi_k]}{\mathrm{d}t}, \ (k = 1,2,3,4), \\ J\frac{\mathrm{d}^2\theta(t)}{\mathrm{d}t^2} + K_{fv}\frac{\mathrm{d}\theta(t)}{\mathrm{d}t} + M_r \mathrm{sign}\frac{\mathrm{d}\theta(t)}{\mathrm{d}t} = m_e, \end{cases}$$

où: $[i_k]$ représente la matrice colonne des courants, $[R]$ – la matrice diagonale des résistances de phases, $[\psi_k]$ – la matrice colonne des flux totals, J – le couple d'inertie total réduit à l'arbre du MPP, considéré constant, K_{fv} – coefficient de frottement visqueux, M_r – le couple résistant réduit à l'arbre du MPP, considéré constant, m_e – le couple électromagnétique développé par le moteur, θ – l'angle mécanique instantané du roteur.

Le flux ψ_k de l'équation de tensions peut être exprimé en fonction des inductivités des enroulements et des courants qui les parcourent:

$$(2) \qquad \psi_k = \sum_{j=1}^{4} L_{kj} i_k,$$

où:

$$L_{kj} = \begin{cases} \text{l'inductivité statique propre de la phase } k, \text{ pour } k = j; \\ \text{l'inductivité statique mutuelle entre les phases } k \text{ et } j, \text{ pour } k \neq j. \end{cases}$$

Au cas du MPP à réluctance variable, polystatorique, les inductivités mutuelles des phases peuvent être considérées nulles, compte tenu que les phases sont disposées sur des circuits magnétiques séparés. Toutefois si on néglige la saturation du circuit magnétique, l'inductivité propre L_k de la phase k est fonction seulement de l'angle θ qui définit la position du roteur:

$$(3) \qquad L_k = L_0 + L_1 \cos\left[Z_r\theta(t) - (k-1)\frac{\pi}{2}\right], \ (k = 1,2,3,4),$$

où: L_0, L_1 sont des constantes qui dépendent des paramètres constructifs du moteur, Z_r – nombre de dents rotoriques.

Tous calculs effectués, le système des équations des tensions prend la forme:

$$(4)\qquad \begin{cases} u_k = \left\{R_k + L_1 Z_r \omega \sin\left[Z_r\theta - (k-1)\frac{\pi}{2}\right]\right\} i_k + \\ \qquad + \left\{L_0 + L_1 \cos\left[Z_r\theta - (k-1)\frac{\pi}{2}\right]\right\} \frac{\mathrm{d}i_k}{\mathrm{d}t} \\ \omega(t) = \frac{\mathrm{d}\theta(t)}{\mathrm{d}t},\ (k = 1,2,3,4), \end{cases}$$

où $\omega(t)$ est la vitesse angulaire du MPP.

Le couple électromagnétique développé par le MPP polystatorique, négligeant la saturation du circuit magnétique, est donné par la relation:

$$(5)\qquad m_e = -\frac{1}{2} L_1 Z_r \sum_{k=1}^{4} i_k^2 \sin\left[Z_r\theta - (k-1)\frac{\pi}{2}\right].$$

Pour réaliser le modèle du converteur on a choisi un schéma d'alimentation à deux tensions, le passage de la tension de forçage à celle de maintient étant, dans le moment quand on atteint un seuil prescrit du courant de la phase, égal avec le courant nominal.

L'équation de la tension sur une phase quelconque k du moteur est:

$$u(t) = \begin{cases} U_2 & \text{pour } 0 \le i_k \le I_{\text{nom}},\ 0 \le t \le t_c; \\ U_1 = U_{\text{nom}} \le U_2 & \text{pour } i_k = I_{\text{nom}},\ t_c \le t \le T - t_s; \\ -U_2 & \text{pour } i_k \le I_{\text{nom}},\ T - t_s < t \le T; \\ 0 & \text{pour } i_k = 0,\ t > T. \end{cases}$$

où: U_2 représente la tension de forçage, U_1 – tension nominale du MPP, t_c – temps de croissance du courant de phase, t_s – temps de suppression (de décroissance) du courant de phase, T – période de commande du MPP.

Pour la suppression on a utilisé la méthode à diode et résistance connectées à la tension de suppression U_2.

3. Résultats obtenus

La simulation numérique a été réalisée utilisant le paquet de programmes MATLAB (SIMULINK) [3],[4]. On alimente une seule phase, le roteur démarre de la position initiale $\theta_0 = 0$ et il se dirige vers la position stable la plus rapprochée $\theta(t) = \theta_{\text{pas}} = 1,8°(Z_r = 50)$, de sorte que la réluctance magnétique soit minimale.

Ci-dessous sont présentés les résultats de la simulation à savoir les grandeurs mécaniques qui définissent le mouvement du roteur: l'angle mécanique instantané θ (Fig.1), la vitesse angulaire ω (Fig.2), le couple développé par le moteur m_e (Fig.3) et le courant dans la phase alimentée pour certains régimes de travail: a) commande à haute fréquence, charge nominale (Fig.4), b) commande à haute

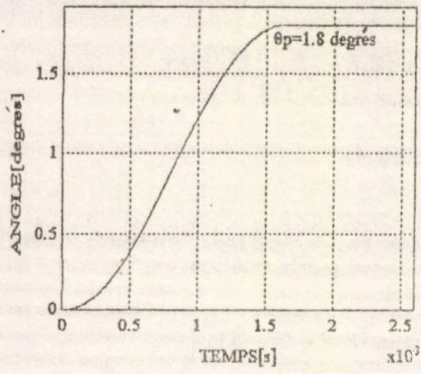

Fig. 1.– L'angle mécanique.

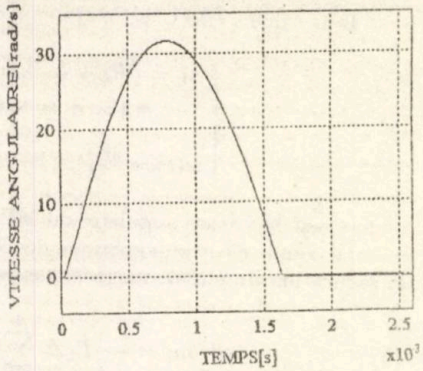

Fig. 2.– La vitesse angulaire.

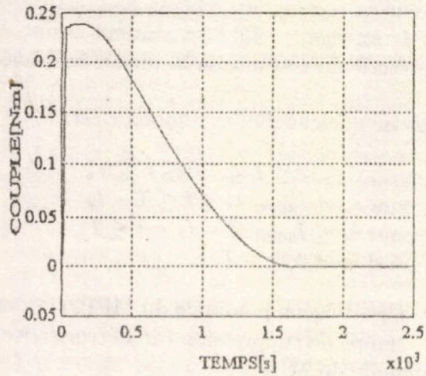

Fig. 3.– Le couple moteur.

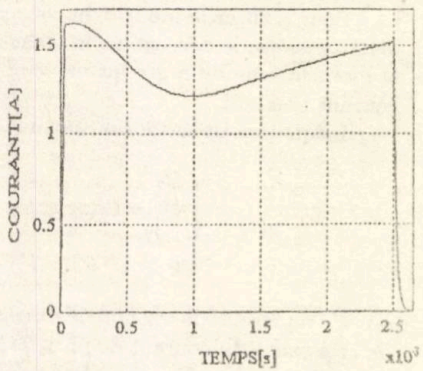

Fig. 4.– Le courant de phase. haute fréquence, charge nominale.

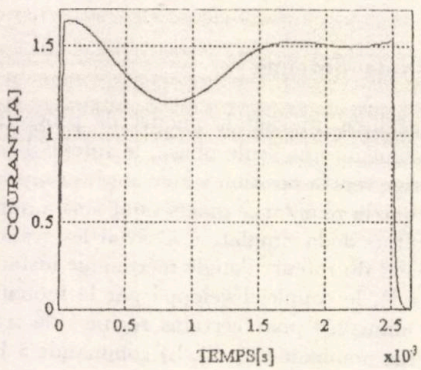

Fig. 5.– Le courant de phase, haute fréquence, sans charge.

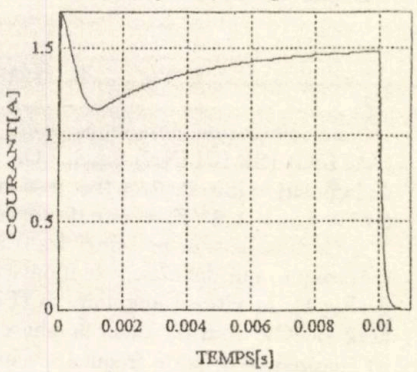

Fig. 6.– Le courant de phase, basse fréquence, charge nominale.

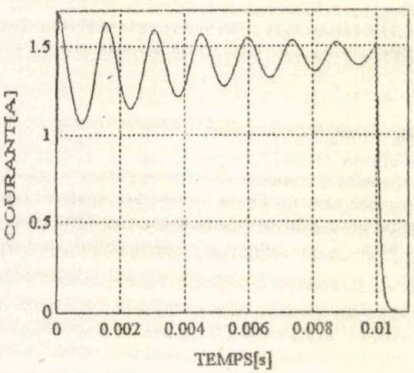

Fig. 7.– Le courant de phase, basse fréquence, sans charge.

fréquence, sans charge (Fig.5), c) commande à basse fréquence, charge nominale (Fig.6), d) commande à basse fréquence, sans charge (Fig.7).

4. Conclusions

La simulation numérique du système converteur–moteur–charge met à la disposition de l'utilisateur un instrument utile et précis.

Le modèle choisi reproduit avec une précision suffisante le comportement physique du système. Par l'examination de la forme d'onde du courant dans la phase alimentée on observe l'existence des points d'extrémum; le premier – point de minimum – fournit une information concernant la position du roteur, qui est utilisée pour la commande en boucle fermée sans capteur incrémental.

Reçue le 15 décembre 1994

Université Technique „Gh. Asachi", Jassy, Chaire d'Utilisations, Entrainements électriques et Automation

BIBLIOGRAPHIE

1. K u o B.C., K e l e m e n A., *The Incremental Motion Control Systems* (en Roumain). Ed. Tehnică, Bucureşti, 1981.
2. A c a r n l e y P.P., *Stepping Motors: a Guide to Modern Theory and Practice.* Peter Peregrinus, Oxford, 1992.
3. * * * MATLAB for Windows User's Guide, March 1992.
4. * * * SIMULINK User's Guide, March 1992.
5. G o e l d e l C., *Contributions à la modélisation, à l'alimentation et à la commande des moteurs pas à pas.* Thèse de Docteur ès Sciences, I.N.P.L., 1984.

CONTRIBUŢII PRIVIND COMANDA FĂRĂ TRADUCTOR DE POZIŢIE A SISTEMELOR DE ACŢIONARE ELECTRICĂ CU MOTOARE PAS CU PAS

(Rezumat)

Se studiază simularea numerică a regimului de păşire pentru un motor pas cu pas (MPP) cu reluctanţa variabilă cu patru faze, alimentat de la un convertor cu două tensiuni.

Modelul matematic liniar în coordonate reale al MPP conduce la o ecuaţie diferenţială puternic neliniară care nu poate fi rezolvată analitic. Integrarea numerică a acestei ecuaţii evidenţiază existenţa unor puncte de extremum în forma de undă a curentului în faza alimentată, primul dintre acestea, un minim, putând fi folosit la comanda MPP în buclă închisă fără traductor de poziţie.

BULETINUL INSTITUTULUI POLITEHNIC DIN IAŞI
Tomul XLI (XLV), Fasc. 3–4, 1995
Secţia III
ELECTROTEHNICĂ. ENERGETICĂ. ELECTRONICĂ

D.C. 621.8; 669

MATHEMATICAL MODEL FOR STABILIZED STATE OF ELECTRICAL DRIVE SYSTEMS USED IN METALLURGICAL INDUSTRY

BY
IULIAN GRAUR, GR. TAŞCĂ, ADRIAN GRAUR, DRAGOŞ TAŞCĂ,
M. ALBU, MIHAELA MAREŞ, DORIN LUCACHE and V. HORGA

1. Introduction

In the principal production divisions of metallurgical industry there are used electrical drive systems (EDS) for which become necessary the study of some stabilized functioning modes, particular solutions of some first order, with constant coefficients, linear differential equations which have as right member a periodical function which satisfy the Dirichlet criterion [1],...,[14].

In this case, Fourier series of the input function $M_s(t) = f(t)$ are used, but, due to the difficulties encountered in the calculus of the amplitudes and initial phases of the component harmonics and having in view that in more cases is necessary, for a satisfactory precision, to utilise a big number of harmonics, in the last time, concentrate solutions are used [1],...,[14], with finite number of terms, easier to calculate.

The study, research and analysis of functioning states of the EDS impose the necessity of determining and representing the variation curves of the motor torque and of the duration of a functioning cycle.

The characteristic example of functioning states with variable and duration loads specific to the equipments of metallurgy is represented by the drive systems with rolling mills.

In previous papers [11],[12] there have been established the relations for the computation of states of some drive systems working according to the diagrams of loading with periodical load shocks under the form:

$$(1)\qquad \begin{aligned} &\text{a)} \quad M_{m_k}(t) = c_k e^{-t/T_m} + D_k(t - T_m) + E_k, \\ &\text{b)} \quad \Omega_{m_k}(t) = \Omega_{ON} - K_m M_{m_k}(t),\ t \in [t_{k-1}, t_k], \end{aligned}$$

where it has been noted:

$$C_k = \frac{T_m}{1 - e^{t_n/T_m}} \left[\sum_{j=1}^{k-1} a_j e^{(t_j + t_n)/T_m} + \sum_{j=k}^{n} a_j e^{t_j/T_m} \right],$$

$$a_k = \frac{M_{s_k} - M_{s_{k-1}}}{t_k - t_{k-1}} - \frac{M_{s_{k+1}} - M_{s_k}}{t_{k+1} - t_k}, \quad D_k = \frac{M_{s_k} - M_{s_{k-1}}}{t_k - t_{k-1}},$$

$$E_k = \frac{M_{s_{k-1}} t_k - M_{s_k} t_{k-1}}{t_k - t_{k-1}}, \ (k = 1, 2, ..., n),$$

the other notations having the significance precised in [11],[12].

In this paper, having in view the research results indicated in [11], it is established the peculiar form of the relations for the computation of stabilized state of drive systems functioning after load diagrams with variable and duration load shocks of a special form, specific to the equipments of metallurgy.

2. Calculus Algorithm

For determination of the relations concerning the stabilized functioning regime of EDS with rolling mills is considered the general case of a load diagram, with variable and duration loads, of a special form, periodical for $t > 0$, having T_c as period (Fig.1), ($M_{s_{ktot}} = M_{s_k} + M_0 + M_{d_k} \approx$ const. [2]).

The developed resistant static torque is:

$$(2) \quad M_s(t) = M_{s_k} = M'_{s_{k-1}} = \text{const.}; \ t \in [t_{k-1}, t_k], \ (k = 1, 2, ..., n), \ t_0 = 0.$$

The stabilized electromagnetic torque, developed by the drive electric motor and corresponding to the load interval k, done by relation $(1\,a)$, has the form [12]:

$$(3) \quad M_{m_k}(t) = \frac{T_m}{1 - e^{t_n/T_m}} \left[\sum_{j=1}^{k-1} a_j e^{(t_j + t_n)/T_m} + \sum_{j=k}^{n} a_j e^{t_j/T_m} \right] e^{-t/T_m} + \\ + D_k(t - T_m) + E_k, \ t \in [t_{k-1}, t_k],$$

where $a_1, ..., a_n$, $D_1, ..., D_n$ and the free terms $E_1, ..., E_n$ have the form [8]:

$$a_k = \frac{M_{s_{k+1}} - M_{s_{k-1}}}{T_m}, \quad D_k = \frac{M_{s_k} - M_{s_{k-1}}}{t_k - t_{k-1}} \text{ and } M_{s_k} = M_{s_{k-1}},$$

which involve

$$D_1 = D_2 = \cdots = D_n = 0, \quad M_k = \frac{M_{s_{k-1}} t_k - M_{s_k} t_{k-1}}{t_k - t_{k-1}} = M_{s_k}.$$

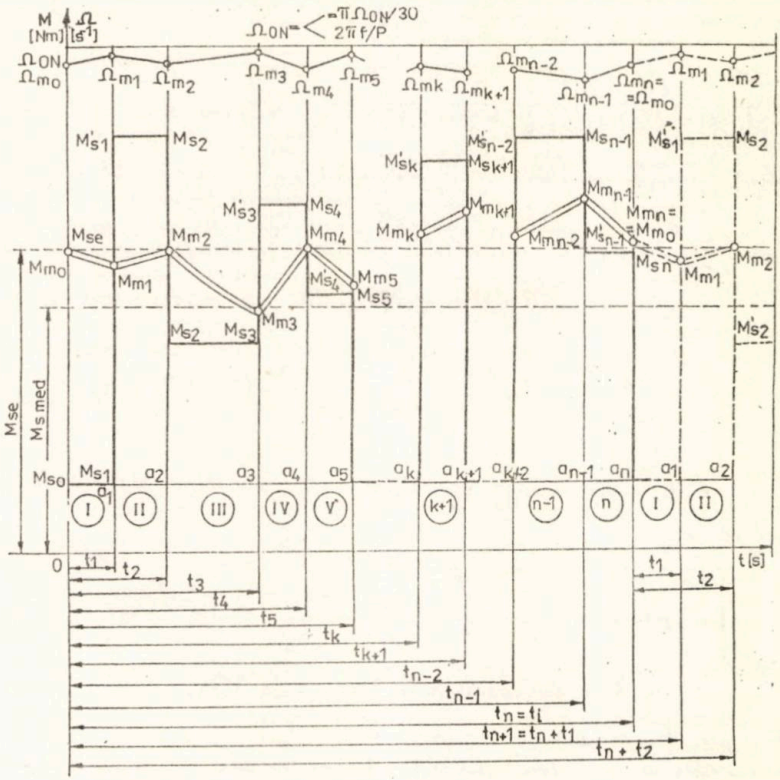

Fig. 1

In this case the relation (3), written for the load interval k, becomes:

$$M_{m_k}(t) = \frac{T_m}{1 - e^{t_n/T_m}} \left[\frac{M_{s_2} - M_{s_0}}{T_m} e^{(t_1+t_n)/T_m} + \frac{M_{s_3} - M'_{s_1}}{T_m} e^{(t_2+t_n)/T_m} + \cdots \right.$$

$$\left. \cdots + \frac{M_{s_n} - M'_{s_{n-2}}}{T_m} e^{t_n/T_m} \right] e^{-t/T_m} + M_{s_k}, \quad t \in [t_{k-1}, t_k] \tag{4}$$

and

$$M'_m(t) = \frac{T_m}{1 - e^{t_n/T_m}} \left[\sum_{j=1}^{k-1} \frac{M_{s_{j+1}} - M'_{s_{j-1}}}{T_m} e^{(t_j+t_n)/T_m} + \right.$$

$$\left. + \sum_{j=k}^{n-1} \frac{M_{s_{j+1}} - M'_{s_{j-1}}}{T_m} \right] e^{-t/T_m} + M_{s_k}, \quad t \in [t_{k-1}, t_k].$$

Simplifying by T_m and regrouping the resistant static torques in a natural order (s. (2)), the relation (4) becomes:

$$(5) \qquad M_m(t) = M_{m_k}(t) = C'_k e^{-t/T_m} + E'_k, \; t \in [t_{k-1}, t_k], \; (k = 1, 2, ..., n-1),$$

with $M_{m_1}(0) = C'_1(0) + E'_1(0)$, $(t = 0)$, and where was used the notations:

$$C'_k = \frac{1}{1 - e^{t_n/T_m}} \left\{ M_{s_1} \left[e^{t_1/T_m} - e^{(t_1+t_n)/T_m} \right] + \sum_{j=2}^{k-1} M_{s_j} \left[e^{(t_{j-1}+t_n)/T_m} - \right. \right.$$

$$\left. - e^{(t_j+t_n)/T_m} \right] + M_{s_k} \left[e^{(t_{k-1}+t_n)/T_m} - e^{t_k/T_m} \right] +$$

$$\left. + \sum_{j=k-1}^{n} M_{s_j} \left(e^{t_{j-1}/T_m} - e^{t_j/T_m} \right) \right\}, \; (k = 1, 2, ..., n-1)$$

and

$$E'_1(0) = M_{s_0}, \quad E'_1 = M_{s_1}, \; ..., \; E'_k = M_{s_k}, \; ..., \; E'_n = M_{s_n};$$

finally it results:

$$(6) \qquad \begin{cases} M'_{m_k}(t) = C'_k e^{-t/T_m} + E'_k, \\ \Omega_{m_k}(t) = \Omega_{ON} \left[1 - \frac{s_N}{M_N} \left(C'_k e^{-t/T_m} + E'_k \right) \right], \end{cases} \quad t \in [t_{k-1}, t_k].$$

3. The Program and The Logic Diagram

The program used for solving the established algorithm contains four moduli:

a) the data input modulus (marked with A in the logic diagram (Figs.2 *a* and 2 *b*)) contains all data inputs operations;

b) the B modulus calculates the values of C'_k and E'_k coefficients, performing previously the two sums from the mathematical model; these sums are contained in the S_1 and S_2 variables;

c) the D_i subprogram modulus; this is a FUNCTION type subprogram and it has as input parameter a real number (a time moment), furnishing the k index of the time interval $[t_{k-1}, t_k]$ which contains the time moment;

d) the C modulus calculates and prints the values for $M'_m(t)$ and $\Omega_m(t)$, using the D_i subprogram.

4. Conclusions

1. The analysis of the obtained results shows that the exponential form of the solutions for $M'_m(t) = f_1(t)$ and $\Omega_m(t) = f_2(t)$ has the advantage of a high speed of calculus and eliminates many difficulties and incertitudes of the determination and the verification of the EDS parameters in a direct way on anyone of the intervals of charge graph.

2. The mathematical model $M'_m(t) = f_1(t)$ and $\Omega_m(t) = f_2(t)$ and the computer program established and presented in this paper are used in the computer

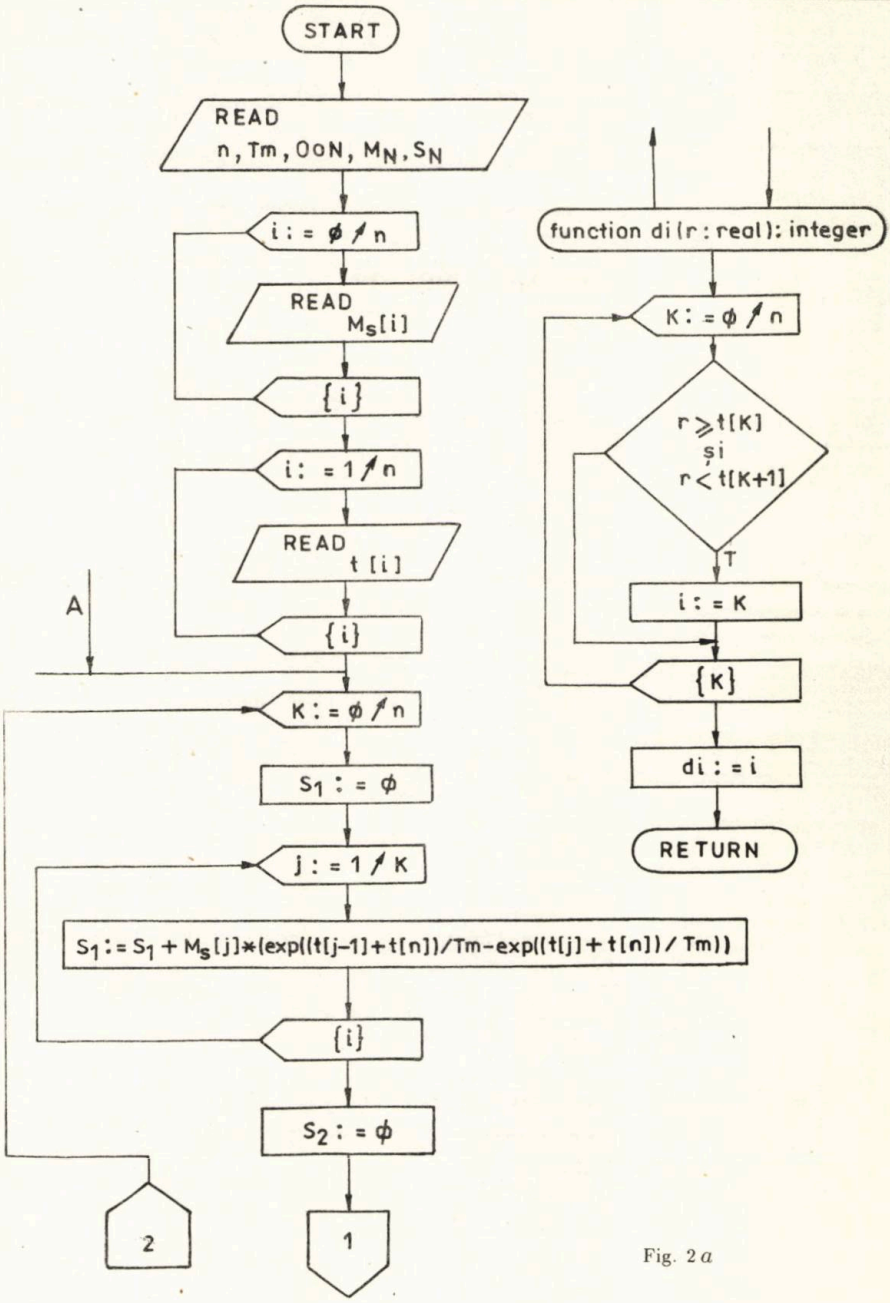
START
READ
n, Tm, OoN, M_N, S_N
i : = ϕ / n
READ
M_S[i]
{i}
i : = 1 / n
READ
t [i]
{i}
A
K : = ϕ / n
S_1 : = ϕ
j : = 1 / K
$S_1 := S_1 + M_S[j]*(\exp((t[j-1]+t[n])/Tm - \exp((t[j]+t[n])/Tm))$
{i}
S_2 : = ϕ
2
1
function di (r : real): integer
K : = ϕ / n
r ≥ t[K] şi r < t[K+1]
T
i : = K
{K}
di : = i
RETURN

Fig. 2 *a*

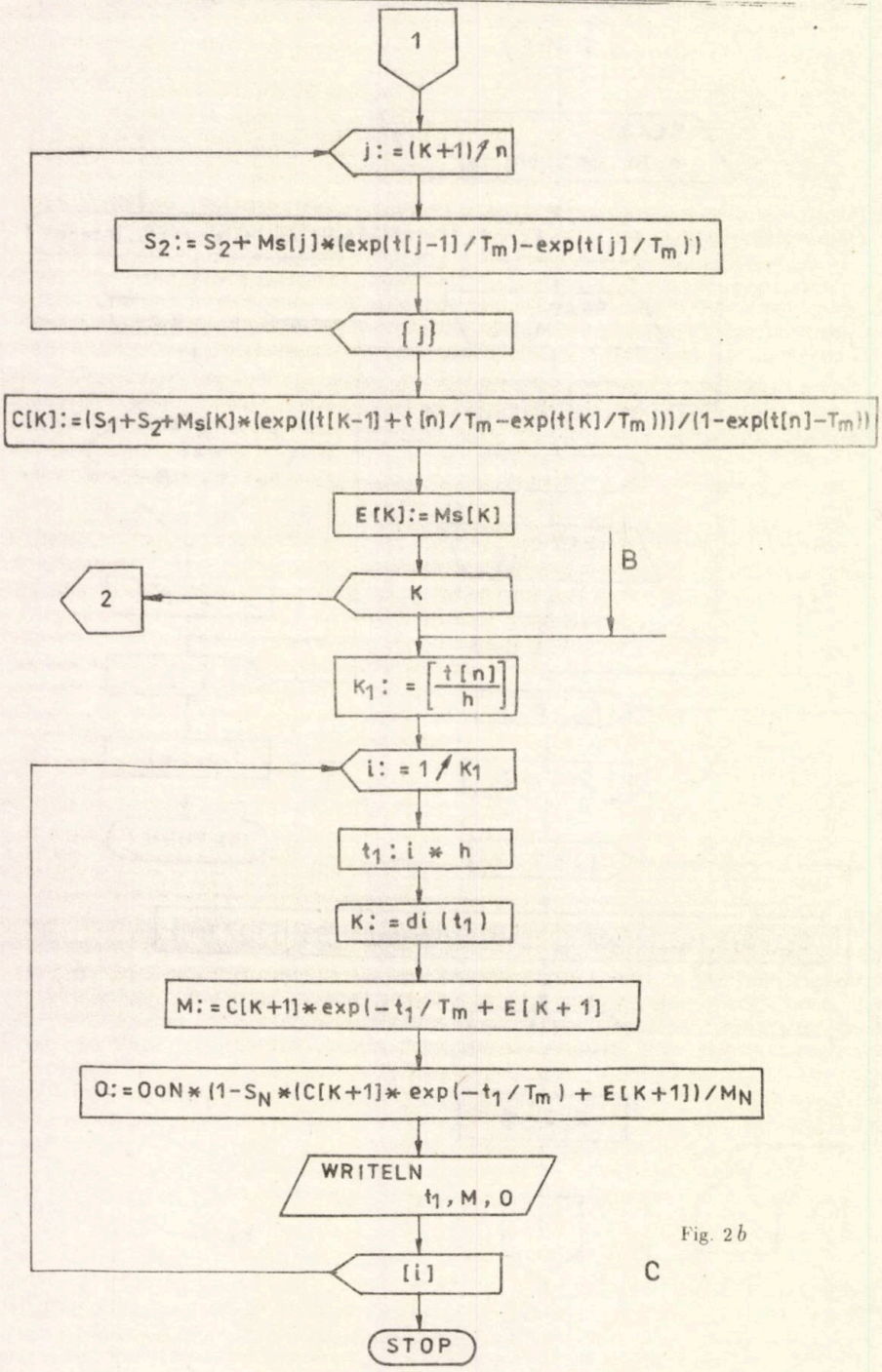
1
j: = (K+1) / n
S2: = S2 + Ms[j] * (exp(t[j-1] / Tm) - exp(t[j] / Tm))
{j}
C[K]: = (S1 + S2 + Ms[K] * (exp((t[K-1] + t[n] / Tm - exp(t[K] / Tm))) / (1 - exp(t[n] - Tm))
E[K]: = Ms[K]
B
2
K
K1: = [t[n] / h]
i: = 1 / K1
t1: i * h
K: = di (t1)
M: = C[K+1] * exp(- t1 / Tm + E[K + 1]
O: = OoN * (1 - SN * (C[K+1] * exp(- t1 / Tm) + E[K+1]) / MN
WRITELN
t1, M, O
[i]
C
STOP

Fig. 2 *b*

simulation of the stabilized modes of the EDS for metallurgic machines with constant time and inertia moment, periodic charge strikes.

Received, March 10, 1994

Technical University "Gh. Asachi", Jassy,
Department of Industrial Utilizations,
Electric Drives and Automation,
University "Ştefan cel Mare", Suceava
and
A.I.A., Jassy

REFERENCES

1. Boţan N.V., *Bazele calculului acţionărilor electrice.* Ed. Tehnică, Bucureşti, 1970.
2. Braşovan M., Seracin E., *Metode noi de proiectare a acţionărilor electrice.* Ed. Acad. Române, Bucureşti, 1968.
3. Caba S., *Proiectarea acţionărilor electrice.* Inst. polit., Iaşi, 1989.
4. Diaconescu M., *Studii privind determinarea principalilor parametri ai sistemelor de acţionare electrică.* Ph.D. Diss., Polyt. Inst., Jassy, 1974.
5. Ganciu T., Taşcă Gr., *About the Choice of Drive Motors for Equipments with Aleatory Load.* 5-th Nat. Conf. on Electr. Drives, Jassy, May 15-17, 1986.
6. Kelemen A., *Acţionări electrice.* EDP, Bucureşti, 1976.
7. Popescu Şt., Taşcă Gr. et al., *Mathematical Model and Computer Simulation for the Starting of Pumping Units.* 7-th Nat. Conf. of Electr. Drives, Galatzi, 1990.
8. Rusu N., *Contribuţii la optimizarea funcţionării laminoarelor reversibile de tip bluming.* Ph.D. Diss., Polyt. Inst. "Traian Vuia", Timişoara, 1981.
9. Saal C., *Neue Ergebnisse im Bereich der Stossantriebe.* Bul. Inst. polit., Iaşi, **XXV (XXIX)**, *1-2*, s.III (1979).
10. Seracin E., Popovici D., *Tehnica acţionărilor electrice.* Ed. Tehnică, Bucureşti, 1985.
11. Taşcă Gr., *Contribuţii la calculul cuplului motor stabilizat al unor motoare rotative funcţionând cu şocuri de sarcină periodice.* Bul. Inst. polit., Iaşi, **XXVI (XXX)**, *1-2*, s.III, 103-112 (1980).
12. Taşcă Gr., *Calculul cuplului motor stabilizat şi al vitezei unor motoare rotative funcţionând cu grafice de sarcină cu şocuri periodice de formă particulară, caracteristice sectoarelor agricole şi zootehnice.* Bul. Inst. polit., Iaşi, **XXX (XXXIV)**, *1-4*, s.III, 95-104 (1984).
13. Taşcă Gr., *Asupra determinării puterii motorului electric de acţionare a presei mecanice PMT-5 de balotat paie şi fân.* Bul. Inst. polit., Iaşi, **XVIII (XXII)**, *3-4*, s.III, 149-155 (1972).
14. Taşcă Gr., *Experimental Research of the Stabilized State of Electrical Drive Systems Used in the Industry of Processing Fodders.* 6-th Nat. Conf. on Electr. Drives, Timişoara, May 13-14, 1988.

MODEL MATEMATIC PENTRU CALCULUL REGIMULUI DE FUNCŢIONARE STABILIZAT AL UNOR SISTEME DE ACŢIONARE ELECTRICĂ UTILIZATE ÎN INDUSTRIA METALURGICĂ

(Rezumat)

Pe baza rezultatelor cercetărilor din [7],[11],[12] se stabileşte modelul matematic (forma particulară a soluţiilor) pentru calculul regimului stabilizat al sistemelor de acţionare electrică ce funcţionează după grafice de încărcare cu şocuri de sarcină variabile şi de durată specifice utilajelor din industria metalurgică.

BULETINUL INSTITUTULUI POLITEHNIC DIN IAŞI
Tomul XLI (XLV), Fasc. 3-4, 1995
Secţia III
ELECTROTEHNICĂ. ENERGETICĂ. ELECTRONICĂ

D.C. 621.314.2

FROM PLANNED MAINTENANCE TO OPPORTUNE MAINTENANCE

BY

FLORIN MUNTEANU, D. IVAS and GERARDUS-CHRISTOFFEL PAAP

1. Introduction

In this paper a new application of an original device to improve power transformer reliability is demonstrated. This device can be used as a part of a system for self-checking, self-diagnosis and monitoring to improve reliability according to the new principle of reliability engineering: it is economically sound to change planned maintenance into an opportune one. The probability of establishing conditions of failure exist and action to remove them before the fault appears, improve the system's availability.

2. Reliability of Power Transformers

The reliability of power transformers is a much discussed subject [3],...,[5] because of its economic and technical importance. Because the transformer's load capability depends on the hottest-spot temperature (HST) the probability problem is complicated, since the HST depends on many random variables: load, ambient temperature and forced outage rate of parallel operating transformers.

2.1. Actual Load Model for Reliability Calculations

For the calculation of the transformer reliability parameters, which depend on the HST, a two-step representation of the daily load curve is used. The method of converting the actual load cycle into a two-step representation load cycle as suggested in [6] is shown in Fig.1, where S_p^i is the peak load, t_{Li} – the duration of the equivalent peak load, S_2^i – the equivalent peak load and S_1^i – the equivalent low load. The latter three parameters describe the two-step representation of the i-th daily load curve. The equivalent peak load for the i-th load cycle, S_2^i, is the r.m.s. value of the load during the interval, in which the load is higher than a preselected level, γS_p^i, $(\gamma < 1)$. According to the Loading Guide [6], the r.m.s.

value for the equivalent peak load should not be less than 90% of the maximum integrated half-hourly demand. Therefore the value of γ was chosen as 0.89.

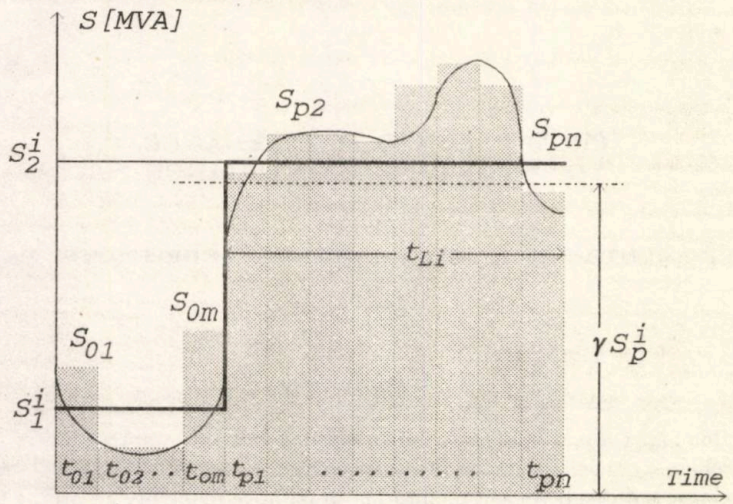

Fig. 1.– Equivalent load cycle.

The equivalent loads, S_2^i, S_1^i, can be expressed by:

$$(1) \qquad S_2^i = \sqrt{\frac{\sum_{i=1}^{n} S_{pi}^2 t_{pi}}{\sum_{i=1}^{n} t_{pi}}} \quad \text{and} \quad S_1^i = \sqrt{\frac{\sum_{i=1}^{m} S_{0i}^2 t_{0i}}{\sum_{i=1}^{m} t_{0i}}},$$

where $S_{p1}, ..., S_{pn}$ and $S_{01}, ..., S_{0m}$ are the various load steps in the actual curve.

The equivalent peak and minimal load as a fraction of the transformer rated power, S_r, for an i-th daily load cycle, k_2^i, k_1^i, are given by:

$$(2) \qquad k_2^i = \frac{S_2^i}{S_r}, \qquad k_1^i = \frac{S_1^i}{S_r}.$$

2.2. An Industrial Power-transformer Application

Let the load diagram of a substation transformer be like that in Fig.1. The two-step representation of this daily load is quite good in this case. However, for an industrial transformer supplying an arc furnace, an equivalent two-step daily load curve is not realistic. Over a period of time the large current results in losses, which can be described as the I^2t effect. These losses are considerably higher than

those that should be calculated on average half-hourly readings of demands as the Loading Guide has established. Consider the four sets of load currents varying in time around a 1.0 pu level, as shown in Fig.2 *a*. In case *i*, the heating effect of a load current of 1.0 for 1.0 pu time is $(1.0)^2 \times 1 = 1.0$. In case *ii*, where the current variation is ±0.2 pu, also over 1.0 pu time, the I^2t effect is $[(1.2)^2+(0.8)^2]/2 = 1.04$. Thus, although the average current in the latter case is still 1.0, the heating effect has increased by 4%. Similarly, in case *iii* the heating effect has increased by 16% and in case *iv* by 64%. The trend of the heating effect is shown in Fig.2 *b*.

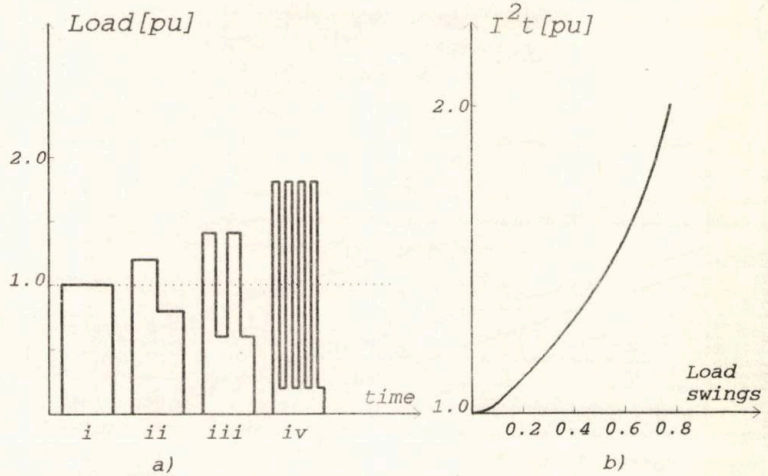

Fig. 2.– Effect of current, swings on I^2t: *a* – varying load patterns for I^2t calculations; *b* – variation of I^2t effect with load swings.

Thus, for widely varying short-time current swings as appear in arc-furnace loads, the actual cumulative I^2t effect is considerably greater than would be expected from the average half-hourly demand values. The conclusion is that in determining the HST for reliability calculations, taking m and n values for sampling the load curve (s. Fig.1) is of extreme importance in calculating an equivalent two-step load, which of course has different parameters than the usual one.

2.3. Load and Ageing Effect

The reliability of a transformer is directly related to that of its insulation materials. It is known that these materials lose their mechanical and electrical properties faster when conductor temperature increases (ageing effect). To evaluate this effect, it is usual to define the Expected Life (EL, [h]) of the transformer insulation and to express its temperature dependence as

$$\text{EL} = \exp\left(A + \frac{B}{273 + \theta_{hs}}\right), \tag{3}$$

where θ_{hs} is the HST, [°C], and A and B are constants that depend on the type of transformer. The EL does not define a time span between EL and the time that the transformer insulation is definitely destroyed. Actually, a transformer can be used for a much longer time than its EL.

Assuming that a transformer is in operation at a constant rated HST, $\theta_{hs} = 98°C$, Eq. (3) gives an expected life which may be defined as Rated Expected Life (REL). The values of θ_{hs} are 98°C according to IEC [6], 65°C winding temperature rise. The loss of life, in percent of the REL, can be expressed by

$$\Delta L\% = 100 \frac{\Delta t}{\exp\left(A + \frac{B}{273+\theta_{hs}}\right)}, \tag{4}$$

where Δt is expressed in hours.

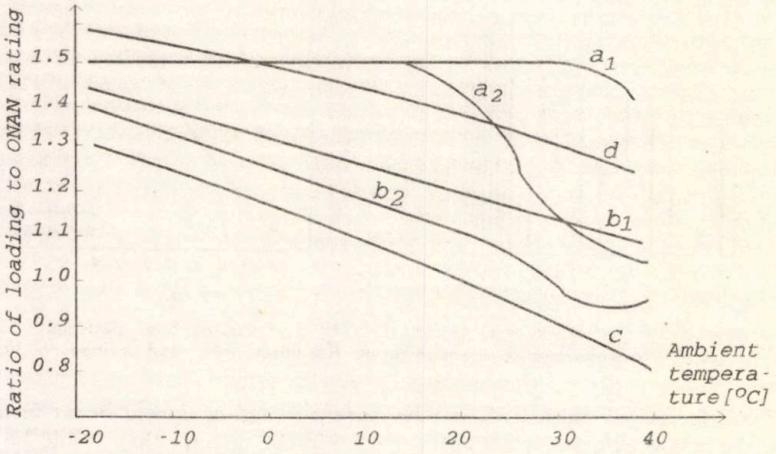

Fig. 3.– ONAN overloading capability.

The values of the temperatures used in Eqs. (3) and (4) are limited up to a critical HST, which may cause immediate transformer insulation failure. The value of the maximum permissible HST for a 65°C winding temperature rise is 140°C according to IEC. Since the relationship between load and HST is rather complex and also depends on the transformer construction, various approximate formulas are available. A commonly used formula is

$$\text{HST} = T_{0t} + k(T_{wa} - T_{0a}), \tag{5}$$

where T_{0t} is the top-oil temperature, T_{wa} – the average winding temperature, T_{0a} – the average oil temperature and k – a constant with values between 1.1 and 1.3. Fig.3 shows the ONAN transformer loading capability which depends on the ambient temperature and previous loading. Curve c corresponds to a constant load

for 24 hours. It shows that the transformer can be operated at a rated load at an ambient temperature of 20°C without affecting the nominal expected life. The load can increase to 1.3 times the rated load at −20°C and decrease to 0.85 times the full load at 40°C. Curve d shows the loading limit by which rapid deterioration and damage of the insulation takes place when the maximum load should be applied continuously. Curves a and b give the transformer's loading capability as per historical data. Curve a takes into account that the transformer previously operated at maximum load for 2 hours, and curve b for 8 hours. Evaluating these curves, it is clear that the transformer load can be higher for curve a than for b. Curve a_1 holds for the case where, in the past, the previous loading was 0.25 times the transformer rated load, while it was 0.9 times for curve a_2.

3. Determination of "Preventive Reliability Alarm" Conditions

On the basis of the foregoing theoretical and technical principles we establish if and when conditions leading to a transformer failure exist and present a practical and efficient device to start a preventive reliability alarm signal.

3.1. Probabilistic Approach

To calculate the HST it is necessary to determine the time of fault initiation on the load curve, t_f. For the calculation of the expected value of the fault initiation, $E(t_0)$, it is assumed that the time between two forced outages, t_F, and the duration of the equivalent peak load, t_L, are exponentially distributed with probability density functions given by:

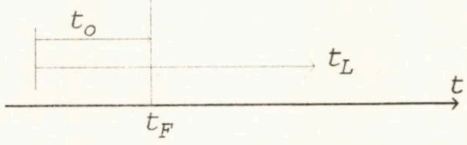

Fig. 4.– Definition of $F_{t_0/t_L}(t)$.

$$f_{t_F} = \lambda \exp(-\lambda t) \quad \text{and} \quad f_{t_L} = \lambda_L \exp(-\lambda_L t), \tag{6}$$

where λ is the outage rate and $1/\lambda_L = T_L$ – the mean duration of an equivalent peak load. For a given t_L, the conditional distribution function, $F_{t_0/t_L}(t)$, is defined (Fig.4) by relation:

$$F_{t_0/t_L} = p(t_0 \leq t) = p(t_F \leq t/0 < t_F \leq t_L), \tag{7}$$

where t_0 is the time of fault initiation during the equivalent peak load, t_F – the time between two forced outages and t_L – the duration of the equivalent peak load.

The conditional probability can be expanded as follows:

$$(8) \qquad F_{t_0/t_L}(t) = \frac{p(t_F \leq t \cap 0 < t_F \leq t_L)}{p(0 < t_F \leq t_L)} = \begin{cases} 1, & t > t_L, \\ \frac{p(0 \leq t_F < t)}{p(0 < t_F \leq t_L)}, & 0 < t \leq t_L. \end{cases}$$

This yields, for $0 < t \leq t_L$, to:

$$(9) \qquad F_{t_0/t_L}(t) = \frac{\int_0^t \lambda \exp(-\lambda\tau)\mathrm{d}\tau}{\int_0^{t_L} \lambda \exp(-\lambda\tau)\mathrm{d}\tau} = \frac{1 - \exp(-\lambda t)}{1 - \exp(-\lambda t_L)}, \quad t_L \neq 0.$$

The probability density function, $f_{t_0/t_L}(t)$, is:

$$(10) \qquad f_{t_0/t_L}(t) = \frac{\mathrm{d}}{\mathrm{d}t} F_{t_0/t_L}(t) = \begin{cases} 0, & t > t_L, \\ \frac{\lambda}{1-\exp(-\lambda t_L)}, & 0 < t \leq t_L. \end{cases}$$

The expected value of t_0, $E(t_0)$, can be expressed by the conditional expected value, $E(t_0/t_L)$, as follows:

$$(11) \qquad E(t_0) = E[E(t_0/t_L)]$$

with

$$(12) \qquad E(t_0/t_L) = \int_{-\infty}^{+\infty} t f_{t_0/t_L}(t)\mathrm{d}t.$$

From (10) and (12), it results the expected value $E(t_0/t_L)$ namely:

$$(13) \qquad E(t_0/t_L) = g(t_L) = \int_0^{t_L} \frac{t\lambda \exp(-\lambda t)}{1 - \exp(-\lambda t_L)}\mathrm{d}t = \frac{1}{\lambda}\left[1 - \frac{\lambda t_L \exp(-\lambda t_L)}{1 - \exp(-\lambda t_L)}\right]$$

and from (11) and (13) the expected value by t_0, $E(t_0)$:

$$(14) \qquad E(t_0) = \int_0^{+\infty} g(t)\lambda_L \exp(-\lambda t)\mathrm{d}t.$$

The function $g(t_L)$ can be approximated by:

$$(15) \qquad g(t_L) \approx \frac{t_L}{2}, \quad (t_L \neq 0),$$

which yields to:

$$(16) \qquad E(t_0) = \int_0^{+\infty} \frac{t_L}{2}\lambda_L \exp(-\lambda_L t)\mathrm{d}t = \frac{1}{2\lambda_L} = \frac{T_L}{2},$$

where T_L is the duration of an equivalent peak load. Therefore, when the load is S_2^i, it is possible that a fault appears after $T_L/2$. The preventive reliability alarm signal starts and the opportune maintenance can be fixed after x, $(x = 1, 2, ...)$, signals.

3.2. Deterministic Approach

This time we do not use the equivalent load cycle and the resultant value S_2 but the real daily, hourly, etc., load cycle which depends greatly on the load type. The deterministic approach is a result of the following two judgements:

a) When the future transformer's life has a random nature because of the random nature of the future load and the ambient temperature, the past life is a deterministic one.

b) The deterministic recent past operating conditions predict the future of the transformer so that the maintenance program can be adapted to these conditions.

There are two technical possibilities to adapt the maintenance shedule to the transformer stresses.

a) *Direct Determination of the HST*

It is not difficult to calculate the HST using relation (5) by measuring T_{0t}, T_{wa} and T_{0a}, to count every HST>98°C and to modify the maintenance program. In practice, changing the maintenance program is only necessary when excessive HSTs are met and not in the case of long lastings HSTs below the specified boundary values.

The thermal protection usually does not take into account the number of times the load exceeds a preselected overload value which has a cumulative effect on insulation materials and, consequently, on the transformer reliability.

b) *The Two Time-load Steps Method*

This method uses an original electronic device [2] as a new application for preventive reliability alarm signal generation and a more comprehensive logic than those used before. An extensive description of this device is presented in [2]. Fig.5 shows only the black-box scheme where BCW, BCT are two identical blocks for energy and real-time counting and A is a circuit for energy-dependent signal counting. The signals are received from the energy–frequency convertor EFC. A' is the same circuit for time dependent signals received from TFC. B is a circuit to display the energy (B' – real time), C – a circuit to preselect the total energy W_d (C' – real time T_d) reserve, D – a circuit to preselect and to display the partial energy W_a (D' – real time T_a) reserve, E – a circuit to detect the partial energy (E' – real time) consumption and F a circuit to detect the total energy (F' – real time) consumption. BDL is a logic decision block, where G is a sequential decision circuit, H – the reset circuit and I – the preset circuit. L is the preventive alarm circuit and M – the amplifier circuit.

For reliability, the operating logic principle of this device is important. We presume that from the start of operation the transformer has an initial transport

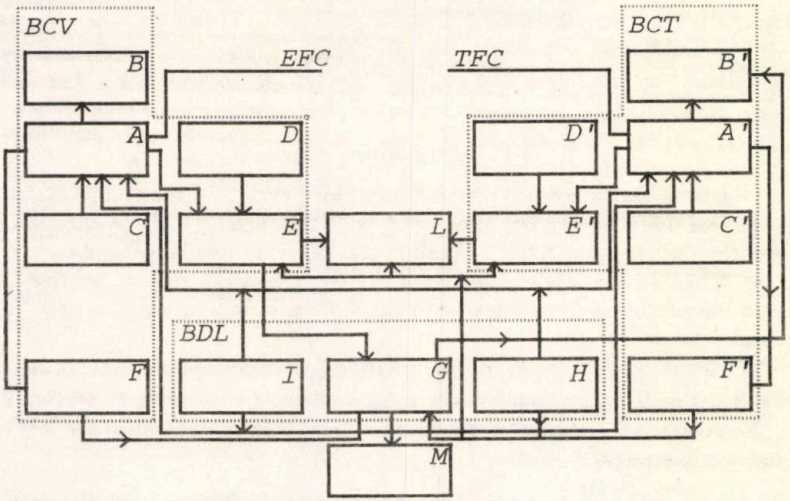

Fig. 5.– Black-box diagram of the electronic device for preventive reliability alarm.

capacity of W_L, [MWh], which could be established as:

$$W_L = S_r T_L, \tag{17}$$

where S_r is the rated transformer power and T_L – technical operating time established in relation to REL (s.(3)).

For maintenance, we can preselect partial values $W_a < W_c$ for energy and $T_a < T_c$ for time, which yield the average power value:

$$S_a = \frac{W_a}{T_a} \tag{18}$$

and partial values W_a, $(W_a < W_c < W_L)$, for energy and T_a, $(T_a < T_c < T_L)$, for time, which yield the average power value:

$$S_c = \frac{W_c}{T_c}. \tag{19}$$

The energy value W_a and the time T_a are introduced to generate a preventive alarm, while exceeding these values will change the maintenance program. The selection of the W_a, W_c, T_a and T_c values is most important. These constants depend on the transformer type (ONAN, ONAF, OFAF) and on the load type (special industrial loads, like those in Fig.2 or usual loads, like those in Fig.1). Usual values for T_a and T_c are expressed in hours and only in special cases it is necessary to introduce extreme values like tenths of minutes for chaotic and excessive loadings or days or

Table 1

Case	Time succession				Operating mode after:			
	t_1	t_2	t_3	t_4	t_1	t_2	t_3	t_4
1	W_a	T_a	W_c	T_c	PRA	–	RA+CM	NOC
2	W_a	T_a	T_c	–	PRA	–	NOC	–
3	W_a	W_c	T_a	T_c	PRA	RA+CM	NOC	–
4	T_a	W_a	W_c	T_c	–	–	RA+CM	NOC
5	T_a	W_a	T_c	–	–	–	NOC	–
6	T_a	T_c	–	–	–	NOC	–	–

even weeks or months for compensation between seasonal overloads and underloads. It is possible to preselect all these values.

Table 1 shows all possible time sequences of preselected values of T_a, T_c, W_a and W_c. T_a and T_c have a normal real-time succession, while W_a and W_c depend on the transformer load. Table 1 includes also the device action according to every sequence, in fact showing its operating mode and the essence of conception. PRA is the preventive reliability alarm, RA – the reliability alarm. CM means change of maintenance program and NOC – starts a new operating cycle.

4. Conclusions

The proposed methods are suitable for practical implementation in power systems to increase the reliability observability. Literature refers not only to transformers but also to high-voltage SF6 circuit breakers to change the planned maintenance into the new economically opportune maintenance.

The probabilistic approach to chaotic industrial loads and two alternatives of a deterministic one to enable adequate self-diagnosis and monitoring techniques for these components to improve their reliability are presented.

Received, December 14, 1994

Technical University "Gh. Asachi", Jassy,
Department of Energetics
and
Delft University of Technology,
Power Systems Laboratory,
Netherlands

REFERENCES

1. K e c e c i o g l u D., *Reliability Engineering Handbook.* Vol.I and II, Prentice-Hall, New Jersey, 1991.
2. M u n t e a n u Fl., Romanian Patent, *95084* (1988).
3. L a k e r v i E., H o l m e s E.J., *Electricity Distribution Network Design.* P. Peregrinus Ltd, U.K., 1989.
4. A l b e r t H., F l o r e a I., *Industrial Consumers Supply from Power Networks* (in Romanian). Ed. Tehnică, Bucureşti, 1987.
5. B r a u n s t e i n A., E l m a k i s D., *Calculation of Substation Reliability Indices Based on Hottest-spot Temperature of the Power Transformer.* Proc. of the 9-th Power Syst.

Comput. Conf., Portugal, 1987.
6. * * * *Guide for Loading Mineral Immersed Power Transformers up to and Including 100 MVA, with 55° C and 65° C Winding Rise.* ANSI/IEEE, C57.92, 1981.

DE LA MENTENANŢA PLANIFICATĂ LA MENTENANŢA OPORTUNĂ

(Rezumat)

Se prezintă o metodă probabilistică şi una deterministă pentru autodiagnoza şi monitorizarea componentelor sistemelor electroenergetice în scopul creşterii fiabilităţii. Transformatorul de putere serveşte pentru a demonstra modul de utilizare a acestor metode. Durata prestabilită de funcţionare ca parametru de fiabilitate dependentă de solicitările termice ale izolaţiei cauzate de suprasarcini şi modul de monitorizare a temperaturii punctului cald al înfăşurării sunt considerate pentru sistemul propus de urmărire a fiabilităţii. Este detaliat şi modul de utilizare a unui dispozitiv electronic original.

BULETINUL INSTITUTULUI POLITEHNIC DIN IAŞI
Tomul XLI (XLV), Fasc. 3–4, 1995
Secţia III
ELECTROTEHNICĂ. ENERGETICĂ. ELECTRONICĂ

C.D. 621.311.003

LES PARTICULARITÉS DES MODÈLES D'OPTIMISATION EN ÉNERGÉTIQUE DANS L'ÉTAPE ACTUELLE

PAR
GH. CÂRŢINĂ, VIRGIL ALEXANDRESCU et GH. GEORGESCU

1. Introduction

Assez souvant, dans les problèmes d'électroénergétique, on se trouve devant un choix très large de solutions possibles. De plus, compte tenu de la très longue durée de vie de l'équipement (câbles, postes de transformation, etc.) il faut que les décisions prises tiennent compte de cette période. Afin de trouver la solution la plus raisonnable on cherche de réduire la somme des coûts d'investissement et de pertes. On considère que tous les autres coûts sont généralement indépendants de la solution adoptée. Afin que la comparaison des diverses solutions soit significative, tous les coûts sont transformés en valeurs actualisées au niveau de la première année.

Généralement, le modèle mathématique d'optimisation comporte une fonction objectif et une ou plusieures restrictions. La fonction objectif fournit une grandeur scalaire, par exemple des coûts, qu'il s'agit de les réduire en appliquant les méthodes d'optimisation. Parmi les méthodes d'optimisation celles heuristiques sont de plus en plus utilisées. Elles se caractérisent par le principe de passer en revue toutes les combinations possibles entre les différentes valeurs des paramètres, de calculer la fonction objectif et de sélectionner la solution optimale en comparant les valeurs de calcul de la fonction objectif. Pour réduire le nombre des possibilités envisagées le réalisateur du programme peut éliminer un ensemble d'arborescences de l'arbre de décision s'il considère que les combinaisons qu'il contient n'apporteront pas la solution optimale (il y a le risque de passer à côté de la solution optimale) en raison de la mauvaise définition des règles de sélection ou de leur inadéquation au problème posé [1].

En dépit de cet inconvénient l'expérience pratique des méthodes heuristiques est positive dans l'ensemble. Elles restent dans la plupart des cas l'unique moyen de trouver une solution au problème en discussion.

2. Les caractéristiques générales des problèmes d'optimisation en énergétique

Le choix des solutions suivant les critères d'optimisation présente aujourd'hui au moins deux caractéristiques [2].

Premièrement il s'agit de l'apparition et d'évolution spectaculaire, dans les pays industriels, du management de la consommation de l'énergie, basé sur l'introduction des technologies de pointe [3].

La deuxième particularité, se référant spécialement à notre pays, concerne l'installation d'une période d'inflation de longue durée avec un taux assez grand et variable. Par l'inflation on comprend généralement l'augmentation des prix. Ce phénomène ne conturne pas, à une autre échelle, même les pays les plus développés (des taux d'inflation entre 2% et 15%). L'inflation provoque des incertitudes dans les milieux des affaires spécialement quand il s'agit d'un taux variable. Généralement d'autant le taux d'inflation est plus grand, tant sa fluctuation est plus importante. Dans ces conditions il est difficile, pour les firmes, d'évaluer leurs coûts et leurs bénéfices, ainsi qu'il est difficile d'estimer à longue terme le taux annuel d'inflation. Quant à la question de la prévision de charge électrique pour les usagers, le problème n'est pas moins compliqué. Compte tenu que notre pays traverse une période de grands changements économiques il n'est pas justifié d'utiliser les méthodes connues de prévision de la charge surtout dans le secteur industriel. Pour une entreprise il est difficile d'arriver à séparer dans son analyse du passé, comme dans son effort de prévision, les parts des effets conjucturels et des évolutions structurelles.

3. Le calcul du coût des pertes d'énergie

Pour calculer le coût des pertes d'énergie il faut partir de la prévision de charge. La prévision de charge des postes de transformation constitue une donnée clé du problème d'optimisation.

La plus suggestive représentation des puissances solicitées est celle basée sur les graphiques de charge (quotidiens, hebdomadaires, mensuels, annuels). La modélation des graphiques de puissances actives et réactives des noeuds du réseau électrique par des séries de temps s'avère suffisamment précise par rapport au processus réel.

En général, une série de temps, $Y_0(t)$, a trois composants [4]:

$$Y_0(t) = Y_T(t) + Y_C(t) + Y_S(t), \tag{1}$$

où: $Y_T(t)$ représente le composant tendance générale, $Y_C(t)$ – le composant cyclique (périodique), $Y_S(t)$ – le composant stochastique (aléatoire).

Les composants tendance générale peuvent être expliqués par la politique économique, l'essor ou la régression économique. Les composants cycliques sont

dûs à la périodicité de certaines activités quotidiennes, à la succession des saisons, etc. Pour calculer les coefficients des premiers deux composants on utilise la méthode des moindres carrés (par rapport aux charges survenues par le passé). Pour estimer les paramètres du modèle autoregrésif – le composant stochastique – les meilleurs résultats sont obtenus avec l'algorithme L e v i n s o n [4]. À l'aide des données, le programme de prévision peut définir une grille de charge par poste et par année jusqu'à l'achèvement de la période d'étude.

À longue terme et même à moyen terme dans la situation actuelle de l'économie il est difficile et risquante l'utilisation des séries de temps pour la prévision de la charge surtout dans le secteur industriel.

Quant à la demande d'électricité des clients résidentiels, tant comme niveau qu'au forme, elle est étroitement liée à leur mode de vie et évolue donc en fonction de multiples et profondes transformations des moeurs et des techniques. C'est-à-dire que la courbe de charge des clients résidentiels est appellée à se modifier au cours des années et que celle de l'an 2000 sera loin d'être une simple exploitation de la courbe de charge de 1992.

Un solution pour le calcul des pertes d'énergie dans ce cas est d'utiliser les valeurs caractéristiques du processus aléatoire correspondant: les valeurs moyennes et les covariances des puissances actives et réactives. Ainsi on peut calculer les pertes d'énergie pendant une période, T, avec une erreur assez faible (moins que 0,6%) en utilisant la relation [5]:

$$\mathrm{DW} = [\mathrm{DP}(P,Q)]_m T = [\mathrm{DP}(P_m,Q_m) + \mathrm{COR}(P,Q)]T, \tag{2}$$

où $\mathrm{DP}(P_m,Q_m)$ représente les pertes de puissance dans le régime permanent caractérisé par les valeurs moyennes des puissances aux noeuds du réseau.

La correction $\mathrm{COR}(P,Q)$, d'environ 3...5% par rapport à $[\mathrm{DP}(P,Q)]_m$ – la moyenne des pertes de puissance – est calculée en fonction des covariances des puissances actives et réactives. Donc, afin d'accéder au coût des pertes il est nécessaire d'effectuer l'estimation des valeurs caractéristiques des puissances actives et réactives considérées comme variables aléatoires de même que l'estimation des intervalles de confiance correspondants.

4. Le critère de la valeur nette actualisée

Le critère de la valeur nette actualisé, VAN, a pour expression [6]:

$$\mathrm{VAN} = B_0 - C_0 + \sum_{i=1}^{T}(B_t - C_t)\frac{(1+i_t)^t}{(1+a_t)^t}, \tag{3}$$

où B_t, C_t représentent le bénéfice, respectivement le coût de l'activité dans l'année t; i_t, a_t – le taux d'inflation, respectivement, d'actualisation dans la même année.

À son tour le taux d'actualisation contient quatre composants:

$$a = d + i + r + m, \tag{4}$$

où: d est l'intérêt, i – le taux d'inflation, r – le taux du risque de l'investissement, m – le taux de dépréciation de la monnaie nationale par rapport aux devises.

De l'analyse de plusieurs critères il en résulte que le critère VAN est le plus opportun du point de vue de l'efficience économique. Il indique, pour chaque solution, la mesure de sa compétitivité. Si VAN>0, l'investissement est rentable.

La solution optimale est celle qui assure VAN=max. À partir de l'expression (3) on peut en déduire les expression du bénéfice marginal, BM, et du coût marginal, CM. BM et CM représentent le bénéfice, respectivement, le coût, rapportés à une unité supplémentaire d'activité. Une personne raisonnable décidera de déployer une certaine activité si le bénéfice marginal dépasse le coût marginal de celle-ci. Donc, l'extension d'une activité est justifiée jusqu'au moment où BM=CM. L'utilisation de la relation (3) avec i et a variables implique des difficultés assez grandes provenant de l'estimation des valeurs pour i_t et a_t. Une certaine simplification est obtenue si on utilise un seul paramètre constant, le taux d'actualisation „sans inflation", a', donné par la relation:

$$\frac{1+i}{1+a} = \frac{1}{1+a'}, \tag{5}$$

d'où il résulte

$$a' = \frac{a-i}{1+i}. \tag{6}$$

Pour les variations des taux d'actualisation et d'inflation entre les limites prévisibles, a=20...70%, i=10...60%, dans le Tableau 1 sont sont présentées les valeurs du taux d'actualisation „sans inflation", a'. Pour les valeurs les plus probables du taux d'actualisation „sans inflation" sont calculées les moyennes géométriques correspondantes.

Tableau 1

Les valeurs du taux d'actualisation „sans inflation", [%]

$a-i$	Taux d'actualisation, a, [%]						Moyenne
%	20	30	40	50	60	70	géométrique
10	9	8,3	7,6	7,1	6,6	6,2	7,40
20	–	18,1	16,0	15,3	14,2	13,3	15,29
30	–	–	27,0	25,0	23,0	21,0	23,90

5. Conclusions

Les problèmes clé de l'optimisation en énergétique sont le critère d'optimisation et le calcul des pertes d'énergie.

Pour le calcul des pertes d'énergie on peut utiliser l'estimation des valeurs caractéristiques des puissances actives et réactives considérées comme variables aléatoires.

Comme critère d'optimisation on peut utiliser la valeur nette actualisée, avec un taux d'actualisation „sans inflation" de l'ordre $a'=10{,}63...13{,}89$, dont les fondements doivent être réalisés d'une manière plus précise, suivant le cas.

Reçue le 4 janvier 1994

Université Technique „Gh. Asachi", Jassy, Chaire d'Energétique

BIBLIOGRAPHIE

1. F r e u n d H., W e l l s s o n W.H., *Planification des réseaux de distribution au moyen de techniques d'optimisation assistées par l'ordinateur.* II-ème Colloque sur la distribution „Qualité de service futur", Lisbonne, 25-28 octobre 1989.
2. C â r ţ i n ă Gh., I v a s D., *Problema criteriilor de optimizare în perioada actuală.* III-ème Symp. „Optimisation du développement et de l'exploitation des installations énergétiques", Faculté d'Électrotechnique, Jassy, **I**, 1991, 116-120.
3. T a l u k d a r S., G e l l i n g s C., *Load Management.* IEEE Press, NY, 1986.
4. C â r ţ i n ă Gh., *La prévision à court terme de la consommation de l'énergie électrique.* Bul. Inst. polit., Iaşi, **XXXIV (XXXVIII)**, *1-4*, s.III, 79-84 (1988).
5. C â r ţ i n ă Gh., *Le calcul des pertes d'énergie dans les réseaux maillés.* Bull. ASE/UCS, **74**, *21*, 1220-1224 (1983).
6. S l o m a n J., *Economics.* Harvester Wheatsheaf, New York–London–Tokyo–Singapore, 1991.

PARTICULARITĂŢILE MODELELOR DE OPTIMIZARE ÎN ENERGETICĂ ÎN ETAPA ACTUALĂ

(Rezumat)

Se prezintă modul în care trebuie modificată funcţia obiectiv pentru a ţine seama de particularităţile etapei actuale (rata mare de inflaţie etc.).

BULETINUL INSTITUTULUI POLITEHNIC DIN IAŞI
Tomul XLI (XLV), Fasc. 3–4, 1995
Secţia III
ELECTROTEHNICĂ. ENERGETICĂ. ELECTRONICĂ

D.C. 621.316.11

CONSUMER CATEGORY IDENTIFICATION IN DISTRIBUTION NETWORKS USING HOPFIELD NETS

BY

M. GAVRILAŞ and GH. GEORGESCU

1. Introduction

Almost all present day practices in the optimal control and planning of urban rural power distribution networks use a repetitive load flow analysis, corresponding to different operating conditions, each of them associated to specific loads or consumers.

A frequent approach classifies the consumers from distribution networks according to different typical load curves [1], [2]. These and few other information (such as the value of the load at a certain hour of the day or the daily energy consumption) have proved sufficient to accurately reconstruct the real load curves of consumers in urban and rural distribution networks.

Meanwhile accurate results in the optimal control or planning of power distribution networks need the most accurate possible representation of the loads. On the other hand the load structure changes frequently and therefore influences on the accuracy of load flow analysis.

Nowadays most of the electric utilities hold in their Data Base numerous typical load curves built up by statistically processing a great number of actual load curves recorded in the nodes of the distribution networks. However a complete and exact use of this information supposes its permanent update according to the quantitative and the qualitative changes occurring in the evolution of the loads. In this way the monitoring of these changes and the update of the typical load curves in accordance to this evolution would be useful.

Using such an updated Data Base the recognition of new types of loads that could appear in the network or the structure identification in the case of complex loads would be possible.

This paper is intended to emphasize the possibility of using Artificial Neural Nets in order to build up and operate with such a Data Base. This task could be accomplished into two stages: the recognition or identification of a typical load curve and the decomposition of a complex load into a known number of typical loads.

2. Consumer Category Identification Using Hopfield Neural Nets

This paper deals with only the first of these stages. This one can be formulated as a problem of recognition, filtering or completion of a real load curve to obtain a typical one. The answer to this problem can be obtained using a H o p f i e l d Neural Net (HNN) [3].

In the power systems area the HNN is mainly used as an optimizer as for example for state estimation, optimal load flow, unit commitment and economic dispatch [4].

The principle of HNN uses the "error surface" with "valleys" associated to local or global minima which in fact correspond to the patterns in the learning set [5].

In the specific case of consumer category identification the HNN will be trained using as patterns the typical load curves and thus a "valley" on the "error surface" will capture a specific type of load.

Since the considered below HNN is of discrete type the load curves have been represented using seven binary inputs (± 1) for each level. For the usual values in the typical load curves this real-to-binary conversion ensures an acceptable accuracy, i.e. the errors do not exceed 2%.

The analysis was conducted for two separate groups of typical load curves which differ one another by the number of hourly levels taken into consideration, i.e. typical load curves with 12 (TC12) and 24 (TC24) hourly levels.

The learning patterns for the HNN considered were chosen accordingly:

a) 9 typical load curves for the TC12 associated to urban or rural domestic consumers, hotels, hospitals, department stores, etc. for a summer/working day operating condition;

b) 36 typical load curves for the TC24 associated to the same consumers for the four annual characteristic operating conditions (summer–winter/working–leisure day).

After the learning stage has been passed on an analysis of the HNN performances having in view its accuracy in recognizing, filtering or completing different patterns of typical load curves.

2.1. Recognition

This stage was performed using the same typical load curves as in the learning set. All these curves have been recognized after a single cycle of the HNN, which shows a successful pass through the learning stage.

2.2. Filtering

In order to test the performances of the HNN in cleaning out a noisy pattern several load curves generated on the bases of typical load curves and a random noise were considered. As an example, in Fig.1 are shown three pairs of noisy and corresponding typical load curves towards which the HNN has converged. These curves refer to urban/rural domestic loads and hospitals. From reasons of a simpler representation here and below the examples refer to the TC12 curves but similar conclusions have been found for the TC24 ones.

This analysis shows that the HNN filters the real load curve and converges towards a typical one after a number between 18 and 27 cycles, depending on the noise level and the shape of the curve presented as the input of the net.

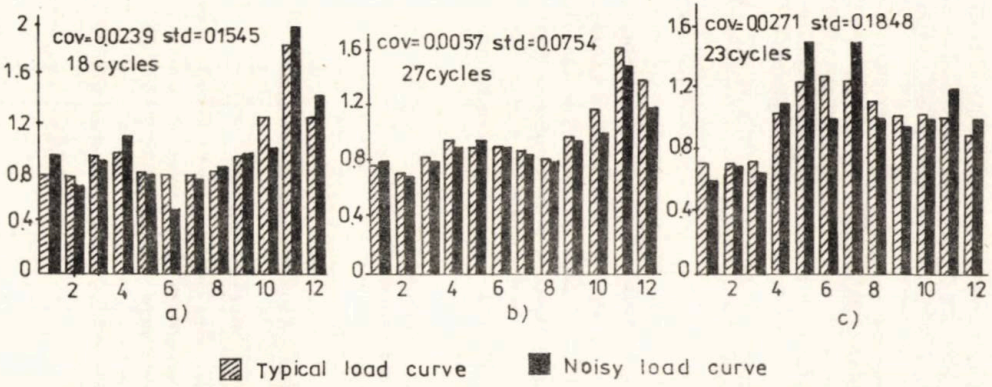

Fig. 1.– Typical and noisy load curves for urban-domestic (a),rural-domestic (b) and hospitals (c) type consumers.

Fig.1 shows also the variance, the standard deviation and the number of cycles requested by the HNN to converge towards a learning pattern. These values could suggest the idea that the smaller the variance or standard deviation between the real and the typical curves are, less cycles the HNN goes through until convergence. However such a conclusions can not be sustained since the performances of the net depend not only upon these statistical parameters but also upon the shape of the load curve. For example though the real curve in Fig.1 *b* seems to be a good approximation of the typical one, it also comes closely to the typical curve in Fig.1 *a* and thus the HNN will need few more cycles to separate the wrong from the right pattern.

2.3. Completion

In this case the process starts from an incomplete pattern (i.e. a load curve which contains values for few hourly levels, the others being left to 0) and in certain conditions, succeeds to complete the missing hourly levels in accordance to the corresponding typical load curve.

The analysis of this task proved that under certain conditions the completion could be perfect even with only two known levels in the load curve, as shown in Table 1. However such an accuracy is possible only in that case when the missing values (denoted by zeros) do not overlap upon portions of other typical load curves described by weak changes in the load. This situation is described in Table 2. Here, for the first seven patterns the load curve is correctly completed. On the contrary for the last two patterns the unknown values (the zeros) overlap upon portions of significant weak variation of other typical load curves and consequently the original pattern will not be completed.

Table 1

Typical Load Curves Completion

(0 – unknown, x – known hourly levels)

Typical load curve	Particular cases								
	1	2	3	4	5	6	7	8	9
0.7927	0	0	0	0	0	0	0	0	0
0.7697	0	0	0	0	0	0	0	0	0
0.9403	x	0	0	0	0	0	0	0	0
0.9564	x	x	0	0	0	0	0	0	0
0.8183	x	x	x	0	0	0	0	0	0
0.7959	x	x	x	x	0	0	0	0	0
0.7871	x	x	x	x	x	0	0	0	0
0.8214	x	x	x	x	x	x	0	0	0
0.9374	x	x	x	x	x	x	x	0	0
1.2577	x	x	x	x	x	x	x	x	0
1.8568	x	x	x	x	x	x	x	x	x
1.2662	x	x	x	x	x	x	x	x	x
Cycles until convergence	4	5	7	8	9	10	12	14	14

Table 2

Typical Load Curves Completion;
Successfully: Cases 1–7; Unsuccessfully: Cases 8, 9
(0 – unknown, x – known hourly levels)

Typical load curve	Particular cases									Alternate typical load curves	
	1	2	3	4	5	6	7	8	9	store	school
0.7927	x	0	0	x	x	x	x	0	0	0.0107	0.0457
0.7697	x	0	0	0	0	0	0	0	0	0.0107	0.0457
0.9403	0	x	0	0	x	0	0	0	0	0.0107	0.0457
0.9564	0	x	0	0	0	x	0	0	0	0.2293	0.9302
0.8183	0	0	x	0	0	0	x	0	0	1.8096	2.4848
0.7959	0	0	x	0	0	0	0	0	0	1.8935	2.3507
0.7871	0	0	0	0	0	0	0	x	0	1.9078	1.8645
0.8214	0	0	0	0	0	0	0	x	0	2.1808	1.7851
0.9374	0	0	0	0	0	0	0	0	x	1.9935	1.7743
1.2577	0	0	0	0	0	0	0	0	x	1.9322	0.5821
1.8568	0	0	0	x	0	0	0	0	0	0.0107	0.0457
1.2662	0	0	0	0	0	0	0	0	0	0.0107	0.0457
Cycles	13	14	18	16	17	14	17	–	–	–	–

These few remarks and the analysis accomplished for the TC12 curves considered have proved that five arbitrarily known values of the hourly levels in a typical load curve are a guarantee for its correct completion. As for the TC24 curves this minimal number of known hourly levels grows up to seven.

It is important to emphasize that since the completion could be though as an extreme case of filtering (when the unknown values are alter to zero) it is to suppose that a correct completion of a typical load curve could be accomplished even with altered values of the known hourly levels. However these alterations must not be too important since the missing values already represent themselves significant changes in the shape of the pattern to complete.

3. Conclusions

The model of the HNN described in this paper, meant for the processing of typical load curves, is useful for classifying different types of consumers from the nodes of a power distribution network.

Once the HNN has been trained the recognition of any typical load curve from the training set is instantaneous (in one cycle of the net). The HNN could be used successfully to identify the type of the consumer even in the case of load curves altered by a certain noise. Also this identification is still possible for incomplete load curves, when only few hourly levels are known.

Received, October 13, 1994

Technical University "Gh. Asachi", Jassy,
Department of Energetics

REFERENCES

1. Codiasse A.M., Guillevic M., Giraud D., *Connaissance des charges moyenne tension en vue de leur prise en compte dans les études de planification.* Rev. Gén. de l'Électr., *7-8* (1982).
2. Georgescu Gh., Poeată Al., Poeată N., *Contribuţii la modelarea sarcinilor din nodurile reţelelor electrice de distribuţie urbane.* Bul. Inst. polit., Iaşi, **XXIX (XXXIII)**, *1-2*, s.III (1983).
3. Gavrilaş M., Georgescu Gh., *Consumer Category Identification of the Loads from Electric Distribution Systems Using Artificial Neural Networks.* Bul. Inst, polit., Iaşi, **XL (XLIV)**, *1-4*, s.III (1994).
4. * * *, *Artificial Neural Networks for Power Systems – A Literature Survey.* CIGRE TF 38-06-06, August 1993.
5. Beale R., Jackson T., *Neural Computing – An Introduction.* Adam Hilger Publishing, 1990.

IDENTIFICAREA CATEGORIEI CONSUMATORILOR DIN REŢELELE ELECTRICE DE DISTRIBUŢIE FOLOSIND REŢELE NEURONALE ARTIFICIALE DE TIP HOPFIELD

(Rezumat)

Clasificarea consumatorilor din reţelele electrice de distribuţie este posibilă folosind Reţele Neuronale Artificiale de tip Hopfield (RNAH). După antrenare, RNAH permit identificarea categoriei de consum, după curbele de sarcină tip, chiar şi în cazul unor grafice de sarcină incomplete sau alterate de un anumit zgomot.

BULETINUL INSTITUTULUI POLITEHNIC DIN IAŞI
Tomul XLI (XLV), Fasc. 3–4, 1995
Secţia III
ELECTROTEHNICĂ. ENERGETICĂ. ELECTRONICĂ

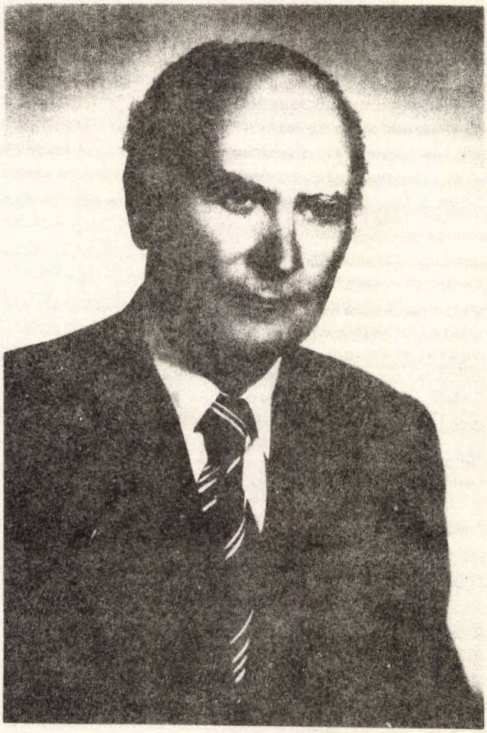

DUMITRU BĂRBULESCU

1919–1995

Le 11 mai 1995 a rendu son âme, foudroyé par une crise cardiaque, dans son laboratoire de recherches, le professeur dr.ing. Dumitru B ă r b u l e s c u. C'est une perte irréparable pour l'enseignement supérieur électrotechnique de Jassy où il a déployé une activité intense près d'un demi siècle, en conduisant pendant les deux dernières décennies le département de Mesures Électriques, jusqu'à sa retraîte.

Né le 20 décembre 1919 à Jassy, dans une famille modeste, D. B ă r b u l e s c u a suivi d'abord les cours du Lycée National puis ceux de l'École Militaire en se distinguant comme un élève très doué. Promu sous-lieutenant il a combattu, pendant la guerre, d'abord sur le front d'Est et puis sur celui d'Ouest. Cité mainte fois par ordre de jour il a été décoré avec l'hautes ordres, en soyant démobilisé avec le grade de lieutenant.

Pendant les années 1945–1949 il a suivi les cours de la Faculté d'Électromécanique (devenue dès 1948 d'Électrotechnique), de l'École Polytechnique „Gh.Asachi" de Jassy, en obtenant le titre d'ingénieur électricien. Remarqué comme un étudiant excellent il a été retenu dans l'enseignement

supérieur, en étant nommé assistant le 1-er octobre 1949. Il monte succésivement tous les degrés universitaires devenant professeur en 1970, au département de Mesures Électriques où il a resté jusqu'à sa retraîte, en 1990. Doué avec des qualités pédagogiques remarquables D. B ă r b u l e s c u a été apprécié toujours comme un professeur d'élite par des dizaines de générations d'étudiants.

En même temps le professeur D. B ă r b u l e s c u a manifesté, en permanence, un très vif intérêt pour la recherche scientifique. Soutenant, en 1962, une thèse de doctorat élaborée sous la direction du feu professeur Vasile P e t r e s c u, il a déployé, pendant plus de trois décennies une intense activité de recherches scientifiques concrétisée en plus de 60 de travaux publiés dans les revues de spécialité tant roumaines qu'étrangères. Les thèmes abordées appartenaient surtout au domaine des Mesures Électriques, en bénéficiant d'appréciations favorables dans les cercles de spécialistes. À ces travaux on peut ajuter nombre de livres dans le même domaine, édités sur plan local ou bien national, qui ont trouvé une large audience parmi les étudiants, les doctorands et les spécialistes travaillant dans l'industrie. D. B ă r b u l e s c u a dirigé avec compétence et dévouement de nombreuses thèses de doctorat, dans sa spécialité, de sorte qu'on peut affirmer sans aucune réserve qu'il est devenu chef d'école dans le domaine des Mesures Électriques, un digne successeur de son illustre prédécesseur, le professeur V. P e t r e s c u.

Pédagogue éminent, doublé par un chercheur scientifique dont les travaux sont hautement appréciés par les spécialistes, le professeur Dumitru B ă r b u l e s c u a été, avant tout, un homme dans la plus noble acception de ce mot. Sa rectitude morale bien connue par ses collègues et les étudiants, son incapacité d'accepter des compromis indignes, sa exigence envers ses collaborateurs et surtout envers lui même, sa loyalité à l'égard de ses amis, sa modestie bien connue et surtout sa probité menée jusqu'à l'extrême l'ont caractérisé pendant toute sa vie.

Par la disparition inattendue du dr.ing. Dumitru B ă r b u l e s c u l'enseignement supérieur technique perd un professeur d'élite; les collaborateurs et ses amis ressentent douloureusement sa disparition et ils garderont pour toujours son souvenir inoubliable.

H. Rosman

BULETINUL INSTITUTULUI POLITEHNIC DIN IAŞI
Tomul XLI (XLV), Fasc. 3–4, 1995
Secţia III
ELECTROTEHNICĂ. ENERGETICĂ. ELECTRONICĂ

RECENZII — BOOK REVIEWS

WEHINGER H. (federführend), *Explosionsschutz elektrischer Anlagen.* Expert Verlag, Renningen, 1995, 332 S., ISBN 3-8169-0961-2.

Die sicherheitstechnischen Aufgaben in Unternehmungen, welche brennbare Flüssigkeiten und Gase lagern oder verarbeiten – vor allem in der chemischen und petrochemischen Anlagentechnik – nehmen mit der starken Ausweitung dieses wichtigen Industriezweiges einen besonderen Platz ein. In diesem Themenband werden die notwendingen Grundlagen kurz erläutert. Vor allem werden alle Probleme der Prüfung und des Einsatzes explosionsgeschützter Betriebsmittel möglichst praxisnah dargestellt. Dabei wird insbesondere aus Sicht der Betreiber auf Planung, Installation, Betrieb und Instandhaltung eingegangen, und es werden die für den Betreiber notwendingen Maßnahmen erläutert.

Das Buch ist Pflichtlektüre für Ingenieure und Techniker der Elektroindustrie, die bei der Herstellung, Prüfung und Installation explosionsgeschützter Betriebsmittel und Anlagen tätig sind, Fachleute der chemischen und petrochemischen Industrie und der zuständigen Aufsichtsorgane, die derartige Anlagen planen, betreiben und überwachen.

I n h a l t: Planung explosionsgeschützter elektrischer Anlagen – Explosionsgeschützte Maschinen und ihre Schutzeinrichtungen – Explosionsgeschützte Schalt- und Steuertechnik – Das Prüf- und Bescheinigungsverfahren der Physikalisch-Technischen Bundesanstalt – Auswahlkriterien für explosionsgeschützte elektrische Betriebsmittel – Errichtung und Betrieb elektrischer Anlagen – Betrieb und Instandhaltung von explosionsgeschützten elektrischen Anlagen.

KLOTH ST., DUDENHAUSEN H.-M., *Elektromagnetische Verträglichkeit.* Expert Verlag, Renningen, 1995, 172 S., ISBN 3-8169-1207-9.

Dieses Buch bietet das nötige theoretische und praktische Know-How, um elektronische Geräte so zu konstruieren, daß sie ein geringstmögliches Maß an Störanfälligkeit aufweisen. Ein EMV-gerechtes Gerätedesign ist nicht nur für die Ausfallsicherheit eines Systems von Bedeutung, sondern wird vom Gesetzgeber ab 1996 für viele elektronische Geräte generell verlangt!

Dieses Buch zeigt besonders für den EMV-Anfänger, welche Maßnahmen und Faustregeln bereits bei der Konstruktion eines Gerätes beachtet werden müssen, um den zukünftigen Anforderungen an EMV gerecht zu werden.

Das Buch ist für Studenten, Ingenieure, Elektroniker, Physiker und Interessierte gleichermaßen geeignet. Die Problematik der EMV wird von Anfang an geschildert, so daß keinerlei Vorkenntnisse auf diesem Gebiet notwendig sind.

BONFIG K.W. (federführend), *Feldbus-Systeme.* Expert Verlag, Renningen, 1995, 202 S., ISBN 3-8169-1141-2.

Für die computerorientierte Meß- und Prüftechnik hat der Feldbus zentrale Bedeutung gewonnen. Über den Feldbus erfolgt der Informationsfluß zwischen Sensoren, Aktuatoren und dem Prozeßleitsystem. Nur mit einem Feldbus können die besonderen Vorteile und Möglichkeiten der modernen Digitaltechnik, die inzwischen in nahezu allen Meß-, Prüf- und Automatisierungsmitteln Einzug gehalten hat, auch in einem kompletten System ausgeschöpft werden.

Der Themenband ist für Ingenieure, Physiker und Informatiker bestimmt, die sich über die wichtigsten konkurrierenden Feldbussysteme, über ihre Konzepte und Eigenschaften sowie über die technische Realisierung informieren möchten.

I n h a l t: Überblick über verschiedene Konzepte für Bus-Systeme – Der Profi-Bus – Der P-NET-Bus – Der Interbus S – Der Bitbus – Entwicklung von der Smart-Technik zum herstellerunabhängigen Bedienkonzept – CAN, ein Auto-Bus – Das DIN-Meßbus-Konzept.

ORSZÁGOS KÖZPONT 1883 MŰSZAKI INFORMÁCIÓS KÖNYVTÁR

ISSN 0258-9109